MODELING OF VEGETATED FLOWS WITH UNCERTAINTY ESTIMATION

AFIS OLUMIDE BUSARI

Ph.D

The Hong Kong Polytechnic University

2016

The Hong Kong Polytechnic University

Department of Civil and Environmental Engineering

Modeling of Vegetated Flows with Uncertainty Estimation

Afis Olumide BUSARI

A thesis submitted in partial fulfillment

of the requirements for the

degree of Doctor of Philosophy

October, 2015

Certificate of Originality

I hereby declare that this thesis is my own work and that, to the best of my knowledge and belief, it reproduces no material previously published or written, nor material that has been accepted for the award of any other degree or diploma, except where due acknowledgement has been made in the text.

BUSARI Afis Olumide

Abstract

Vegetation growth in natural and artificial waterways (open channels) is desirable due to ecological and environmental concern. It can be actively used as a flood management tool, and to enhance the sustainability and restoration of ecosystem. Its growth in channels, however, increases the hydraulic resistance and leads to energy loss, which can be problematic. The consequence is the decrease in mean velocity, thereby reducing the channel conveyance capacity. The hydraulic resistance produced by sparsely distributed vegetation stems has been well studied while the effect of dense vegetation on hydraulic resistance has not been thoroughly investigated. Numerous studies of flow through vegetation in open channels are often based on cylindrical shape elements. Scarcity of data through review scrutiny reveals there is a need for more laboratory studies on flows over blade-type vegetation, and investigation of the effect of different vegetation distribution pattern on hydraulic roughness parameter. In addition, the field conditions are always with uncertainty. There is a practical need to investigate the propagation of uncertainty in the flow and vegetation parameters towards the uncertainty in hydraulic roughness parameter.

The objectives of this work are: (*i*) to develop a hydraulic roughness model for submerged flexible vegetation; (*ii*) to acquire experimental data of flows through blade-type vegetation under emergent and submerged conditions; (*iii*) to clarify the inconsistent findings of previous research by investigating the dependency of the bulk drag coefficient (C_d) on plant distribution pattern instead of the solid volume fraction (ϕ), through the experimental study of the sheltering and channeling effect of vegetation

stems on the behaviour of flow through emergent and submerged vegetation; (i*v*) to propose empirical equations relating C_d to the lateral and longitudinal spacing of stems for both submerged and emergent conditions; and (*v*) to assess the propagation of uncertainties in the modelling of vegetated flow. To achieve the above objectives, this study is subdivided into four parts.

Firstly, this study used Spalart-Allmaras model to generate synthetic velocity profile data for hydraulic roughness determination. In the model, turbulence is simulated by the closure with a modified length scale which is dependent on the vegetation density and vegetation height to water depth ratio. Flexibility of vegetation is accounted for by using a large deflection analysis. The model has been verified against available experiments. Based on the synthetic data an inducing equation is derived for submerged flexible vegetation, which relates the Manning roughness coefficient to the vegetation parameters, flow depth and a zero-plane displacement parameter. The derived equation has been verified using well-documented experimental data as well as field data. The equation performed better than the existing equations especially for submerged flexible vegetation. Generally, the predictive capability of these equations depend largely on the C_d values.

Secondly, a systematic laboratory study has been carried out to investigate the effect of the distribution pattern of vegetation stems on the hydrodynamics of gradually varied flow (GVF) through emergent blade-type vegetation. The drag induced by flow through vegetation is affected by the velocity, shape of vegetation stems and wake interference among stems. Previous studies have accounted for the interference effects generally by relating C_d of vegetation to the solid volume fraction ϕ of the vegetated

zone and the results were found to be inconsistent. The C_d values are well documented for cylindrical shape while that for blade type vegetation is less reported, and the drag characteristics for the two shapes can be different. In this work, a blade-type finite artificial vegetation patches of solid volume fractions ranging from 0.005 to 0.121 have been used and the stem Reynolds number tested ranges from 500 – 2600. The longitudinal water surface profiles have been measured and the effect of increasing areal density of vegetation with respect to varying longitudinal and lateral spacing under the flow conditions is examined. The momentum equation that relates the vegetation resistant force and water surface profile has been used to obtain the value of C_d. The results shows that C_d decreases with increasing stem Reynolds number, decreases with increasing ϕ at fixed lateral spacing due to sheltering effect, and increases with ϕ at fixed longitudinal spacing due to channeling effect. The inertial contribution due to pressure loss in the stem wake decreases with increase in transverse and longitudinal spacing, while the effects of viscous shear stress, vortex shedding and jet spreading increases with the increase in longitudinal spacing over the experimental range. An empirical equation relating C_d to the lateral and longitudinal spacing instead of ϕ has been obtained and validated.

Thirdly, the hydrodynamic behaviour of GVF through submerged blade-type vegetation is investigated. The distribution layouts of stems are similar to those cases of emergent vegetation. The blade Reynolds number Re ranges from 670 to 1150 and six flow rates are used in each set of the experiments. The vertical profiles of stream-wise velocity have been measured using Acoustic Doppler Velocimeter (ADV). The theoretical longitudinal momentum equation relating the vegetation resistant force,

water surface slope and mean velocity in the vegetation layer is used to determine the C_d value. Using a regular-array pattern of vegetation elements, the interference effects have been studied independently by varying the longitudinal element spacing (S_x) and lateral element spacing (S_y) respectively. The results showed that the distribution pattern of vegetation elements can exert significant effect on the C_d values, and the associated flow characteristics, including flow adjustment length, peak Reynolds stress and flow division in the clear water zone and vegetation zone. An empirical equation relating C_d to the lateral and longitudinal spacing is proposed for submerged flexible vegetation. For the same vegetation distribution pattern, the C_d values obtained for submerged and emergent conditions are similar for cases with high areal density of vegetation.

Lastly, numerical simulation of flows over dense vegetation has been carried out using the experimentally determined C_d as input. The flow evolution within the vegetation patches and the clear water zone due to sheltering and channeling effects among vegetation stems have been successfully replicated. For practical applications, the accuracy of the prediction by the proposed equations and numerical model is further assessed. The sources of uncertainty are due to the limitations of the equations/model and the variability of the input vegetation and flow parameters. The uncertainty of the inducing equations and numerical model in the estimation of the roughness coefficients is expressed by the Normalized Root Mean Square Deviation (NRMSD) and the propagation of the uncertainty due to the variability of the vegetation and flow parameters existing in nature is investigated by using the method of Unscented Transformation (UT). The method is found efficient and gives a more accurate estimation of the mean roughness (or drag) coefficients. By measuring the vegetation

and flow parameters with uncertainty ranges, the inducing equations together with the UT method can be used to compute the mean and covariance of the Manning roughness (or drag) coefficient.

In summary, this study contributes to the knowledge and understanding of vegetated flows. It advances the previous studies in that the dependence of the hydraulic roughness parameter (drag coefficient) on the distribution pattern of vegetation has been investigated and the propagation of the uncertainty in the parameter estimation has been quantified. The proposed equations and numerical model have been verified against experiments and can be applied to conditions where laboratory and field study have not been performed. The model thus will be useful for river/wetland restoration and vegetation management projects.

List of publications arising from the thesis

Journal publication

Busari, A.O and Li, C.W., (2016). Bulk drag in a regular array of emergent vegetation stems under gradually varied flow. Journal of Hydro-environment Research, volume 12, pp 59 - 69.

Busari, A.O and Li, C.W., (2015). A hydraulic roughness model for submerged flexible vegetation with uncertainty estimation. Journal of Hydro-environment Research, volume 9, issue 2, pp 268 – 280.

Conference paper

Busari, A.O and Li, C.W., (2015). Modeling of gradually-varied flow through submerged semi-rigid blade-type vegetation**.** Presented at the 36th IAHR World Congress 28 June – 3 July, 2015 Delft-The Hague, the Netherlands.

Busari, A.O and Li, C.W., (2015). A laboratory study of gradually varied flow through semi- rigid emergent blade-type vegetation. Proceedings of Engineering Mechanics Institute (ASCE) 2015 International conference. January 7 - 9, 2015 at the Hong Kong Polytechnic University, Hong Kong SAR, China.

Busari, A.O and Li, C.W., (2013). A hydraulic roughness model for submerged flexible vegetation. Proceedings of 35th IAHR World Congress, September 8-13, 2013 at Chengdu, China.

Acknowledgements

Gratitude to the Research Grant Council of the Hong Kong Special Administrative Region and the Hong Kong Polytechnic University for giving me the opportunity to study in Hong Kong as well as providing financial support.

My profound gratitude to my supervisor, Professor, Chi-Wai Li of the department of Civil and Environmental Engineering, for his helpful suggestions, constructive critics, incredible patience and technical advice during this research work. I am glad to have worked with you as a PhD student. Your encouragement gave me hope even when the going was tough.

My sincere thanks to my examiners: Prof. Onyx W.H Wai (Chairman Board of Examiners), Dr. K.M LAM (The University of Hong Kong) and Prof. Koji SHIONO (Loughborough University, UK) for their constructive criticism and comments.

Heartfelt thanks to all Professors in the departments of Civil and Environmental Engineering, Mechanical Engineering and Applied Mathematics, the Hong Kong Polytechnic University for sharing their knowledge during my course work.

Many thanks to Mr. K.H. Leung, the hydraulic laboratory technical staff for his assistance during the experiment. I am also indebted to all my research group colleagues for the support giving to me during the after-normal hour laboratory work.

I sincerely appreciate my guardian, Sheu Ahmad Tijani Lawal for the great role he has played in making my dream a reality.

Special thanks to my son, Ahmad Eniola for his understanding. I owe you God - bless and wishing you the best.

Thanks to all friends who in one way or the other have contributed to the success of my stay in Hong Kong.

Table of contents

List of Figures

List of Table

List of Plates

Nomenclature

Alphabetical Symbols

A_0 = Blade spacing (m)

B = Channel width, m

C (= 1.8614) = Constant

C_0 = Coefficient of discharge

C_d = Bulk drag coefficient over the entire canopy length

C_h = Chézy resistance coefficient

c_{b1} constant (= 0.1355)

c_{b2} constant (= 0.622)

c_{n1} constant (= 7.1)

c_{w2} constant (= 0.3)

c_{w3} constant (= 2)

d = Turbulence length scale (m)

E = flexural stiffness (N/m^2)

F_i (= F_x,) is the resistance force component in the direction of flow (N/m^3)

f = Darcy-Weisbach friction factor

F_d = Drag force

f_d = Non-dimensional or dimensionless drag force

Fr = Froude number

f_{rk} = Drag force parameter (m^{-1})

f_v = Vegetation resistance parameter (-)

g = Gravitational acceleration, (m/s^2)

h = Water depth measured from the bottom (m)

h_d = Averaged deflected height (for flexible stem experiments), (m)

h_p = Penetration depth (m)

h_v = Undeflected canopy height (for stem experiments), (m)

I = Second moment of area (m^4)

k = Turbulent kinetic energy ($m^2\ s^{-2}$)

L_v = Length of VP (m)

L = Turbulent length scale (m)

M = Bending moment (Nm)

n = Vegetative Manning's roughness coefficient ($m^{-1/3}s$)

N = number density of gravel bed (m^{-2})

Q = Flow rate, (m^3/s or m^3/hr)

Q_v = Flow rate in the vegetation region (m^3/s)

Q_a = Flow rate in the clear water region (m^3/s)

$Q_{in} = Q$ = Total flow rate in the open channel (m^3/s)

Re = Reynolds number;

R = Hydraulic radius (m)

R^2 = Square of correlation coefficient;

S_y = Lateral stem spacing (m)

S_x = Longitudinal stem spacing (m)

S_0 = S = Bed slope (-)

S_w = Average water surface slope

u = Depth averaged velocity (m/s)

U = Cross-sectional averaged pore velocity (m/s)

u, v, w = Instantaneous velocity components in x, y, z directions (m/s)

$\bar{u}$, $\bar{v}$, $\bar{w}$ = Time-averaged velocity components in x, y, z directions (m/s)

u', v', w' = Fluctuating velocity components in x, y, z directions (m/s)

u^* = Bed-shear velocity (m/s)

$-u'w'$ = Reynolds shear stress per unit mass (m^2/s^2)

w = Width of stem (m)

x, y, z = Rectangular Cartesian coordinates (m)

z = Vertical distance from the bottom (m)

z_o = Zero-plane displacement parameter

z_o', = Modified zero-plane displacement parameter

Greek Symbols

α' *(=0.5)* = constant

β' *(= 0.7)* = constant

λ = Frontal area of vegetation per unit volume (m^{-1})

δ = Deflection in x-direction (m)

δ_e = Penetration scale (m)

κ = Karman constant

ν_m = Kinematic molecular viscosity (m^2/s)

ν_t = Kinematic eddy viscosity (m^2/s)

ρ = Water density (kg/m^3)

ϕ = Stem average solid volume fraction (-)

Abbreviations

1D	One-Dimensional
2D	Two-Dimensional
3D	Three-Dimensional
ADV	Acoustic Doppler velocimetry
COR	Correlation
HD	High density
K-H	Kelvin-Helmholtz
LES	Large Eddy Simulation
NSE	Navier Stoke Equations
Q3D	Quasi-three-dimensional
SNR	Signal-Noise-Ratio
SP	Sigma points
UT	Unscented Transformation
VP	Vegetation patch

1 Introduction

1.1 Preamble

Vegetated flows encompass a wide range of environmental flow regimes. Vegetation- flow interactions are common problems in the design of river restoration schemes, studies of flood risk and sediment transport, therefore, are of practical interest to ecologists, hydrologists and hydraulic engineers. Recently, engineering projects for the restoration of river basins toward natural developments are popular owing to the increase in the awareness of the need of ecological and environment preservation. In artificial channels, gravels with growing vegetation are generally used to control soil erosion and to maintain the ecological balance.

Decades ago most of the flood control channels in Hong Kong and other countries in the world were constructed with plain concrete. To enhance sustainable development, some channels are now rehabilitated using ripraps/hollow concrete blocks with growing vegetation to control soil erosion and to restore the natural habitat, thereby promoting eco-friendly design practice. Accommodation of vegetation in drainage design will serve as a restoration means for the lost mangroves in many countries due to urban development. The naturalization of water channels however increases the flow resistance and requires widening of the channel cross section. The problem of hydraulic resistance by vegetation and its effects on channel conveyance and drainage capacity is not unique to one country, but a global concern.

In order to address this issue, numerous research works have been carried out including field and laboratory studies, analytical and numerical studies, and most often,

a combination of approaches for validation to understand the behaviour of vegetation in natural and artificial waterways (i.e., open channels). The effect of vegetation on flow resistance has called for hydraulic roughness determination to estimate the conveyance capacity of river channels. The estimation of hydraulic roughness has been an issue of concern in the research arena mainly because of the variability and interrelated vegetation parameters and its effect on flow.

Vegetative roughness coefficient is an important parameter in the design of hydraulic structures, estimation of velocity distribution and as well as in the precise computation of energy losses (Temple, 1986; GU, 2007 and Azamathulla et al, 2012). Generally, most rigid channel linings have Manning's roughness coefficient (*n*) that is approximately constant, although, the value of *n* increases for shallow flows, but the effect is often neglected in design. In case of flexible vegetation that replicates natural cases along the river channel, the estimation of hydraulic roughness is crucial because of its pressing significance in drainage design and its complicated nature due to the associated behaviour of vegetation parameters with flow. Nevertheless, many equations have been proposed for the Manning's roughness coefficient for submerged rigid/flexible vegetation, but still no valid conclusion. This inconclusiveness has led to doubts about the tentative resistance equation to be used as a tool for the design of vegetated open channel flows especially for flexible and /or highly dense vegetation.

Presently, with an increase in the global concern for environmental sustainable development, the research community, industries, non-governmental organizations and government have realized the need to improve, protect and preserve/restore natural/artificial vegetation in our waterways/drainage systems. Review of the previous

research studies reveal the relentless effort of researchers through data collection and analysis, designing, implementing laboratory/field studies and numerical simulation of natural processes, in order to understand the behaviour and the hydrodynamic effect of vegetation. Most of these studies focused on emergent flexible/rigid vegetation and submerged rigid vegetation (Wu and He, 2009; Stone and Shen, 2002; Lopez and Garcia, 2001; Kutija and Hong, 1996; Enduran and Kutija, 2003; Nezu and Sanjou, 2008; Dupont and Brunel, 2009; Fathi-Magadam and Kouwen, 1997, Dhamasiri et al, 2012; Tanini and Nepf, 2008; Cheng and Nguyen, 2011; Cheng, 2011). In case of submerged flexible vegetation, the hydrodynamics of flow becomes more complicated basically because the type, distribution pattern, areal density and flexibility of the canopy in an open channel flow can affect the channel morphology, resulting into change in velocity and shear stress distribution, turbulence structure and coherent motion of flow (Dunn et al, 1996; Ikeda and Kanazawa, 1996; Jarvela, 2005; Kubrak et al, 2008; Takaaki and Nezu, 2010). These changes are related to the vegetal drag which can have strong influence on sediment transportation (resulting into erosion or deposition) and aquatic lives.

Although, the hydrodynamics of vegetated flows has been extensively studied, there are still many issues awaiting clarification. For examples; (i) the hydraulic resistance produced by sparsely distributed vegetation stems has been well studied while the effect of dense vegetation on hydraulic resistance has not been thoroughly investigated; (ii) numerous studies of flow through vegetation in open channels are often based on cylindrical shape elements, whereas other geometrical shapes similar to plants found in nature are rarely study; (iii) scarcity of data through review scrutiny reveals

there is a need for more laboratory studies on flows over blade-type vegetation and; (iv) investigation of the effect of different vegetation distribution pattern on hydraulic roughness parameter deserve research attention. In addition, the field conditions are always with uncertainty. There is a practical need to investigate the propagation of uncertainty in the flow and vegetation parameters towards the uncertainty in hydraulic roughness parameter.

One possible approach to understand the uncertainty in vegetation roughness parameter is to investigate the effect of interference mechanisms on drag coefficient. More so, the effects of lateral and/or longitudinal variation of vegetal stem spacing on hydrodynamic drag need to be investigated. Therefore, a better understanding of this approach will be greatly advantageous to the river restoration/ drainage design in terms of the estimation of drag coefficient, determination of hydraulic roughness and deepen our understanding of flow dynamics in vegetated open channel flow modeling.

Upon advancement in computer knowledge, models now play vital role towards improving the understanding of hydrodynamics of flows, simulating flow behavior and, assist in the design of hydraulic structures. As a result of constant improvement in the numerical computation, one has the ability to represent hydrodynamic processes with increasing level of details. Since models are now essential decision support system, hence, there is a need to analyze the uncertainty contribution of vegetation parameters and flow conditions in the model predictions in order to assess the confidence levels of numerical prediction subjected to multi-dimensional parameters. Uncertainty estimation has gained applications in hydrologic modeling, whereas uncertainties in hydraulic modeling is often ignored (Sowinski, 2006). Usually, performances of

numerical models are often based on agreement between the field or laboratory results and numerical results. The uncertainties in the vegetative (input) parameters are rarely considered and their relative importance to model response is needed. These input uncertainties manifest in the model resulting into uncertainties in the model predictions. In order to understand the effect of these uncertainties and improve our confidence level in these models to an extent of ensuring their use in the design, the performance of empirical equations/numerical model needs to be examined. With this being done, our predictions (that is, model outcomes) can then be applied to conditions where laboratory or field study have not been performed.

The scarcity of data through review scrutiny reveals there is a need for more laboratory studies on flows over blade-type vegetation, and investigation of the effect of different vegetation distribution pattern on hydraulic roughness parameter. Also, gradually varied flows occur in nature rather than the assumption of uniform flow condition. In addition, the field conditions are always with uncertainty. There is a practical need to investigate the propagation of uncertainty in the flow and vegetation parameters towards the uncertainty in hydraulic roughness parameter. Due to the complexity and practical limitation of some uncertainty techniques during review, this study introduces a practical technique of **U**nscented **T**ransformation (UT) to propagate the uncertainties in the modeling of vegetated flows.

1.2 Context of the study

The thesis combines modeling of dense vegetated flow (using blade-type elements) with the analysis of uncertainty in the estimation of the hydraulic resistance

parameters. This combination aims to deepen our understanding of the modeling of high density vegetated flow with respect to the relative uncertainties of vegetation resistance parameters through error uncertainty in input parameters and empirical equations/numerical model using UT method.

1.2.1 Modeling of vegetated flows

The knowledge of restoration of river basins toward natural development requires understanding of the behaviour of vegetated channels in river engineering, for proper design of drainage control channels and for decision making on river management. Typical examples are questions related to safety against flooding, discussion regarding nature rehabilitation, channel maintenance planning and technical problems. The accommodation of vegetation in rivers, floodplain and drainage channel have to consider their influence on flow and sediment transport through the channel. Hence, systematic understanding of the hydrodynamics of the system with natural variation of vegetation parameters defined by roughness coefficient is required to satisfy the planning and design specification in engineering to cater for the consequences as well as management practice.

Many investigators (e.g., Kutija and Hong, 1995; Lopez and Garcia, 2001; Velasco et al, 2008; Jia et al, 2008 and Zhang et al, 2012) have carried out research towards improving the understanding and prediction of capabilities concerning vegetated flow channels through efforts into the development of numerical model systems which incorporates modules that estimate flow velocity in vegetation channels. Therefore, accurate estimation of bulk drag coefficient which is an important vegetation roughness parameter is required to enhance the predictive capability of these numerical

models. This drawback is also applicable to numerous physical models from previous studies where efforts to estimate the bulk drag coefficient were based on solid volume fraction of vegetation, whereas the effects of distribution pattern of plants can play a significant role.

1.2.2 The need for uncertainty estimation

Hydrodynamic models for vegetation flows are often deterministic in approach, that is, the results are given in terms of unique values of velocity and pressure in time and space. On the other hand, as for natural processes these results may not be exact, as modeling of vegetated flows involves many uncertainties. For example, the vegetation stem diameter varies from plant to plant, is spatially non-uniform, plant heights exhibit natural variation in space and time, and many more regarding vegetation parameters such as variation in stiffness and vegetation densities. This natural variation of vegetation variables result in uncertain hydraulic roughness estimates. The key parameter to the roughness estimate is the vegetal bulk drag coefficient. In the simulation of vegetated flows, C_d is an important input parameter to the theoretical, (semi)empirical or numerical model and its accurate estimation is essential. The areal density of vegetation (or vegetation density) has been found to be dynamic in time and space in a broad range of scale (Poggi et al, 2004). The output of the model usually presents one out of many possible velocity profiles. Most especially, the characteristics of flexible, submerged vegetation have made hydraulic resistance a variable (in time and space) whose measure depends on flow phenomena and plant characteristics (Bakry et al, 1992; Stephan and Gutknecht, 2002; Yang and Choir, 2010; Li and Xie, 2011).The variability produces underestimation or overestimation of the hydraulic roughness and

resulting in variation in water level and conveyance capacity. The uncertainty in the estimation of roughness parameter such as C_d has to be quantified and minimized possibly by identifying the relative importance of vegetative parameters. With this being done, our predictions (that is, model outcomes) can then be applied to conditions where laboratory or field study have not been performed. By understanding of these surrounding uncertainties using UT method rather than ignoring it leads to correct or at least an appropriate estimate of conveyance capacity of drainage systems.

1.3 Aim

The aim of this study is to contribute to the knowledge and understanding the hydraulic drag coefficient for modeling of highly dense vegetated flows using interference effects among vegetation stems and investigate the influence of vegetative parameters in the model prediction (e.g., roughness coefficient or channel discharge) using UT method of uncertainty estimation.

1.4 Objectives

The specific objectives of this research are as follows:

i. To develop a hydraulic roughness model for submerged flexible vegetation;
ii. To acquire experimental dataset for flows through blade-type vegetation under emergent and submerged conditions;
iii. To clarify the inconsistent findings of previous research by investigating the dependency of the bulk drag coefficient (C_d) on plant distribution pattern instead

of the solid volume fraction (ϕ), through the experimental study of the sheltering and channeling effect of vegetation stems on the behaviour of flow through emergent and submerged vegetation;

iv. To propose empirical equations relating C_d to the lateral and longitudinal spacing of stems for both submerged and emergent conditions;

v. To examine the predictive capability of numerical model with Spalart – Allmaras (S-A) turbulence closure by simulating fully developed open channel flow over submerged canopies and assess propagation of uncertainty in the modeling of vegetated flow.

1.5 Research purpose

The hydraulic resistance produced by sparsely distributed vegetation stems has been well studied while the effect of dense vegetation on hydraulic resistance has not been thoroughly investigated. Numerous studies of flow through vegetation in open channels are often based on cylindrical shape elements. Scarcity of data through review scrutiny reveals there is a concrete evidence for more laboratory studies on blade-type vegetation. The review, also, provides clear explanation of the need for laboratory/field study on the effect of different vegetation distribution pattern on hydraulic roughness parameter. In addition, the field conditions are always with uncertainty. There is a practical need to investigate the propagation of uncertainty in the flow and vegetation parameters towards the uncertainty in hydraulic roughness parameter. In view of the above, this study set out contribution to the knowledge.

This study provides detailed understanding of the influence of interference effects (i.e. *Sheltering* and *channeling* effects) on hydraulic roughness coefficient. These two effects have been identified to illustrate the inconsistency in the previous works that relates bulk drag coefficient to solid volume fraction (ϕ) of vegetation elements instead of lateral and longitudinal spacing. It can be demonstrated that the relationship between C_d and ϕ for a fixed Reynolds number is not unique. The study uses blade-type vegetation as obstruction elements, thereby, providing dataset on blade-type vegetation for future studies and increase the confidence level of numerical modeling of vegetated flows. Understanding the "*sheltering*" and "*channeling*" effects can be useful for river restoration. The former can be used as an erosion control mechanism and to provide a favorable habitat for aquatic animals. The latter can enhance solute transport and reduce sediment accumulation. To strike a balance between the ecological preservation and hydraulic resistance reduction, vegetation management can take account the interference effects among individual stems. In particular, it will contribute to the accuracy and safe engineering design of sustainable flood control channels with vegetation when using numerical models.

Numerical simulations need to provide a physical explanation of the flow phenomenon in vegetated waterways. A major obstacle in the numerical modeling of vegetated flow is the estimate of the (form) drag and the complexity of interrelated vegetative parameters as well as flow characteristics. This study provides extensive discussion on the influence of interference effects on drag coefficient, mean velocity profiles and Reynolds stress profiles. The phenomena is replicated using a numerical model, the uncertainty in the estimate of C_d and its variance with flow, plants

distribution and vegetation parameters will not only identify which parameter requires further study, but also give insight into the possible options for the management of vegetated waterways.

1.6 Overview of thesis

This thesis consists of eight chapters. The first chapter provides the introductory aspect of the thesis. The remaining seven chapters are structured as follow:

- ***Chapter two*** reviews the studies of vegetated channel flows and uncertainties in the modelling practice. The modeling practice is discussed under three heading namely: physical, analytical and numerical modeling approaches. Further review on the hydraulic resistance model with respect to the significance of vegetative drag is reported. Finally, it reviews uncertainty in the modelling practice; the challenges in the classification of uncertainties due to different nomenclature from different field of studies; the available methods of uncertainty analysis including their applicability, advantages and limitations.
- ***Chapter three*** presents the development of a proposed hydraulic roughness model for submerged flexible vegetation. The model verification as well as comparison with existing empirical models is extensively discussed.
- ***Chapter four*** describes the completeness of the methodology for the laboratory studies of gradually varied flow through emergent and submerged semi-rigid blade-type vegetation. This chapter serves as a background for chapters five and six.

- ***Chapter five*** investigates the interference effects among the vegetation stems through laboratory flume measurements of gradually flow through emergent blade-type vegetation elements. The longitudinal and lateral spacing between adjacent vegetation elements are changed in different sets of experiments to identify the mechanism of flow interference and present results using bulk drag coefficient and normalized drag force parameter.
- ***Chapter six*** provides a systematic study of hydrodynamic the interference effects/mechanisms among vegetation stems through submerged vegetation under a gradually-varied flow condition. The results are discussed based on lateral (longitudinal) spacing, effect of vegetal distribution patterns on bulk drag coefficient, proposed equation for computing bulk drag coefficient. Finally, comparison is drawn between the estimated bulk drag coefficients for emergent and submerged cases.
- ***Chapter seven*** studies the uncertainty analysis of vegetated flow modeling using the numerical model, the model is used to reproduce the flume experiments conducted in chapter (6) and discuss the results. In explicit form, the chapter assesses the input and modeling errors of the fitting equations and 1-D model using NRMSD method and the error propagation is carried out using UT method of uncertainty analysis.
- ***Chapter eight*** gives the conclusion on the results of the hydraulic roughness model for submerged vegetation as well as the present laboratory and numerical studies. It also highlight issues that need to be address in the future work as recommendation.

2 Literature review

2.1 Introduction

This chapter review the previous work on modeling of vegetated flows as well as methods of uncertainty estimation.

2.2 Modeling of Vegetated Flows

The restoration of natural riverine environment is a significant task in river management worldwide. This prompts the hydraulic research in vegetated flows in streams, rivers and coastal waters. Vegetation is an indicator of richness and diverse living resources with possession of great environmental and socio-economic importance for many countries of the world (DSD/ Moc MacDonald, 2009). The growth of natural vegetation in waterway and wetlands is favored because of its ecological and environmental importance (Lopez and Garcia, 2001; Li and Yu, 2010). Vegetation can trap and stabilize sediment along waterways as well as to reduce river bed erosion (Wilson, 2007; Jia et al, 2008; Tanino and Nepf, 2008; HUAI et al, 2009; Okamoto and Nezu, 2010; Zhang et al, 2012). It can improve water quality, reduce turbidity, induces biological purification processes, hence reduce discharged nitrates and phosphates in rivers (Velasco et al, 2003; Nezu and Sanjou, 2008). It can also attenuate flood waves and protect coastal and riparian against flooding (Cheng and Nguyen, 2011, Busari and Li, 2014); provide habitat resources and river aesthetics (Pirim et al, 2000; Li and Yan, 2007); balance the global ecosystem (Vassilios, 2000), and enhance ecological equilibrium (Defina and Bixio, 2005). Lastly, it can provide a source of livelihood for aquatic animals (Li and Xie, 2011) and interestingly, a valuable resource for public environmental education and scientific research (DSD/ Moc MacDonald, 2009).

Therefore, the understanding of the hydrodynamics of vegetation for ecological and environmental sustainability is paramount.

An understanding of flow resistance and conveyance capacity is the basic knowledge required by hydraulic engineers for the design and planning of ecological friendly open channels. Based on the structural measures, the design of flood control system usually will include a variety of conveyance channels called flood control channels. Flood control channels should behave in a stable and predictable way to ensure a known flow capacity will be available for a planned flood event. Since the occurrence of soil erosion cannot be circumvented for a flood flow, vegetated channel linings which are environmentally friendly are temporarily or permanently required to enhance channel stability.

Vegetated flows are usually simulated in the laboratory where the flow rate and water level can be controlled, whereas numerical modeling is useful in tackling problems outside the laboratory conditions or in field studies. According to the response of vegetation stems to water flow, aquatic vegetation can be classified as inflexible (rigid) and flexible. In both cases the vegetation could grow above (emergent) or beneath (submerged) the water level of the river channels. Vegetation which is rigid or flexible, submerged or emergent has been studied by various investigators. For example, the hydraulic roughness induced by emergent flexible vegetation was studied by Noarayanan et al. (2012), the hydrodynamic of flows over submerged flexible vegetation was studied by Jarvela (2002, 2005), Defina and Bixio (2005), Carollo et al. (2005), Wilson (2007), Su et al, (2003) have classified riverine vegetation into three categories as follows:

(i) flexible or inflexible according to the flexural rigidity of the vegetation;

(ii) emergent or submerged according to the height of vegetation and the water depth;

(iii) dense or sparse according to the area density of vegetation.

2.2.1 Flexible and rigid vegetation

The rigidity of vegetation affects the hydraulic resistance of vegetation. Typical examples of flexible vegetation include herbaceous plants, grasses, bushes and reeds, and typical of examples of rigid vegetation include woody or arborescent plants. Both flexible and stiff materials have been used by researchers to simulate these natural elements in the laboratories. Rigid vegetation (mimicked by nails, metal rods and Plexiglas cylinders) is easier to simulate in the laboratory, but less realistic. The physics of flows through rigid vegetation is simpler than that of flexible vegetation as less controlling parameters are involved. The study of flows through rigid vegetation thus is easier and paves the way for the more complicated study of flows through flexible vegetation (Dunn et al, 1996).

For the modeling of flexible vegetation in the laboratory, plastic strips or nylon filaments are commonly used (Kouwen and Li, 1980; Ikeda and Kanazawa, 1996; Velasco et al, 2008; Zeng, 2012). It has been established that both natural and simulated flexible vegetation have three fundamental flow regimes: stiff, bending and prone (Kouwen and Li, 1980; Takaaki and Nezu, 2010). The degree of bending is dependent on the fluid force striking on the stems. The estimation of hydraulic resistance induced by flexible vegetation is difficult due to the followings:

- Vegetation of medium flexibility oscillates in the flow with characterized wavy motion (Carollo, 2002; Stephan and Gutknecht, 2002).
- Coherent vortices exist near the top of plants (Ikeda and Kanazawa, 1996; Zeng, 2012)
- Vegetation of high flexibility can interact with ambient flow (Kouwen and Li, 1980; Takaaki and Nezu, 2010; Li and Xie, 2011);
- The deflection of stem can be very large under high flow (Stephan and Gutknecht, 2002; Li and Xie, 2011)

Velasco, et al, (2003) experimentally observed that increasing flow and relative submergence reduces the resistance to flow for flexible vegetation. They observed that the deflected plant height is directly related to the effective roughness of the vegetation.

2.2.2 Emergent and submerged vegetation

Schematic diagrams showing flows through emergent and submerged vegetation are shown in Figure 2.1. The variables are defined as flow depth (h), stem height (h_v) mean channel velocity (U), u_a and u_v are the average velocity in the clear water layer and vegetation layer respectively. A distinguished feature of flexible submerged vegetation is that the drag coefficient decreases with bending (Carollo et al, 2005). The phenomenon is generally more complicated for submerged condition (Kutija and Hong, 1996; Jarvela, 2005).

Nept and Vivoni, (2000) classified submerged vegetation flow using submergence ratio (h/h_v). Submerged condition is more complicated than the emergent condition basically because of the interaction between the vegetated layer and clear

water layer, and also the effect of coherent motion at the top of the vegetation may affect the drag coefficient in submerged condition (Stone and Shen, 2002).

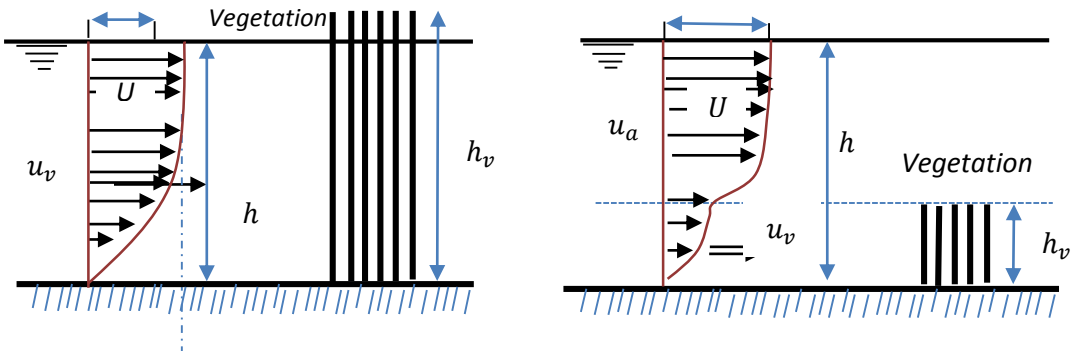

(*a*) Emergent case (*b*) Submerged case

Figure 2.1: Schematic diagrams of flows through emergent and submerged vegetation

2.3 Physical modeling and field measurements

Many experimental studies of vegetated flows have been carried out. In laboratory the flow conditions and the vegetation parameters can be easily controlled. The results can be analyzed with less uncertainty. Field measurements can give realistic vegetated flow behaviors to supplement other studies.

Carollo et al, (2002) experimentally investigated the effect of vegetation density and relative submergence on velocity profiles of flexible vegetation in an open channel flume. They observed that, the relative submergence greatly influenced the location of the zone of logarithmic velocity profile, whereas the vegetation density provides no significant influence. The effect of the vegetation density (*N* = number of stems per unit area) is predominant on the shape of the velocity profile. As *N* increases, the flow

velocity within the vegetation layer decreases and the velocity in the surface layer increases.

Jarvela, (2005) performed experiment on the flow structure above the flexible vegetation in a laboratory flume using Acoustic Doppler Velocimetry (ADV) device for flow measurement. The experiments were carried out on natural vegetation (wheat) of 280 mm and 2.8 mm average length and width respectively. The average vegetation density was found to be 1200 stems/ m^2. The water level ranged from 0.3m-0.71m and the bed-slope ranged from 0.02 - 0.36%. The submergence ratio or relative submergence was in the range of 1.8 - 5.5. The velocity profile measured above the vegetation matched well with the modified log law by Stephan, (2002). It was observed that the maximum Reynolds stress and turbulent intensity lied approximately above the level of deflected canopy height. The author found that the shear velocity (equation 2.1) defined as a function of the deflected height was proper to be used in the conventional hydraulic resistance equations. The predicted flow velocities agreed well with the experimental results.

$$u_* = \sqrt{g(h - h_d)S} \tag{2.1}$$

where g is the gravitational constant (m/s^2); h is the water depth (m); h_d is the mean deflected height of plant (m) and; S is the bedslope (%). More significantly, the friction factor, f was found to be dependent on the deflected height of flexible vegetation, the flow velocity and depth of flow.

Nikora et al, (2008) examined in field the effects of vegetation on hydraulic roughness in five small streams in New Zealand for a duration of six months. The ranges

of stream width, depth and bed-slope covered are (1.7 - 8.2m), (0.12 - 0.65m) and (0.005 - 0.6%) respectively. Water levels were measured at every 20 - 30 minutes interval to monitor the hydraulic conditions and obtain the water surface slopes. Spectra-Physics Laser-plane level and a custom-built hydrostatic measurement device were used for the measurement. The distance between the measurement cross sections was 1-2 channel widths. The velocity measurement was taken using ADV and the flow regimes were subcritical and turbulent all through. About seven species of vegetation were found dominant in the study area ranging from filamentous alga/vascular plants of high or moderate flexibility and floating canopy form characteristics to aquatic bryophyte of low flexibility. The plants were very dense. The areal and volumetric densities were determined in the laboratory and the vegetation porosity estimated. The vegetation porosity was found higher than *0.98*, therefore effect of water displacement by plants on computed hydraulic parameters is negligible. The analysis of the field data was presented in terms of three roughness parameters: Manning's *n*, friction factor, *f* and Chezy's, C_h, which are interrelated as

$$n = \frac{h^{2/3} S^{1/2}}{U} = \frac{h^{1/6}}{C_h} = h^{1/6} \left(\frac{f}{8g}\right)^{1/2} \tag{2.2}$$

Based on the variation of hydraulic and vegetation parameters among sites and seasons, they found that the hydraulic roughness parameters are highly correlated with the relative submergence (h/h_v), with $R^2 > 0.89$. The relationship between the hydraulic roughness and vegetation parameters are shown in equations 2.3, 2.4 and 2.5.

$$n = n_l e^{\left(\alpha_n \frac{h_v w}{h B}\right)} \tag{2.3}$$

$$f = f_l e^{\left(\alpha_f \frac{h_v w}{h\ B}\right)} \quad (2.4)$$

$$C_h = C_l e^{\left(\alpha_C \frac{h_v w}{h\ B}\right)} \quad (2.5)$$

where;

$h_v =$ Patch-averaged height of plant (m)

$w =$ Cross-sectional mean width vegetation patches (m)

$B =$ mean flow width (m)

$\alpha_n, \alpha_C = -0.5\alpha_f$ are coefficients.

The coefficients $n_l, f_l\ and\ C_l$ were found to be approximately the same for many sites and their corresponding values are 0.025, 0.065 and 34.6 respectively.

Additionally, Nikora et al claimed that the effect of plants species and patch patterns are insignificant, whereas vegetation patch height and width are the main parameters for the determination of hydraulic roughness in vegetated streams.

On the flow resistance law, Takaaki and Nezu, (2010) measured the velocity structure and coherent motion in open channel flows with rigid and flexible vegetation using Particle Image Velocimetry (PIV) technique. They examined the characteristics of flow resistance in flexible vegetation by varying the vegetation length. Vegetation motion in flexible canopy was classified as either swaying (that is non-organized waving) or Monami (organized waving). A good correlation between the zero-plane displacement and mean deflected plant height signifies the importance of mean deflected height of vegetation as a parameter for describing the influence of roughness

on the overall flow field. The friction factor, *f* was found to decrease with increase in Reynolds number (*Re*) as observed by Jarvela, (2005) and was smaller for flexible canopy than that for rigid canopy, implying that the flow resistance is reduced due to the deflection of flexible vegetation. For the turbulent structure, the turbulent shear stress was high with sharp peak near the vegetation edge for swaying or rigid canopy, and was smaller with milder peak for Monami canopy. The vertical distribution of the time-averaged vorticity showed that large-scale coherent vortices were generated at the vegetation edge. For Monami canopy, vegetation elements are deflected significantly resulting in weaker and smaller vortices when compared with those of rigid vegetation.

Zhong et al, (2010) investigated the hydraulic resistance of submerged vegetation with varying flow condition in a closed plexiglass-flume of length 3.7m, width 0.2m and depth of 0.1m, which can produce flow velocity of up to 6.75m/s. Natural vegetation was used with sediments at the bed. The flow regime was turbulent in hydraulic rough region. The hydraulic head was measured using two piezometer orifices located at some distance upstream and downstream of the vegetation region. The velocity was increased with time until scouring occurs to obtain critical shear stress on the bed and the corresponding friction velocity. The results showed the relationship between the shear stress above the vegetation and mean velocity is non-linear. D-W friction factor (herein refers to as friction factor) reduces with increase in flow velocity at high Reynolds number. The growth status of the vegetation, flow intensity (i.e., velocity variation) and duration during the scouring process were found to be the main factors affecting the variation of friction factor. The variation of flow velocity and duration during the scouring process indicated that friction factor is not only a function of flow velocity but

highly dependent on the ratio of deflected height of vegetation to the flume hydraulic radius.

2.4 Analytical models

Klopstra et al. (1997) suggested analytical equations for the velocity distribution in vegetated flows. The Boussinesq hypothesis was used to obtain velocity profile within the vegetation layer, whereas Prandtl mixing length approach was used to describe the logarithmic velocity profile for the flow in the surface layer. The average flow velocities within vegetation layer (u_v) and surface layer (u_a) were combined to form the mean average velocity over the entire flow depth given as follows:

$$u = \frac{h_v}{h} u_v + \frac{h - h_v}{h} u_a \tag{2.6}$$

The mean velocity in the vegetation layer is defined as:

$$u_v = \frac{2}{k\sqrt{2\Delta}} \left(\sqrt{C' e^{h_v \sqrt{2\Delta}}} + u_{vo} \right) + \frac{u_{ao}}{h_v \sqrt{2\Delta}} ln \left[\frac{\left(\sqrt{C' e^{h_v \sqrt{2\Delta}}} + u_{vo}^2 - u_{vo} \right) \left(\sqrt{C' + u_{vo}^2} + u_{ao} \right)}{\left(\sqrt{C' e^{h_v \sqrt{2\Delta}}} + u_{vo}^2 + u_{so} \right) \left(\sqrt{C' + u_{vo}^2} - u_{vo} \right)} \right] \tag{2.7}$$

The u_{vo} and u_{ao} are the characteristic constant flow velocity in vegetation layer and surface layer respectively. The variables $\Delta = {f_{rk}}/{2\alpha'}$ and $f_{rk} = C_d N w$, whereas α' is the turbulent length scale given by:

$$\alpha' = 0.0227 {h_v}^{0.7} \tag{2.8}$$

The variable C' is given as:

$$C' = \frac{2gS\frac{(h-h_v)}{\alpha'}}{\sqrt{2\Delta}\left(e^{h_v\sqrt{2\Delta}}\right)+e^{-h_v\sqrt{2\Delta}}} \quad (2.9)$$

The mean velocity in the surface layer is defined as follow:

$$u_a = \frac{u_*}{\kappa(h-h_v)}\left(\left(h-(h_v-Nw)\right)ln\left(\frac{h-(h_v-Nw)}{z_o}\right) - Nw.\,ln\left(\frac{Nw}{z_o}\right) - (h-h_v)\right) \quad (2.10)$$

z_o is the roughness length scale, w is the stem width of vegetation, κ is the Von Karman constant and u_* is the shear velocity for the surface vegetation zone and it is given as:

$$u_* = \sqrt{g\left(h-(h_v-p)\right)S} \quad (2.11)$$

The penetration depth, p is obtained from the following expression

$$p = \frac{1+\sqrt{1+\frac{4{E_o}^2\kappa^2(h-h_v)}{gS}}}{\frac{2{E_o}^2\kappa^2}{gS}} \quad (2.12)$$

Where E_o is defined as:

$$E_o = \frac{\sqrt{2\Delta\left(C'e^{-h_v\sqrt{2\Delta}}+C'e^{h_v\sqrt{2\Delta}}\right)}}{2\sqrt{C'e^{-h_v\sqrt{2\Delta}}+C'e^{h_v\sqrt{2\Delta}}}+u_{vo}} \quad (2.13)$$

The equations were validated using experimental data set on artificial rigid vegetation. The complexity of the equations could be a limiting factor for its practical applicability.

A model that is applied to the entire bulk flow was proposed by Stone and Shen, (2002). The model was built on the assumption that the water weight component in the stream-wise direction is balanced by the flow resistances (that is, bed and vegetation

drag). Usually, the bed drag is much lesser than the vegetation induced drag and could be neglected for high vegetation density. For a unit bed area, the equation is

$$\rho g S\left(1-\frac{\pi w^2 N}{4}\frac{h_v}{h}\right)=\frac{1}{2}C_d\rho w N h_v\frac{{u_v}^2}{\left(1-w\sqrt{N}\right)^2} \quad (2.14)$$

Stone and Shen (2002) considered dense vegetation and took the effect of solidity parameter into consideration. The total volume occupied by vegetation elements was deducted from the entire bulk flow in order to obtain the water volume. The mean velocity is thus related to stem layer velocity using plant - flow depth length scale and is expressed by:

$$u=u_v\sqrt{\frac{h}{h_v}} \quad (2.15)$$

The substitution of equation (2.15) into equation (2.14) yielded the flow resistance equation in terms of mean velocity.

$$u=\sqrt{\frac{2gS}{f_{rk}}}\left(1-w\sqrt{N}\right)\sqrt{\left(\frac{h}{h_v}-\phi\right)\frac{h}{h_v}} \quad (2.16)$$

Where ϕ is the solid volume fraction occupied by the plant stems and it is given by

$$\phi = \frac{\pi N w^2}{4} \quad \text{(for circular elements)} \quad (2.17)$$

The practical limitation of the model of Stone and Shen is that the model is restricted to rigid vegetation and is valid for a limited range of flow velocity.

Gu (2007) derived analytical solutions of velocity distribution in vegetative flow using the two layer approach of velocity profile assuming a constant velocity throughout

the vegetation layer (the same concept as Temple, 1986). Above the vegetation layer, Gu obtained the velocity profile using Prandtl mixing length theory based on the assumption of turbulent flow. The shear stress equation for the vegetated channel was given by:

$$\tau = \rho g S(h - z) \tag{2.18}$$

where h is the total depth of flow, z is the distance from channel and S is the energy slope. The author defined the zero-plane displacement equal to the vegetation height. From the derived velocity equation (2.19), using the principle of flow continuum and conservation of momentum in a control volume, a relationship between the shear stress due to vegetation and Manning's n induced by vegetation was obtained.

$$u = u_v + \frac{\sqrt{gS}}{\kappa}\left[\begin{array}{c} 2\sqrt{h-z} - \sqrt{h-h_v} - \sqrt{h-0.94h_v}.\, ln\left(\frac{\sqrt{h-0.94h_v}+\sqrt{h-z}}{\sqrt{h-0.94h_v}-\sqrt{h-z}}\right) + \\ \sqrt{h-h_v}.\, ln\left(\frac{\sqrt{h-0.94h_v}+\sqrt{h-h_v}}{\sqrt{h-0.94h_v}-\sqrt{h-zh_v}}\right) \end{array}\right] \tag{2.19}$$

By increasing the flow depth, the emerged condition gradually becomes submerged. The analysis showed that the flow resistance is mainly characterized by the flow depth, flow velocity, type and density of vegetation. The results were compared with the experimental flume data through $n \sim h$ relationship for different vegetation densities. A good agreement was obtained between the theoretical and experimental results. It was observed that for $h/h_v > 2$ the Manning's n can assume a uniform value. Nevertheless, the effect of momentum absorption area of vegetation and flexibility were not considered. The method is, however, unsuitable for submerged flexible vegetation.

Huai et al., (2009) carried experimental study on submerged rigid vegetation of of low density ($\phi = 0.002$) using regular array of cylinders of 0.006m diameter under steady uniform flow condition. The flow rate was varied while the bed slope was fixed ($S = 0.004$). The vertical distribution of the mean stream-wise velocity is obtained. To develop a mathematical model for submerged vegetation, the entire flow region of the velocity profile was divided into 4 regions (external region, upper vegetation, transition and viscous region). By applying the theory of Karman similarity, the authors improved the mixing length expression and proposed analytical solution to predict the vertical distribution of stream-wise velocity in the external region.

2.5 Numerical modelling

The formulation of most numerical models for vegetated flows is based on the spatially averaging of the Reynolds Averaged Navier Stokes (RANS) equations. Drag on vegetation stems is spatially averaged to give momentum source terms in the equations.

Lopez and Garcia, (2001) developed two 1-D models by double averaging the conservation equations. Turbulence was modelled by $k-\varepsilon$ or $k-\omega$ two-equation closure. The drag due to vegetation was taken into account in the momentum equation, as well as in the equations for kinetic energy k and dissipation rate ε, or ω. Laboratory experiments were carried out to provide data for the verification of the numerical models. The experiments were conducted in tilting flume of length 19.5m, width 0.91m and depth 0.61m. The set up was under uniform flow condition. Rigid, submerged vegetation were simulated using cylindrical wooden dowels of 6.4mm and 120mm width and height respectively. The vegetation densities were in the range of 30 - 350

stems/m^2, the flow Reynolds number ranged between 57,000 and 240,000. The experimental flows were generally subcritical and fully turbulent. The comparison between the computed and laboratory results showed that the $k-\varepsilon$ model slightly over-predicted the mean velocities above vegetation layer, while the $k-\omega$ model predicted the mean velocities correctly. The Reynolds stresses and turbulent kinetic energy were found to be maxima at the top of vegetation layer. Moreover, for the variation of Manning's roughness coefficient with vegetation density, the Manning's roughness coefficient appears to be constant for the region of low plant density and linearly increases with plant density.

Erduran and Kutija, (2003) developed a quasi-three-dimensional (Q3D) model for submerged canopy. The model coupled the finite volume solution of 2-D shallow water equations with a finite difference solution of NSE for vertical velocity distribution and included additional term that accounted for drag forces in both set of the equations. The vertical shear stresses were computed from two different approaches: the eddy viscosity with correction term and combination of eddy viscosity and mixing length model of turbulence. The flexibility of the vegetation was analyzed based on theory of small deflection analysis. The model replicated well the velocity profile of the experimental data set for rigid vegetation. More so, they varied plant stiffness and measured the deflection at the tip of the vegetation for a given plant height and of varying water depth. It was observed that the deflection of vegetation decrease with increase in stiffness. However, the model could not account for deflection of highly flexible vegetation. The velocity profile was almost divided into three regions. The first region is the near bed region where bed friction dominates (corresponding to Zone 1

and 2, according to the categorization of Velasco et al, (2008) and the pressure-driven layer by Zeng, (2011)). The second region is where the velocity profile is more or less of convex shape (Zone 3 – internal region, according to Velasco et al. (2008), and the mixing layer by Zeng (2011). The third zone is where the profile is concave in the surface region (Zone 4 – external region according to the categorization of Velasco et al. (2008), and the logarithmic layer by Zeng (2011)).

Velasco et al, (2008) studied the flexural properties of vegetation and their effects on flow behaviors. One dimensional model was developed from simplified RANS equations and modified mixing-length model of turbulent closure. In the model the resistance parameters were calibrated and verified using experimental data measured in a flume covered with flexible vegetation. The model coupled the hydrodynamic and mechanical behaviour of flexible vegetation. The former accounted for the velocity profile as well as the turbulent shear stress distribution while the latter gave the canopy deflection subjected to water flow. The transversal deformation profile y(z) is given by equation (2.20).

$$\frac{\partial^2 y}{\partial z^2} = -\frac{M}{EI} \qquad (2.20)$$

where y is the transverse deformation, M is the moment (*Nm*), z is the adopted coordinate for the vertical, longitudinal direction of the stem, E and I are the stiffness modulus (N/m^2) and inertial moment (m^4) respectively.

Based on force consideration, the flow through and above vegetation is separated into the following four different zones (as shown in Figure 2.2):

Zone 1 - Viscous region, where viscous forces are predominant and velocity gradient are high.

Zone 2 – Shear-less region, where the turbulent shear stress is negligible, also called penetration depth region, *p*.

Zone 3 - Internal region, below $z = h_v$ where the gravity shear stress balanced both the vegetative and turbulent stresses.

Zone 4 - External region ($h_v < z \leq h$) above the canopy, where drag force is zero.

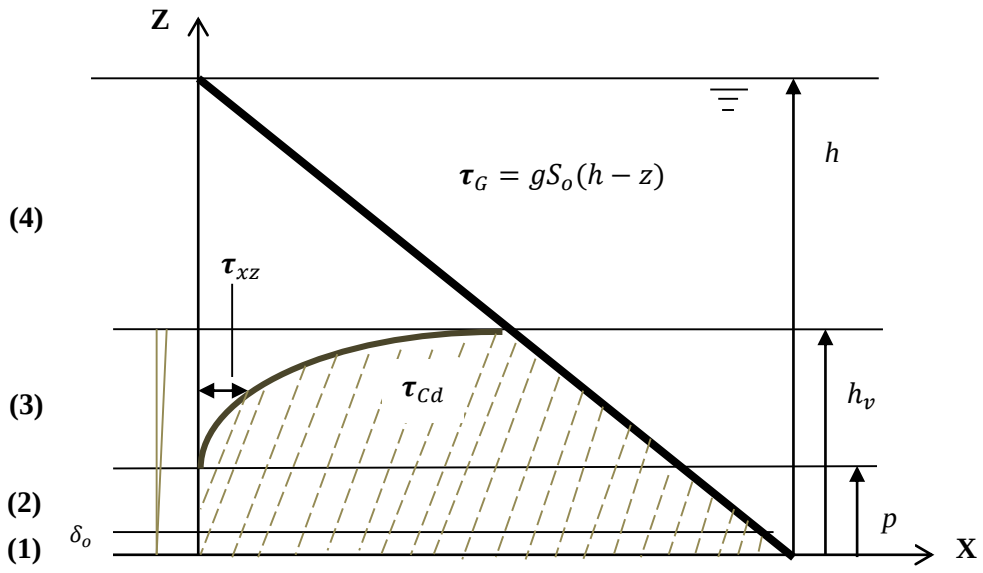

Figure 2.2: Shear balance scheme for high vegetative momentum absorption capability (Adapted from Velasco et al, 2008).

The model required several tunable parameters, including the drag coefficient. It was tested for submerged flexible vegetation by varying the submergence ratio from

1 to 2.7 while maintaining a constant bottom slope. The computed results generally are in agreement with the experimental data in terms of velocity profile and turbulent shear stress.

Kubrak et al, (2008) developed a 1-D steady state model for predicting the vertical profiles of horizontal flow through and above flexible vegetation in an open channel. The model considered channel bottom roughness and drag exerted by the submerged flexible stems. The model is based on the theory of analysis of forces acting on the volumetric element surrounding a given number of flexible stems of vegetation under the assumption of uniform and steady flow conditions. The analysis was based on two layers approach: vegetation and surface layers, unlike the four layer approach adopted by (Velasco et al, 2008). The drag force was defined as a function of Reynolds number and the shear stress terms defined using Prandtl mixing length concept. The mixing length is expressed as ($l = \kappa(z)$) where z is any distance from the channel bed and $\kappa = 0.41$ (von Karman constant). The differential equations obtained for the vegetation layer and surface layer were solved using explicit finite difference scheme with the associated boundary conditions in the computational domain. The bed shear velocity was related to the water velocity at the roughness height of the bed and uniform velocity above the vegetation zone. The model was tested against the set up flume experiment, which consists of varying vegetation density and bed slopes. The result showed a good agreement. From the results, it was deduced that the flow condition is dependent on bed slope, bed roughness, flow depth, mixing length, vegetation density, width of plant and stiffness.

A summary list of numerous work on vegetated flow including the key vegetative parameters and related findings is presented in Table 2.1.

Table 2.1: Vegetated flows: key parameters and findings

Investigator	Key parameter(s)	Inference
Carollo, et al., 2002	h_v and N	Relative roughness (h_v/h) influences the location of zone of logarithmic velocity profile, whereas N determines the shape of the velocity profile.
Jarvela, 2005	h_v (specifically h_d for highly flexible vegetation)	The Reynolds stress, $-(\rho u'w')_{max}$ correspond to h_d. The h_d/h can significantly affect hydraulic roughness
Nikora et al., 2008	The h_v relative to flow depth as well as plant width, w.	Vegetation patch heigh and width are the
Takaaki and Nezu, 2010	Z_o and h_d	Z_o is strongly correlated with h_d which indicates the importance of h_d as a vegetative parameter for describing hydraulic roughness
Zhong et al., 2010	h_d	The mean flow velocity and friction factor are affected by h_d/h.
Gu,2007	h_v	For $h/h_v > 2$; Manning's roughness coefficient (n) can be assumed to take a uniform value.
Lopez and Garcia, 2001	N	The n value is approximately constant at low value of N (<< 100) and increases linearly with N.

2.6 Hydraulic roughness determination

Accurate determination of the hydraulic roughness of a vegetated channel is of engineering significance. Numerous efforts have been made to develop resistance law

for vegetated channel flows. Fathi-Maghadam and Kouwen, (1997) developed a mathematical model that establish relationship between roughness conditions and flow conditions to enhance estimation of roughness on floodplain. They derived a resistance equation by applying dimensional analysis to the vegetation and flow parameters. In their study, the derived equation (2.21) was substantiated with flume experiment by measuring the parameters *U, h, A* and *EI*. Equation (2.21) is a functional relationship between a resistance coefficient equivalent to the nearly submerged condition and flow induced deformation of vegetation. The drag forces on selected plants (cedar and pine) were measured using a load cell, the velocity was measured upstream of the model plants using miniature propeller current meter, *A* was measured by photographic means and *EI* was measured by subjecting trees to damping, the natural frequency of the vibration is defined from the rate exchanges of kinetic and potential energy when plant stem vibrates. The kinetic energy is proportional to the square of the velocity of element mass, while the potential energy is proportional to the square of the elastic strains. The functional relationship for the estimation of the resistance to flow in emergent flexible vegetation is as follows

$$C_d \left(\frac{A}{\forall}\right) h_v = \left(\frac{\rho U^2 h^4}{EI}\right) \qquad (2.21)$$

The dimensionless parameter on the left hand side represents the friction factor divided by the relative submergence.

where;

A = deflection of plant foliage area, i.e., Momentum absorbing area;

$\forall = \lambda h_v$, λ = bed area covered by vegetation.

The variation of friction factor with velocity for cases of different flow depth confirmed that the drag force increased linearly with the velocity. The drag coefficient and hence hydraulic roughness decreased with velocity due to deflection of plant stem and reduction of foliage area.

Stone and Shen, (2002) performed laboratory study on the hydraulic resistance characteristics of open channel flow with both emergent rigid and submerged rigid vegetation. Based on the momentum balance, they developed an analytical flow resistance equation and conveyance formula. The equation was validated using experimental results. The authors considered the solidity (i.e., deduction of fraction of control volume occupied by vegetation from the weight component of water) and bed friction contribution in their analysis. They found that expressing the drag force using the maximum velocity in the vegetation layer rendered the bulk drag coefficient close to that of a single cylindrical stem. They proposed a resistance equation which is a function of stem size, vegetation density and flow depth.

Carollo et al, (2005) observed that the application of the well-known Kouwen's method overestimated the flow resistance in an open channel with flexible vegetation. The coefficients in the logarithmic equation of flow resistance were subsequently recalibrated against their experimental data. It was analyzed dimensionally (using π-theorem and the condition of incomplete self-similarity), they concluded that at high vegetation density, the shear Reynolds number has to be included along with submergence ratio in the flow resistance equation.

Wilson, (2007) experimentally investigated the variation of hydraulic roughness parameters with flow depth and observed that the Manning's roughness coefficient increases with decreasing flow depth reaching an asymptotic constant at high submergence depth ratio. The value of the constant is dependent on the height of vegetation and other vegetation parameters. Uncertainty arose due to the difficulty in the determination of flexibility of individual plants which were of high variability. Large variations in modulus of elasticity, size and shape can occur among samples. The author queried the correlation of deflected height of plant as a function of flexural rigidity because densely packed plants will possess different bending properties when compared with an individual plant.

Baptist et al. (2007) proposed three equations describing the submerged vegetation induced resistance from different angles. The equations are in the form of Chezy equation with the hydraulic roughness described by the Chezy coefficient. The first equation was based on the analytical approach which assumes logarithmic (log-law) variation of velocity in the non-vegetation layer and a well-defined physics-based velocity distribution in the vegetation layer. The second equation was based on a two-layer approach. In the vegetation layer the velocity is assumed constant and determined from the solution of the momentum equation. In the surface layer the velocity profile is determined by the log-law. For comparative study later, these equations are transformed into the Manning's equation form using the relationship described in equation (2.2). The analytical expressions of the resulting Manning roughness coefficient are shown in equation (2.22) and equation (2.23).

$$n = \frac{h^{\frac{1}{6}}}{\sqrt{\left(\frac{2g}{f_v}+n_b\right)+\frac{(h-h_v)^{3/2}\frac{\sqrt{g}}{\kappa}ln\left(\frac{h-h_v}{ez_o}\right)}{h^{3/2}}}} \tag{2.22}$$

$$n = h^{-4/3}\left\{\begin{array}{l} L\left[2\left(u_v-\sqrt{a'+u_o^2}\right)+u_o ln\left(\frac{(u_v-u_o)\left(\sqrt{a'+u_o^2}+u_o\right)}{(u_v+u_o)\left(\sqrt{a'+u_o^2}-u_o\right)}\right)\right] \\ +\frac{\sqrt{g(h-h_v)}}{\kappa(h-h_v)}\left[(h-d)ln\left(\frac{h-d}{z_0}\right)\right]-(h_v-d)ln\left(\frac{h_v-d}{z_0}\right)-(h-h_v)\end{array}\right\} \tag{2.23}$$

$$a' = \frac{2Lg(h-h_v)}{c_p\ell\exp(k/L)} \tag{2.24}$$

where;

z_o = roughness length

L = length scale

d = zero-plane displacement.

ℓ = mixing length

c_p = turbulence intensity

u_v and u_o are the corresponding velocities at depth $(z) = h_v$ and 0 respectively

The third equation is based on the analysis of the synthetic data generated by a 1-D k-ε model using the genetic programming approach. The model describes vegetation as rigid cylinders and accounts for horizontal flow condition through simplification of the full 3-D Navier-Stokes equations. The hydraulic roughness equation obtained from this

approach was found to produce results of good agreement with experimental data. The resulting expression of Manning roughness coefficient is given by

$$n = \frac{h^{\frac{1}{6}}}{\sqrt{\left(\frac{2g}{f_v}+n_b\right)+\frac{\sqrt{g}}{\kappa}ln\left(\frac{h}{h_v}\right)}} \tag{2.25}$$

Where $f_v = f_{rk}$. h_v and n_b is the bed roughness which is negligible for smooth flume beds.

Recently, Yang and Choi, (2010) applied the concept of two-layer approach to vegetation-flow model also. The velocities in the vegetation layer and surface layer were separately considered. Using the continuity equation, the average velocity over the whole depth was computed and the equation was substituted into the Manning's formula. A semi-analytical vegetative roughness equation is obtained as follows

$$n = h^{2/3}\left[\sqrt{\frac{2gh}{\lambda C_d h_v}} + \frac{C_u\sqrt{gh_s}}{\kappa}\ln\left(\frac{h}{h_v}\right) - \frac{h_s}{h}\frac{\sqrt{gh_s}}{\kappa}\right]^{-1} \tag{2.26}$$

Where flow depth, $h = h_v + h_s$, and C_u is a parameter depending on vegetation density λ (Yang and Choi, 2009; Yang and Choi, 2010).

More recently, Cheng, (2011) proposed a flow resistance formula still using the two-layer averaging velocity approach. The resulting averaged velocity vegetation layer and surface layer is substituted into the Chezy's formula. Using the relationship between the Chezy coefficient (C_h) and Manning's coefficient (n), the model is given by

$$n = h^{1/6}\left[\sqrt{\frac{\pi g(1-\phi)^3 w}{2\phi C_d h_v}}\ (\frac{h_v}{h})^{1.5} + 4.54\sqrt{g}\left(\frac{h_s\,(1-\phi)}{\phi w}\right)^{0.0625}\left(\frac{h_s}{h}\right)^{1.5}\right]^{-1} \tag{2.27}$$

2.6.1 Drag in simulated vegetation

In the hydraulic roughness equations proposed above, all the flow and vegetation parameters can be measured and quantified relatively easily, except the drag coefficient. The estimation of vegetation induced-drag is therefore critical in the modeling of vegetated flows (Dunn et al, 1996; Nepf, 1999, Tanino and Nepf, 2008; Li and Xie, 2011). The calculation of drag force is a usual form of problems in engineering fluid mechanics often solved by experimentation (Fathi-Maghadam and Kouwen, 1997). The dynamic of drag force on a flexible plant is complicated as the force changes when the plants bend and streamline with the flow (Wilson et al, 2008). Most laboratory models for vegetated flow simulate vegetation in laboratory flume with cylindrical objects based on the assumption that the flow Reynolds number is sufficiently high and only form drag dominates. The form drag force exerted by a single infinite cylinder stem in a uniform flow velocity, u_u is parameterized through drag coefficient as follows:

$$F_d = \frac{1}{2}\rho A C_d u_u^2 \tag{2.28}$$

where;

F_d = drag force ; ρ = fluid density

A = obstructed area of the cylindrical object and;

C_d = drag coefficient

The pressure on the cylinder can be integrated over the entire surface of the cylinder to give the drag force. More conveniently, the drag force is determined using a

momentum balance analysis. The water velocity is measured and the only unknown parameter C_d is solved for (Dunn et al, 1996; Huthoff and Augustijn, 2006).

It has been established by previous researchers that C_d on an isolated cylinder is dependent on the Reynolds number *Re(w)*. In Figure 2.3, the experimental data and empirical curves for the variation of C_d and *Re(w)* are shown (White, 1991, pp 181; Cengel and Cindala, 2010, pp 607). White proposed the following simple curve-fit equation:

$$C_d = 1 + 10Re_w^{-2/3} \tag{2.29}$$

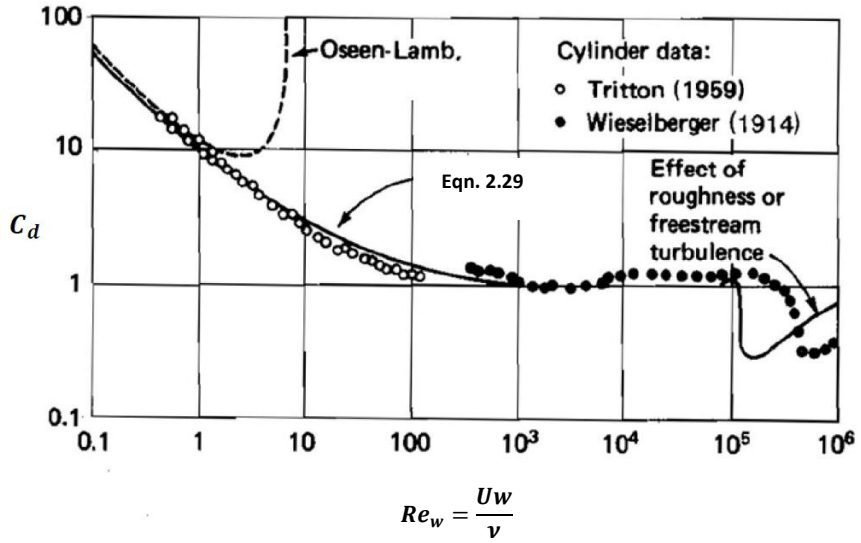

Figure 2.3: *Re* – C_d curve for an isolated cylinder (White, 1991)

From the *Re* – C_d curve, in the moderate range of $10^3 \leq Re(w) \leq 10^5$, C_d is relatively constant (approximately 1.2). Experiments showed that at low turbulence intensities the value of C_d will fall below the standard curve, whereas at high turbulence intensities (> 10%), the value of C_d will be above the curve. Further increase in turbulence leads to increase in C_d with less dependency on *Re*.

Many studies showed that as the number of vegetation element increases the estimation of drag becomes more problematic. The flow interference between the vegetation elements (i.e. cylinder strips) varies and dependent on the spacing, pattern as well as flow characteristics. Drag in vegetated channels is complicated by the non-uniformity of velocity profiles, turbulence and free surface effects (Dunn et al, 1991; Nikora et al, 2008; Miler et al, 2012). The extent of this complication poses a limitation on the use of equation (2.28) for vegetated open channels. Instead a bulk or mean drag coefficient is proposed as follows:

$$F_d = \frac{1}{2}\rho A C_d u^2 \tag{2.30}$$

where C_d is the characterized (bulk) drag coefficient based on the average drag force on the vegetation stem and therefore assumed to be constant with the vegetation height. Efforts have been made by researchers to measure C_d in the laboratory and in the field.

Wilson et al, (2008) experimentally studied the contribution of plant's foliage to the total plant's hydrodynamic drag using vegetation with different biomechanical properties and physical forms (foliage type and stem form). The considered species are pine and ivy stipes. The drag force (F_d) on a single plant was measured by two strain gauges. The foliage impact were examined for each specimen in terms Manning's roughness and drag force ratio. They measured the F_d (for plants with and without foliage) as a ratio of difference between the bending moments measured by strain gauges and the distance between the gauges. The flow velocity was measured by area mean velocity method. Wilson et al. defined a parameter C_dA_p, the product of wetted

frontal projected vegetation area and drag coefficient, and expressed it as a function of the measured F_d and velocity ($C_d A_p = 2F_d/\rho u^2$). By evaluating the F_d ratio (= F_d with foliage / F_d without foliage) the contribution of the foliage to total drag is assessed. Pine plant showed a streamline ability which is a distinct feature of flexible vegetation, as the F_d ratio decreased with increasing velocity, whereas for Ivy the F_d ratio appeared relatively constant with increasing velocity indicating the approach of point of maximum streamlining. The ratio of Manning's coefficient, *n* ratio (*n* with foliage / *n* without foliage) was evaluated. The *n* ratio – velocity plot indicated that the increase in velocity led to the decrease in *n* ratio. The ratio is dependent on the foliage area to the total plant projected area contribution; flexibility and streamline ability of plant under a given range of velocity; and Reynolds number. They showed that for a plant with large effective frontal foliage area, the flexibility of plant and its streamline ability will reduce the total drag.

Li and Xie, (2011) proposed an empirical equation to account for flexibility of plant under uniform lateral distributed load for different velocity profiles using the theory of large deflection. By applying dimensional analysis to a plant stem subjected to uniform lateral distributed water load (*q*), they arrived at the following empirical equation:

$$\frac{h_d}{h_v} = \psi \frac{q {h_v}^3}{EI} \tag{2.31}$$

where h_v and h_d are the actual height and deflected height of the plant respectively. The empirical parameter ψ can be obtained by considering different values of distributed loads. The equation indicated that highly flexible plants are largely deflected under flow

and hence, the drag force is reduced considerably. They extended their study to the effect of foliage on drag coefficient, it is known that when plants experienced water flow, deflection of stems occurs and leaves are streamlined along the flow (Kouwen and Li 1980; Wilson, 2007; Wilson et al, 2008; Tanini and Nepf, 2008; Takaaki and Nezu, 2010; Li and Xie; 2011; Wu and Yang, 2011 and Miler et al, 2012). The phenomenon is described using fluid flow-inclined thin plate analogy. Li and Xie related the expression to the product of C_dA_p normalized with $C_{do}A_{po}$ corresponding to the non-deflected condition. They were able to derive an empirical equation based on the assumption that the average width of foliage is constant with the flow velocity. The proposed empirical equation fitted against experimental data sets (including data of Wilson, et al. 2008) showed a reasonable agreement and can be used to estimate C_d for flexible vegetation. Table 2.2 showed the summary of the estimates of $\overline{C_d}$ used in various vegetation models. Most of researcher explicitly recognized the epistemic uncertainty (due to lack of knowledge) of the precise value of $\overline{C_d}$ as well as its variance with vegetation parameters and flow characteristics.

Table 2.2: Summary of bulk drag coefficient measurements in turbulent shear flows in water

Researcher	Material classification	Material shape	Computational method	Nature of study	C_d value
Yang and Choi, (2010)	Flexible and Rigid	Polythene films and cylindrical wooden dowels	Empirical model	Laboratory	1.11 – 1.15
Stone and Shen, (2002)	Rigid	Cylinders	Empirical model	Laboratory	0.96 - 1.11
Lopez and Garcia, (2001)	Rigid stems	Cylinders	k – ε model and k – ω model	Computational	1.13
Dunn et al, (1996)	Flexible and rigid	Plastic straws and cylindrical wooden dowels	Empirical model	Laboratory	1.13± 0.15
Saowapon and Kouwen, (1989)	Flexible plastic	Cylinders	Empirical model	Laboratory	Varies from 0 to 2.0

2.6.2 Effect of wake interference on stem drag coefficient

To investigate wake interference effects in an array of cylinders, Tanino and Nepf, (2008) carried out laboratory measurement of the depth-averaged drag coefficient in random arrays of rigid emergent cylinders. The solid volume fraction (ϕ) varied between 0.091 and 0.35 and the stem Reynolds numbers varied from 25 – 685. Their analysis showed that the drag coefficient can be expressed in the following form:

$$C_d = 2\left(\frac{\varphi_0}{Re} + \varphi_1\right) \tag{2.32}$$

where φ_o is a function of ϕ, and φ_1 is a constant.

The first term on the right hand side of equation (2.32) represents the drag force per unit mass due to viscous shear stress. The last term of the above equation represents the inertial contribution due to pressure loss in the cylinder wake. The value of C_d were

obtained using the measured mean velocity and the pressure gradient obtained with the use of mounted pressure gauges upstream and downstream of the flow. They recognized large uncertainties in the measured C_d at small ϕ, small cylinder height and low Re, hence, discarding all measurement with error greater than 25% of the estimated C_d.

The drag coefficient decrease monotonically with increasing Re (w) and increased with (ϕ). They also demonstrated that C_d of an isolated cylinder is lesser than that in a random array for the Re (w) conditions studied for $\phi \leq 0.35$. The prediction of the drag parameter and C_d were obtained by interpolation of $\boldsymbol{\varphi_o}$ and $\boldsymbol{\varphi_1}$. The predictions are, however, valid for 30 < Re (w) < 700. The $\boldsymbol{\varphi_o}$ is systematically independent on ϕ; for ϕ = 0.091, $\boldsymbol{\varphi_o}$ increase from 25 ± 12 and remain constant at 83.4 at ϕ = 0.15 – 0.35. $\boldsymbol{\varphi_1}$ is linearly related with ϕ, and it is given by

$$\varphi_1 = (0.46 \pm 0.11) + (3.8 \pm 0.5)\phi \tag{2.33}$$

The Manning's coefficient is related to the depth-averaged drag coefficient, solid volume fraction and stem diameter has given by

$$n = \frac{R^{\frac{2}{3}}}{(1-\phi)^{\frac{3}{2}}} \sqrt{\frac{C_d}{2g}}\lambda \tag{2.34}$$

where R = hydraulic radius.

Nepf (1999) developed a wake interference model to account for the reduction of drag coefficient of a cylinder in an array. The model predicts that the bulk drag coefficient decreases with the increase in solid volume fraction ϕ. Stone and Shen, (2002), however, found that the bulk drag coefficient increases with the solid volume fraction for an array of cylinders with staggered arrangement. The use of the velocity

between the stems as the velocity scale reduces the bulk drag coefficient which becomes closer to that of an isolated cylinder. Similarly, Kothyari, et al., (2009) measured directly the drag on a single cylinder within a staggered array of cylinders and found that the stem drag coefficient increases logarithmically with ϕ.

Recently, Cheng and Nguyen, (2011) developed a formula for estimating C_d for cylindrical stem in array of cylinders and based the analysis on two categories of experimental dataset (i.e., randomly distributed and staggered pattern). The authors redefined hydraulic radius by taking into consideration the size, stem configuration and channel characteristics and provide a friction factor for open channel with vegetation. The Reynolds number, shear velocity and vegetation friction factor were defined in using vegetated-related hydraulic radius r_v as characteristic length. The usual bulk mean velocity in the vegetated induced drag formula was replaced by averaged- pore velocity.

After lengthy derivation, a semi-analytical equation for the drag coefficient was obtained. The analytical based approach was affirmed using laboratory experiment consisting 143 runs with varying vegetation density and stem diameters. The results indicated that the use of vegetated-related hydraulic radius as characteristic length for defining Reynolds number for emergent vegetated open channel flow rather than stem diameter yields better results. Furthermore, data from previous studies assert the proposed characteristic length. The result demonstrated that for the same Reynolds number, there is no significant difference in the C_d values based on the pattern of arrangement of cylinders and more significantly, the drag coefficient decrease monotonically as Reynolds number increases (as observed by Tanino and Nepf, 2008 using stem diameter as characteristic length for Re). Based on the best-fit function of

experimental dataset, a formula for estimating drag coefficient in array of cylinders for emergent rigid vegetation is proposed as

$$C_d = \frac{130}{r_{v^*}{}^{0.85}} + 0.8\left[1 - exp\left(-\frac{r_{v^*}}{400}\right)\right] \quad (2.35)$$

where $r_{v^*} = 24 - 5000$. Details of the model can be found in Cheng and Nguyen (2011).

2.7 Uncertainties: classification and challenges

It is a general belief that we not know "reality" and "uncertainty" always exists (Van der Merwe, 2004). The often synonymous words to "uncertainty" as described by (Van Gelder, 2000; Haldar and Sankaran 2000, and Hayes, 2011) are randomness, variability, irregularity, unpredictability, un-sureness, ambiguity, stochasticity and so forth. Therefore, from the word variability leading to randomness, we cannot avoid uncertainties in the design and planning of Civil engineering works. The recognition of the need to incorporate the concepts of uncertainty in Civil Engineering receives more and more attention. The knowledge of statistical modeling has provided engineers with a tool for making decisions under uncertain conditions (Ang and Tan, 1975; Hayes, 2011). In this section, the trend in the uncertainty analysis in numerical modeling was studied and the available methods of propagating uncertainty with their merits and limitations summarized.

2.8 Definition of uncertainty

At all times, in many circumstances, we all find ourselves in a state of uncertainty. Haldar and Sankaran, (2000) define uncertainty as the occurrence of multiple outcomes without any pattern. It is the degree of ignorance or state of incomplete knowledge (Beven, 2009). Raadgever et al, (2011) describes uncertainty as a situation in which there is no unique and complete knowledge of the system to be managed. Van Asselt, (2000) and Walker et al, (2003) defines "uncertainty as any deviation from the unattainable state of completely deterministic knowledge of relevant system". In addition, from a statistical point of view, Li et al, (2011) defines uncertainty as the dispersion of a measured or estimated value of measurement around its true value. From this perspective, we observe that measurements are error bounded implying no exactness in planning and design as well as decision making. It can be deduced that uncertainty exists in as much as the probability of an event occurring is not zero or one (Van Gelder, 2000 and Eric, 2002). As a result of this, the uncertainty needs to be analyzed. Analysis of uncertainties can be simplified by classifying uncertainties as a basis for the method of analysis (Van de Klis, 2003 and Hayes, 2011).

2.9 Classification and types of uncertainties

Van Asselt, (2000, p 75-118) and Van Asselt and Rotmans (2002) classified uncertainties into two: sources and types. The former is due to variability (or randomness) and lack of knowledge (or incompleteness of information) while the latter describes how uncertainty manifest itself in modeling. In a more explicit form, Walker et al, (2003) based their classification on three dimensions of uncertainty: location, level

and nature. The word "sources" have been used by various authors to refer to "causes" of uncertainty (Sigel et al, 2010; Raadgever et al, 2011 and Hayes, 2011). A diverse of variability and degree of lack of knowledge is shown in Figure (2.4).

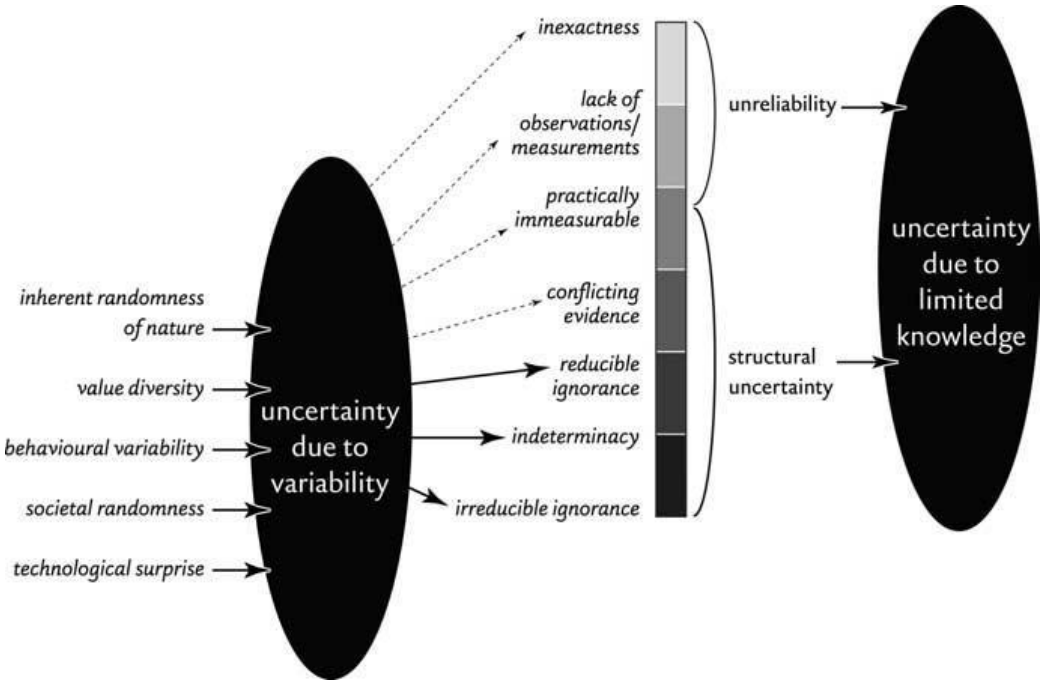

Figure 2.4: Typology of sources of uncertainty (Van Asselt and Rotmans, 2002)

The types of uncertainty based on the classification by Van Asselt and Rotmans (2002) are technical, methodological and epistemological uncertainties. The first one is simply due to unreliability based on the quality of data that is used to describe the system. It could result from the aggregation (of temporal and spatial scale) through simplification owing to unavailable data and approximation. For example, uncertainty in model quantities (such as parameters, input and initial states). The second one is

associated with lack of knowledge or uncertainty about model form. For example, if uncertainty is inherent, what analytic tools and which methods are appropriate? How do we differentiate what we know and what is uncertain? These questions require knowledge about model structure, functional relationship and choice of algorithms. The last one is based on the concept of the phenomenon. It is simply the uncertainty about the completeness of the model or its adequacy. It arises from variability and structural uncertainty. The key question regarding this type of uncertainty is whether the description, theory or model relates to the real, variable world.

2.9.1 Comparison of classification of uncertainties by different researchers

According to Walker, et al, (2003) uncertainty is not simply the absence of knowledge. It could be inexactness, unreliability and border with ignorance. Based on this, they classified uncertainty on three dimensional scales in relation to model-based decision support system, they are: location, nature and level of uncertainty. The authors believe that understanding of the various dimensions of uncertainty will assist modelers to identify, give clear distinction, and priority to critical uncertainties.

The various levels of uncertainty are distinguished as: determinism, statistical uncertainty, recognized uncertainty and total uncertainty (Walker, et al, 2003). The progressive transition from determinism to total ignorance is shown in Figure 2.5.

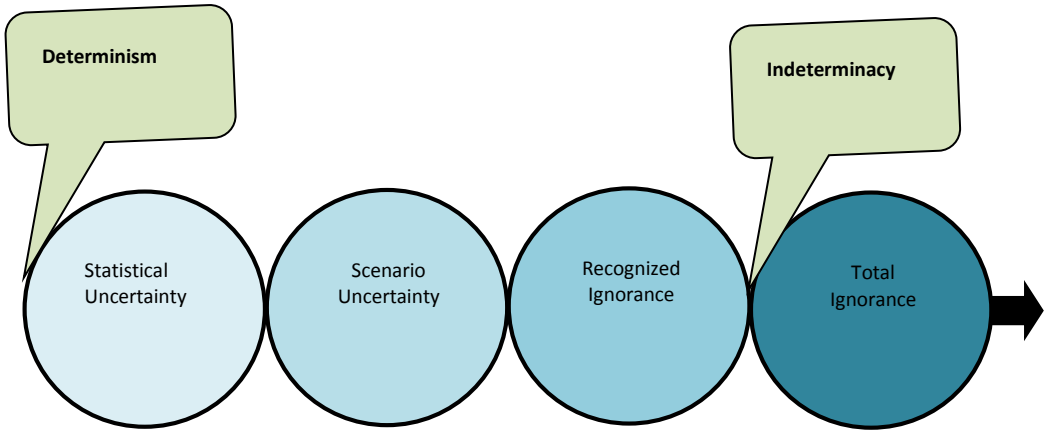

Figure 2.5: The progressive transition between determinism and total ignorance (Adapted from Walker, et al, 2003).

A careful observation shows that a good comparison can be drawn from the classification of uncertainties reported by the researchers. Even though, a single classification that captures different categories of uncertainties may not exist (Hayes, 2011). A comparison has been made based on the methods of Van Asselt (2000), Van Asselt, and Rotmans (2002) and Walker, et al, (2003) and in a more general form is presented in Figure (2.6) which shows the relationship between the different categorization given to the various classes of uncertainty irrespective of their nomenclature.

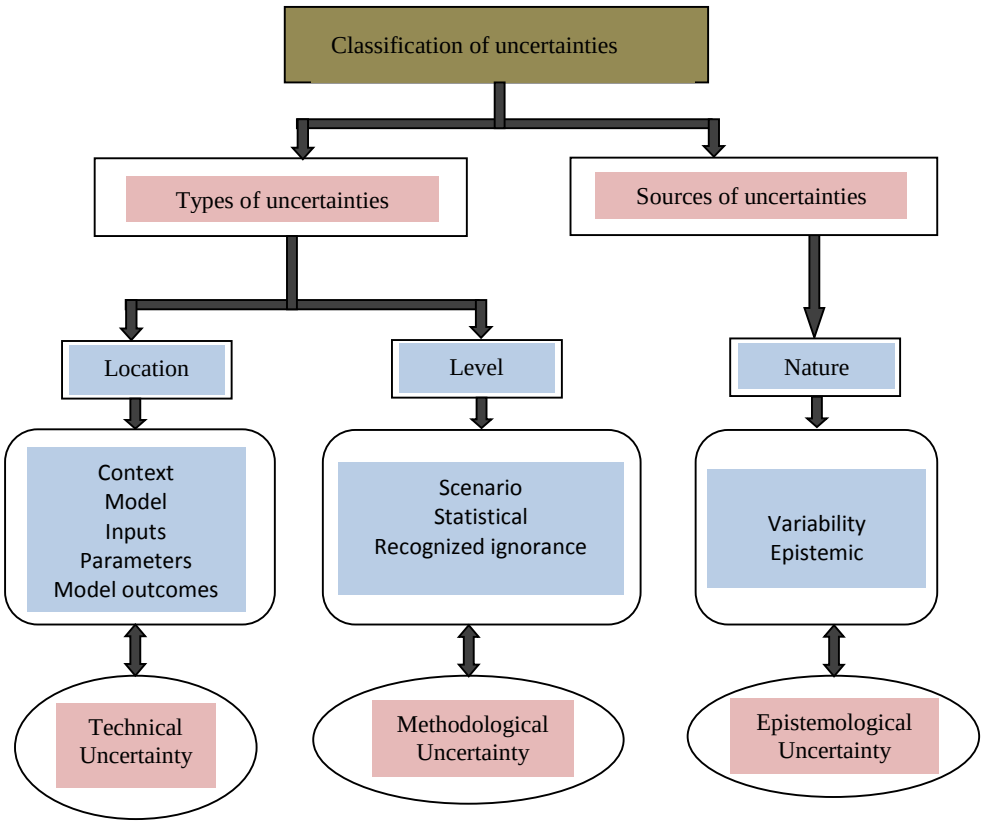

Figure 2.6: Generalized form of classification based on comparison of existing methods of classifying uncertainties found in the literature.

2.9.2 Challenges in the classification of uncertainties

Regal et al, (2002; 2004) recognizes two sources of uncertainty: Linguistic and epistemic uncertainty. Linguistic uncertainty arises from the vagaries of language, it is very important for the assessment and communication of risk in the qualitative uncertainty analysis. It is not related to this study. Its comprehensive review can be found from (Regal, et al, 2002; Hayes, 2011). Most of the authors distinguished variability from epistemic uncertainty (Walker, et al, 2003; Ascough et al, 2009; Burgan

et al, 2010 and Hayes, 2011). Uncertainty arising from variability is as a result of natural and/or artificial induced variation in observation in time and space. It is often distinguished from epistemic uncertainty because it cannot be eliminated or reduced with further studies and additional information. It is therefore, an unavoidable reality of the real-world.

Xu et al. (2010) classified uncertainty into three categories: data uncertainty, model uncertainty and other uncertainties (which include quantifiable uncertainties such as system domain grid scale and systematic error). This classification is summarily and in principle the same with Van Asselt, (2000) and Van Asselt and Rotmans (2002) and was consistently adopted by Van der Klis (2003) when accounting for uncertainty in river bed morphology.

Hayes, (2011) classified uncertainty into four categories namely: variability uncertainty, epistemic uncertainty, linguistic uncertainty and decision uncertainty. From the above study, it is difficult to have a clear distinction between these categories because the existing classifications are different between disciplines driven by different domains as well as the objectives and the available data for analysis. Therefore, no single classification can capture the categorization of sources of uncertainty found in the literature. Regan et al, (2002) and Hayes, (2011) categorized the following: model uncertainty, completeness (i.e. the uncertainty when enumerating all possible outcomes), scenario uncertainty, subjective judgments (when interpretation of data is insufficient to make a reliable judgment), systematic uncertainty and sampling uncertainty (e.g. density function of a variable) under epistemic uncertainty because they occur due to insufficient or lack of data, understanding and knowledge about the

phenomenon. Subjective judgement is particularly important in qualitative uncertainty analysis since it relies exclusively on the form of information. Subjective judgement contributes to uncertainties both in the parameter and model structure uncertainty.

Variability is further categorized into natural variation and inherent randomness (Van Asselt, 2000; Van Asselt and Rotmans 2002; Aven, 2010; Hayes, 2011; Abdel-Khalik, et al, 2013). The former is the variability that occurs naturally in the *location* (that is within the context, model, inputs and parameters) in time and space. For example, the time variation in the growth of plant can have an effect on the flexural rigidity and plant height, the spatial variation can be the change in the plant diameter. The inherent randomness explains the repeated processes with no detectable deterministic trait because there is no substantial information to completely describe the dynamics of the process, for example, the ecosystem and weather system. For these reasons, variability has been treated separately from epistemic uncertainty by many authors because of its distinguished characteristic i.e., it cannot be reduced. Generally, the data used to represent variability in an uncertainty analysis are often a sub-set of the population of interest. Therefore, statistical techniques are required to test for the adequacy within a data set (Aven, 2010; Hayes, 2011 and Abdel-Khalik, et al, 2013).

2.10 Uncertainty techniques

In section 2.9, the analysis of the causes and types of uncertainty found in the literature were explored. Most importantly, the authors' argument about classification were compared and one can observe with conclusion that authors were saying almost

the same thing in different ways. This is shown in (Figure 2.6), with this understanding of uncertainty, one can easily demarcate between less uncertain and high uncertain issues, reducible and irreducible uncertainty. The issue now is how to deal with high uncertainty. On another hand, how do we treat uncertainties? Is there a general technique for addressing this issue or the dimension of uncertainty dictates the technique for analyzing uncertainty?

Morgan and Henrion, (1990) outlined the different ways to represent uncertainty about empirical quantity (that is, the measured properties of the real-world systems) by a probability distribution. Firstly, in the event of having empirical data directly relevant to the quantity, statistical techniques can be used to select appropriate distribution and estimate its parameters. Secondly, in the presence of little or no knowledge about the quantity before seeing the observation, standard classical statistical methods can be used. Thirdly, in case of little knowledge and reasoning about the quantity, the prior knowledge can be added to the observed evidence to obtain posterior distribution using Bayesian methods. Lastly, where no direct relevant observation of the quantity is available, analyst may directly wish to express opinion by subjective probability distribution. For empirical parameter or chance variable, mode of treatment is probabilistic and parametric analysis.

Ferson and Ginzburg, (1996) identified two causes of uncertainty: variability and ignorance. The authors argued why the two sources of uncertainty requires different methods for propagation when information is limited for risk assessment. They claimed that distinguishing between the two sources of uncertainty is not enough, but they should be propagated with different methods. Interval analysis was suggested for the

propagation of ignorance through mathematical expression, but not the classical form of probability theory. In addition, they claimed that the method of interval analysis is generally enough to account for uncertainties from both sources. However, the method overestimates the dispersion in the case of variability if the correlation between the input parameters is specified. To cater for the variability with known dependencies, probability theory should suffice for propagating random variability. Since both uncertainties are usually encountered in real - life situation, they suggested approach such as probability bound analysis which is faithfully to both methods to be used in uncertainty propagation.

Van Asselt, (2000, pp 92 - 107) stated three approaches often used for analyzing uncertainty in model-based decision support based on causes and types of uncertainty, they are: sensitivity analysis, probability - based methods and formal scenario analysis. Sensitivity analysis simply means studying the effect of parameter variations and initial values on model predictions (outcomes) to account for the relative importance of the variables. The approach usually applied statistical techniques. Individual and/or joint parameter variation, sensitivity coefficient (or differential sensitivity analysis), response - surface method are some of the methods for sensitivity analysis. Among the frequently used probability methods is the Bayesian approach, where probability are defined and interpreted as subjective "degrees of beliefs". Probability calculus requires information regarding the distribution of the uncertain inputs or parameter. This may be determined using statistical fit or assumed by analyst based on experts' opinion. In this case, the uncertainties propagate through the model and the output variables show probability

distributions or 95 - percentile in statistical measures. This is often done using sampling techniques.

Formal scenario analysis is based on possible future states by making judgement on or evaluation of different sets of assumptions. Model runs are performed using sets of parameter values and results are compared. This technique targets to understand the variation of future states. It is surprising that validation could be a technique for analyzing uncertainty! Usually, it is a means testing the performance of model, which implies that the completeness of a model is measured by validation analysis. Therefore, validation remains the only method for reducing uncertainty model validity (Van der Kliss, 2003; Xu and Mynett, 2006; Hayes, 2011). The methods of analyzing uncertainty in terms of causes of uncertainty and types of uncertainty are given in Table 2.3 and Table 2.4 respectively.

Table 2.3: Potential methods in addressing different sources of uncertainty (Van Asselt, 2000)

S/n	Sources or causes	Method
1.	Lack of observation/ measurements	• Probability - based methods • Formal scenario - analysis
2.	Inexactness	• Probability - based methods • Formal scenario - analysis
3.	Ignorance	• Validation • Qualitative scenario development • Interactive problem and uncertainty structuring
4.	Indeterminacy	• Qualitative scenario development • Interactive problem and uncertainty structuring
5.	Natural randomness	• Stochastic modelling
6.	Value diversity	• No methods
7.	Behavioural variability	• Scenario - approaches
8.	Societal randomness	• Scenario - approaches
9.	Technological surprise	• No methods

Table 2.4: Methods of uncertainty analysis in terms of types of uncertainty (Van Asselt, 2000)

Uncertainty		Method	Output
Uncertainty in model quantities	Uncertainties in input data	• Sensitivity analysis • Probability - based methods • Formal scenario - analysis	• Role of uncertainties in input data in model run • Propagation of probabilities input data to outcomes • Effect from uncertain socio-economic inputs on outcomes
	Parameter uncertainties	• Sensitivity analysis • Probability - based methods	• Role of uncertainties in input data in model run • Propagation of probabilities input data to outcomes
Uncertainty about model form	Uncertain equations	• Sensitivity analysis in the form of meta-modelling	• Insights into crucial equations
	Model structure uncertainties	• No methods	
Uncertainty about model completeness	Uncertainty about model validity	• Validation	• Insights into model performance

Regan et al, (2002) from ecological point of view reckoned with two causes of uncertainty: epistemic and linguistic uncertainties. The author agreed with Van Asselt, (2000) that model uncertainty apart from the difficulty to quantify, is also impossible to eliminate. The only way of getting appropriate model for prediction is through validation analysis. For the subjective judgement that may arise as a result of data interpretation or due insufficient data to make reliable statement about parameters, subjective (or Bayesian) probability is allowed based on degrees of belief about the event from experts. The author queried the claimed benefit of the approach because degrees of belief are often not precise. A suggested approach is the imprecise probabilities in form of interval analysis, where upper and lower bounds are defined for

the event. Table 2.5 shows the summary of various sources of epistemic uncertainty with the appropriate general methods of propagation.

Table 2.5: Methods of analyzing epistemic uncertainty (Regan et al, 2002)

Sources of uncertainty	Method of treatments
Epistemic uncertainty	
• Measurement error	• Statistical techniques; intervals
• Systematic error	• Recognize and remove bias
• Natural variation	• Probability distributions; intervals
• Inherent randomness	• Probability distributions
• Model uncertainty	• Validation; revision of theory based on observation; analytic error estimation (for meta – models)
• Subjective judgement	• Degrees of belief; imprecise probabilities

Judging from risk assessment point of view, Aven, (2010) argued that the appropriate method of analyzing uncertainty depends on the relevant available data and the aim of the analyst/expert. He claimed that if the analyst aimed to obtain an objective description of unknown quantities, then the frequentist probabilities and not the subjective probabilities is the best method. However, where data is limited or understanding hinder the use of statistical techniques to produce probabilistic assessment, then, expert judgement is required in form of subjective probability, preferably called "Knowledge-based probability" (Aven, 2010). In this case, the uncertainty will be assessed based on judgement of knowledge and assumptions, whereby the expert assign probability through knowledge transformation. The

conclusion could differ for different analysts, but the judgment is considered valuable based on the competency of the experts in the field of analysis.

2.11 Uncertainty analysis

Uncertainty analysis is the study of how the different uncertainties in the input and parameters constitute the uncertainty of the model output. The advantages of an uncertainty analysis are that (Erik, 2002; walker et al., 2003 and Van der Klis, 2003, hall et al., 2009):

i) it provides the possibility to judge the acceptability of the accuracy of the model results for a specific purpose;

ii) it gives the framework to evaluate whether it is possible to improve accuracy when necessary;

iii) it can guide data collection so that the model accuracy is enhanced at reasonable data collection cost and;

iv) it serves as objective for further research to improve the relevant model or which parameter requires further studies.

Judging from above, performing an uncertainty analysis includes (Van Der Klis, 2004; Padulo et al, 2007; Tomblin, 2012):

- Identification of important uncertainties (sensitivity analysis),
- Quantification of important uncertainties,
- Quantification of the effect of those uncertainties on the model outputs (which is simply the propagation of uncertainty through system analysis) and

- Interpretation of the uncertainty in the model results.

In this study, analyses shall be based on extensive laboratory experiments and the inventory of several configurations of different water levels, vegetation heights, drag coefficients and vegetation densities using numerical model. The effect of the variation on the model output will be measured and quantified. The available methods are different for different problems arising in order to estimate the validity and reliability of the output results. They are often classified by stages depending on authors' interest. In this review, uncertainty measures are categorized into two: local methods and global methods.

The local methods are sensitivity coefficient or indirect method often called Brute-force method (Tomlin, 2012), method of elasticity, also referred to as local sensitivity analysis (Ramroth et al, 2006; Edoardo et al, 2010) or normalized Brute-force method (Tomlin, 2012) and the Gaussian 1^{st} order approximation, often called local uncertainty method (Li et al, 2011 and Tomlin, 2012).

The assumptions of linear response and uncorrelated inputs are the limitations of the local sensitivity and uncertainty analysis. Notwithstanding the limitations, this method has been found applied to majority of sensitivity analysis in hydrology and hydraulic engineering (e.g., Kabala, 2001; Chen and Chen, 2003; Horritt, 2006; Wu and Mohanty, 2006; Podsechin et al, 2006 and Hall, et al, 2009). By excluding the nonlinear effects with parameter correlations may be misleading. The best option then, is to apply global methods (Tomlin, 2012 and Abdel-Khalik, et al, 2013). The overall aim of a global uncertainty analysis is to determine the joint pdf of predicted model from the joint pdf of the model input parameters. To do this, on one hand, the joint pdf of all

parameter is required. For multi-dimensional parameters, it may be necessary to screen less important parameters to minimize computational cost using Morris method (e.g.,Morris, 1991; Xu and Mynett, 2006; Ziehn and Tomlin, 2008; Ziehn et al, 2009 and Kumar and sung, 2011; Confalonieri, et al, 2010; Tomlin, 2012; King and Perera, 2013).

2.12 Brief review of methods of propagation of uncertainties

2.12.1 Stochastic methods

Stochastic methods portray the variability of large complex system behaviour. The mathematical models that describe the processes surrounding this system behaviour often display the following properties (Taylor and Karlin, 1998, pp 5 - 18; Van Vuren, 2005):

(i) Numerous input and output variables;

(ii) Time consuming mathematical models;

(iii) Modulations to the model are tedious and time-consuming;

(iv) Model input variables are correlated;

(v) The models are difficult to compress into a single system of equations;

(vi) The associated marginal distribution function (MDF) of the model inputs are often non-Gaussian;

(vii) The model outputs are non-linear multivariate dependent functions of the input variables.

The problem statement is usually how to obtain the mean and covariance of model output given the mean(s) and covariance(s) of stochastic vector. The purpose of a stochastic method is to quantify uncertainties (statistical characteristics) in the model output. In addition, it can be used to estimate the relative contribution of various sources of uncertainty in the model input variables in relation to the total uncertainty in the model prediction. Typical examples of common stochastic methods are ***Monte Carlo Simulation*** (MCS), ***Numerical Integration Method*** (NIM), ***First Order Reliability Method*** (FORM), for example (Van der Klis, 2003; Gates and Al-Zahrani, 1996; Morgan and Henrion, 1990), ***Response Surface Replacement Method*** (RSRM) and ***Stochastic Differential Equations*** (SDE). These methods have been discussed extensively in literature (Morgan and Henrion, 1990; Haldar and Sankaran, 2000; Tyagi and Haan, 2001; Van der Klis, 2003; William et al, 2003; Van Vuren, 2005; Padulo et al, 2007; Ata, 2007; Coleman and Steele, 2009; Tomblin, 2012).

Using criteria based on linearity, complexity of the system and the applicability of the models as tool in engineering practice. NIM is often not recommended because the method requires numerous model evaluations. The RSRM, also, could be impractical as hydrodynamic models are too complex to be adequately replaced by a simplified meta-model. Van Vuren, (2005) on this basis emphasized the inadequacy of this method in morphodynamics models. The SDE method is associated with description of the state and physical system behaviour in terms of probability. The procedure is too mathematical, involving many concepts of calculus and numerical approximation. The laborious steps may not be applicable in practice. For these reasons, these methods are not considered any further in this study. However, NIM has been used

in chapter seven (7) to verify the performance of Unscented Transformation (Sigma – point) approach.

The advantages of MCS are (Van der Klis, 2003):

- Easy to implement, flexible and robust method for solving many problems;
- No need to discretize continuous distributions;
- The non-linearity characteristic of the model is maintained;
- No restrictions to the magnitude or nature of model input uncertainties, as far as they can described in statistical terms;
- The method can provide information about complete probability distribution of the model output as well as all its statistical properties;
- The precision of the estimate of the output distribution can possibly be obtained from the output samples using standard statistical methods.

MCS is seems to be "the only method capable of estimating the cumulative distribution function of the model output for highly non-linear and/or complex system relationship" (Melching, 1995; Van der Klis, 2003). The main limitations of MCS are:

- Occurrence of clusters in some regions and gaps in other regions;
- Time consuming simulations or the computational complexity of the method constitute a practical issue;
- The application of this method to high-dimensioned systems is rare in practice.

The issue of computational complexity was addressed by Morgan and Henrion (1990) and was adopted by Van der Klis, (2003) for the analysis of technical uncertainty using Sobek model for river bed morphology. Morgan and Henrion provide explicitly a

method that assist to decide the number of runs necessary to achieve required degree of accuracy. Generally, MCS results are often used as check of results for other solutions techniques (Van der Klis, 2003; Abrishamchi et al, 2005; Hall et al, 2009 and Camacho and Martin, 2013). Because of its significant merits, MCS has been used in various research fields, like hydrology (Gates and Al-Zahrani, 1996), thermal modeling (Ramroth et al, 2006), ecological modeling (Larocque et al, 2008), water quality modeling (Osidele et al, 2006; Carrasco and Chang, 2005; Hamed and El-Beshr, 2004; McIntyre, 2004; Mailhot and Villeneuve, 2003).

An improvement on MSC is the ***Latin Hypercube Sampling*** (LHS), a technique developed to reduce the variance of the statistical errors in the Monte Carlo Simulation results, thereby reducing its required computational effort. LHS is popular among the variance-reduction techniques. The techniques increase the efficiency and accuracy of the simulation methods of uncertainty estimation by using a relatively small number of simulations (Morgan and Henrion, 1990; Haldar and Sankaran, 2000; Mckay et al, 2000; Helton and Davis, 2002; Hamed and El-Beshr, 2004; Tomblin, 2012). The method have been successfully applied to different fields (e.g., Helton, 1999; Yu et al, 2001; Kapelan et al, 2006; Turanyi, 2008; Karanki et al, 2010). Its limitations are that it is computationally expensive for large parameter models and its application to high-dimensioned systems is rarely practical.

Another important method of uncertainty analysis is the ***Bayesian approach*** where multi-dimensional integrals only in linear, Gaussian systems are tractable and the closed-form recursive solution exists in some restricted cases for example using the universal Kalman filter and grid-based filters (Jazwinski, 1970; Van der Merwe, 2004;

Speyer and Chung, 2008, pp 119-145; Mochnac et al, 2009; Kessler, 2012). Under the assumption of linearity and Gaussian probability densities, the celebrated Kalman filter method seems to be the optimal (and exact) solution to the Bayesian estimation problem (Norgaad et al, 2000; Van der Merwe, 2004; Luo and Moroz, 2009). Kalman filter is known as optimal estimator as it minimizes the mean square error of the estimated parameter, provided the distribution is Gaussian. The method is so popular for following reasons:

- The structure and optimality yielded good practical results.
- It is convenient for online real time processing.
- Ease of formulation with basic understanding of implementation.

Generally, real world systems are often nonlinear, non-Gaussian. Numerous approximate solutions available including Monte Carlo Simulation (MCS) have been extensively discussed (Collins, 2003; Van der Merwe, 2004; Ata, 2007; Speyer and Chung, 2008, pp 241-249; Evangelos, 2009, pp 55-80; Kessler et al, 2012). Besides, the accuracy as well as the validity of the assumption (in simplified form) depends on the nature of extrapolated problem under consideration, thereby making certain approximate methods more suitable than others.

The Gaussian approximate methods are capable of modeling pertinent density in the Bayesian recursion (by Gaussian distributions). It includes ***Kalman filter*** (KF), ***Extended Kalman filter*** (EKF) and ***Gaussian sum filters*** (GSF) (see Figure 2.7). The highlighted methods have gain a lot of attention in research works due to their low computation cost and relative eases of implementation (Van der Merwe, 2004; Speyer and Chung, 2008; Evangelos, 2009). The solutions are based on the underlying

assumption that a consistent minimum variance estimator of the posterior density can be obtained through propagation and update of the first and second order moments of the actual densities (Van der Merwe, 2004). Although the EKF shows significant application as it is applicable to nonlinear Gaussian systems by linearization of the system using first – order truncated Taylor series expansion. The flaws of this approach is that it is more reliable only when the higher order terms of the nonlinear functions almost zero. In other words, in means that it is more efficient when the first order terms dominate. Additionally, the method linearize around the mean value of the distribution which may not be practically a representative sample. The details of inaccuracy of this method have been documented (Van der Merwe, 2004, pp 35-40).

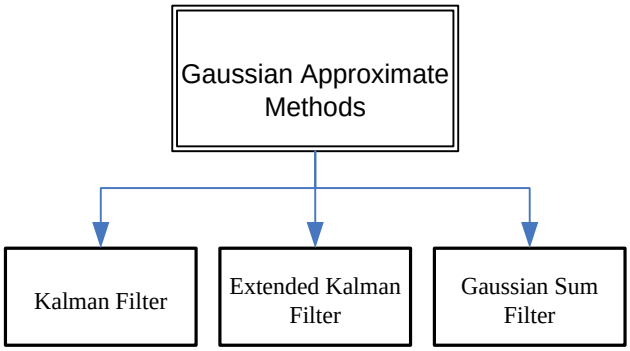

Figure 2.7: Modeling methods in Bayesian Recursive Estimation

Kalman filter approach has been defined as "the minimum-variance state estimator for linear dynamic systems with Gaussian or non-Gaussian distribution" (Simon, 2010). Kalman filter can be derived using several approaches, either by assuming Gaussian distribution of the process and of the initial state in order to obtain the posterior distribution of the states given the observations and using the mean of the resulting distributions to estimate the state or the combination of the recursive weighted

least-squares method with weighting of the previous estimate of the states to obtain additional measurement (Mochnac et al, 2009).

The main limitation of KF method is that it requires linear model. Generally, KF addresses problem by estimating the state $x \in \Re^n$ of a discrete-time controlled process governed linear SDE where the posterior pdf is Gaussian for every time step (Kalman, 1960; Julier, 2002; Daum, 2005; Simon, 2010). Systems found in practice usually have non-linear measurement – processes relationship and often, the pdf is non-Gaussian. In this case the well-known Kalman filter when applied to a linearized version such systems loses its optimality, therefore, different approach is required to tackle such problem (e.g., approximate grid-based method or extended Kalman Filter. These methods are referred to as sub-optimal algorithms (Arulampalan, 2002; Mochnac et al, 2009; He and Herose, 2013).

The ***Extended Kalman filter*** is an extension of the KF. The EKF is a standard procedure of solving non-linear system problem and had gained wider practical application. The EKF linearizes the measurement equations and state update about the predicted state at a nominal point via Taylor expansion (Van der Merwe and Wan, 2004; Schneider and Geogakis, 2013; Mansouri et al, 2013). This prediction is often not accurate practically. The refinement of the estimate can be done through re-evaluating the estimate around the new estimated state nominal point and the procedure is simply referred to as "Iterated EKF". It has been explained as "an ad hoc state estimator that only approximates the optimality of Baye's rule by linearization" (Welch and Bishop, 2006). The derivation of EKF has been provided by (Julier et al, 2000; Welch and Bishop, 2006). Also, in the same conceptual principle Norgaard et al, (2000) used

function evaluations in the interpolation formula of EKF as a replacement to Taylor's formula. The difference alone could be seen in the update of the covariance matrices which enhance easy implementation. The method has been widely used in hydrological forecasting of stream flows and long-range horizon water levels including (Koutsoyiannis et al., 2008; Londhe and Charhate, 2010; Muluye, (2011).

The limitations of the approach are, firstly, linearization of non-linear function via Taylor expansion with neglected higher order terms which produces poor approximation especially when the error propagation are not well approximated by linear function. Secondly, Jacobian matrix must exist for linearization to be applied, which is not always the case for discontinuous systems. However, the non-triviality of Jacobian matrices in most applications as well as its associated implementation complications remains issue. In order to address the deficiencies associated with linearization, the unscented transformation (UT) was developed to give a more explicit and direct mechanism information for the mean and covariance transformation (Julier and Uhlmann, 2004).

The ***unscented Kalman Filter***, (UKF) is a discrete KF where unscented transformation is used to obtain the mean and covariance update. In this approach, the estimated mean and covariance of the observation and Kalman gain in the EKF are replaced by sigma point and then propagated through the model (Van der Merwe and Wan, 2004). Sigma points provide accurate approximation to evaluate *n*-dimensional integrals. Although EKF and UKF yield same results for linear model, UKF provide better approximation for non-linear functions. In addition, no Jacobians are required for the Unscented Kalman Filter, but still demands Gaussian distributions for

implementation (Gove and Hollinger, 2006. Simon, 2010; Girish and Ravindra, 2010). The accuracy of UKF is largely superior to the EKF (Daum, 2005; Luo and Moroz, 2009). The general formulation of Kalman Filter using the UT approach has been described explicitly (see Julier and Uhlmann, 2004).

2.12.2 Unscented transformation method

The Unscented Transformation (UT) is based on the notion that "it is easier to approximate a probability distribution than to approximate non-linear model or transformation" (Julier et al, 2000; Julier and Uhlmann, 2004). The UT, especially in form of the UKF, has principally replaced the EKF in many nonlinear model applications, including for spacecraft and air navigation (Xiaojun et al, 2010; Bruno et al, 2011)). The illustration of the approach goes thus: for the input variable, select a set of points called sigma points deterministically from the representative mean and covariance. Then, the nonlinear function or simulation is applied to each point and the corresponding transform points are obtained in form of model predictions. Set the weighted points to reflect certain properties of the variable (see detail in the method overview).The statistics of the model outputs can be calculated to form an estimate of the predicted mean and covariance (Julier et al, 2000; Julier, 2002; Julier and Uhlmann, 2004).

2.12.3 Sigma point approach

The Sigma Point (SP) technique was introduced by Uhlmann and Julier in the early 1994 and has been found to be optimal state estimate of non-linear stochastic models in signal processing (Simo and Jouni, 2010). The approach is based on the concept that it is easier to approximate probability distribution than to approximate non-

linear model or transformation. Padulo et al, (2007) analyzed of uncertainty propagation in the computer system analysis using different methods. The compared methods are method of moment (MM), Gaussian quadrature (GQ), and Monte Carlo Simulation. In addition, their study presented two methods based on sigma point approach; they are Unscented Transformation (UT) and Divided Difference Filter (DDF). Their study mainly focused on the propagating uncertainty by comparing these methods with the conventional methods (MM, MCS) through the analysis of system so as to procure a probabilistic description of the constraints and objective functions. By using mathematical analyses and numerical examples, Padulo et al showed that SP methods could provide better estimates of mean and variance with less computational cost.

The significant merit of the method is that it is derivative-free and requires *2m* or *2m +1* function evaluations for each analysis. It overcomes the limitation of the EKF, as it does not linearize non-linear functions, but fully exploits nonlinear functions. There are other methods of data assimilation for example UKF and Ensemble Kalman Filter (EnKF) approaches do not linearize either, but the distribution has to be Gaussian. The EnKF and UKF have been found to produce better state estimation that EKF, however, the problem of non-Gaussianity is not addressed using EnKF method (Colburn et al, 2011). At this point SP surpasses the existing methods in its application to non-linear function, non-Gaussian distribution and high dimensional systems (Luo et al, 2010). Sigma point approach requires less function evaluations and has been found as an alternative to Monte Carlo Simulation in various disciplines (Padulo et al, 2007; Menezes et al, 2013; Stephanie et al, 2013). A flow chart for SP approach is as shown in Figure 2.8. The approach is flexible, easy to apply.

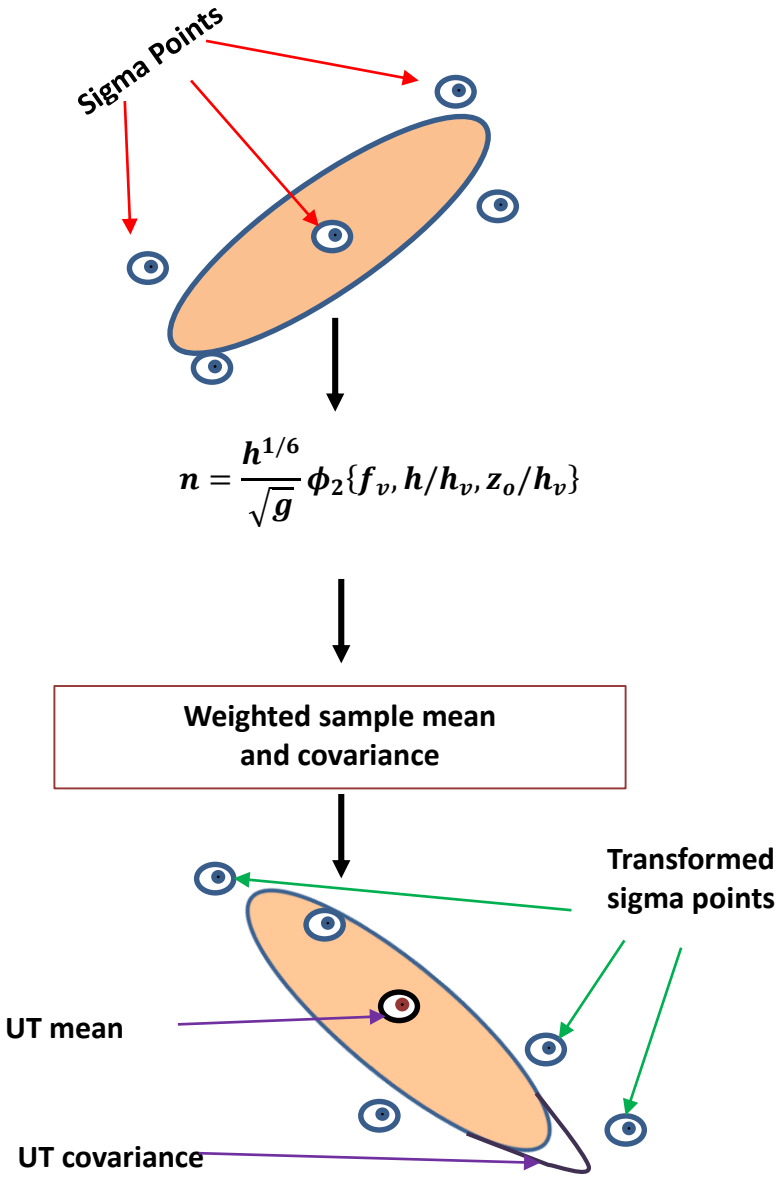

Figure 2.8: A flow chart for UT (Sigma points) method of uncertainty propagation

The method has been applied to modulation schemes in signal processing and communication channels and was found to be as accurate as MCS and relatively faster than other existing stochastic methods including MCS also it does not require in-depth knowledge of the probability distribution (Kim et al, 2010; Menezes et al, 2013). The SP approach has gained tremendous application in the field of computer and electrical engineering (e.g., Van der Merwe and Wan, 2004; Wang et al, 2008). In the field of spacecraft navigation, Xiaojun et al, (2010) mentioned that the SP technique yield lower relative state estimation errors with faster convergence rates than the other techniques. Similarly, Bruno et al, (2011) studied the choice of state estimation algorithm performance of varying stochastic methods on the flight path reconstruction, they concluded that SP technique in terms of accuracy substantially outperform the EKT and UKT in the covariance estimate.

Recently, Stephanie et al, (2013) apply the technique to calibrate the electromechanical cardiac model for 16-dimensional systems in order to understand and enhance the treatment of cardiovascular diseases involving wide spectrum of therapy and was found to produce faster parameter calibration.

Evaluating the mean and covariance of the function accurately requires the approximation of the input variables up to m^{th} order. The approximation of this approach is correct up to the third order for the covariance. The error introduced in the fourth and higher orders are due to the function of k_o and matrix square root. In case where a different distribution is assumed for the input variable, a different choice of k could be more appropriate (Julier et al, 2000; Julier and Uhlmann, 2004; Kim and Park, 2010).

2.13 Summary

This chapter provides thorough review on impact of vegetation on the velocity profile and most significantly on flow resistance. To begin with, the importance of vegetation was studied. Also, the studies of open-channel flows with emerged and submerged cases using physical and numerical modeling approaches by different investigators have been reviewed. The assessment of the existing studies reveals that study on emergent/ submerged rigid vegetation and its relevance in waterways and riparian zone is well-documented, whereas further study is required for dense submerged flexible vegetation. Aquatic plants found in nature are species with stems of high flexibility and density, e.g., Chondrus cripus, (see Boller and Carrington, 2006) and Glyceria fluitans, Ranunculus penicillatus, Myriophyllum alterniflorum and Fontinalis antipyretica (see Miler, 2012). The hydrodynamics of vegetated river system includes a dynamic feedback among flow characteristics, vegetation characteristics (morphology and size), channel characteristics and sediment transport. Based on this, the conveyance of an open channel flows depend on flow conditions and vegetation characteristics, such as vegetation density, plant height, size, shape and flexibility.

In general, the flow characteristics vary in space causing change in velocity resulting in bending and compaction of vegetative species, thus, affect hydraulic roughness. Flexible plant species often adapt to this situation by streamlining and re-establishing a new dynamic equilibrium state through reconfiguration due to change in shape and size and, hence, drag reduction. Previous studies have focused on hydraulic roughness model using rigid cylinder analogy. Therefore, the knowledge of hydraulic roughness to flexible vegetation is still not fully explored.

The observation of the previous inconsistent results that the drag coefficient increases with ϕ (Tannio and Nepf, 2008, Kothyari, Hayashi and Hashimoto, 2009), and the drag coefficient decreases with ϕ (Nepf, 1999, Mattis et al., 2015) needs thorough assessment. The study of influence of lateral and longitudinal spacing ratio among vegetation stems on drag coefficient for emergent and submerged vegetation can advance the understanding of flow resistance. Based on this, a reliable estimate of C_d can be made. There is need for collation of experimental dataset that shows (lateral and longitudinal spacing) variation of areal density for blade type vegetation.

One of the prominent features of this research is the modeling of vegetated flow in which proper estimate of C_d will yield better conveyance capacity of drainage system. By doing these, data from physical models can be simulated in the numerical model and assessment of the confidence levels of numerical prediction subjected to large dimension of input parameters can be made.

The slope of tangent sensitivity, method of elasticity, and Gaussian approximations can be classified as local measures of uncertainty method. The methods may not be practically applicable to vegetation parameters due non-linearity of the problems. For example, vegetal drag depends of many parameters such as areal density, flow depth, plant flexibility and geometry of plants. These parameters are mutual correlated. Therefore, uncertainty in drag coefficient (C_d) or other parameters using discharge as the response variable will require more practical approach. To this end, unscented transformation (sigma point approach) is introduced to analyze uncertainty in model quantities in vegetated open channel flows. The review of literature shows that Unscented Transformation approach has gained application in diverse multidisciplinary

field, it is practical and easy to apply. This method has not been applied to the field of fluid mechanics or hydraulics to the best of the author's knowledge. Therefore, it is introduced in this study and its applicability to hydraulic of vegetated flow is studied in chapter 7.

3 Hydraulic roughness model for submerged flexible vegetation

3.1 Model selection

Submerged vegetation is a key component in natural and restored rivers. The hydraulic resistance produced by submerged flexible vegetation depends on many factors, including the vegetation stem size, plant height, number density and flow depth. Although various hydraulic roughness equations have been reported in literature (e.g. Kouwen and Li, 1980; Baptist et al., 2007: Brian and Shen, 2002; Choi and Yang, 2010 and Cheng, 2011), these equations are mainly developed for emergent vegetation or submerged rigid vegetation. A hydraulic roughness model covering submerged flexible vegetation thus is required.

In this chapter, a numerical modeling approach is used to generate synthetic velocity profile data for hydraulic roughness determination. Models that portray nature may be difficult to develop most especially for turbulence modeling. Nevertheless, a model should consider important parameters that simulate the physical processes and provide insight of the natural processes. Such model when provided with adequate input data is expected to replicate experimental and field results to a reasonable extent.

In the present model turbulence is simulated by the Spalart-Allmaras closure with a modified length scale which is dependent on the vegetation density and water depth to vegetation height ratio. The velocity - stem height relationship is determined by large deflection analysis using Euler- Bernoulli theory of bending which has been found to be more accurate than the commonly used small deflection theory of Timoshenko (Paul et al., 2014). This model was developed by Li and Zeng (2009) and verified against

available experiments. Based on the synthetic data an inducing equation is derived, which relates the Manning roughness coefficient to the vegetation parameters, flow depth and a zero-plane displacement parameter. The derived equation is compared with an existing equation, as well as the data sets of flume experiments conducted by various researchers. The predictive capability of the derived equation is subsequently tested in field conditions. This indicates that the model is not just only a research tool, but can be implemented in real-world practical application under specific conditions.

3.2 Numerical methodology

In this study-the 1-D version of the model is used because most vegetated flows are unidirectional and, with shallow flow depth. Multi-dimensional models require more computational effort and are not efficient for the generation of a large number of synthetic data.

3.2.1 Governing equations

The primary quantities to describe an open-channel flow are the velocity and pressure. For water (a Newtonian fluid), the flow is incompressible and is governed by the Navier –Stokes equations (NSE). The 1D version of the equations can be written as follows.

Continuity equation

$$\frac{\partial u_i}{\partial x_i} = 0 \qquad \text{i=1} \qquad (3.1)$$

Momentum equation in horizontal direction:

$$\frac{\partial u_i}{\partial t} + u_j \frac{\partial u_i}{\partial x_j} = \frac{\partial}{\partial x_j}\left[\nu_m \left(\frac{\partial u_i}{\partial x_j} + \frac{\partial u_j}{\partial x_i}\right) + \frac{\tau_{ij}}{\rho}\right] - \frac{1}{\rho}\frac{\partial p}{\partial x_i} - \frac{1}{\rho}F_i + g_i \quad I=1, j=3 \qquad (3.2)$$

where x_i $(= x_1)$ = coordinate in horizontal direction *(m)*; u_i $(= u_1)$ = time averaged velocity in horizontal direction (*m/s*); $u_j = 0$; t = time (*s*); ρ = fluid density (kg/m^3); ν_m = molecular viscosity (m^2s^{-1}); $\tau_{ij} = -\rho u_i' u_j'$ = Reynolds stresses (N/m^2); p = pressure (N/m^2) is assumed to be a constant; $F_i = F_x$ (N/m^3) is the resistance force components per unit volume induced by vegetation in *x* directions. g_i = is the x-component of the gravitational acceleration and is set to gS_o, where S_o = channel bottom slope.

The Reynolds stresses are represented by eddy viscosity model:

$$\frac{\tau_{ij}}{\rho} = -\overline{u_i u_j} = -2\nu_t \left(\frac{\partial u_i}{\partial x_j} + \frac{\partial u_j}{\partial x_i}\right) - \frac{2}{3}\delta_{ij}k \quad i=1, j=3 \qquad (3.3)$$

where $k = {}^1/_2\,\overline{u_i' u_i'}$= turbulent kinetic energy (m^2s^{-2}) which can be absorbed into the pressure gradient term and ν_t = eddy viscosity (m^2s^{-1}).

The eddy viscosity ν_t is specified by the Spalart-Allmaras (SA) turbulence model which involves the solution of a new eddy viscosity variable ν. The version of the model used is for near-wall region and moderate Reynolds number, which is most relevant to the present problem (Spalart and Allmaras, 1994).

3.2.2 Closure model

The Spalart- Allmaras (S-A) one equation turbulence model is is simpler compared to the well-known $k - \varepsilon$ model and has been found successful in the modeling of vegetated flows (Li and Yan, 2007; Li and Yu, 2010; Li and Zhang, 2010; Paul et al,

2014). The model is applicable to near–wall region and for moderate Reynolds number. It describes the convective transport, along with the production, diffusion, and destruction of eddy viscosity. Detail of the closure model can be found in (Spalart and Allmaras, 1994; Sebastien et al, 2002; Li and Yan 2007; Li and Zeng, 2009; Zeng, 2012).

$$\frac{\partial \nu}{\partial t} + u_j \frac{\partial \nu}{\partial x_j} = C_{b1}\tilde{S}_\nu \nu + \frac{1}{\rho}\left\{\frac{\partial}{\partial x_j}\left[(\nu + \nu_m)\left(\frac{\partial \nu}{\partial x_j}\right)\right] + C_{b1}\left(\frac{\partial \nu}{\partial x_j}\frac{\partial \nu}{\partial x_j}\right)\right\} - C_{w1} f_w \left(\frac{\nu}{d}\right)^2 \quad (3.4)$$

The eddy viscosity is defined as

$$\mu_t = \rho \nu f_{\nu 1} = \rho \nu_t \quad (3.5)$$

where

$$f_{\nu 1} = \frac{\chi^3}{\chi^3 + C_{\nu 1}^3} \text{ with } \chi = \frac{\nu}{\nu_m} \quad (3.6)$$

The vorticity magnitude S_ν is modified as:

$$\tilde{S}_\nu = S_\nu + \frac{\nu}{\kappa^2 d^2} f_{\nu 2} \text{ with } S_\nu = \sqrt{\omega_j \omega_j} \quad (3.7)$$

$$f_{\nu 2} = 1 - \frac{\chi}{1 + \chi f_{\nu 1}} \quad (3.8)$$

$$f_w = g\left[\frac{1 + C_w^6}{g^6 + C_w^6}\right]^{1/6} \text{ with } g = r + C_{w2}(r^6 - r), \quad r = \frac{\nu}{\tilde{S}_\nu \kappa^2 d^2} \quad (3.9)$$

Constants of the model are: $\kappa = 0.41;\ \sigma = 2/3;\ C_{b1} = 0.1355;\ C_{b2} = 0.622,\ C_{\nu 1} = 7.1;\ C_{w1} = \frac{C_{b1}}{\kappa^2} + \frac{1 + C_{b2}}{\sigma};\ C_{w2} = 0.3;\ C_{w3} = 2\ and\ d =$ length scale.

The S-A closure model has been basically developed for aerodynamic flows. It is intrinsically a transport equation for the eddy viscosity was developed under the well-known Boussinesq hypothesis. It has been successfully applied in the modeling of free-shear flow, wall-bound flow and separated flow problems.

The resistance force due to vegetation is defined by the quadratic friction law. The average force per unit volume within the vegetation domain is given by

$$f_i = \frac{1}{2}\rho C_d w u_i \sqrt{u_j u_j} \qquad i=1 \tag{3.10}$$

Where C_d = drag coefficient of stem, w = width of stem. The drag force resulted from wake formation downstream of the stem. The average force per unit volume within the vegetation domain is obtained by

$$F_i = N f_i = \frac{1}{2}\rho C_d N w u_i \sqrt{u_i u_j} = \frac{1}{2}\rho f_{rk} u_i \sqrt{u_j u_j} \qquad i=1 \tag{3.11}$$

where N = vegetation density (defined as number of stems per unit area, $1/\mathrm{m}^2$) and $f_{rk} = C_d N w$.

In case of wall bounded shear flow, the turbulence length scale d is proportional to the distance from the point of interest to the channel bed. In the presence of vegetation, the turbulence eddies above the vegetation layer may not reach the channel bed, thus there will be reduction in the turbulence length scale. One approach to simulate the reduction in the turbulence length scale is to introduce a zero plane displacement parameter, Z_o. The turbulence length scale of a point at level Z is obtained by

$$\begin{cases} L = Z - Z_o, & Z > h_d > Z_o \\ L = Z\,(h_d - Z_o)/h_d\ , & Z < h_d \end{cases} \tag{3.12}$$

where h_d is the deflected height of vegetation (m).

3.2.3 Flexibility (Large deflection analysis)

Natural vegetation bend easily in high flow and the deformation of the top of vegetation can be of the same order as the deflected plant height. Hence, the classical analytical expression for transducer deformation which is based on theory small deformation as previously used (Kutija and Hong, 1996; Erduran and Kutija, 2003; Kubrak, et al, 2008) may not be adequate for vegetation with high flexibility. The selected model uses a large deflection analysis based on the Euler-Bernoulli law for bending of a slender transducer has been used to determine the large deflection of plant stem (Li and Xie, 2011).

In the analysis each vegetation stem is modeled as a vertical in-extensible non-prismatic slender transducer of length, $\boldsymbol{l}$. The water flows produces variable distributed loads $q_x(s)$ on the transducer along the *x*-direction as shown in Figure (3.1). From Euler-Bernoulli law, the local bending moment is proportional to the local curvature.

$$M(s) = EI(s)\frac{\frac{d^2\delta}{ds^2}}{1-\left(\frac{d\delta}{ds}\right)^2} \tag{3.13}$$

where, M is the bending moment (Nm), s is the local ordinate along the transducer,

E is the modulus of elasticity (N/m^2), I is the Second moment of area (m^4) and,

δ is the deflection in x - direction (m).

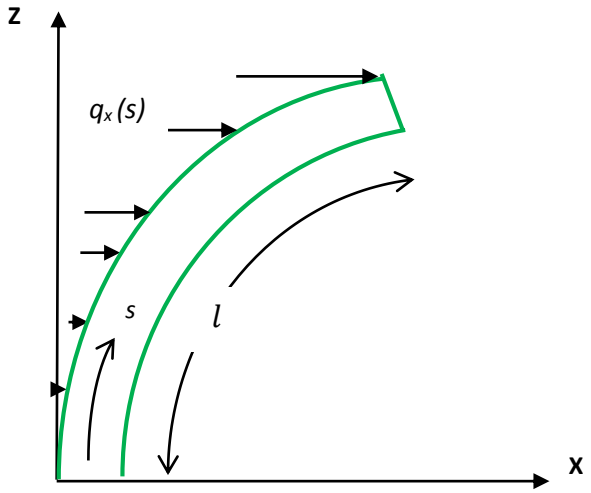

Figure 3.1: Schematic diagram of large deflection of a transducer carrying distributed load.

The equilibrium of forces and momentum gives

$$\frac{d^2M}{ds^2} + \frac{dM}{ds}\frac{\frac{d\delta d^2\delta}{ds\,ds^2}}{\left[1-\left(\frac{d\delta}{ds}\right)^2\right]} = -q_x(s)\sqrt{1-\left(\frac{d\delta}{ds}\right)^2} \tag{3.14}$$

Combining of equations the Euler-Bernoulli law (3.13) and the equation of equilibrium of forces and moments (3.14) yielded a fourth order nonlinear equation in the deflection δ

$$\frac{d^2}{ds^2}\left[EI(s)\frac{\frac{d^2\delta}{ds^2}}{1-\left(\frac{d\delta}{ds}\right)^2}\right] + \frac{d}{ds}\left[EI(s)\frac{\frac{d^2\delta}{ds^2}}{1-\left(\frac{d\delta}{ds}\right)^2}\right]\frac{\frac{d\delta d^2\delta}{ds\,ds^2}}{\left[1-\left(\frac{d\delta}{ds}\right)^2\right]} = -q_x(s)\sqrt{1-\left(\frac{d\delta}{ds}\right)^2} \tag{3.15}$$

The vegetation stem is taken as inextensible as the total length remains constant. By dividing the stem into n equal part of constant length Δs, the z-ordinate of the ith node is obtained by

$$z_i = \sum_{j=1}^{i}\sqrt{\Delta s^2 - (\delta_i - \delta_{i-1})^2} \tag{3.16}$$

3.2.4 Numerical methods and Boundary conditions

The deflected height of the stem is then equal to z_n. The equation (3.15) is then solved using a quasi-linearized central finite difference scheme. In order to minimize computational effort, the solution is expressed in non-dimensional form relating the deflected height of vegetation to the applied force, and is approximated by a polynomial.

At the free surface, by neglecting the wind and surface tension, the dynamic condition can be satisfied by specifying zero pressure and zero gradients of velocity component:

$$p = 0 \qquad and \qquad \frac{\partial u_i}{\partial \sigma} = 0 \tag{3.17}$$

At the bottom, the logarithmic law wall function is imposed to calculate the wall shear stress used in diffusion step. The wall function is given by

$$u = u_w \left[\frac{1}{\kappa} ln\left(\frac{u_w z}{\nu_m}\right) + B\right], \; \nu = \kappa \, z \, u_w \tag{3.18}$$

where u_w = wall shear velocity (*m/s*); z = distance from the wall (*m*); and $B = 8.5$. By knowing the velocity at the point next to the wall with distance, z the wall shear stress can be computed iteratively. An extensive description of the numerical scheme and boundary conditions can be found in (Li and Zeng, 2009).

3.3 Model calibration

The number of (uniform) grids used is 41 and the time step size is in the order of 0.0005s to ensure computational stability. Grid convergence study shows that further

reduction of grid size does not affect the results practically. The 1- D model has been calibrated using data from previous experimental works conducted to investigate open channel flows with flexible or rigid submerged vegetation. The detailed description of each experimental works have been given in section 2.3, 2.4 and 2.5 of chapter 2. The following experimental cases of section 3.3.1 through 3.3.6 were simulated using the model. Generally, the dataset contain eight variables, i.e., flow depth (h), energy slope (S), strip width or stem diameter (w), vegetation height (h_v), discharge (Q), flexural rigidity (EI) and number of strips or stems per unit area (N). Two parameters are required to be calibrated: the bulk drag coefficient and the zero-plane displacement parameter. The latter is significant in the clear water zone while the former is important in the vegetation zone.

3.3.1 Mean velocity profile

In the first test, experiments carried out by Lopez and Garcia, (2001) on the mean flow and turbulence structure through submerged flexible vegetation which has been reviewed (see section 2.5) was simulated. The experimental condition is shown in Table 3.1.

Table 3.1: Experimental conditions (Lopez and Garcia, 2001)

Run	*N* (*stems per m^2*)	*h* (*m*)	*w* (*mm*)	h_v (*m*)	**EI* (*Nm^2*)	*Q* (*m^3/s*)	*S* (*%*)
Experiment 1	142	0.34	6.4	0.12	4.75	0.179	0.36

h = water depth, h_v = height of vegetation, $\boldsymbol{N}$ = number of stems/m^2 and EI = flexural rigidity

*Adopted modulus of rigidity

Figure (3.2) showed the comparisons between the numerical results using 1-D and the experimental data of Lopez and Garcia (2001). The computed mean velocities above the vegetation layer obtained through data simulation agreed well with that reported in the experiment. The difference between the presently computed mean velocity above vegetation and the corresponding measured value is less than 7%.

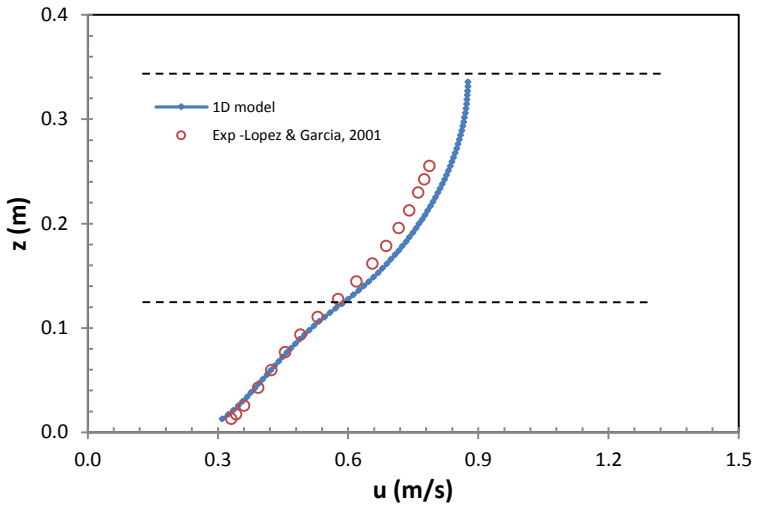

Figure 3.2: Mean velocity profile (Lopez and Garcia, 2001)

3.3.2 Effect of submerged flexible vegetation on flow structure and resistance

For the second test, the flume studies carried out by Jarvela, (2005) investigating the effect of flow structure above flexible vegetation was replicated. The hydraulic conditions are as shown in Table 3.2. The detail experimental work has been reported in section 2.3.

Table 3.2: Experimental conditions (Jarvela, 2005)

Run	*N* *(stems per m^2)*	*h* *(m)*	*w* *(mm)*	h_v *(m)*	*EI* *(Nm^2)*	*u* *(m/s)*	*S* *(%)*
R4-8	12,000	0.707	2.8	0.28	4.35×10^{-5}	0.129	0.02
R4-9		0.704	2.8			0.185	0.03

In Figure (3.3) the computed results are in good agreement with the measured data in the clear water zone and exhibit a low velocity region in the vegetation layer. The results from showed that the model is capable of predicting the velocity above the vegetation layer or surface layer.

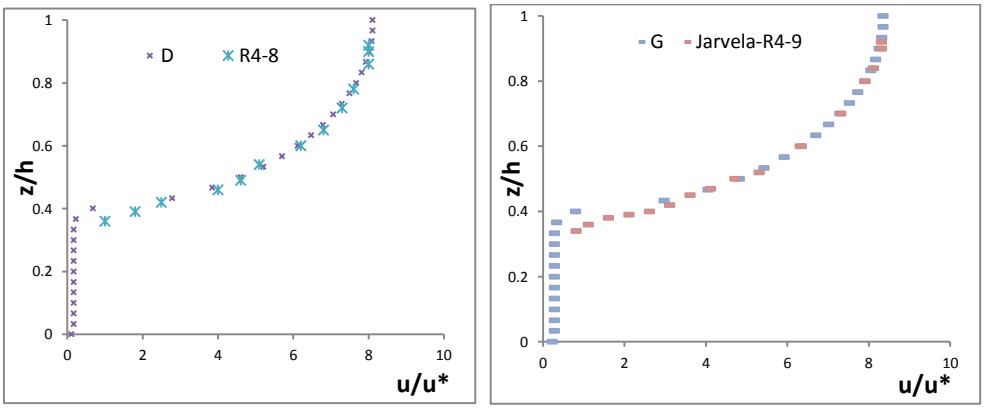

Figure 3.3: Normalized Velocity profile and flow depth
(D and G denote model results).

3.3.3 Effect of relative submergence on mean velocity

In the third test, the effect of flow depth on mean velocity of flow in open channels with vegetation lining was investigated. The experimental condition from Wilson, (2007) was replicated (Table 3.3). In the experiments the flow depth varied from 48mm to 165mm and the corresponding mean velocity was measured. The progressive change in flow velocity due to the increase in water depth is shown in Figure 3.4.

Table 3.3: Experimental conditions (Wilson, 2007)

Run	*N* *(stem per m^2)*	*h* *(m)*	h_v *(m)*	*Q* *(m^3/s)*	*S (%)*
A-2	833,333	0.048 – 0.165	0.016	0.002 – 0.017	0.1

The flexibility of the vegetation (grass) was not determined in the experimental study. The flexural rigidity of grass was calibrated in the simulation to reproduce the observed deflected height. In Figure (3.4), the profile is in non-dimensional form and is obtained by combining the results of several experiments with different h/k ratios. The computed results were almost overlapping with that of experimental data. The results showed a good correlation of trend of variation of the velocity with h/k ratio within the range of selected water depth.

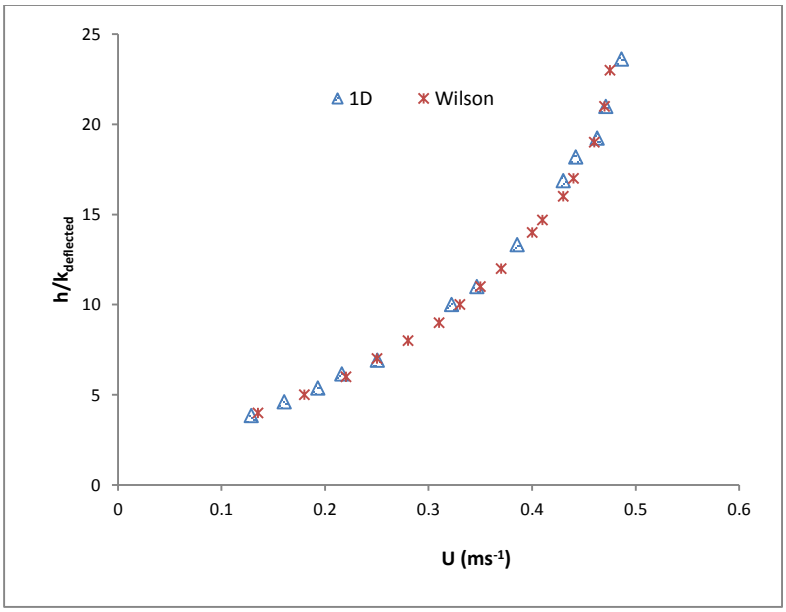

Figure 3.4: Mean velocity with degree of submergence

3.3.4 Flow with submerged rigid vegetation

In the fourth test, the experiment carried out by Huai, et al, (2009) was replicated. The experimental detail can be found in section 2.4 and hydraulic parameters are shown in Table 3.4.

Table 3.4: Parameters of the experiments of Huai et al. (2009) and Kubrak et al. (2008)

Researcher	*N (stems/m^2)*	*h (m)*	*h_v (m)*	*w (m)*	*EI (Nm^2)*	*u (m/s)*	*S (%)*
Huai, et al, 2009	200	0.291	0.19	0.006	3.49	0.127	0.4
Kubrak, et al, 2008	2500	0.239	0.151	8.25e-4	2.0e-04	0.528	0.87

Figure 3.5 show the comparisons between the simulated result and the measured velocity profile. It is clear that the simulated profile agrees well with the measure one.

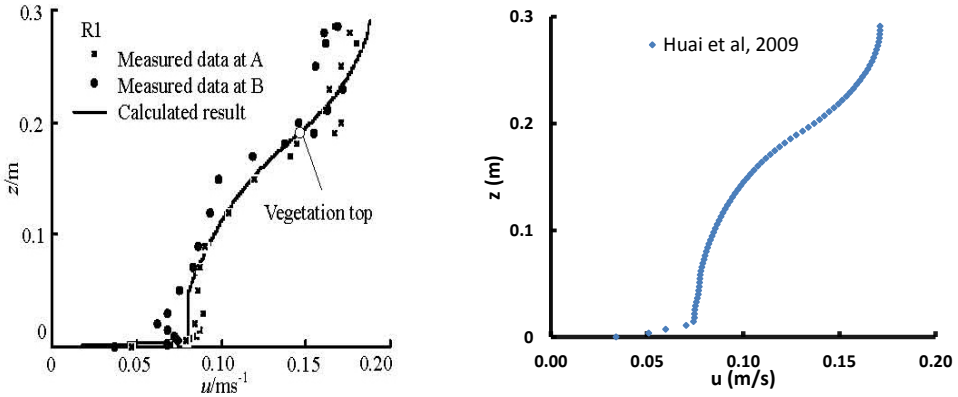

Figure 3.5: Comparison between computed results and measured velocity: Results of Huai et al. (2009) (Left) and present work (Right).

3.3.5 Vertical velocity profile of submerged flexible vegetation

In the fifth test, laboratory experiments in Kubrak et al., (2008) on the velocity distributions through and above submerged flexible vegetation were simulated. Kubrak

et al measured the vertical velocity distributions in a flume containing flexible vegetation under submerged uniform flow condition. The hydraulic parameters are shown in Table 3.4. The present computed results and the measured velocity by the investigators were compared in Figure 3.6, and the agreement is satisfactory.

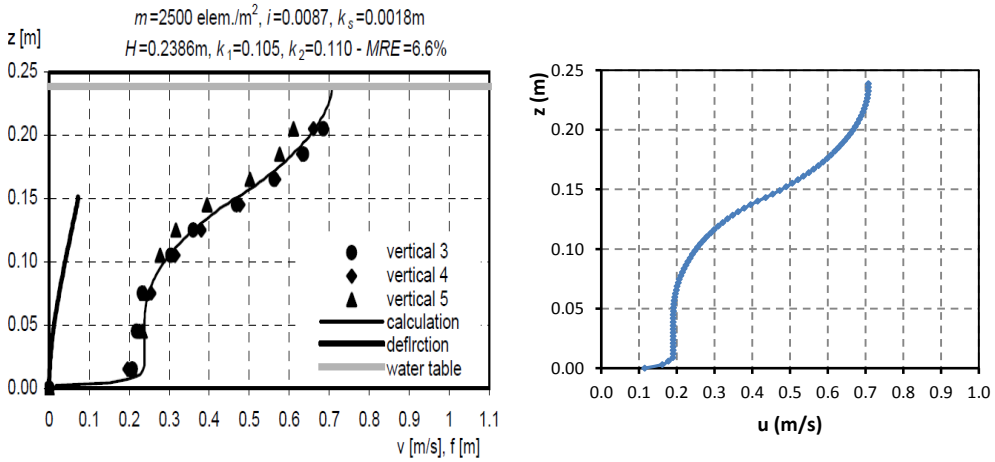

Figure 3.6: Comparisons between computed results and measured velocity: Results of Kubrak et al. 2008 (Left) and present work (Right).

3.3.6 Simulated rigid and flexible vegetation

In the sixth test, the experiments of Dunn et al., (1996) were simulated. The experiments consisted of flows through both flexible and rigid vegetation in a flume of 0.91m wide under steady uniform flow conditions. Commercial drinking straws were used to simulate flexible plants, whereas wooden dowels were used to mimic rigid plants. Experiments 2 and 6 for rigid vegetation and experiments 13 and 15 for flexible vegetation were selected in the present simulation. Mean drag coefficients of 1.1, 1.4, 1.2 and 1.5 were determined in these experiments (2, 6, 13, 15) respectively. Four different plan locations with 10 measuring points in each vertical were considered for each experiment. The hydraulic conditions are as shown in Table 3.5.

Table 3.5: Experimental conditions (Dunn et al, 1996)

Experimental nbr.	***N*** *(stems/m²)*	***h*** *(m)*	h_v *(m)*	***w*** *(m)*	***Q*** *(m³/s)*	***S*** *(%)*
2	172	0.229	0.1175	0.00635	0.088	0.36
6	43	0.267	0.1175	0.00635	0.178	0.36
13	172	0.368	0.152	0.00635	0.179	0.36
15	43	0.257	0.132	0.00635	0.179	0.36

Figures 3.7 and 3.8 showed that the numerical results match well with the experimental results.

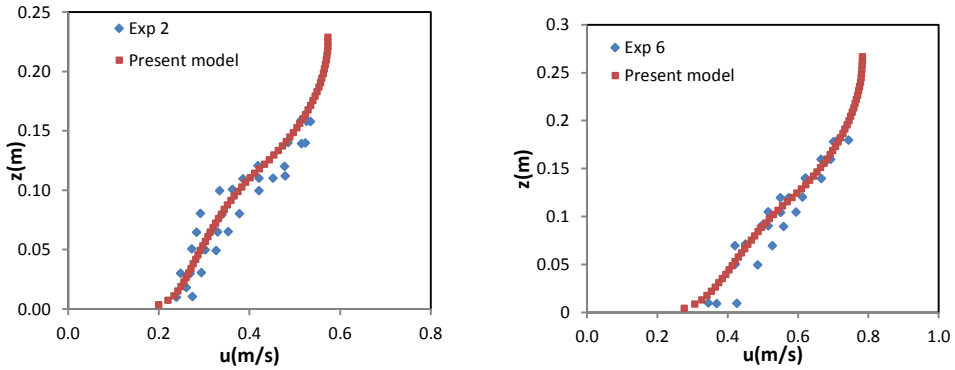

Figure 3.7: Comparison between computed results and measured velocity for flexible vegetation (Data from Dunn et al, 1996)

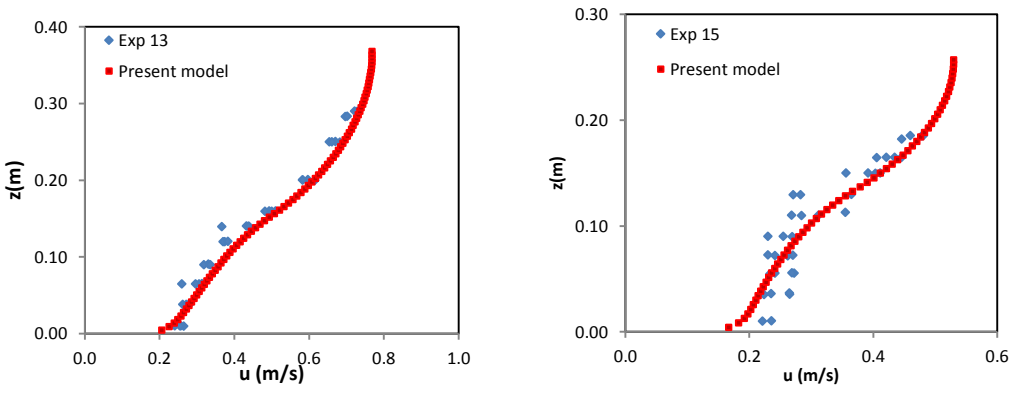

Figure 3.8: Comparison between computed results and measured velocity for rigid vegetation. (Data from Dunn et al, 1996)

Apart from the velocity profile which is of paramount interest in this chapter, the 1-D model produces the vertical distribution of Reynolds shear stresses, turbulence intensity, turbulence kinetic energy as well as the plant's deflected height.

3.3.7 Extensive validation

The capacity of the numerical model in predicting the vegetation induced roughness effect is examined. By computing the velocity profile, the mean velocity can be obtained and the Manning roughness coefficient *n* can be determined using the Manning's equation (2.2). For validating the model, 117 experimental runs based on laboratory flume tests (with varying vegetation parameters, flow depth and channel slope) were obtained from literature and replicated using the 1-D model. In the computations, for cases where drag coefficient is not specified, the value of 1.2 is adopted. More so, where the deflected height is not specified, it will be computed using the large deflection analysis. The Manning's roughness coefficient values obtained from experimental data is computed using equation (2.2) were compared with the computed values. In Figure (3.9), the comparison between measured and calculated *n* values showed good agreement with the available experimental data set, with difference generally within 10%.

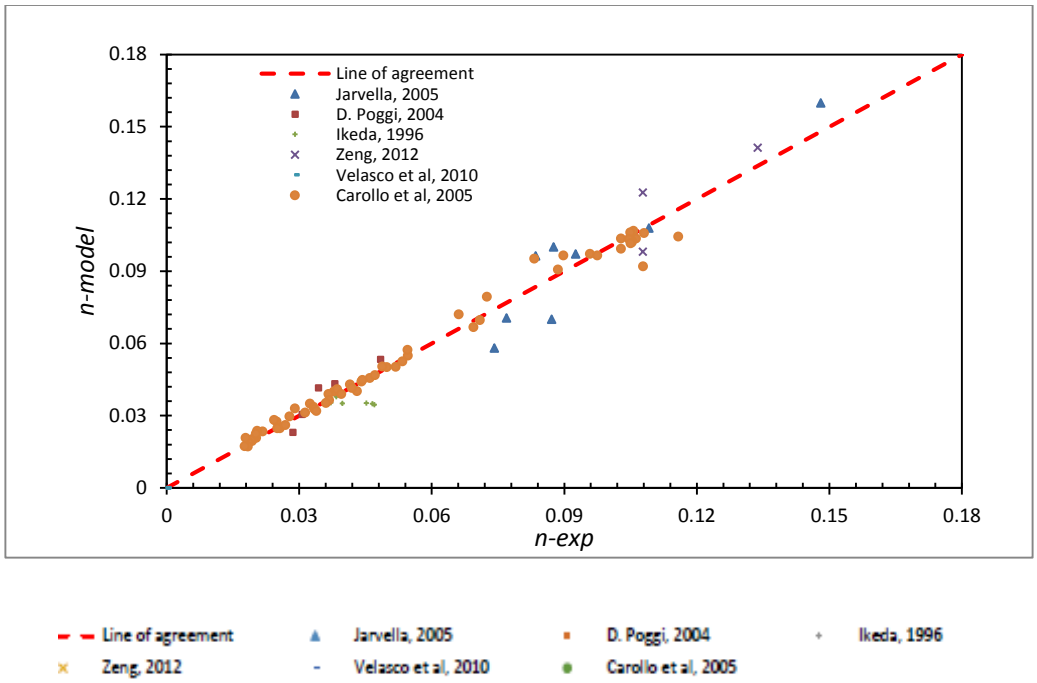

Figure 3.9: Comparison between the measured values and computed values of Manning roughness coefficient ($m^{-1/2}s$)

3.4 Inducing roughness equation for flexible vegetation

In this section, a hydraulic roughness model is proposed for flow over submerged flexible vegetation. A large number of simulations were run for submerged flexible vegetation under varying vegetation parameters, flow depths and zero-plane displacement z_o relating roughness length (equation 3.12 and Figure 3.10) to the total frontal area of vegetation per unit horizontal area.

The zero-plane displacement z_0 is found to be a function of the vegetation parameters. Numerical experiments have been carried out against available experimental data during calibration exercise in (section 3.3) to obtain an empirical equation of z_o which is given by

$$\frac{z_o}{h_v} = \frac{f_v^{\beta'}}{f_v^{\beta'} + \alpha'^{\beta'}} \tag{3.19}$$

where h_v = height of vegetation, $f_v = f_{rk}.h_v$, α' *and* β' are constant and equal to *0.5* and *0.7* respectively. The curve for zero – plane displacement parameter, z_o/h_v against vegetation parameter, f_v is shown in Fig. 3.11. A convergence of the curve is observed, irrespective of the submergence ratio.

The fitting equation (3.19) is in reasonable agreement with the equation (3.20) proposed by (Raupach, 1994).

$$\frac{z_o}{h_v} = 1 - \frac{1 - exp\left(-\sqrt{a_1 FAI}\right)}{\sqrt{a_1 FAI}} \tag{3.20}$$

where $a_1 = 15$ and *FAI* can be related to other parameters in this present study by

$$FAI = Nwh_v = \frac{f_{rk} h_v}{C_d} = \frac{f_v}{C_d} \tag{3.21}$$

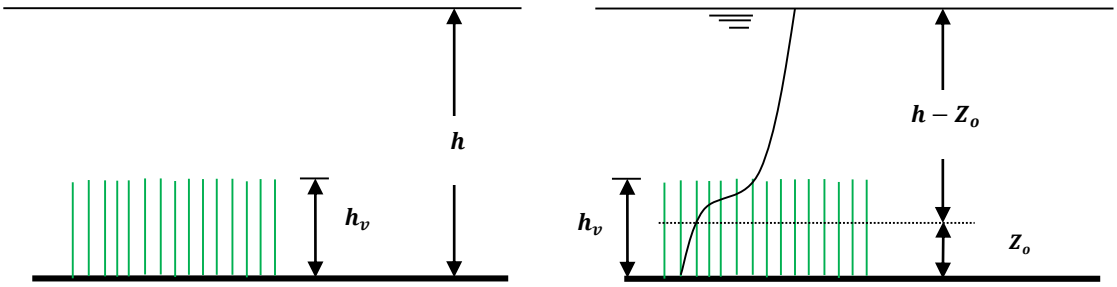

Figure 3.10: Geometrical parameters of submerged vegetation

The Manning's roughness coefficient can be related to the vegetation parameters and flow depth as

$$n = \phi_1\{C_d, N, w, h_v, h, z_o, g\} \tag{3.22}$$

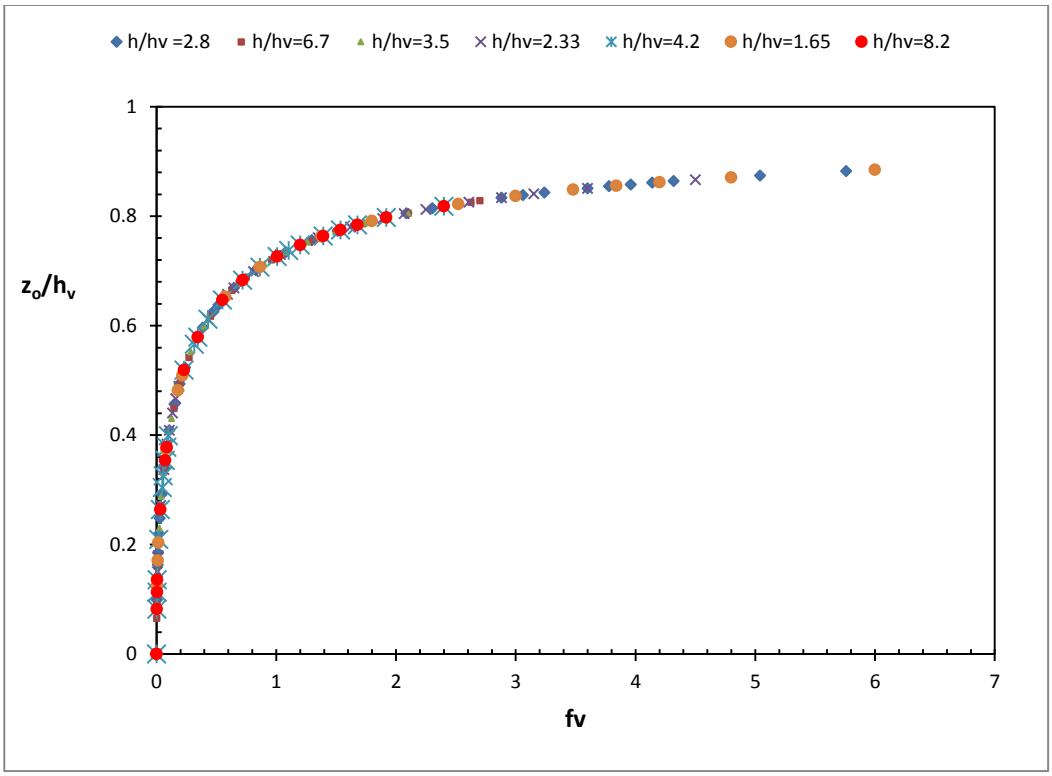

Figure 3.11: Fitting equation for zero-plane displacement and vegetation parameters

The equation can be further simplified to the following non-dimensional form:

$$n = \frac{h^{1/6}}{\sqrt{g}} \phi_2\{f_v, h/h_v, z_o/h_v\} \tag{3.23}$$

3.4.1 Synthetic velocity profile data and fitting of equation

The synthetic velocity profile data were generated for a large number of cases with different vegetation density, flexibility, and submergence ratio as well as zero-plane displacement. Using the synthetic velocity profile, the mean velocity over entire flow depth is computed by averaging the mean depth velocity, hence, the Manning's roughness coefficient (n) is obtained using equation (2.2). The relationship between n and the vegetative resistance parameter (f_v) obtained from the synthetic data is shown in

Figure 3.12 as the dotted blue line. An empirical equation of form (3.24) is proposed. The fitting of the proposed equation with the synthetic data is shown in Figure 3.12.

$$n = \frac{h^{1/6}}{\sqrt{\frac{2g}{f_v}} + A'\frac{\sqrt{g}}{\kappa} ln\left(\frac{h - z_o'}{h_v - z_o'}\right)} \tag{3.24}$$

where von Karman constant, $\kappa = 0.41$ and, A' is an empirical parameter, which is dependent on $\frac{h}{h_v}$ .The parameter, z_o', represents a modified zero-plane displacement parameter and is given by

$$z_o' = z_o exp\left(\frac{-\eta}{f_v^{3/4}}\right) \tag{3.25}$$

where $\eta \approx 3.7$.

In equation (3.24) the variations of submergence ratio with vegetation parameters and zero-plane displacement have shown that the parameter A' is a non-linear function of h/h_v. The fitting of equation (3.25) to the synthetic data from numerical simulation leads to the following quartic polynomial equation

$$A'\left(\frac{h}{h_v}\right) = a_1\left(\frac{h}{h_v}\right)^4 + a_2\left(\frac{h}{h_v}\right)^3 + a_3\left(\frac{h}{h_v}\right)^2 + a_4\left(\frac{h}{h_v}\right) + 0.6026 \ : R^2 = 0.991 \tag{3.26}$$

where a_1, a_2, a_3 and a_4 are constants equal to $0.0043, -0.0608, 0.2550$ and -0.1604 respectively. Figure (3.12) shows that the fitting is the best at lower values of h/h_v, and has larger discrepancy when f_v is low and h/h_v is high (that is, in the low hydraulic resistance range).

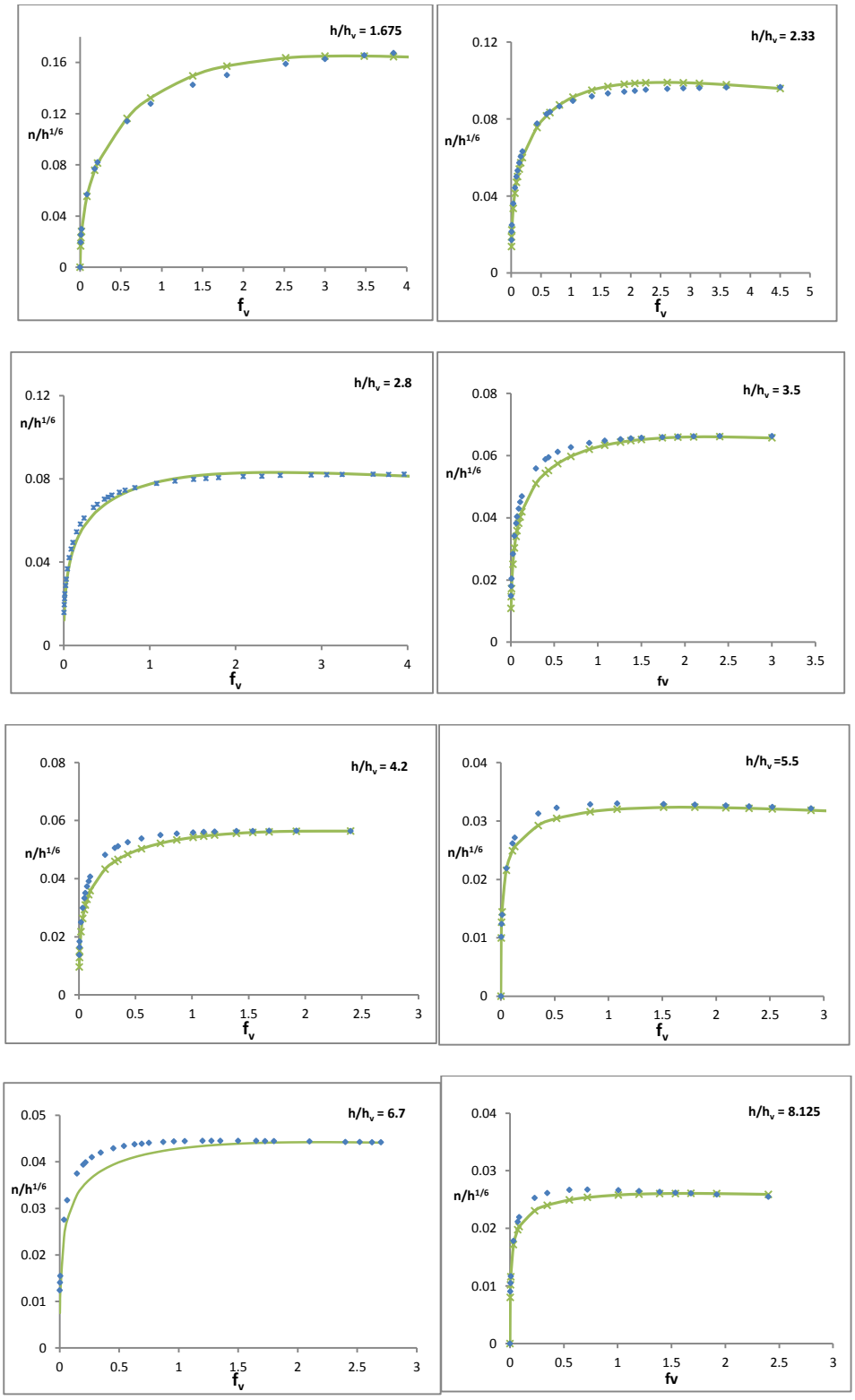

Figure 3.12: Fitting equation (3.24) and synthetic data for different submergence ratio (Blue dots denote synthetic data; green line - fitting equation)

3.4.2 Simplified roughness equation

A simplified form of equation (3.24) can be obtained when exponential function in equation (3.25) approaches 1 at very high vegetation density ($f_v \rightarrow \infty$). In that case, the zero-plane displacement z_o can replace the modified zero-plane displacement parameter, (that is, $z_o' \rightarrow z_o$), then, equation (3.24) takes the following form:

$$n = \frac{h^{1/6}}{\sqrt{\frac{2g}{f_v}+A\frac{\sqrt{g}}{\kappa}ln\left(\frac{h-z_o}{h_v-z_o}\right)}} \tag{3.27}$$

The fitting of equation (3.28) to the synthetic data yields a second order polynomial equation of parameter *A* as a function of the relative submergence h/h_v with correlation coefficient approximately equal to 1 and it is given by

$$A\left(\frac{h}{h_v}\right) = b_1\left(\frac{h}{h_v}\right)^2 + b_2\left(\frac{h}{h_v}\right) + 0.3951 \tag{3.28}$$

where b_1 and b_2 are *0.0165* and *0.0379* respectively.

3.5 Verification of the roughness equations

In the literature, several empirical equations have been proposed for vegetation induced roughness, including Kouwen and Unny (1973) for flexible vegetation; Stone and Shen, (2002); Baptist et al., (2007), Gu, (2007), Yang and Choi, (2010) and Cheng, (2011) for rigid vegetation. The equations are generally of the following form:

$$n = \frac{\boldsymbol{h^{1/6}}}{\sqrt{\boldsymbol{g}}\left[\boldsymbol{a}+\boldsymbol{b}log\left(\frac{\boldsymbol{h}}{\boldsymbol{k_s}}\right)\right]} \tag{3.29}$$

where *a* and *b* are parameters dependent on the flow and vegetation parameters; k_s is a roughness parameter. The specific forms of the equations are as follows:

3.5.1 *Baptist et al. s' roughness model*

The hydraulic roughness model of Baptist et al. (2007) is given by

$$n = \frac{h^{\frac{1}{6}}}{\sqrt{\left(\frac{2g}{f_v}+n_b\right)+\frac{\sqrt{g}}{\kappa}ln\left(\frac{h}{h_v}\right)}} \tag{3.30}$$

where n_b is the bed roughness which is negligible for smooth flume beds and very dense vegetative open-channel flows.

3.5.2 *Yang and Choi's model*

The original form of the model of Yang and Choi (2010), equation (2.26), can be simplified by dividing both the numerator and denominator by$\sqrt{h}$, using $h = h_s + h_v$ and substituting $f_v = C_d N w h_v$, to yield the following equation:

$$n = \frac{h^{1/6}}{\sqrt{\frac{2g}{f_v}+\frac{1}{\kappa}\sqrt{\frac{g(h-h_v)}{h}}\left[C_u ln\left(\frac{h}{h_v}\right)-\left(\frac{h}{h_v}-1\right)\right]}} \tag{3.31}$$

3.5.3 *Cheng's model*

Cheng's model (equation 2.27) can be converted by substituting

$\phi = \frac{N\pi w^2}{4}, \lambda = Nw$ and $f_v = C_d N w h_v$, to the following form:

$$n = \frac{h^{1/6}}{\sqrt{\frac{g(4-\zeta)^3}{32 f_v}\left(\frac{kh_v}{h}\right)^{1.5}+\frac{C\sqrt{g}}{\kappa}\left[\left(\frac{h-h_v}{w}\right)\left(\frac{4}{\zeta}-1\right)\right]^{0.0625}\left(1-\frac{h_v}{h}\right)^{1.5}}} \tag{3.32}$$

where, C = 1.8614, $\kappa = 0.41$ and $\zeta = N\pi w^2$

The proposed models are compared with the existing models using 431 experimental datasets from 18 different investigators. The results are shown in the

Figures 3.13 and 3.14 for cases of rigid vegetation, while Figure 3.15 is for flexible vegetation. Generally, the results depict that the present model yields better results than those of the existing roughness equations, especially for cases of flexible vegetation.

3.6 Field data

Several empirical equations were validated against laboratory measurement data set only (e.g. Klopstra et al, 1997; Stephan and Gutknecht, 2002; Stone and Shen, 2002; Gu, 2007 and Baptist et al, 2007). The present study extends the validation against existing field data. Nikora et al., (2008) conducted field survey to determine the hydraulic roughness of several vegetated streams. The reach lengths of streams vary from 12 to 30m and stream widths vary from 1.81 to 8.06m. The vegetation covered parts of the streams and were in patch form. The stem diameters of the vegetation were between 4-6mm, and vegetation densities were based on the plants characteristics (Bowmer et al, 1995; Hofstra et al, 2006; Kevin et al, 2007 and Nikora et al, 2008) and the distribution of patches. The exact values of vegetation density thus are uncertain, and the values of the parameter f_{rk} is not available and need to be estimated. For the selected densities and taking into account the flexibility of the plants, the drag coefficient is found to be in order of 1 based on sensitivity analysis. The exact value depends on the streamlined flow effect due to vegetation deflection. Figure 3.16 showed the computed Manning's roughness coefficients compared with the field measured values as reported by Nikora et al. The results show a good agreement with the field data.

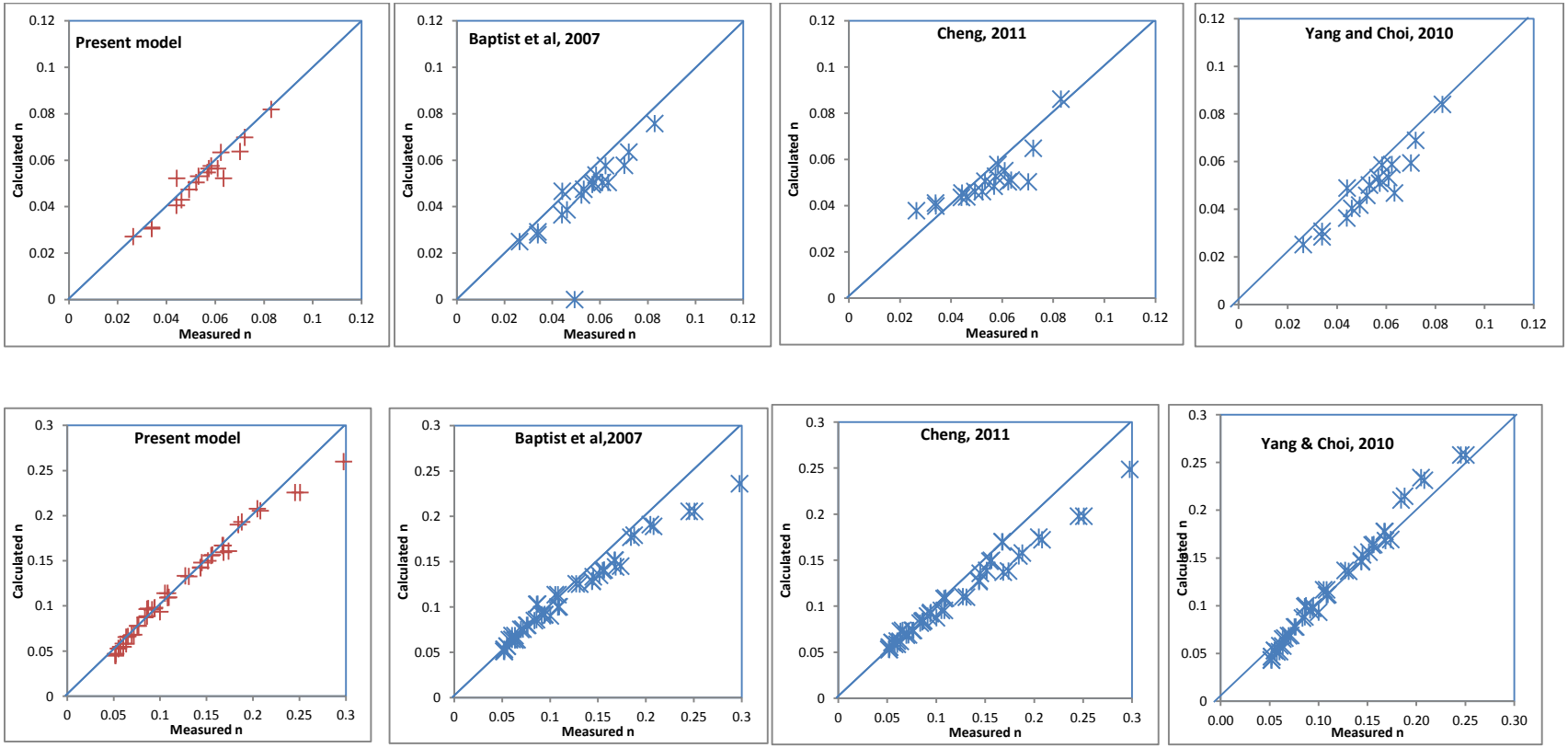

Figure 3.13: Vegetative Manning's roughness, n ($m^{-1/3}s$) comparison, (top row) for Dunn et al., (1996) and (bottom row) for Meijer, (1998).

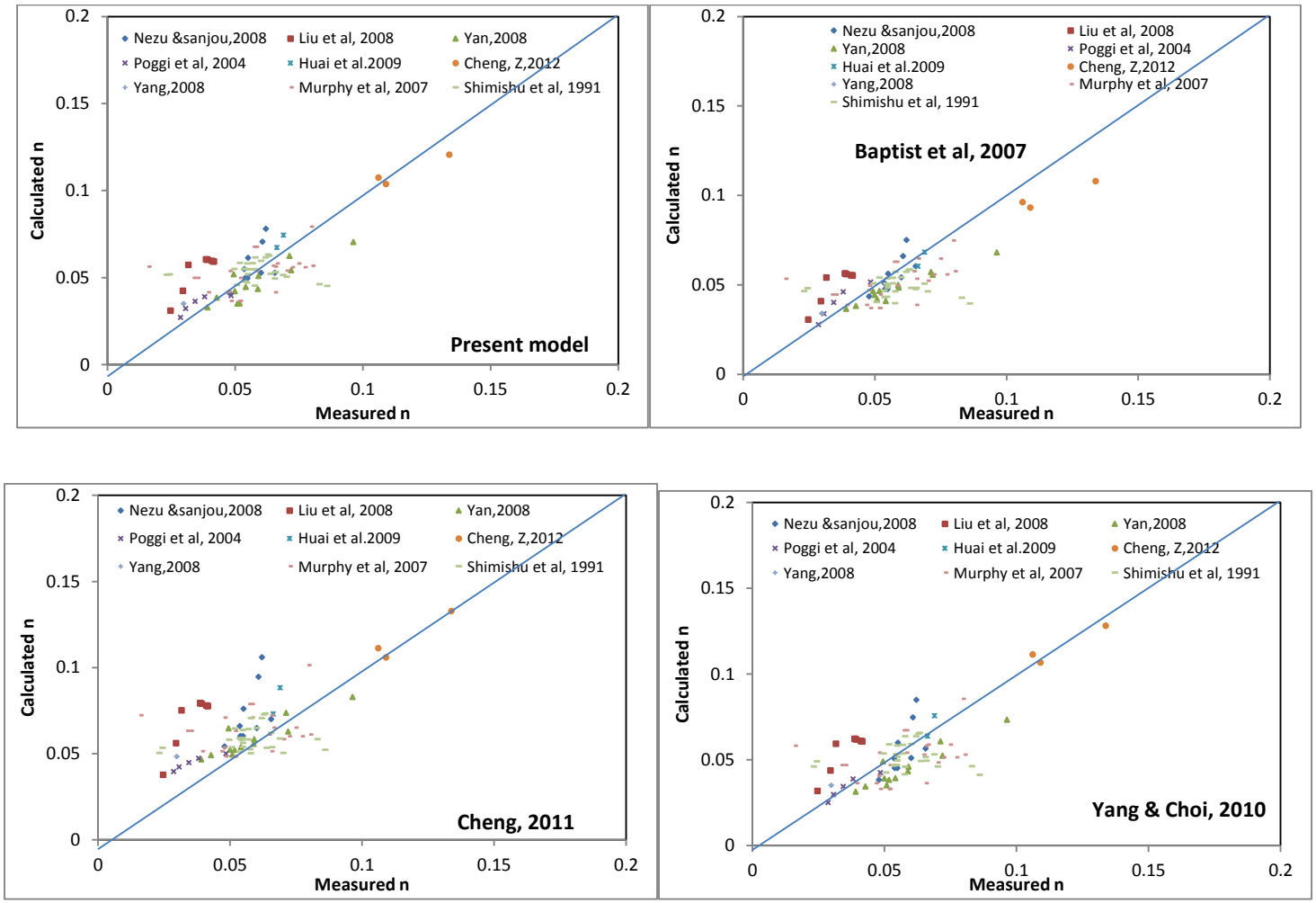

Figure 3.14: Comparison between the measured and calculated values of n ($m^{-1/3}s$) using 85 experimental datasets from nine authors

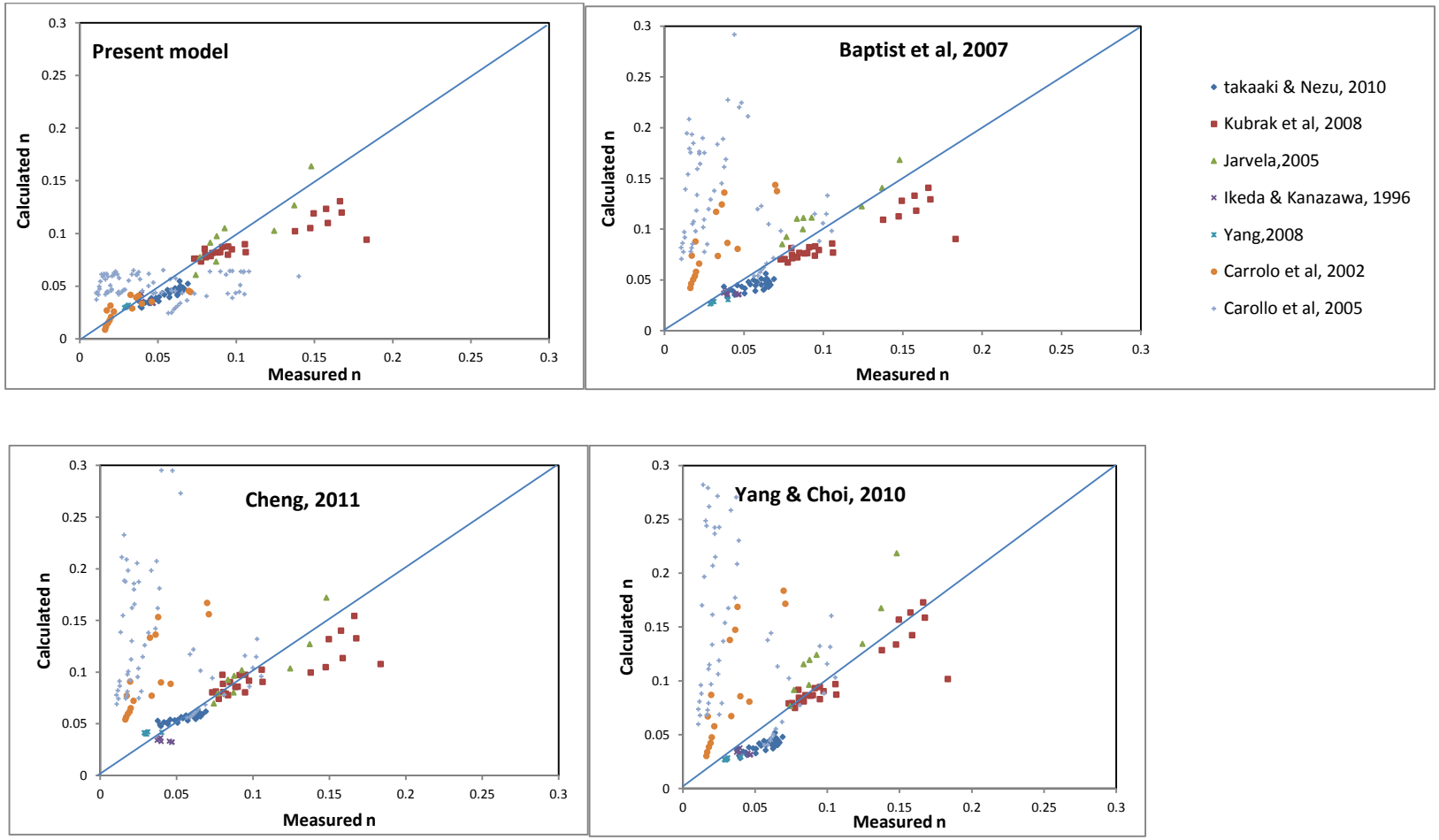

Figure 3.15: Comparison between the measured and calculated values of n ($m^{-1/3}s$) for flexible vegetation

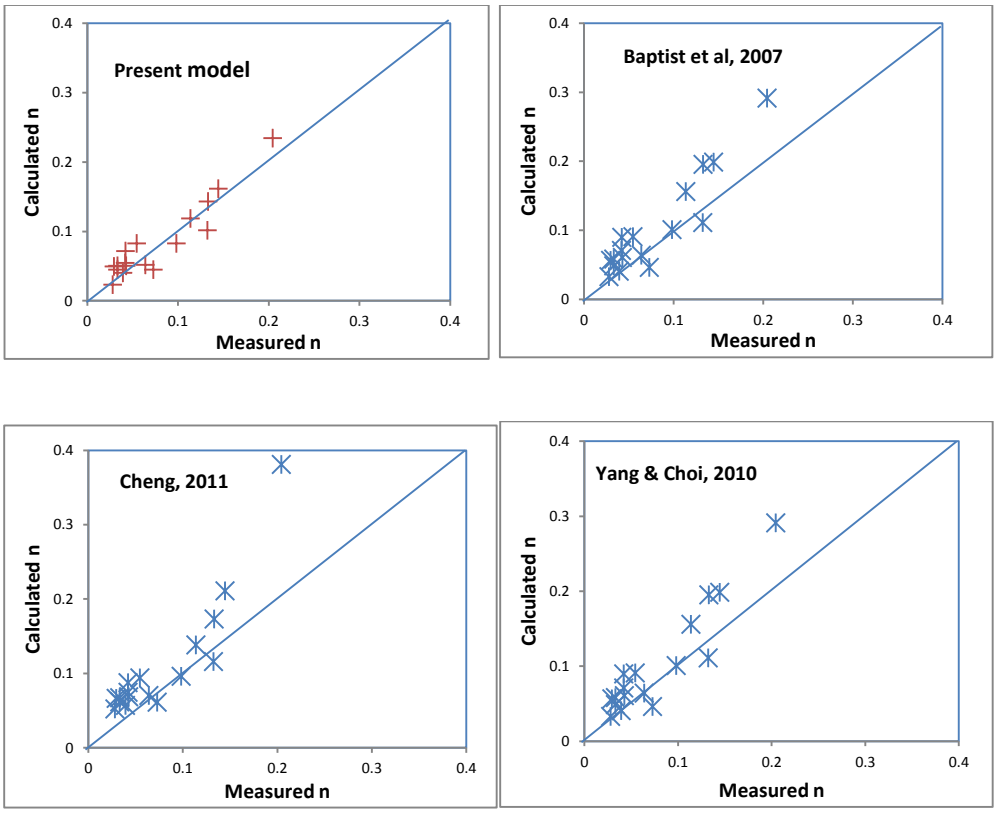

Figure 3.16: Comparison between the field-measured and calculated values of n ($m^{-1/3}s$).

3.7 Summary

A new hydraulic roughness equation has been derived for submerged flexible vegetation. The equation relates the Manning roughness coefficient to the vegetation parameters, flow depth and a zero-plane displacement parameter. The equation is fitted from synthetic velocity profile data generated by a one-dimensional model. The performances of the equations were assessed in two successive stages: comparison with Manning roughness coefficient from experimental data set and then field data. The derived equation and its simplified form have been compared with existing equations

using data set of flume experiments conducted by various researchers for vegetation classified under three categories: type (natural or artificial), areal density (low to high) and flexibility (rigid or flexible). The performance of the equations is generally better than previous equations without the zero plane displacement parameter. The equations have been subsequently applied to the field successfully. The accuracy of the equation is expected to be increased if the drag coefficient can be determined accurately.

4 Laboratory setup for physical modeling description of gradually varied flow through vegetation emergent and submerged flexible blade-type finite vegetation patch

4.1 Experimental techniques

The main objective of this chapter is to provide a step by step description of the laboratory set up to simulate investigate the hydrodynamics of gradually-varied flow through vegetation. The laboratory experiments were conducted in the Hydraulic laboratory of Civil and Environmental Engineering department at Hong Kong Polytechnic University, Hung Hom, Kowloon, Hong Kong. The experimental facilities, model building and measuring devices employed in this study are described as follows:

4.1.1 Tilting, slope – adjustable rectangular flume

The experiments were conducted in a 0.31m wide, 0.40m deep and 12.50m long tilting and slope – adjustable rectangular flume manufactured by GUNT Hamburg, Germany (Plate 4.1). The sidewalls and bottom are made of glass and steel respectively. The longitudinal bed-slope of the flume can be varied from - 0.5 to 2.5%.

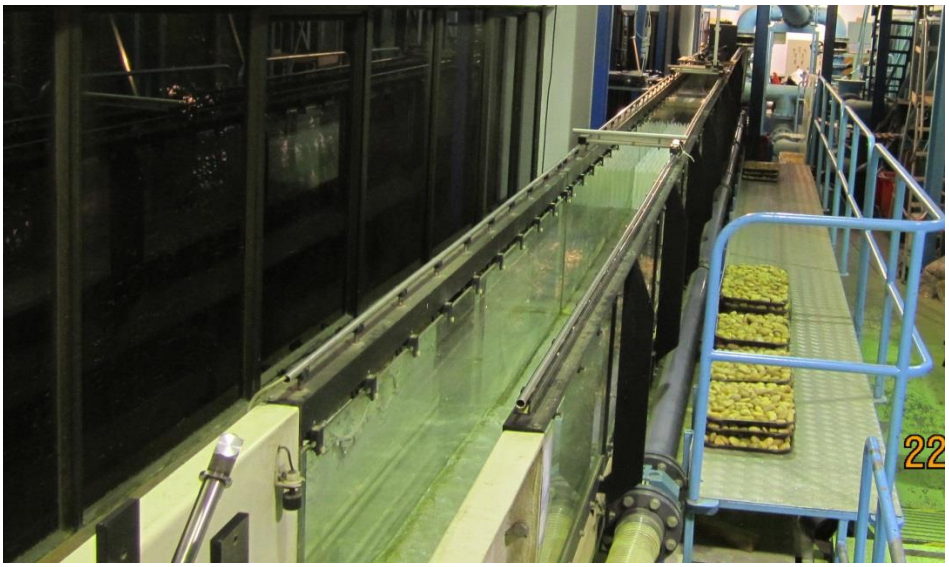

Plate 4.1: Tilting, slope – adjustable rectangular flume

Flow rates were measured from a built-in electromagnetic flowmeter installed in the flow return pipe (Plate 4.9). The flow at the entrance of the channel was straightened using a series of honeycomb grids, thereby preventing the formation of large-scale flow disturbances. The flume received a constant supply of water from a head tank with adjustable tailgate at the downstream end of the flume to regulate the flow depth. Water leaving the flume entered a large sump under the flume, where it was recirculated to the constant head tank with a pump.

4.1.2 Vernier point gauge

The Vernier point gauge was used to measure the flow depth along the flume for both emergent and submerged cases. The channel surface slopes were calculated from longitudinal flow - depth variations, which were measured with a Vernier point gauge with $\pm$1 mm accuracy. Plate 4.2 shows two movable wheeled trolleys located along the double-rail track on the top of the flume which were used to mount the point gauge.

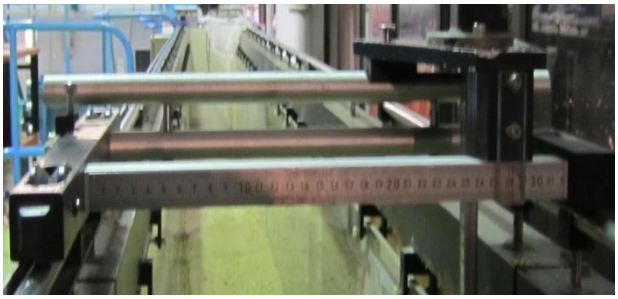

Plate 4.2: Movable wheeled trolleys with Vernier point gauge

4.1.3 Ventrino Velocimeter

A three dimensional Nortek Ventrino velocimeter also known as Accoustic Doppler velocity meter (ADV) was used to measure the instantaneous velocity components of water in an open channel using Doppler Effect. It is remote – sensing, 3-D velocity sensor that uses pulse-to-pulse coherence method of measurement (Lohrmann et al. 1994; Zeng, 2012). ADV's has a variety of configurations; side-looking or down-looking, 2 or 3 dimensional velocities measurements and varieties of set-up configurations depending on the flow conditions. The instrument has gained a lot of application both in the laboratory and field measurement of 2 and 3 dimensional velocities. As shown in Plate (4.3), the probe is side-looking and consists of four receive transducers and a transmit transducer. The four receive transducers are mounted

separately inside a receiver arm and the transmit transducer is located in the centre of the probe. The probe is usually inserted into the flow, but this does not distort the measurement because the sensing volume is several centimeters away from the entire parts of the probe where the beams intersect to reduce flow interference.

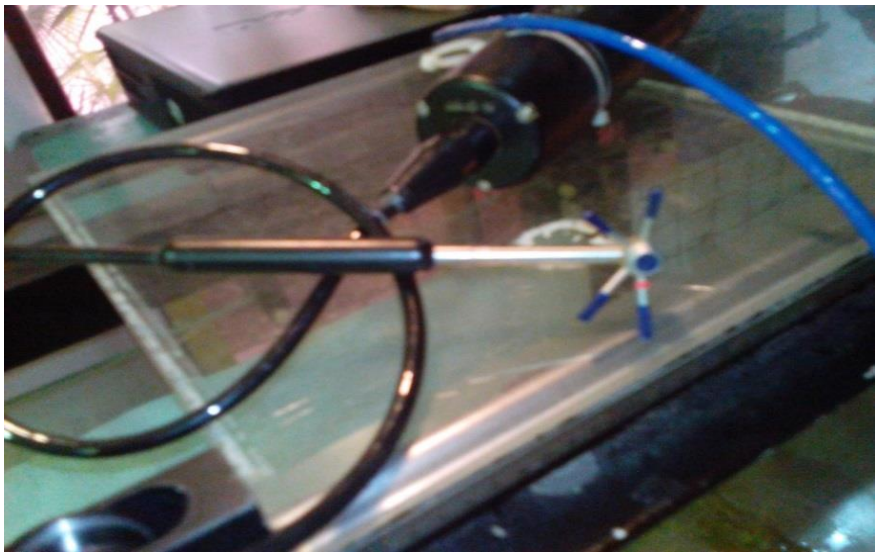

Plate 4.3: 3D Nortek Ventrino Side-looking ADV

At 50mm below the transmit transducer is a sensing (or sampling) volume (see Plate 4.4). The sampling volume is a cylindrical water column with a user defined height of 3 - 15mm and a fixed diameter of 6 mm. Sampling volume of 7mm was used throughout this study. The sampling rate of the ADV is adjustable within the frequency range of (0 – 200Hz). The instruments operate on acoustic frequency of 10MHz. In terms of set-up, it is easy to mount, maneuver and operate within the flow field. The principle of operation follows that the transmit transducer generates acoustic signal that

propagate through the fluid and fraction of the signal is reflected back by the sound scattering particles present in the flow. These particles are assumed to move at the fluid velocity. The receive transducers detect the reflected scattered signal (i.e., echoes) originating at the sensing volume referred to as Doppler shift. The Doppler shift measured at the receivers give an estimate of the flow velocity components. ADV measures velocity of the scattering particles from two consecutive pulses. A computer is connected to the Ventrino to obtain the real time velocity series data. Raw experimental data are gathered using Ventrino plus software. The data were analyzed using simple excel program combined with The WinADV software.

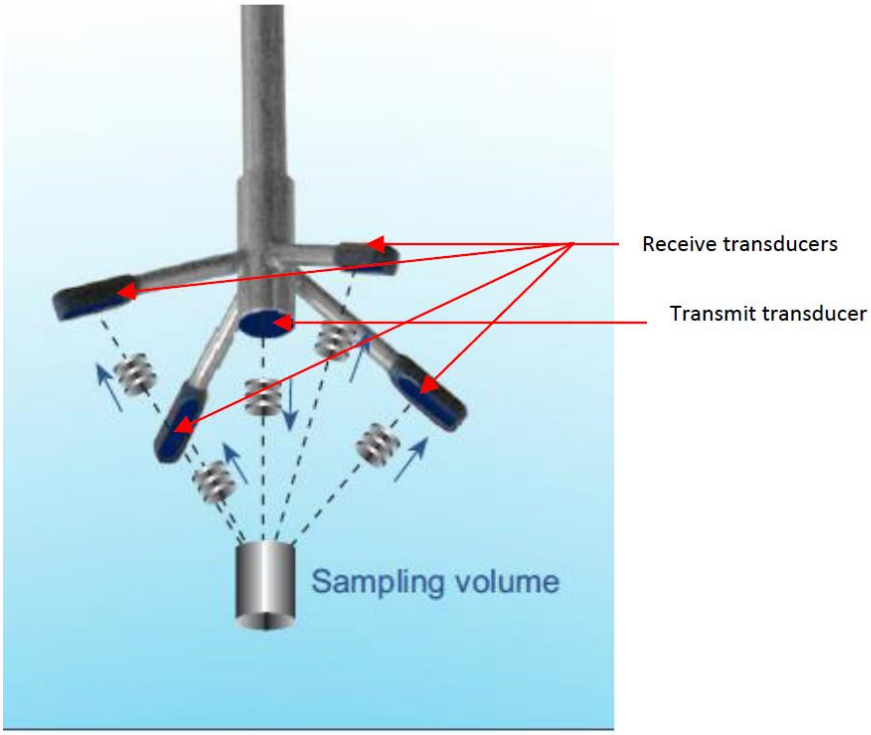

Plate 4.4: ADV probe and schematic view of sampling volume

(Source: Ventrino user guide 2009)

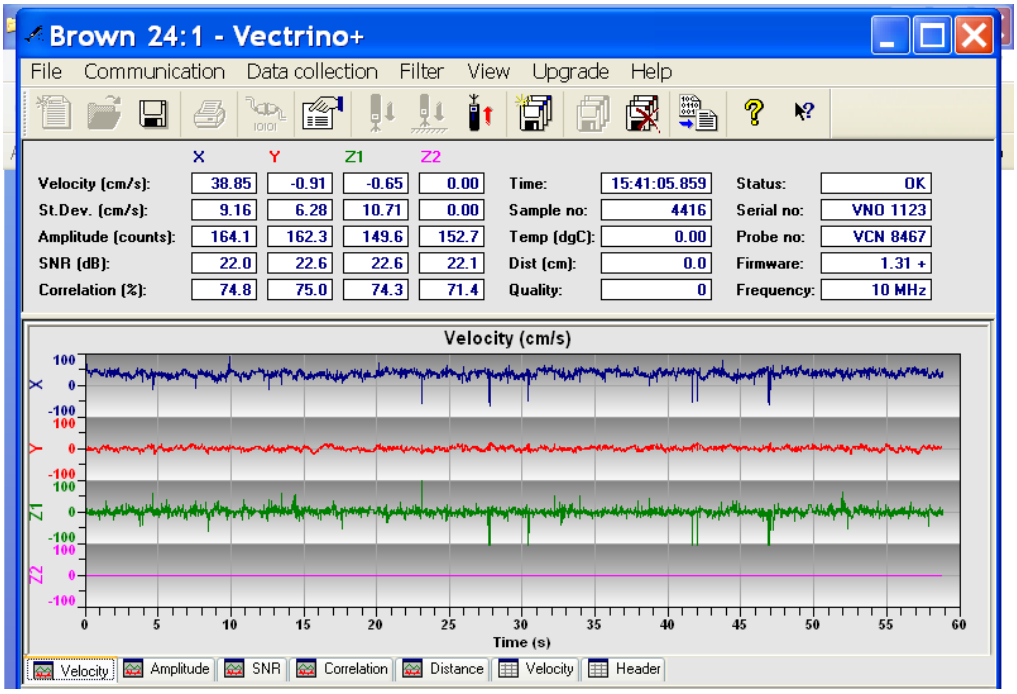

Plate 4.5: Data analysis criteria observation (flow above vegetation)

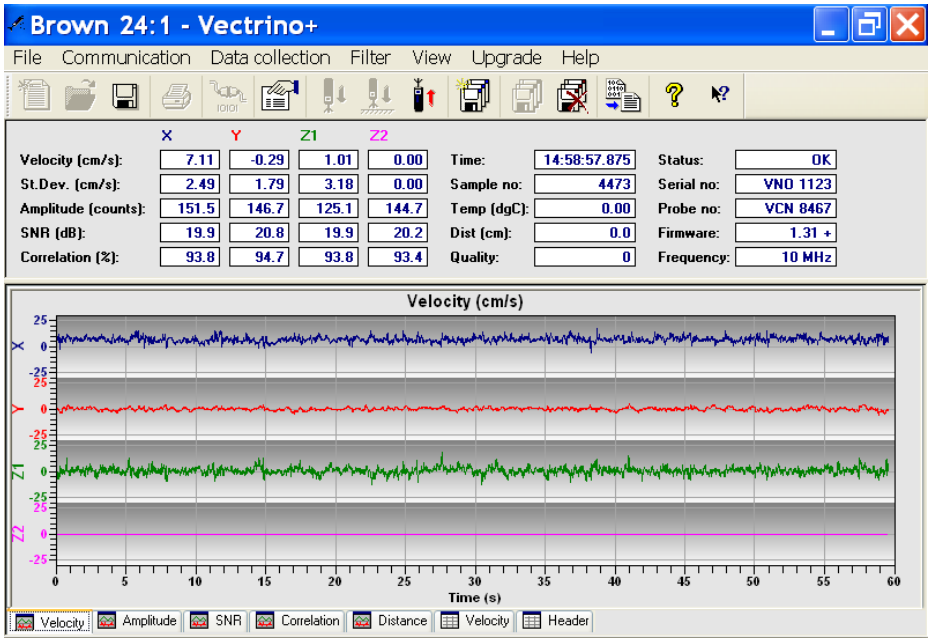

Plate 4.6: Data analysis criteria observation (flow within vegetation)

4.2 Model building

Along the flume was the vegetation patch length of 2.4m long and 0.3 m wide, which represented the flexible vegetation. The vegetation was modeled with arrays of semi-rigid cable tile blades. It is strap-like, thereby resemble sea-grass morphology. The cable tiles were attached to the PVC base boards using adhesive (plate 4.7). The finite artificial vegetation patches of solid volume fractions (ϕ) ranging from 0.005 to 0.121 have been used and the stem Reynolds number ($Re = Ub_v/\upsilon$) ranges from 500 – 2600, where U = cross-sectional averaged pore velocity and υ = kinematic viscosity.

Plate 4.7: Modelled vegetation elements and geometrical characteristics

The spacing of blade elements is different for different boards (see Plate 4.8) and allocation of vegetation patterns is listed in Table 4.1.

Table 4.1: Allocation patterns of vegetation elements

Q (m^3/s)	Spacing (m)	N ($stem/m^2$)	λ (m^{-1})
0.0014 - 0.0083	S_y = 0.0125; S_x = 0.0083	9600	72.32
0.0014 - 0.0056	S_y = 0.0125; S_x = 0.0125	6400	48.19
0.0014 - 0.0056	S_y = 0.0125; S_x = 0.0250	3200	24.10
0.0014 - 0.0069	S_y = 0.0200; S_x = 0.0200	2500	18.83
0.0014 - 0.0083	S_y = 0.0200; S_x = 0.0250	2000	15.06
0.0014 - 0.0084	S_y = 0.0125; S_x = 0.0500	1600	12.05
0.0014 - 0.0085	S_y = 0.0125; S_x = 0.1000	800	6.02
0.0014 - 0.0086	S_y = 0.0200; S_x = 0.0400	1250	9.41
0.0014 - 0.0087	S_y = 0.0200; S_x = 0.0500	1000	7.53
0.0014 - 0.0088	S_y = 0.0200; S_x = 0.0800	625	4.71
0.0014 - 0.0089	S_y = 0.0200; S_x = 0.1000	500	3.77
0.0014 - 0.0090	S_y = 0.0500; S_x = 0.0250	800	6.02
0.0014 - 0.0091	S_y = 0.0100; S_x = 0.0260	400	3.01

The finite artificial vegetation patches are of densities, λ = 72.23, 48.19, 24.10, 18.83, 15.06, 12.05, 9.41, 7.53, 6.02, 4.71, 3.77 and 3.01m^{-1}. The cable tile blade is rectangular in cross section and dimensioned as; height, h_v = 250mm, width, w = 7.53mm and thickness, t_v of 1.68mm. Several experimental and analytical approaches to estimate stem C_d are often based on circular cylindrical elements (e.g., Nepf, 1999; Ishikawa et

al., 2000; James et al., 2004; Liu et al, 2008; Tanino and Nepf, 2008; Ferreira et al., 2009; Kothyari et al., 2009; Stoesser et al., 2010 and Cheng and Nguyen, 2011). Cable tile strips are, however used, because of its preserved flexibility due to the smaller thickness and similar geometry to sea grass. A fixed bed-slope of 1.67% was adopted throughout the experiment. The water levels have been adjusted using the tail gate to satisfy emergent and submerged cases.

Plate 4.8: A sectional plan view of the dense vegetation

($\phi = 0.1214$ and 0.00253 arrays)

The blade-type stems are deployed with a regular rectilinear grid pattern as shown in Figure (4.1). The distribution patterns of vegetation elements have been varied both along and across the stream-wise directions to properly account for the interference effects. The spacing S_y and S_x are measured space from center-to-center of the cable tile laterally and longitudinally respectively.

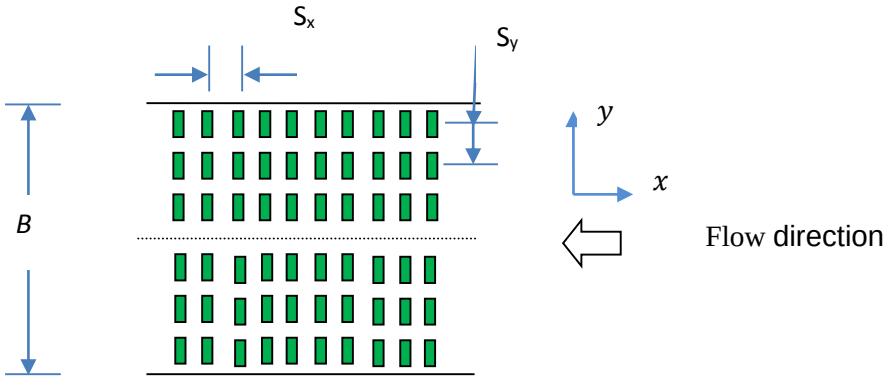

Figure 4.1: Layout of vegetation elements

4.2.1 Measurement techniques

Three parameters were measured for each experimental set up. For submerged vegetation, flow rate was varied and for each flow rate, the water level was measured at intervals along the flume and vertical velocity measured at some selected points within and above vegetation using Acoustic Doppler Velocimeter (ADV). In the case of emergent vegetation only water level was measured at interval for different flow rate. Detail description of measurements is as follows:

4.2.1.1 Water depth and flow rate measurement

A Vernier point gauge (described in section 4.1.2) was used for measuring the water depth and was positioned on the movable wheel trolley at the top of the flume (as shown in Plate 4.2). The water depth was measured at every 5cm along the flume

covering the entire vegetation patch and extending farther from the trailing and leading edges. For emergent cases, the water depth was measured at 13.7cm away from the centerline since the densities are too high. For submerged cases, however, flow depths were measured along the channel centerline. Water flow rate was measured by a built-in electromagnetic flow-meter installed in the flow return pipe (Plate 4.9).

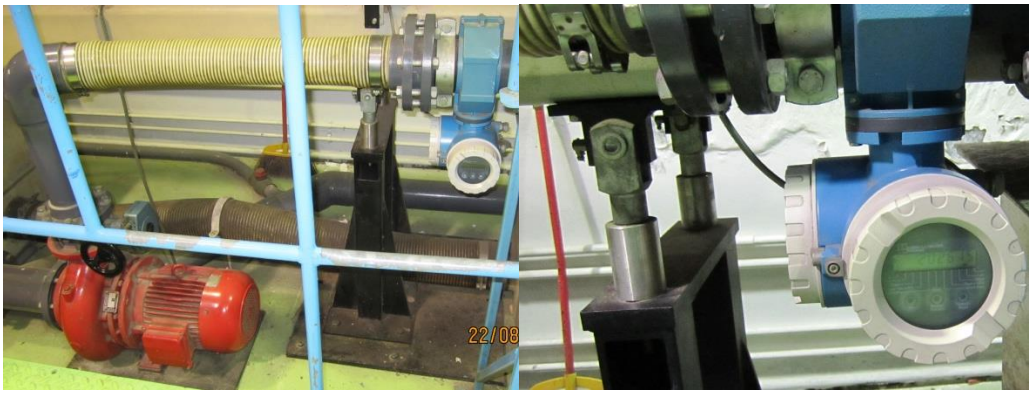

Plate 4.9: Built-in electromagnetic flow meter and pump

4.2.1.2 Velocity measurement

The velocity measurements were carried out using a 3D side-looking Acoustic Doppler Velocimeter (ADV) Vectrino (NORTEK) described in section 4.1.3. Due to the high areal density of the vegetation patch, some blades were removed near the trailing edge for velocity measurements, after water level measurements were completed. To increase the accuracy and reliability of the measurements, the signal-noise ratio (SNR) and the correlation (COR) parameters were evaluated (Zeng, 2012; Wahl, 2000). The raw data were processed if the COR is greater than 70% threshold

and the SNR is greater than 5dB.To capture the turbulence fluctuations, as well as satisfying the SNR and COR requirements, the sampling rate of 75Hz was employed for most experiments except that for cases with $\lambda = 72$ and $48m^{-1}$, the sampling rate was set to 200 Hz and 150 Hz respectively. These setting of sampling rates were based on preliminary investigation by change the sampling frequency and analyzing results to meet the criteria. In addition, the sampling record of 120 s duration was taken at each point to provide reliable estimation of the mean and turbulence quantities. Based on these criteria, more than 75% of the samples were retained in the time series (see Plates 4.5 and 4.6 for screen display during measurement). The criteria is followed throughout the data analysis in this research.

For submerged case, the discharge was varied between 25 m^3/hr and 50 m^3/hr at the interval of $5m^3$/hr. The locations of the vertical velocity measurements were identical for all experiments because the location is far beyond the adjustment length obtained through observations and the empirical equation proposed in Zeng and Li, (2014). The velocity was measured at 10mm interval along the vertical and in some cases at 5mm in the clear water region (i.e., above vegetation layer). The number of velocity measurement along the vertical is not less than 25 for all cases. The longitudinal water depth profile was measured at the middle of the channel using the Vernier point gauge at 5cm interval for cases with S_y = 0.0125m and at 10cm interval for cases with S_x = 0.02m.

The flow is spatially varied due to the finite vegetation patch length. Increasing the discharge leads to the increase in water level, as well as the velocity, particularly in the clear water region. The Reynolds number is defined by blade width scale as $Re =$

$Uw/\boldsymbol{\upsilon}$, where (*U)* and (*w)* are average pore velocity and characteristic blade width, $\boldsymbol{\upsilon}$ is the kinematic viscosity. The side looking ADV measured the velocity at locations at least 2cm below the water surface. The measured velocity profile cannot give the actual mean velocity since the velocity is not uniform across the channel. To estimate the portion of flow within the vegetation region, the following approach is used:

$$Q_v = \left(\frac{Q_1}{Q_1 + Q_2} \right) \times Q_{in}\,; \qquad Q_a = \left(\frac{Q_2}{Q_1 + Q_2} \right) \times Q_{in} \tag{4.1}$$

where Q_v is the flow rate in the vegetation region, Q_a is the flow rate in the clear water region, Q_{in} is the total flow rate in the open channel and, Q_1 and Q_2 are given by $Q_1 = B\int_{z=0}^{z=h_v} U dz$ and $Q_2 = B\int_{z=h_v}^{z=h} U dz$ respectively, *B* is the channel width and *z* is the vertical ordinate. Experiments have shown that the increase in the total flow rate Q_{in} mainly increases the flow rate in the clear water zone, whereas the flow rate within the vegetation zone is almost constant.

It was observed that the simulated plants were deflected (most significantly at the leading edge) and swayed during the experiments (Plate 4.10). The deflection is however small due to the high flexural rigidity of vegetation. Generally, the deflected height exceeded 98% of the original height.

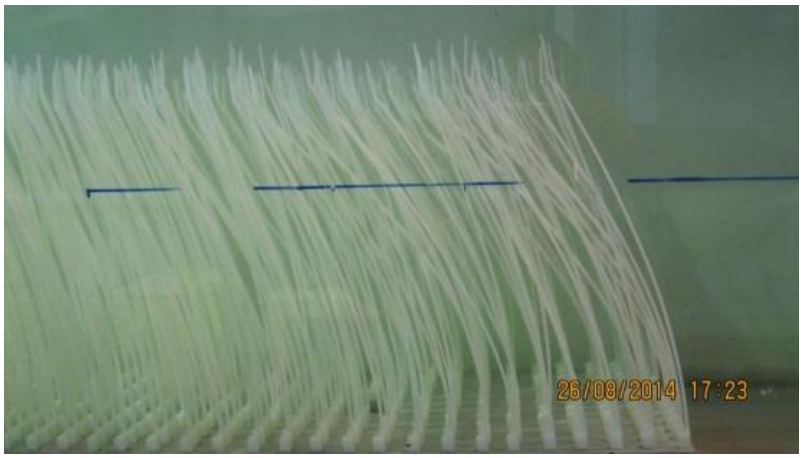

Plate 4.10: Swaying plants

4.2.2 Manning's roughness determination and experimental measurement uncertainty

Manning's equation is the most frequently used approach to calculate the friction head loss open channel flow. The influence of vegetation parameter and flow conditions can lead to varying Manning coefficient. From the laboratory study, knowing the mean cross sectional velocity ($\overline{U}$) in the open channel, the Manning coefficient (n) can be obtained for uniform flow using equation (2.2). For dense vegetation is given as follows:

$$n = \frac{1}{\overline{U}}(h - h_d)^{2/3} S^{1/2} \qquad (4.2)$$

The measured average velocity profile obtained using ADV is obtained along centerline of the flume channel. It cannot give the actual mean velocity since the velocity is not uniform across the channel, hence, the Manning's coefficient is underestimated. Figure (4.2) shows the exaggerated transverse distribution of mean velocity across the channel. The mean average velocity profile measured in this study slightly over estimate the

mean velocity since the measurement is taken at almost the center of the channel (b = $B/2$).

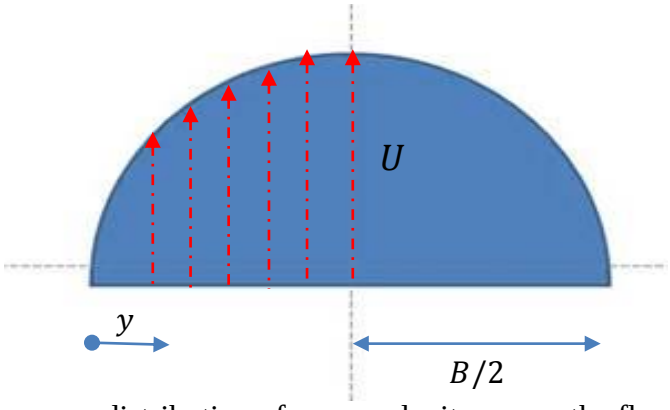

Figure 4.2: Transverse distribution of mean velocity across the flume channel

Uncertainty, therefore, will exist in the measure velocity profile and needs to be estimated. Taking the measured mean average velocity at the centerline as U (see equation 4.1), the theoretical lateral distribution of mean velocity over the profile, $\bar{U}$ is estimated as follows (Ludovic et al., (2015):

$$\bar{U}(z) = \frac{2}{B}\int_0^{B/2} U(z)\left(\frac{2y}{B}\right)^{1/7} dy \tag{4.3}$$

where y is the lateral ordinate.

The uncertainty in the measurement is expressed as:

$$\bar{U} = \frac{1}{1+\psi}U \tag{4.4}$$

where ψ is the correction coefficient in the measurement, hence, estimated in section 6.8 of Chapter 6.

4.3 Summary

A detail description of approach to the study of interference effects on flow resistance parameter, the bulk drag coefficient has been given. This chapter aims to provide a systematic approach to the study of hydrodynamic the interference effects/mechanisms among vegetation stems under a gradually-varied flow condition. The details of the theory of the experiments, interference effects, experimental results and discussion for emergent flow condition and submerged flow conditions are given in chapter 5 and chapter 6 respectively.

5 Gradually varied flow through emergent vegetation patch of high areal density

5.1 Introduction

A complete methodology adopted in this chapter has been described in chapter 4. In chapter 2, section 2.6, it has been pointed out that the key parameter for the quantification of the flow resistance in vegetated waterways is the drag coefficient. The influence of this parameter on flow resistance has been duly examined in section 3.3 of chapter 3. A number of important findings on flow resistance, though, have been obtained from previous studies using the principal assumption that plants are treated as rigid cylinders (i.e., Rigid Cylinder Analogy (RCA) e.g., Nepf, 1999; Ishikawa et al., 2000; James et al., 2004; Liu et al, 2008; Tanino and Nepf, 2008; Ferreira et al., 2009; Kothyari et al., 2009; Stoesser et al., 2010; Cheng and Nguyen, 2011).

Fathi-moghadam and Kouwen, (1997) reported that vegetation density is the dominant parameter for unsubmerged case irrespective of the species, shape and distribution. Not many researchers studied the effect of shape and vegetal density on the vegetation drag (Armanini et al. 2005), however, James et al. (2004), measured vegetal drag for both flexible and inflexible stems by considering various areal densities and the stem drag coefficient was related to the average flow velocity. Righetti, (2008) carried out a series of experiments with drag and velocity measurements on unsubmerged and submerged (real) flexible vegetation, but considered only two different plants densities, in order to distinguish between plant drag and shear stress. The results showed that C_d is highly dependent on vegetation density. Similarly, areal distribution of vegetation has been found to have a strong effect on the vegetation drag coefficient and hence, the fluid

force on the vegetation (Kouwen and Fathi- Moghadam, 2000; Armanini et al. 2005). Wu et al., (1999) developed equations for vegetal drag coefficient for non-submerged vegetation under uniform flow condition using rubberized fibers. They concluded that C_d depends on a vegetative characteristic number which is related to the biomechanical properties of the plants. In fact, various studies suggested different trends for bulk drag coefficient against vegetation density (λ) for cylinder arrays.

Nepf (1999) developed a wake interference model to account for the reduction of drag coefficient of a cylinder in an array. The model predicts that the bulk drag coefficient decreases with the increase in solid volume fraction ϕ. The model results were supported by some available experimental data (Kays and London, 1955, Zdravkovich, 1993).

On the contrary, Stone and Shen, (2002) found that the bulk drag coefficient increases with the solid volume fraction for an array of cylinders with staggered arrangement. The use of the velocity between the stems as the velocity scale reduces the bulk drag coefficient which becomes closer to that of an isolated cylinder. Tanino and Nepf, (2008) carried out experiments to determine drag in a random array of cylinders and found that the bulk drag coefficient increases with ϕ. Kothyari, et al., (2009) measured directly the drag on a single cylinder within a staggered array of cylinders and found that the stem drag coefficient increases logarithmically with ϕ.

For emergent vegetation will high areal density, uniform flow condition seldom occurs and the flow will be gradually varied. Li and Tam, (2002) have studied simulated semi-rigid vegetation (using black rubber rods) under gradually varied flow condition with gentle bed-slope of 1:1000. The longitudinal momentum equation was used to

determine the bulk drag coefficient through the matching of the computed and measured water surface profiles. While the use of circular cylinders to simulate vegetation stems is common, some species of vegetation are of blade type. There is not much study of vegetated flows with blade type elements. Available works include Nezu and Sanjou, (2008) and Yang and Choi, (2009). All these work focus on the flow and turbulent characteristics of the vegetation under submerged condition.

The above works indicate that the bulk drag coefficient may not solely dependent on the solid volume fraction. The distribution pattern of the stems in the array will be important. The present study aims to investigate the interference effects among the vegetation stems through laboratory flume measurements of gradually flow through blade-type vegetation elements. The longitudinal and lateral spacing between adjacent vegetation elements are changed in different sets of experiments to identify the mechanism of flow interference. The bulk drag coefficient for the entire canopy is determined based on the longitudinal momentum equation for gradually varied flow. An empirical formula relating C_d and the longitudinal and lateral stem spacing is proposed.

5.2 Wake interference effect of flow through emergent blade-type vegetation

Vegetation of finite length and width along river channels are not uncommon. For dense vegetation, the hydraulic resistance force offered by the vegetation is often very high and exceeds the gravitational force provided by the bed slope. A water surface profile will be developed to provide the required gravitational force. As a result of this,

the flow is often non-uniform and the water surface profile is gradually varied. This flow condition can be simulated in the laboratory.

The bulk drag coefficient (C_d) for each stem is the parameter to be determined in the laboratory. The trend of C_d with stem density for specific Reynolds number and its dependent on the pattern of stem distribution have been established in this study. Previous studies generally related the bulk drag coefficient of vegetation to the solid volume fraction ϕ of the vegetated zone and the results were found to be inconsistent. Its decreasing or increasing trend with increasing stem density has been discussed extensively in this study using interference mechanisms. Using this mechanism the distribution pattern of stem arrays is studied. The effect of longitudinal spacing at fixed lateral spacing (referred to as sheltering effect) and the effect of lateral spacing at fixed longitudinal spacing (referred to as channeling effect) were studied separately. These effects can be significant for same density arrays, but different distribution patterns.

The fundamental mechanics of vegetation-flow interaction is complicated (as explained in chapter 2). This is because the interrelated variables need to be accounted for; hence, predicting a widely applicable flow resistance law remained an open research area. Within the blade stems, both the form and friction drag are identifiable sources of flow resistance. The latter is due to tangential, viscous shear force between the blade surface and the flow; hence, it is strongly related to the total wetted surface area and roughness of the stem. The form drag, on the other hand, results from the normal forces between the water and blade stem: the pressure on the downstream side is reduced due to flow separation around the blade stem, resulting in a force applied to the blade directed downstream. In principle, the blade exerts an equal and opposite (upstream)

force on the water. The physics becomes more complicated with increasing areal density of blades due to interference effects (as discussed in the next paragraph) and deflection of upstream approaching flow away from the closely packed blades. This phenomenon (of deflected flow) has been explicitly discussed (see White and Nepf, 2007; Zong and Nepf, 2010; Nepf, 2012; Zeng and Li, 2014).

Interference effects on C_d discussed in this study are flow channeling and sheltering effects based on wake formation and scale of eddies. If a stem is situated behind an adjacent stem, it will be subjected to lower velocity of flow due to blocking effect of the upstream stem. If the location is close to the upstream stem, the wake behind the upstream will be interfered with the eddy scale limited by the stem spacing. The reduction in the velocity and the eddy size will lower the pressure drag. The overall drag reduction effect is referred herein as *sheltering effects*. The effect dampen eddies in the flow to scale of blade spacing. Increasing S_x increases the scale of eddies, there is a significant pressure drop (water level drop) for the flow through the constriction between two adjacent blades as shown in plate and water surface profile (see Plate 5.2). It affects the adjacent downstream blades as follows as S_x is increased: i) blockage by neighbouring blades reduces; ii) wake turbulence speed up its point of separation from the downstream blades resulting into pressure drop around the blades leading to higher drag; iii) the downstream velocity is increased in the wake, resulting in higher energy of flow and thus, a higher drag.

On the contrary, if a stem is situated closed to an adjacent stem transversely, the width of the flow path will be narrowed. The velocity of the flow in the narrow gap will be significantly increased due to continuity requirement. A significant portion of

pressure energy will then be converted into the kinetic energy, leading to a further decrease of the pressure at the wake region behind the stem. The drag will then be increased due to the larger pressure difference across the stem. As the lateral spacing increases, the more the pressure energy converted to kinetic energy. The *channeling effect* is used herein to describe the overall drag increase effect (see Plate 5.1). Its hydrodynamics of flow is simulated by changing lateral spacing S_y (at fixed S_x). As S_y increases, the flow is relatively comparable to flow in open water. The hydrodynamic drag, therefore, decreases with stem drag coefficient due low pressure gradient and wake interference.

The "*sheltering*" and "*channeling*" effects can be useful in river restoration. The latter can enhance solute transport and reduce sediment accumulation. The former can be used as erosion control mechanism and provide favorable habitat for aquatic animals. To strike a balance between maintaining ecological preservation and reduction of hydraulic resistance, vegetation management can take account the interference effects among individual stems as serve as a possible scenario.

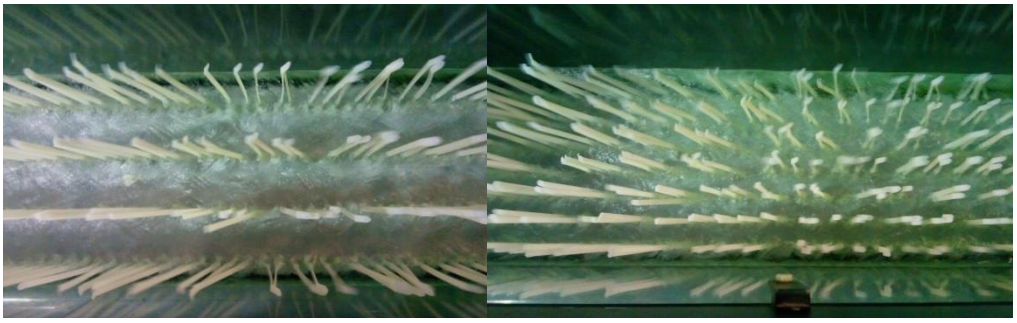

Plate 5.1: Snapshots of flow through simulated vegetation with constant S_x

The key hydraulic parameters for the emergent case are as shown in Table 5.1 and Table 5.2 for fixed lateral spacing and fixed longitudinal spacing respectively. In Table 5.1, the spacing was varied longitudinally between 0.0083m and 0.10m corresponding to spacing ratio between 1.1 and 13.3 respectively, whereas Table 5.2 displays hydraulic condition where the spacing was varied laterally between 0.02m and 0.10m corresponding to spacing ratio between 2.66 and 13.3 respectively. The experimental conditions are selected on the basis of relating the centre-to-centre spacing between blades to width of the blade in order to achieve the goal of high density vegetation. The discharge was varied between 5m^3/hr and 30 m^3/hr at the interval of 5m^3/hr. The lateral gauging position was fixed throughout the experiment.

Table 5.1: Experimental conditions for emergent case (Constant lateral spacing)

Allocation patterns of vegetation elements (m)	Q (m^3/s)	h_{av} (m)	u (m/s)	Re (-)	Fr (-)	λ (m^{-1})
		S_y = constant				
	0.0014	0.0612	0.0833	627	0.1074	
	0.0028	0.1030	0.0990	745	0.0985	
S_Y = 0.0125	0.0042	0.1351	0.1132	853	0.0984	72.29
S_x = 0.0083	0.0056	0.1675	0.1217	917	0.0950	
	0.0069	0.1972	0.1292	973	0.0929	
	0.0083	0.2284	0.1339	1008	0.0894	
	0.0014	0.0724	0.0673	507	0.0799	
S_Y = 0.0125	0.0028	0.1213	0.0804	605	0.0737	48.19
S_x = 0.0125	0.0042	0.1608	0.0910	685	0.0724	
	0.0056	0.1973	0.0988	744	0.0711	
	0.0014	0.0682	0.0684	515	0.0836	
S_Y = 0.0125	0.0028	0.1116	0.0837	630	0.0800	24.10
S_x = 0.0250	0.0042	0.1466	0.0955	719	0.0797	
	0.0056	0.1763	0.1060	798	0.0806	
	0.0014	0.0496	0.0922	694	0.1321	
S_Y = 0.0125	0.0028	0.0895	0.1022	769	0.1090	
S_x = 0.0500	0.0042	0.1194	0.1149	865	0.1062	12.05
	0.0056	0.1458	0.1255	945	0.1049	
	0.0069	0.1655	0.1381	1040	0.1084	
	0.0014	0.0485	0.0934	703	0.1354	
S_Y = 0.0125	0.0028	0.0771	0.1174	884	0.1351	
S_x = 0.1000	0.0042	0.1008	0.1347	1015	0.1355	6.02
	0.0056	0.1258	0.1439	1083	0.1295	
	0.0069	0.1402	0.1614	1215	0.1376	

Table 5.2: Experimental conditions for emergent case (Constant longitudinal spacing)

	S (m)	Q (m^3/s)	h_{av} (m)	u (m/s)	Re (-)	Fr (-)	λ (m^{-1})
		0.0014	0.0587	0.0763	575	0.1006	
		0.0028	0.0916	0.0978	737	0.1032	
S_y	0.02	0.0042	0.12	0.1120	843	0.1032	18.83
S_x	0.02	0.0056	0.147	0.1219	918	0.1015	
		0.0069	0.168	0.1333	1004	0.1039	
		0.0014	0.057	0.0786	592	0.1051	
S_y	0.025	0.0028	0.093	0.0964	726	0.1009	15.06
S_x	0.02	0.0042	0.12	0.1120	843	0.1032	
		0.0056	0.142	0.1262	950	0.1069	
		0.0069	0.164	0.1366	1029	0.1077	
		0.0083	0.182	0.1477	1112	0.1105	
		0.0042	0.081	0.1659	1250	0.1862	
S_y	0.04	0.0056	0.097	0.1848	1391	0.1893	9.41
S_x	0.02	0.0069	0.112	0.2000	1506	0.1908	
		0.0083	0.126	0.2133	1607	0.1919	
		0.0097	0.139	0.2256	1699	0.1932	
		0.0042	0.074	0.1816	1368	0.2132	
S_y	0.05	0.0056	0.0903	0.1985	1494	0.2109	7.53
S_x	0.02	0.0069	0.105	0.2133	1607	0.2102	
		0.0083	0.118	0.2278	1715	0.2117	
		0.0097	0.131	0.2394	1803	0.2112	
		0.0042	0.064	0.2100	1581	0.2650	
S_y	0.08	0.0056	0.074	0.2422	1824	0.2842	4.71
S_x	0.02	0.0069	0.089	0.2517	1895	0.2694	
		0.0083	0.1	0.2688	2024	0.2714	
		0.0097	0.112	0.2800	2109	0.2671	
		0.0042	0.054	0.2489	1874	0.3420	
		0.0056	0.064	0.2800	2109	0.3534	
S_y	0.1	0.0069	0.075	0.2987	2249	0.3482	3.77
S_x	0.02	0.0083	0.085	0.3163	2381	0.3463	
		0.0097	0.092	0.3409	2567	0.3588	

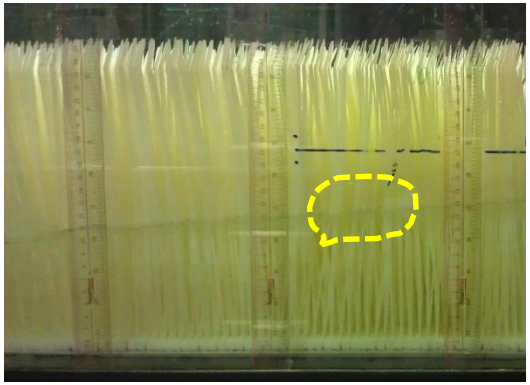

$\lambda = 72.3\ m^{-1}$

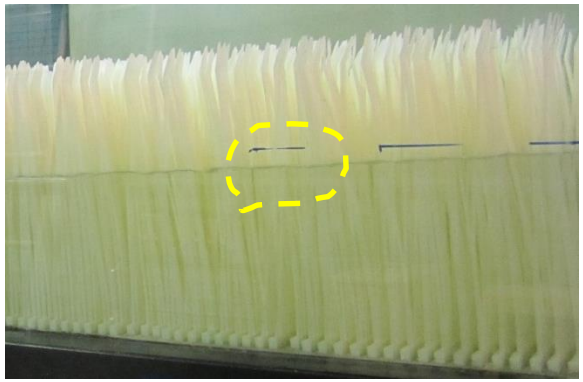

$\lambda = 48.2\ m^{-1}$

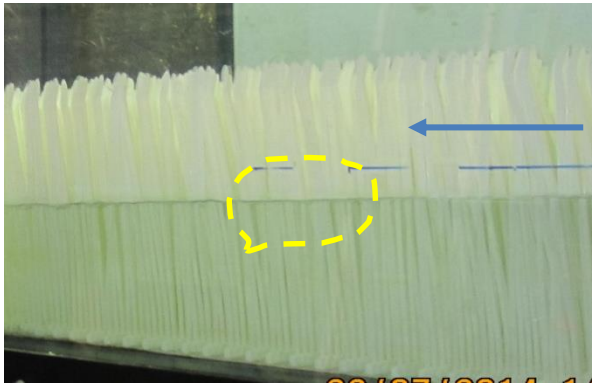

$\lambda = 24.1\ m^{-1}$

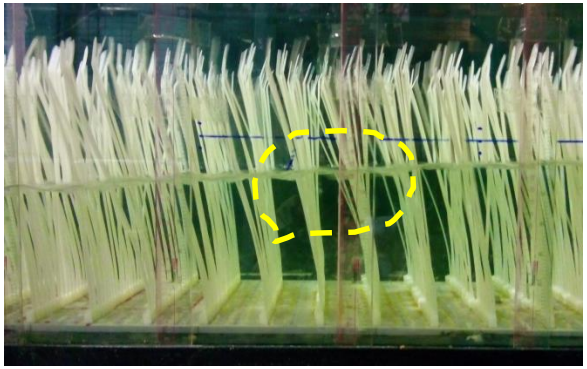

$\lambda = 12.1\ m^{-1}$

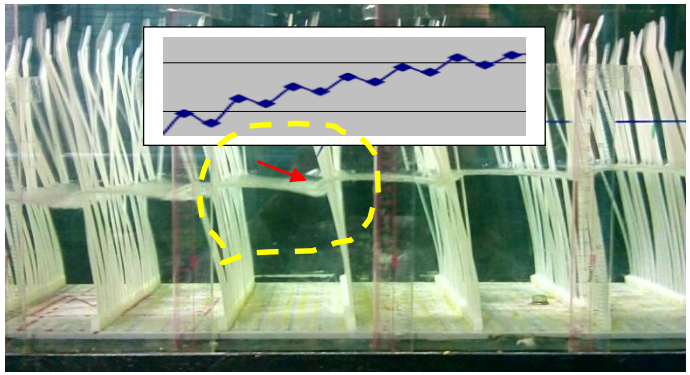

$\lambda = 6.0\ m^{-1}$

Plate 5.2: Snapshots of flow through simulated vegetation with constant S_y

5.3 Theoretical equations

5.3.1 Uniform flow through emergent vegetation

The drag force for each stem blade in stream-wise direction is expressed as

$$F_d = 0.5 C_d \rho h w U^2 \tag{5.1}$$

where C_d (-) is the drag coefficient, ρ is the fluid density *(kg/m^3)*; h is the water depth (*m*); w is the width of stem (*m*); hw is the frontal area and U (*m/s*) is the average pore velocity approaching the stem. For high-density vegetation, the average pore velocity through vegetation as the characteristic velocity for evaluating stem drag is given by

$$U = Q/Bh(1 - \phi l^*) \tag{5.2}$$

in which Q is the flow rate (*m^3/s*), B is the channel width (*m*), $l^* = h_v/h$ is the ratio of wetted length of blades to flow depth, $l^* \cong 1$ for emergent case. $\phi = {wt_v}/{S_x S_y} = Nwt_v = \lambda t_v$ (-) is the average solid volume fraction occupied by vegetation stem and t_v (*m*) is the thickness of the blade. N is the number of vegetation per unit area (*stem/ m^2*). Roughness density λ (*m^{-1}*); S_y and S_x are the lateral and longitudinal centre to centre spacing between blades as defined in Figure (4.1).

The longitudinal momentum equation for a control volume ($B \times \Delta x \times h$, where Δx (m) is the differential longitudinal length) can be given by

$$\rho \frac{\Delta U}{\Delta t} + \rho U \frac{\Delta U}{\Delta x} = -\rho g \frac{\Delta h}{\Delta x} - \tau_s + \rho g S - \frac{1}{2(1-\phi)} \rho C_d \lambda U^2 \tag{5.3}$$

where τ_s*(N/m^2)* is the boundary shear stress, S (-) is the bed-slope, g (*m/s^2*) = acceleration due to gravity, and Δ denotes the differential change. The left hand side of the equation

denotes the rate of change in momentum in the control volume. The first, second, third and fourth terms on the right hand side of the equation are pressure, viscous stress, gravity and vegetation drag respectively.

Generally the boundary shear force is small comparing to the vegetation induced drag force and can be neglected. Assuming the channel is under a steady uniform flow condition, the resulting equation describes the balance between the drag forces as follows:

$$\rho \mathrm{gS} = -\frac{1}{2(1-\phi)}\rho C_d \lambda U^2 \tag{5.4}$$

5.3.2 Gradually varied flow through emergent vegetation

Basically, the assumption of uniform flow eases the interpretation of data as well as enhances the simplification of the method of analysis. Nevertheless, gradually varied type of flow (GVF) is often observed in reality as the hydraulic resistance force offered by the vegetation is often very high for dense vegetation and exceeds the gravitational force provided by the bed slope.

Assuming steady flow condition and neglecting the shear forces at the bed and sidewalls, equation (5.3) becomes:

$$\rho U \frac{\Delta U}{\Delta x} = \rho \mathrm{g}\left(S - \frac{\Delta h}{\Delta x}\right) - \frac{1}{2(1-\phi)}\rho C_d \lambda U^2 \tag{5.5}$$

Utilizing the continuity equation $UhB(1-\phi) = Q$ = constant, we obtain

$$\left(g - \frac{U^2}{h}\right)\frac{\Delta h}{\Delta x} = gS - \frac{1}{2(1-\phi)} C_d \lambda U^2 \tag{5.6}$$

The change in water level in equation (5.6) can be used to describe variation of C_d value along the vegetation patch length. Integrating equation (5.6) between the limits of the initial flow depth, h_o to h with respect to distance x gives the following expression:

$$F(h) = \int_{h_o}^{h} \left(\frac{g - \frac{U^2}{h}}{gS - \frac{1}{2(1-\phi)} C_d \lambda U^2} \right) dh = x + \text{constant} \qquad (5.7)$$

From the measured water surface profile (h against x) for different flow cases, $F(h)$ in equation (5.7) can be evaluated numerically by assuming a value of the bulk drag coefficient which represent the drag coefficient over the entire canopy. Using the trial and errors method, the correct value of C_d gives a straight line of unit slope from the plot of $F(h)$ against x (e.g. Figure 5.1). The measurement uncertainty is related to the coefficient of correlation. Generally, for all the hydraulic conditions, the relative error is less than 2%.

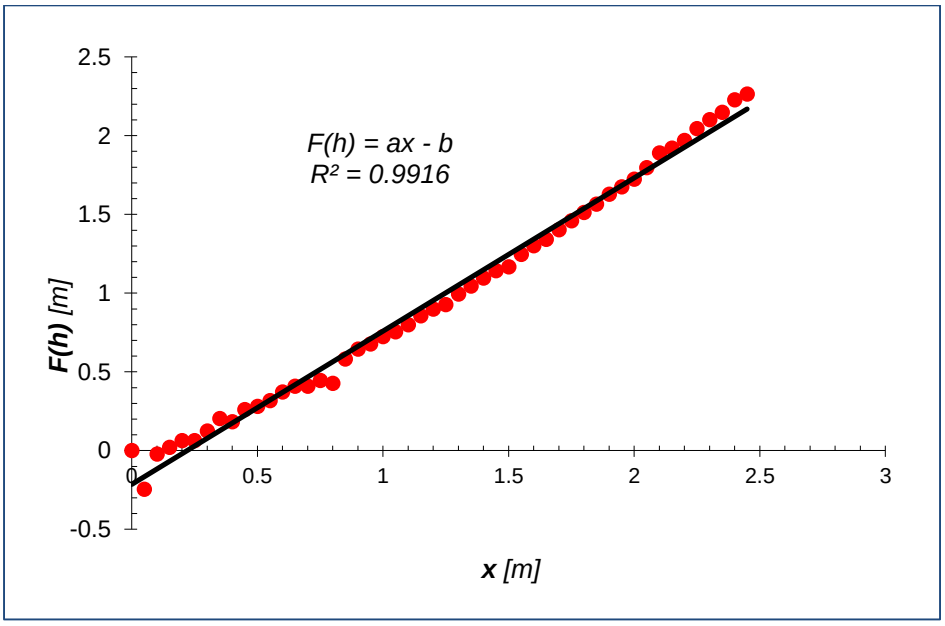

Figure 5.1: Estimation of representative drag coefficient over the entire canopy

The above equation is well applied for flow through dense vegetation (e.g., Plate 4.6). The hydraulic resistance force offered by the vegetation is very high and exceeds the gravitational force provided by the bed slope. A water surface profile will be developed to provide the required gravitational force and a gradually varied flow condition is resulted. The channeling effect can also be related to small orifice analysis for very small lateral spacing of blade width scale. The basic approach is given in section 5.4.

5.4 Analogy between flow through a row of stems and flow through a small orifice

If the flow is relatively undistributed by the upstream and downstream blades, and the transverse spacing is small as compared to the width of blade as shown in Figure 5.2, the orifice flow equation described by equation 5.8 can be used.

$$Q = C_0 A_0 \sqrt{\frac{2(P_1 - P_c)}{\rho}} \qquad (5.8)$$

where

C_0 is the coefficient of discharge, A_0 is the blade spacing, and P_1 and P_c are pressure at 1 and section C respectively.

From Figure 5.2, the fluid flows from the upstream (say section 1) to the spacing or gaps between blades (which can be referred to as orifice). Consequently, the streamlines will have velocity directed towards the centre of the spacing causing the emergent jet to contract, hence the jet's dimension is less that spacing (A_1). The jet

continues to contract and attain its maximum value at section c (known as vena contracta). At this section all the streamlines are taken to be horizontal.

By applying energy equation from section 1 to section c, the head loss is given by

$$h_L = \frac{P_1 - P_c}{\rho g} - \frac{U_c^2 - U_1^2}{2g} \tag{5.9}$$

From the orifice equation 5.8, considering a unit vertical depth of flow,

$$U_1^2 A_1^2 = 2\left(\frac{P_1 - P_c}{\rho}\right) C_0^2 A_0^2$$

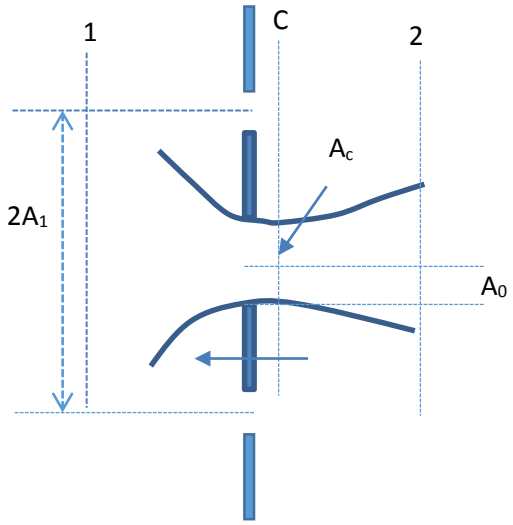

Figure 5.2: Schematic diagram of flow through a row of plates

Dividing throughout by $2g$ it can be shown that

$$\frac{P_1 - P_c}{\rho g} = \frac{A_1^2}{C_0^2 A_0^2} \frac{U_1^2}{2g} \tag{5.10}$$

Combining the orifice equation 5.8 and equation 5.10, it follows that

$$h_L = \frac{A_1^2}{C_0^2 A_0^2}\frac{U_1^2}{2g} - \frac{U_c^2 - U_1^2}{2g}$$

Therefore,

$$h_L = \frac{A_1^2}{C_0^2 A_0^2}\frac{U_1^2}{2g} - \frac{A_1^2}{A_c^2}\frac{U_1^2}{2g} + \frac{U_1^2}{2g}$$

where $A_c = C_c A_0$, hence, the head loss is given by

$$h_L = \left(\frac{A_1^2}{C_0^2 A_0^2} - \frac{A_1^2}{A_c^2} + 1\right)\frac{V_1^2}{2g} \qquad (5.11)$$

Beyond section C, the jet slow down with a negligible divergence and the sectional width of the jet can be assumed equal to the spacing. Hence, velocity of flow is constant.

By applying the momentum equation and energy equation from section 1 to section 2, it can be deduced that

$$h_L = \frac{P_1 - P_2}{\rho g} = \frac{F_D}{\rho g A_1} = C_d\left(1 - \frac{A_0}{A_1}\right)\frac{V_1^2}{2g}$$

Hence

$$C_d = \left(\frac{A_1^2}{C_0^2 A_0^2} + 1 - \frac{A_1^2}{C_c^2 A_0^2}\right)\Big/\left(1 - \frac{A_0}{A_1}\right) \qquad (5.12)$$

Typical values of C_o *= 0.60 - 0.64;* C_c *= 0.64*. A comparison of drag coefficient obtained by equation 5.7 and 5.12 can be drawn.

5.5 Results and discussion

5.5.1 Water surface profiles for flow through vegetation

The results of some measured water surface profiles for different values of λ and flow rates are shown in Figure. 5.3. Observation shows that for all cases, the water depth decreases in the direction of flow. This shows that the resistance force offered by the vegetation is greater than the gravitational force component parallel to the channel bed. Water flow is retarded and a water surface slope steeper than the bottom slope is produced to balance the resistance force generated by vegetation. The computed water surface profiles using best-fit value of C_d are included in (Figure. 5.4). The good agreement between the measured and semi-theoretical results shows the validity of Equation 5.7 and a high reliability of the estimated C_d value. Generally, the water level increases with increase in λ under the same flow rate.

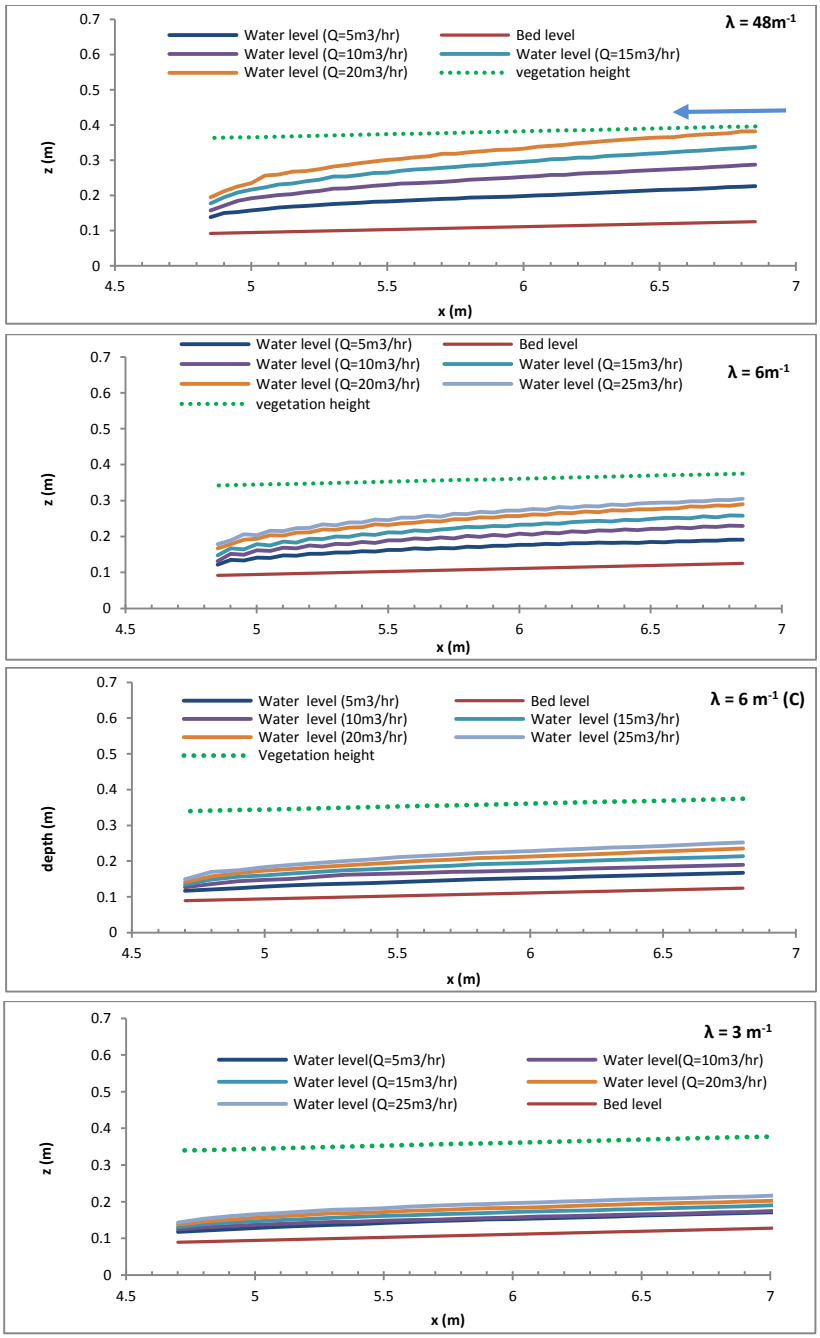

Figure 5.3: Water surface profiles for flow through emergent vegetation

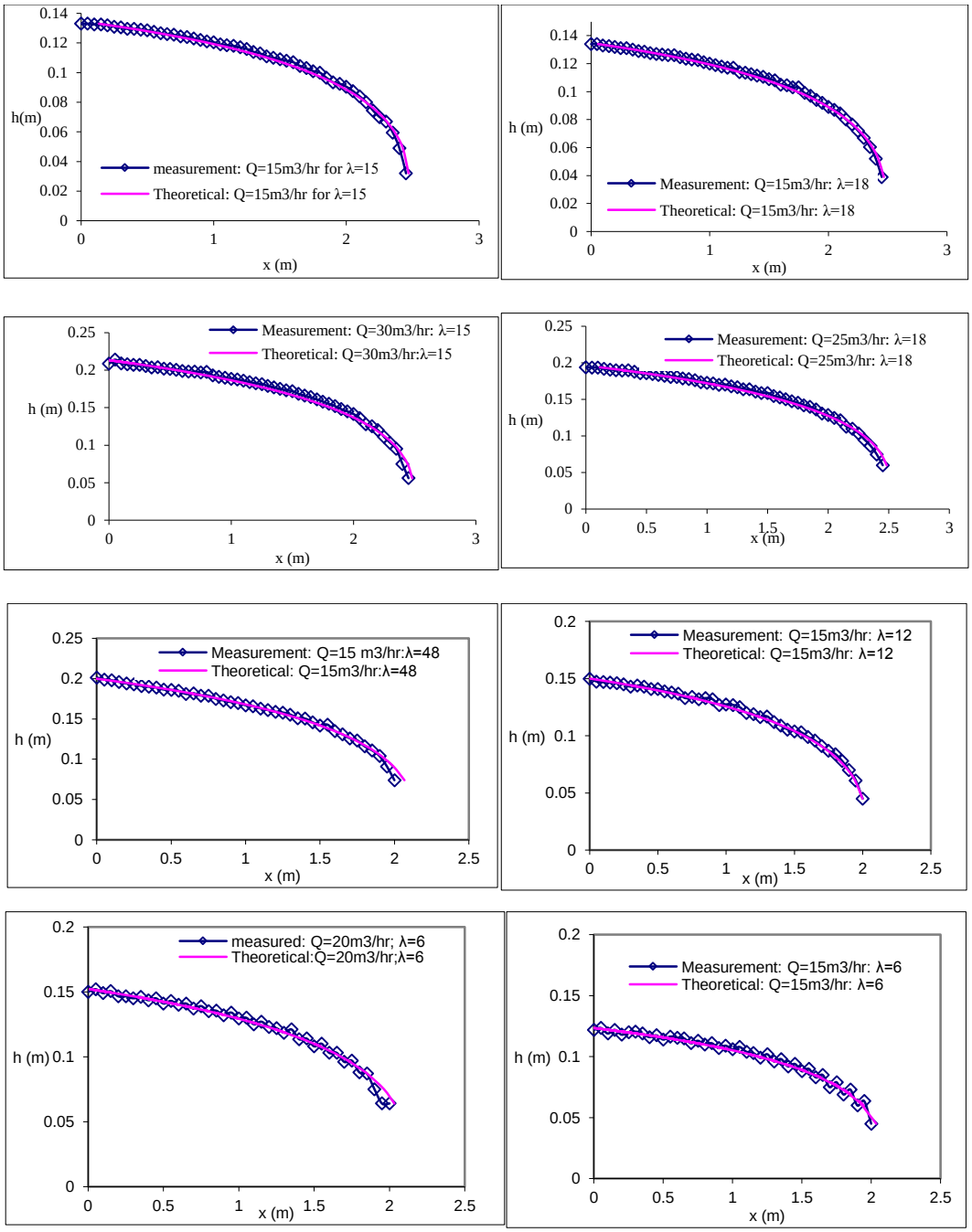

Figure 5.4: Theoretical and observed water surface profiles for flow through emergent vegetation

5.5.2 Flow through simulated vegetation with constant S_x and S_y

For cases with smaller S_y and larger S_x, the channeling effect is apparent. Plate 5.2 shows that there is a significant pressure drop (water level drop) for the flow through the constriction between two adjacent blades for the case $\lambda = 6m^{-1}$ ($S_y = 0.0125m$, $S_x = 0.1m$). At the downstream region of the stems, the velocity decreases due to the shear action. This is similar the spreading of a water jet. Part of the kinetic energy is converted back to the pressure energy when the flow strikes against the downstream blades and an increase in water level is resulted. The process is repeated when the flow encounters another lateral row of blades downstream. Consequently the water level displays a staircase type of profile. When S_x is reduced, the jet spreading effect is not so significant due to the blocking effect of the downstream blades. The velocity in the channel region formed by two adjacent longitudinal rows of blades remains high and there is not so much flow strikes against the blades. The pressure drop across the blades is thus smaller and the water surface profile is smoother (Plate 5.2: $\lambda = 72m^{-1}$, $48m^{-1}$, $24m^{-1}$).

To estimate the energy loss of the flow through a transverse row of stems with narrow openings, an analogy with the orifice flow has been made (section 5.4). The relationship between the drag coefficient C_d and the discharge coefficient C_o, the coefficient of velocity C_v, and the geometric dimensions of the stems has been derived and shown in section 5.4. Using the typical values of the C_o and C_v, the estimated C_d is high and matches the measured value. As an example, if $C_o = 0.7$, $C_v = 1$, $A_1 = 0.0125m$, $A_o = 0.0050m$, equation (5. 12) gives $C_d = 9.4$.

Figure 5.5 shows that the drag coefficient, C_d decreases with increasing stem Reynolds number for the range $500 < Re < 1500$. The drag coefficient exhibits more or

less a linear dependence on the stem Reynolds number. Similar trend had been observed for cylinder arrays of similar range of Re (Tanino and Nepf, 2008; Cheng and Nguyen, 2011). For the set of experiments with S_y fixed, C_d is insensitive to the variation of Re for cases with higher value of λ (Fig. 5.4a). For the set of experiments with S_y fixed, C_d is insensitive to the variation of Re for cases with lower value of λ and higher velocity (Fig. 5.5b).

The experimental results indicates that for cases with S_y fixed, at a smaller value of S_x, the change in velocity will not alter the flow pattern since the wake region is limited by the longitudinal spacing of adjacent blades S_x. The resulting C_d becomes more not less a constant. For a larger value of S_x, the flow pattern is affected by the magnitude of the velocity and a decreasing trend of C_d with Re is resulted. For cases with S_x fixed, at a larger value of S_y, the lateral spacing between adjacent blades is sufficiently wide and the flow pattern is not affected by the variation in velocity. When S_y is small, the interference effect between two laterally adjacent blades becomes strong and is affected by the magnitude of the velocity.

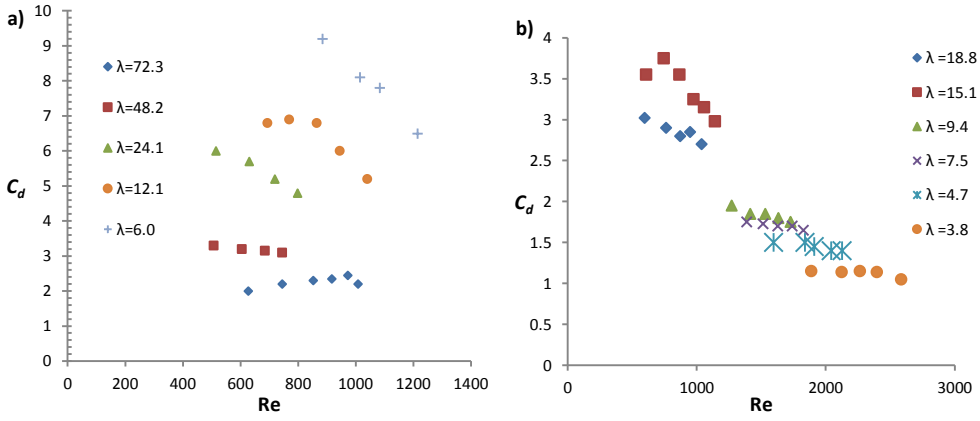

Figure 5.5: Bulk drag coefficient as a function of stems Reynolds number:

a) S_y constant; b) S_x constant

Tanino and Nepf, (2008) studied the dependence of C_d only on Re and vegetation density. In this study the effects of lateral and longitudinal spacing among vegetation has been studied. The two phenomena were studied independently. Figure 5.6a shows that C_d decreases with increasing areal density of vegetation when the transverse spacing S_y is fixed. In this set of experiments the speed up ratio of the flow through the contracting path between two transversely adjacent blades is more or less unchanged since S_y is a constant. The decrease of S_x increases the effect of wake interference induced by the blades, resulting in a lower drag (sheltering effect). Figure 5.6b shows that C_d increases with increasing areal density of vegetation when the longitudinal spacing S_x is fixed. In this set of experiments the wake interference (sheltering) effect is more not less unchanged. The decrease in S_y increases the speed up ratio of the flow through the contracting path in between two transversely adjacent blades, resulting in a higher drag (channeling effect).

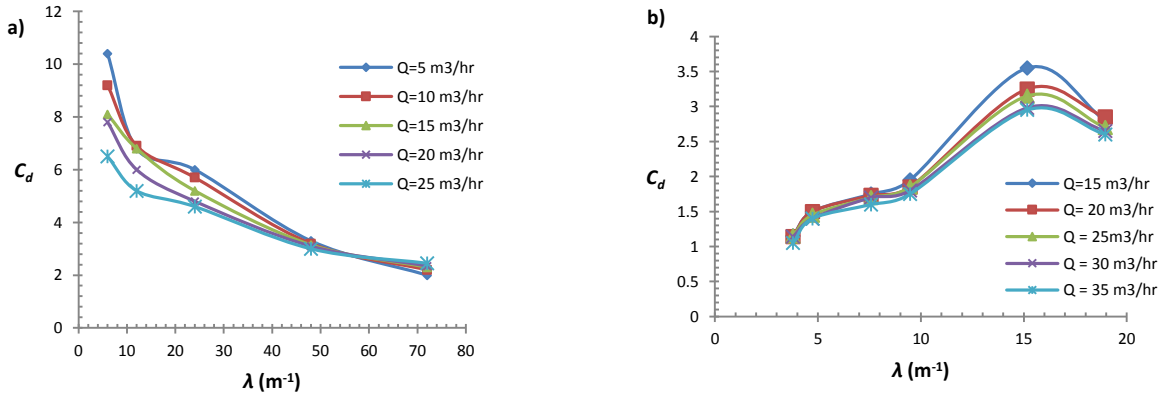

Figure 5.6: Bulk drag coefficient as a function of areal density of vegetation: a) S_y constant; b) S_x constant

For the cases of constant longitudinal stem spacing (channeling effect), the water levels are relatively low due to the high flow velocities, and apparent surface waves were observed. The uncertainties in the C_d values obtained at 5 and 10 m^3/hr flow rates for $\lambda = 6\ m^{-1}$ are high due to the water level measurement uncertainty arising from low water depth and surface waves. In order to reduce the uncertainty in the measurement, $15m^3/hr$ was set as the minimum flow rate.

The increasing trend of C_d with λ in (Figure 5.6b) is supported from the interpolated value in Figure 5.7. For the case of $S_y = 0.0125m$ and $S_x = 0.02m$, $\lambda = 30.1/m$, the interpolated value in Figure 5.10 gives $C_d \sim 4.75$.

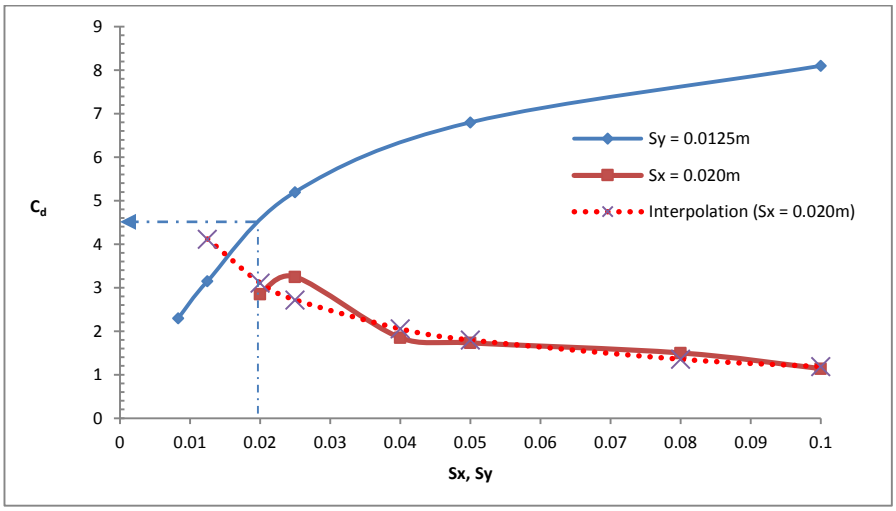

Figure 5.7: Trend analysis of S_x = fixed and error correction by interpolation

To investigate the contribution of the viscous force and pressure force to the total drag force, the normalized drag $f_d = F_d/(\mu U)$ is plotted against Re. Ergun (1952) proposed an equation for drag force in packed columns of the following form:

$$f_d = a_0 + a_1 \mathrm{Re} \tag{5.13}$$

where a_0 represents the contribution of the viscous shear stress on the stem surface, and a_1 represents the contribution of the pressure drop in the stem wake.

Figure 5.8 illustrates the normalized drag force f_d as a function of Re. Normalized drag force has been used by Tanino and Nepf, (2008) for random array of cylinders under low Re, their results is also shown in Figure (5.7). For cases with S_y kept constant, f_d varies approximately linearly with Re for cases with small S_x. For a given Re, f_d increases with decreasing λ, showing that the channeling effect plays a dominant role. For cases with larger S_x, the relationship between f_d and Re deviates from a straight line. If the data are fitted by a straight line, the intercept will give a high value. As the viscous force cannot be so large, the high value of a_o is expected to be caused by the jetting and vortex shedding mechanisms. It is likely the best fit line of the data for cases with large S_x will be a curve bending towards the origin at low Reynolds number. Based on the straight-line fitting, it is found that a_o increases with S_x (see Figure 5.9) indicating that the effects of vortex shedding and jet spreading are more important for larger S_x. The negative value of a_0 at small S_y is probably due to the uncertainty in data fitting. A slight change in the slope of the straight line will easily generate a negative intercept. The coefficient a_1 decreases with increase of S_x showing that the pressure loss ratio due to kinetic energy dissipation decreases with the longitudinal spacing.

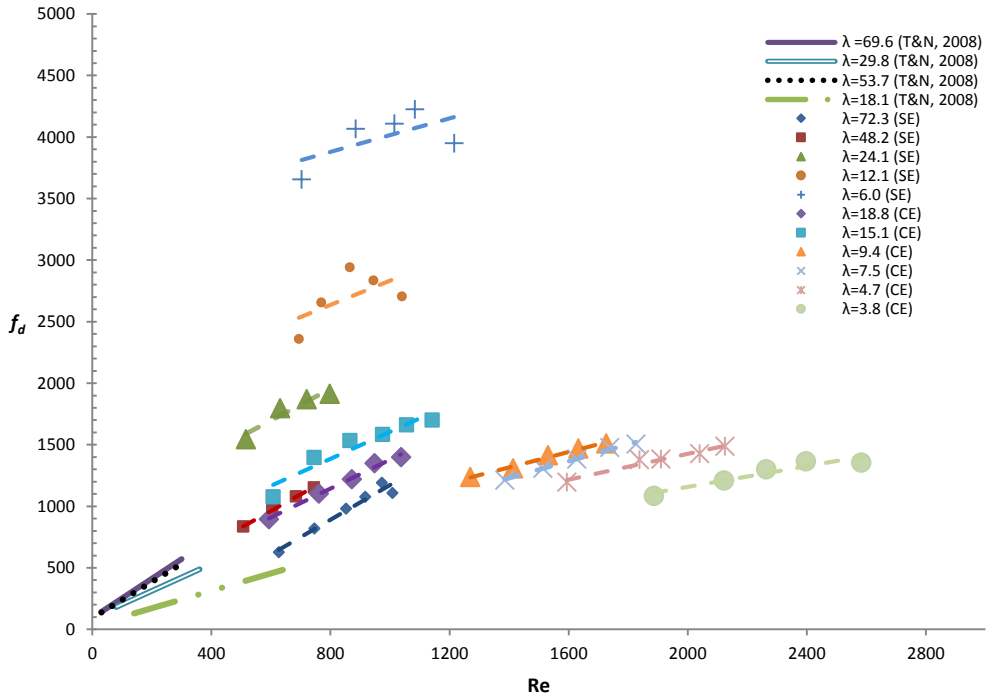

Figure 5.8: Normalized drag force as a function of blade Reynolds number (SE refers to sheltering effect, S_y = constant and CE refers to channeling effect, S_x = constant)

For the cases with S_x kept constant, f_d generally varies linearly with Re. For a given Re, f_d increases with increasing λ, showing that the sheltering effect plays a dominant role. The results are similar and consistent with those obtained by Tanino and Nepf (2008) for closely packed cylinders in the Reynolds number range of 25 - 685 (Figure 5.8). In Figure 5.9, the intercept a_o scatters around a mean value of 350, indicating the contribution of the viscous drag and other mechanisms does not vary significantly with S_y. The slope a_1 decreases with the increase in S_y, showing that the pressure drop ratio decreases with the increase of lateral spacing. This explains that the wider the lateral spacing, the lesser the flow contraction will be. This analysis of

distribution of drag force parameter and Re revealed that flow and wake interference are more influenced by the (longitudinal and lateral) spacing than by vegetation density.

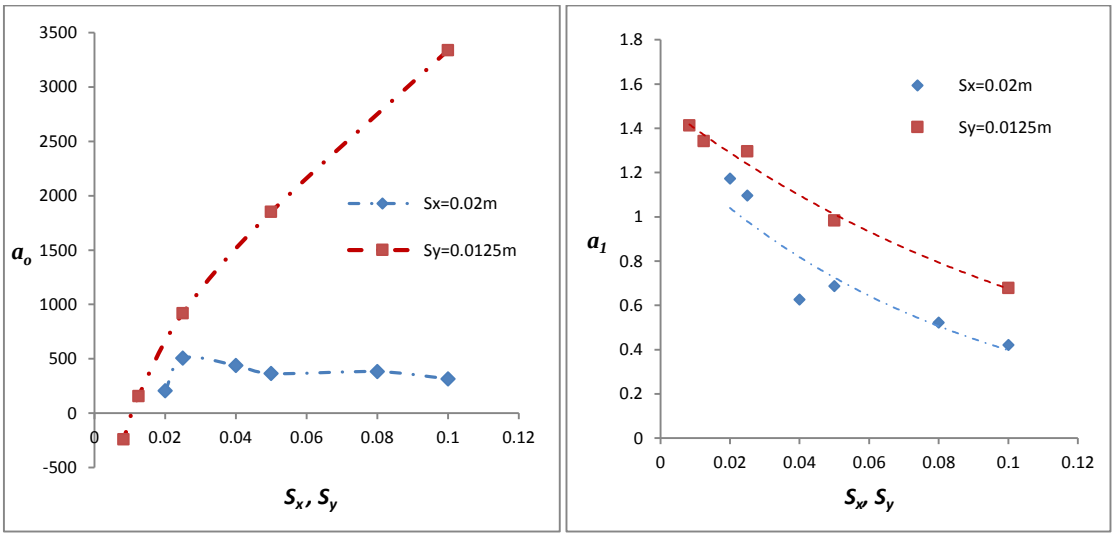

Figure 5.9: Dependency of a_0 and a_1 on lateral (S_y) and longitudinal spacing (S_x)

The variation of normalized drag with Froude number Fr is shown in Figure 5.10. The range of variation of Froude number for each case is narrow, generally within 20% from the mean value. For the cases with S_y = 0.0125m, the normalized drag appears to decrease with the increase in Froude number. The uncertainty can be high as the range of Froude number is narrow. For cases with S_x = 0.02m, the normalized drag appears to be independent of Fr. Therefore it can be concluded that the normalized drag is insensitive to Fr in the range of experimental conditions tested.

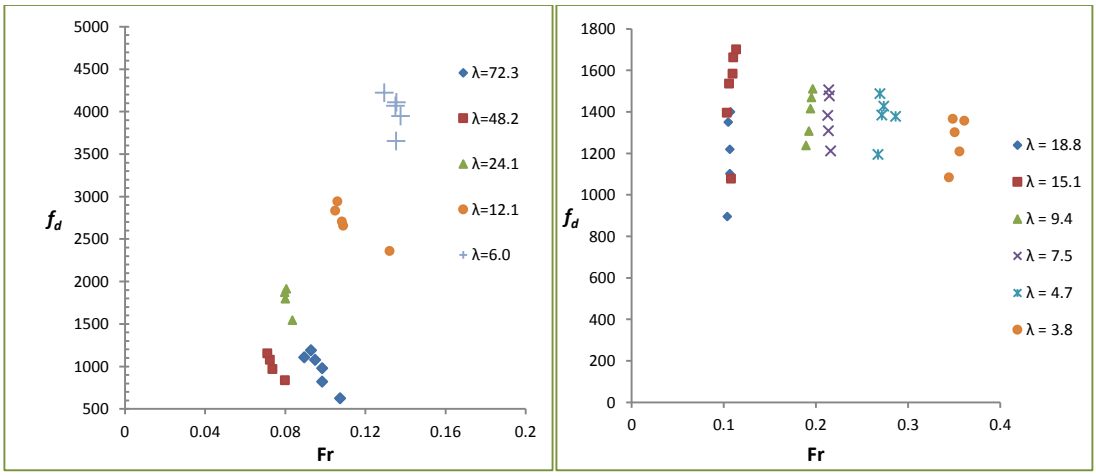

Figure 5.10: Effect of normalized drag force on Froude number

In Figure (5.11), the f_d is strongly correlated to the blade spacing irrespective of the flow rate, and follows a power law relationship. The exponent is dependent on ϕ and flow condition. By varying the longitudinal spacing, the drag force parameter decrease with increasing ϕ because interaction in dense vegetation reduces the flow speed in the canopy relative to distribution of less dense vegetation. In the case of channeling effect, the f_d increases with decreasing lateral spacing due to increasing wake interference.

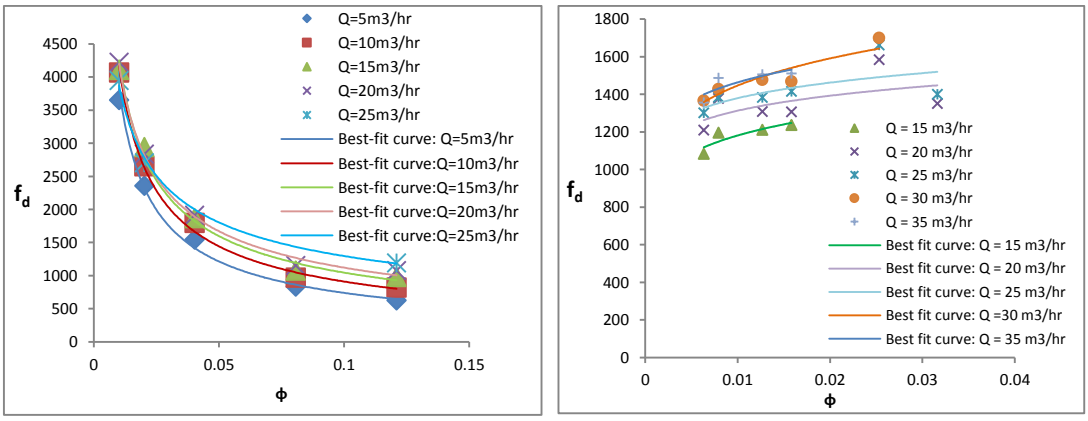

Figure 5.11: Effect of vegetal drag force on blade volume fraction for varying flow rate: Sheltering effect (left), Channeling effect (Right)

5.6 Fitting equation for C_d for flow through emergent vegetation

It is known that for an isolated 2D plate under a high Reynolds number flow the drag coefficient is $C_d = 2$. Ingham et al., (1990) performed experimental investigation for flow through a row standing blades of equal widths and spacing. The flow was found to be symmetrical within the range $0 \leq Re(w) \leq 500$. The results of C_d obtained were comparable to their numerical predictions. The results illustrated that the dependent of drag coefficient (C_d) on mesh size is significant in the range $50 \leq Re(w) \leq 500$. The extrapolation of the results showed that the C_d value is asymptotically equivalent to 2 for the range $50 \leq Re(w) \leq 500$.

Lam and Zou, (2010) have shown the strong effect of aspect ratio (h_v/w) and spacing ratio, not only on the force and pressure characteristics, but wake development behind downstream cylinders. They performed 3D numerical simulations on flow around four cylinders in an in-line square configuration as well as experimental measurements to validate their numerical study. They were able to visualize the flow in a water wind tunnel by investigating the combined influences of aspect ratio and spacing ratio (of equal lateral and longitudinal spacing) on vortex structures, force and pressure coefficient distributions for flow around the circular cylinders at Re = 200. The calculated values of mean C_d were found to be in the range of 1.2 - 1.5 for different spacing ratio and aspect ratio (see Lam and Zou, 2010; Tables 2 and 3; page 486 - 487). Similar study of drag associated with side by side square blades (Alam et al., 2011, Table 1, pp 447 - 448 and their references) measured initial C_d value of approximately 2 for high Re.

Recently, Anagnostopoulos and Seitanis, (2014) carried out numerical simulations of flow past two staggered rows of cylinders in cross-flow. The study focused on varying the longitudinal spacing at fixed Re = 200. The authors specific interest were on the wake width behind the downstream cylinders, dependency of shedding frequency on longitudinal spacing and the correlation between the shedding frequencies past the cylinders of the upstream row and that of the downstream row. The time history of the drag coefficients on cylinders of different longitudinal spacing displayed mean C_d values of approximately 2 (see Anagnostopoulos and Seitanis, 2014; Figures 9, 10 and 17). Also experiments of an isolated 2D plate under a high Reynolds number flow showed that the drag coefficient C_d is 2 (e.g. Hoerner, 1965). Hence, for single blade row; an asymptotic $C_d = 2$ has been obtained.

In this study, experimental results for drag coefficient of multiple blades in the range $500 \leq Re(w) \leq 2600$ by varying the blades longitudinal spacing at constant lateral spacing and vice versa have been obtained. Based on the above finding, an initial value of $C_d(0)$ equal to 2 is obtained and a C_d model for emergent vegetation is proposed as follows:

$$C_d = C_d(0)\{f(S_x)\}\{g(S_y)\} \tag{5.14a}$$

Where $C_d(0) = 2$ for $Re(w) \leq 500$ and

$$\left.\begin{aligned} f(S_x) &= \left\{1 - \beta e^{-K\left(\frac{S_x}{w}\right)}.Re^{-\gamma}\right\} \\ g(S_y) &= \left\{1 + \alpha e^{-L\left(\frac{S_y}{w}\right)}.Re^{-\delta}\right\} \end{aligned}\right\} \tag{5.14b}$$

The fitting of equation (5.14) has been carried out by applying the following condition:

For $S_x \to \infty$; $S_y \to \infty$ and $Re \to \infty$; $C_d \to C_d(0) = 2$

By fitting equation (5.14) with 46 experimental data set using the multiple regression method, a good match between the fitting equation and the data is obtained (Figure 5.12) with the parameters taking the following values: $\beta = 2.35$; $\alpha = 2840$; $K = 0.12$; $L = 0.13$; $\gamma = 0.15$; $\delta = 0.94$. The coefficient of multiple determination (R^2) of the regression is 0.94.

The function $f(S_x)$ describes the hydrodynamics of fluid flow through the blade at varying lateral spacing at fixed longitudinal spacing. The function increases with increasing Reynolds number due high flow velocity, whereas $g(S_y)$ decreases with increasing Re due to decreasing resistance from vegetation.

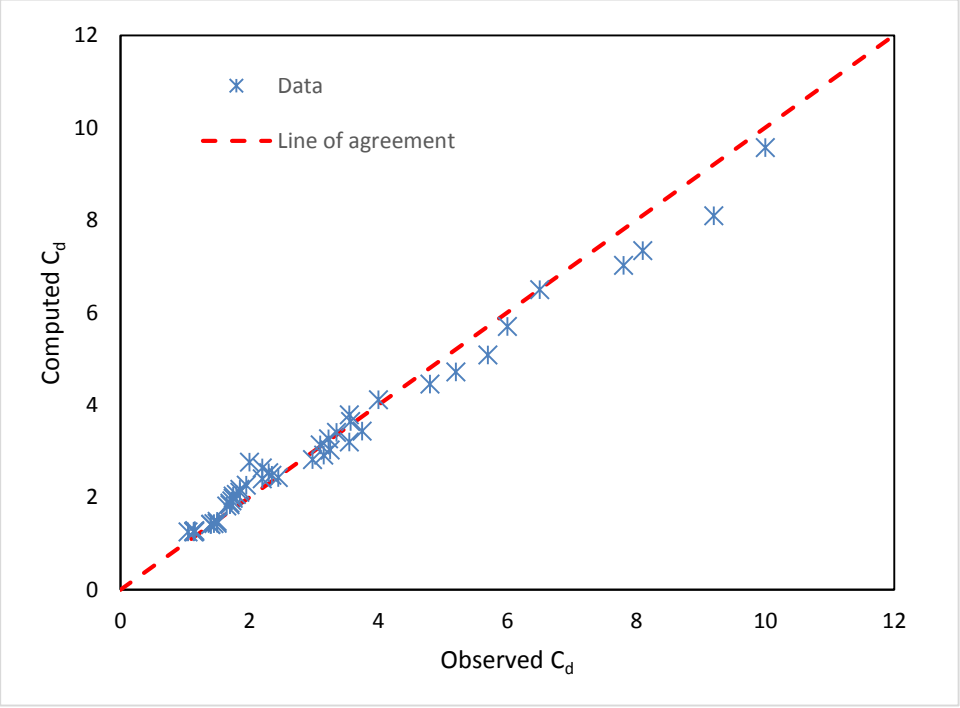

Figure 5.12: Fitting results of C_d using equation 5.14

Another set of data from laboratory experiments have been used to illustrate the predictive capability of equation 5.14. There is no specific reasons behind equation 5.14, other than it fit the experimental dataset better than others considered by the author in this study. Table 5.3 displays experimental conditions. Twenty one (21) sets of data were obtained from laboratory flume experiment for different distribution pattern with varying Reynolds numbers. Nine of the dataset represent the flow condition for sheltering effect (i.e. S_y = fixed and S_x is varied) while the remaining twelve data represent the flow condition for channeling effect (i.e. S_y is varied and S_x = fixed).

Table 5.3: Experimental hydraulic conditions and measured C_d: (emergent case)

S/N	S_y (m)	S_x (m)	Re (-)	C_d (-)
1	0.0125	0.0125	507	3.30
2	0.0125	0.0125	605	3.20
3	0.0125	0.0125	685	3.15
4	0.0125	0.0125	744	3.00
5	0.0125	0.0500	694	6.80
6	0.0125	0.0500	769	6.90
7	0.0125	0.0500	865	6.80
8	0.0125	0.0500	945	6.00
9	0.0125	0.0500	1040	5.20
10	0.0500	0.0250	1200	2.50
11	0.0500	0.0250	1372	2.30
12	0.0500	0.0250	1497	2.40
13	0.0500	0.0250	1603	2.45
14	0.0500	0.0250	1719	2.30
15	0.0500	0.0250	1771	2.40
16	0.1000	0.0250	1194	1.80
17	0.1000	0.0250	2014	1.75
18	0.1000	0.0250	2170	1.70
19	0.1000	0.0250	2322	1.60
20	0.1000	0.0250	2423	1.60
21	0.1000	0.0250	2529	1.55

Equation 5.14 has been used to compute the drag coefficients for the given hydraulic conditions. The measured and the computed drag coefficients are presented in Figure 5.13. It can be seen from the line of agreement that the C_d values are reasonably well predicted using the proposed equation.

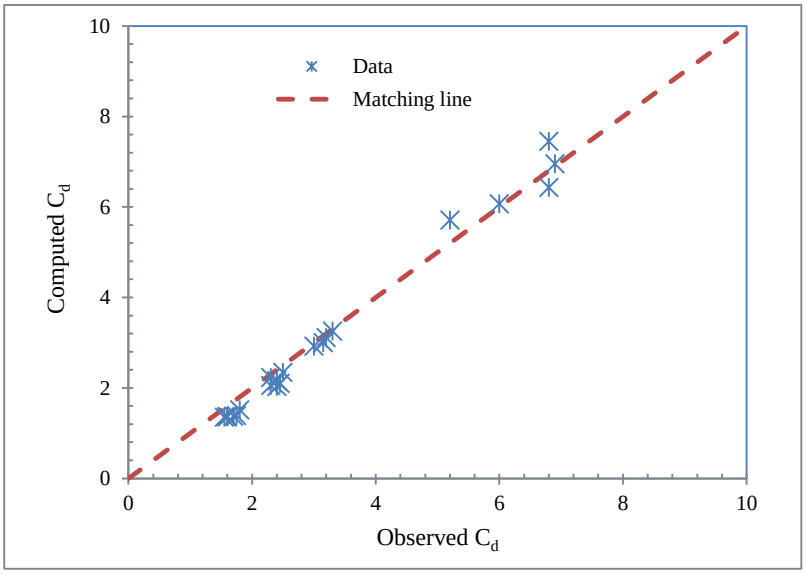

Figure 5.13: Model validation against available experimental dataset

5.6.1 Flow regime map on Sx – Sy plane

The occurrence of mechanism of flow interference (for the sheltering and channeling effects) studied in section 5.5.2 is summarized in the flow regime map as shown in Figure 5.14. The region $C_d < 2$ is dominated by channeling effect while the region with $C_d < 2$ is governed by sheltering effect. Beyond the studied region, denoted by dotted purple line, the drag coefficient is approximately equal two using the equation 5.14.

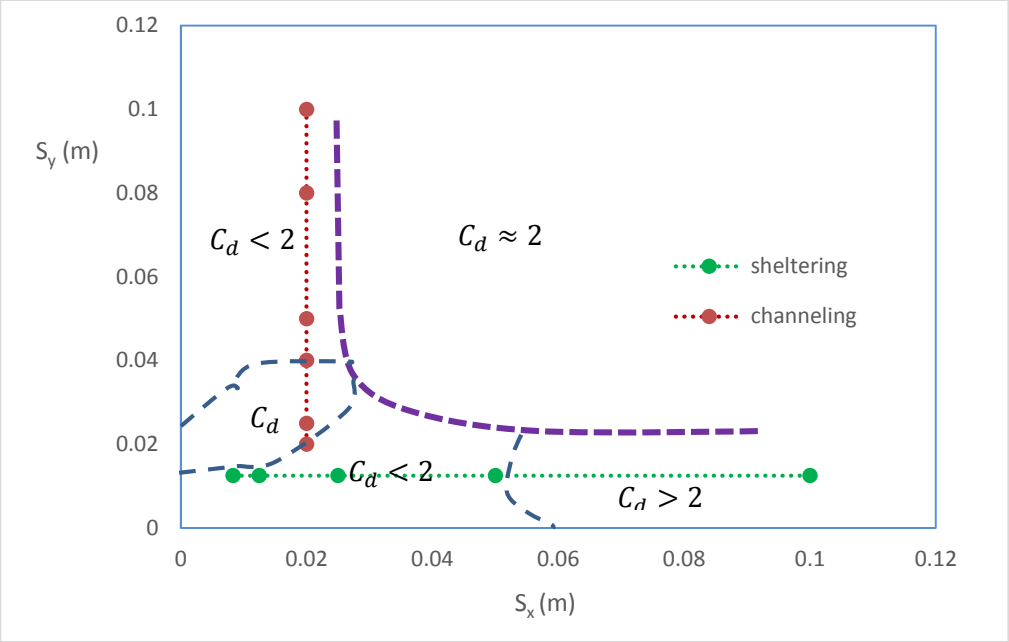

Figure 5.14: Flow regime map for region of occurrence of interference effects (Green line: increasing sheltering effect with decreasing S_x; Red line: increasing channeling effect with decreasing S_y)

5.7 Non-unique relation between C_d and ϕ

In Figure 5.15, based on the fitting equation, it can be demonstrated that the relationship between C_d and ϕ for a fixed Reynolds number is not unique. By fixing S_y and varying S_x, C_d decreases with increasing ϕ. By fixing S_x and varying S_y, C_d increases with ϕ. Figure 5.15 shows the decreasing trend for S_y = 0.0125m, and increasing trend for S_x = 0.02m at constant Reynolds number for both cases (Re = 1000). This observation helps to explain the previous contradictory results that the drag coefficient increases with ϕ (Tanino and Nepf, 2008, Kothyari,et al., 2009), and the drag coefficient decreases with increasing ϕ (Nepf, 1999). The distribution pattern of the individual stems plays a

significant role. Similar trends are observed for normalized drag f_d as f_d is governed by C_d at large Re.

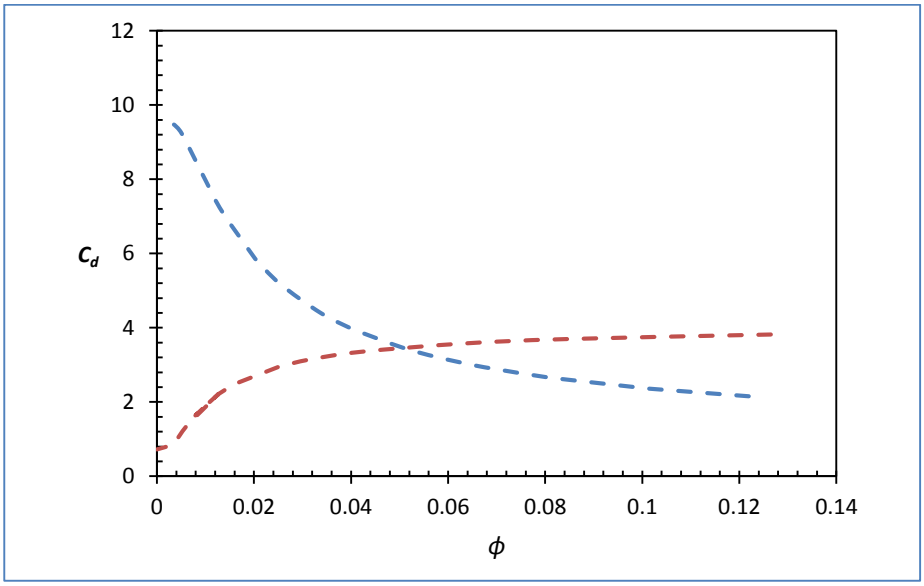

Figure 5.15: Non-unique relationship between C_d and ϕ

(Dotted red line denotes S_x = fixed and the blue line S_y = fixed)

It is noted that the value of C_d is quite large for small S_y and large S_x. The drag in this case is governed by the channeling effect. The transverse gap between the plates is narrow and the velocity of flow through the gap is increased significantly. Comparing to the case with wide gap, more pressure energy is converted into the kinetic energy and the pressure behind the plate is further reduced, resulting in a large drag. The largest drag coefficient computed from the experimental data is about 9, over four times large than that of an isolated plate. This is consistent with the previous works. For example, Tanino and Nepf (2008) found that the drag in a random array of circular cylinders can be three or four times larger than that of an isolated circular cylinder.

5.8 Summary

In this chapter, the hydraulic behaviour of semi-rigid blade type emergent vegetation under subcritical gradually varied flow conditions have been investigated by conducting extensive laboratory experiments on wider range of high areal vegetation density. In the data analysis, the longitudinal momentum equation relating the vegetation resistant force and water surface slope has been used to estimate the bulk drag coefficient C_d. The results showed that C_d decreases with increasing Re, is not dependent uniquely on the solid volume fraction, but depends on the distribution pattern of the vegetation elements. By decreasing the transverse spacing S_y and keeping S_x constant, C_d increases with increasing solid volume fraction due to the channeling effect. By increasing the longitudinal spacing S_x and keeping S_y constant, C_d decreases with increasing solid volume fraction due to the sheltering effect.

The inertia contribution due to pressure loss in the blade stem wake decreases with increase in transverse or longitudinal spacing, while the effects of viscous shear stress, vortex shedding and jet spreading effects increases with increasing longitudinal spacing over the experimental range. The flow through vegetated channel is turbulent and subcritical (Fr <1) as can be observed from (Figure 5.10), as a result, the increasing flow rate does not lead to sudden change in drag coefficient (Figure 5.6). For practical application, an empirical equation that relates C_d to the lateral and longitudinal stem spacing ratios and Re is proposed. A good match between the fitting equation and experimental data is obtained. The empirical equation is further validated using separate experimental dataset.

6 Gradually varied flow through submerged vegetation patch of high areal density

6.1 Introduction

In chapter 5, flow through emergent vegetation was extensively examined and reported. In case of submerged vegetation, the hydrodynamics of vegetated flows in open channels, rivers and streams is complicated due to the wide variation in the flow conditions and vegetation characteristics. Submerged, emergent or floating vegetation will lead to different flow behaviors. In particular, there is an additional flow path over an individual stem at the top. Also the variation in shape, size, structure, distribution pattern and stage of growth of vegetation elements will affect the flows. More complicated cases of flow over submerged vegetation has also been investigated (Nepf, 2012b; Zong and Nepf, 2010; Stoesser et al., 2010; Kothyari et al., 2009; White and Nepf, 2007; Ishiwaka et al., 2000; Wu et al., 1999 and Nepf, 1999). The governing equation for steady flow through vegetation describes the balance of drag force and the flow momentum absorbed by vegetation elements. In case of gradually-varied flow through emergent vegetation, the pressure forces and hence the water surface gradient need to be included in the governing equation. The drag coefficient can be determined by a numerical integration procedure. For flows over submerged vegetation, the determination of flow resistance is more complicated. The resistance force is dependent on the flexibility, frontal projected area and submergence ratio of vegetation (Jarvela, 2004; Stone and Shen, 2002; Jarvela, 2002). More information on the vegetation properties thus is required.

In the determination of vegetation induced hydraulic resistance in open channel flows using theoretical models, semi-empirical models or numerical models, a priori knowledge of the drag coefficient C_d of the vegetation stems is required (Busari and Li, 2015; Jarvela, 2004; Fathi-Moghadam and Kouwen, 1997). For rigid-submerged vegetation, the Rigid Cylinder Analogy (RCA) is, also, commonly used (e.g., Baptist et al., 2007; Huthoff et al., 2007) in which the vegetation stems are treated as rigid cylinders. The flow is then affected by the wake interference among the cylinders (Schoneboom et al., 2011). Aberle and Jarvela, (2013) pointed out that the RCA is not adequate enough for real plants, and the geometric and stiffness properties of vegetation are required for more accurate determination of the drag coefficient.

In numerical simulation, drag coefficient can be obtained from database or using empirical formula. The use of empirical equation is more pronounced and commonly applicable to spherical and cylindrical shapes. However, both sources for obtaining drag coefficient appear to less available for blade-type vegetation. Generally, knowledge of drag coefficient for different distribution patterns of array deserves attention.

In this chapter, focus is on the submerged blade-type vegetation with high areal density. The submergence ratio is relatively low ($h/h_v < 1.6$, h is the water depth and h_v is the vegetation height). The areal density of vegetation gives a resistance parameter $\eta = \lambda h_v$ ($\lambda = Nw$, N($1/m^2$)) is number of stems per unit horizontal area; w(m) is width of stem) which is greater than the threshold value for the generation of canopy scale turbulence defined in Nepf (2012b) and falls in the dense canopy range $\eta \geq 0.23$. Therefore, the behaviour of velocity within the submerged canopy as well as Reynolds stress in the study can be described and classified as high areal density and shallow

submergence. The bed shear force is negligible as compared to the vegetation induced drag.

The main objective of this chapter is to provide a systematic study of hydrodynamic the interference effects/mechanisms (channeling and sheltering) among vegetation stems under a gradually-varied flow condition. Regular arrays of blade-type vegetation stems are employed and each interference effect is studied independently by using appropriate array distribution patterns. For cases with fixed lateral spacing for the study of sheltering effect, the lateral spacing ratio spacing ratio (S_y/w) is 1.7 and the longitudinal spacing ratio (S_x/w) varies from 1.1 to 13.3. For cases with fixed longitudinal spacing for the study of channeling effect, the longitudinal spacing ratio is 2.7 and the lateral spacing ratio varies from 2.65 to 13.1. In the experiments the flow structure is measured and the drag force and hence C_d are obtained through the velocity and surface slope measurements. Based on the analysis results, the inconsistency in the results of previous works whereby the bulk C_d of the vegetation is related to the solid volume fraction (ϕ) of the vegetated zone is addressed. Also, new empirical in terms of longitudinal and lateral spacing ratio) and Reynolds number is proposed for submerged flexible vegetation.

6.2 Theoretical formulation

In unidirectional flow over vegetation, the channel cross-sectional averaged velocity U is given by

$$U = Q \Big/ Bh\left(1-\phi\frac{h_v}{h}\right) \tag{6.1}$$

The total drag force F_d (N) due to pressure differences on the plant surfaces in a unit volume can be defined by

$$F_d = 0.5\lambda C_d \rho h_v U^2 \tag{6.2}$$

The shear force on plant surfaces due to viscous stresses is assumed small and is accounted in the expression of F_d. In the analysis, it is assumed that the only source of energy dissipation is due to current-vegetation interaction. For an open channel flow (of width B) through vegetation, over a small longitudinal distance, Δx, a change in the hydraulic head (water level difference), Δh is resulted. Assuming a steady flow condition and neglecting the boundary shear forces. By applying the principle of conservation of momentum to a control volume ($B \times \Delta x \times h$), the one-dimensional momentum balance equation is as follows:

$$\rho U \frac{\Delta U}{\Delta x} = \rho g S - \rho g \frac{\Delta h}{\Delta x} - \frac{1}{2h(1-\phi\frac{h_v}{h})} \rho C_d \lambda h_v U^2$$

$$\rho U \frac{\Delta U}{\Delta x} = \rho \mathrm{g} \left(S - \frac{\Delta h}{\Delta x} \right) - \frac{1}{2h\left(1-\phi\frac{h_v}{h}\right)} \rho C_d \lambda h_v U^2$$

Rearranging the terms:

$$U \frac{\Delta U}{\Delta x} + g \frac{\Delta h}{\Delta x} = gS - \frac{1}{2h(1-\phi\frac{h_v}{h})} C_d \lambda h_v U^2$$

Utilizing equation 6.1, the momentum equation becomes

$$\frac{C_d \lambda h_v}{2B^2 h^3} \frac{Q^2}{\left(1-\phi\frac{h_v}{h}\right)^3} - gS = -\left(g - \frac{Q^2}{B^2 h^3}\right)\frac{\Delta h}{\Delta x} \tag{6.3}$$

where g (m/s^2) is the gravitational acceleration. The first, second, third and the fourth term of equation (6.3) represents the drag force, body force, pressure force and the rate of change of momentum flow rate respectively. The value of C_d can be evaluated from equation (6.3) by measuring the flow rate and water surface profile.

Alternatively, the drag force can be represented by

$$F_d = 0.5\lambda C_d' \rho h_v U_v^2 \tag{6.4}$$

Where U_v is the longitudinal velocity within the vegetation region, C_d' is the corresponding drag coefficient. The momentum equation then becomes

$$\frac{C_d{}'\lambda}{2hB^2h_v}\frac{{Q_v}^2}{\left(1-\phi\frac{h_v}{h}\right)^3} - gS = -\left(g - \frac{Q^2}{B^2h^3}\right)\frac{\Delta h}{\Delta x} \tag{6.5}$$

where $Q_v = \left(\frac{Q_1}{Q_1+Q_2}\right)\times Q_{in}$ is the flow rate within the vegetation region; Q_{in} is the total flow rate in the open channel, Q_1 and Q_2 are the flow rates based on the measured velocity profiles, given by $Q_1 = B\int_{z=0}^{z=h_v}(udz)$ and $Q_2 = B\int_{z=h_v}^{z=h}(udz)$; B is the channel width and z is the vertical ordinate.

6.3 Details of experiments

The key hydraulic parameters of the experiments are summarized in Tables 6.1 and 6.2. As shown in Table 6.1, for cases with constant lateral spacing of 0.0125m, the longitudinal spacing varies between 0.0083m and 0.10m, corresponding to the spacing

ratio between 1.1 and 13.3 respectively. As shown in Table 6.2, for cases of constant longitudinal spacing of 0.02m, the lateral spacing varies between 0.02m and 0.10m, corresponding to the spacing ratio between 2.66 and 13.3 respectively.

Figure 6.1 shows the schematic diagram of the longitudinal section of the flume. The longitudinal direction is represented as *x*, with subscripts *l*, *a* and *t* denoting the locations of leading edge, adjustment region and trailing edge respectively. A preliminary investigation of the fully developed region was carried out by measuring the vertical profiles of velocity longitudinally. The result suggested that the fully developed region can be estimated using the empirical equation proposed by Zeng and Li, (2014) for the adjustment length of the transitional region of the vegetation patch. Wavy forms of vegetation is not observed in this experiments due low flexibility and high density.

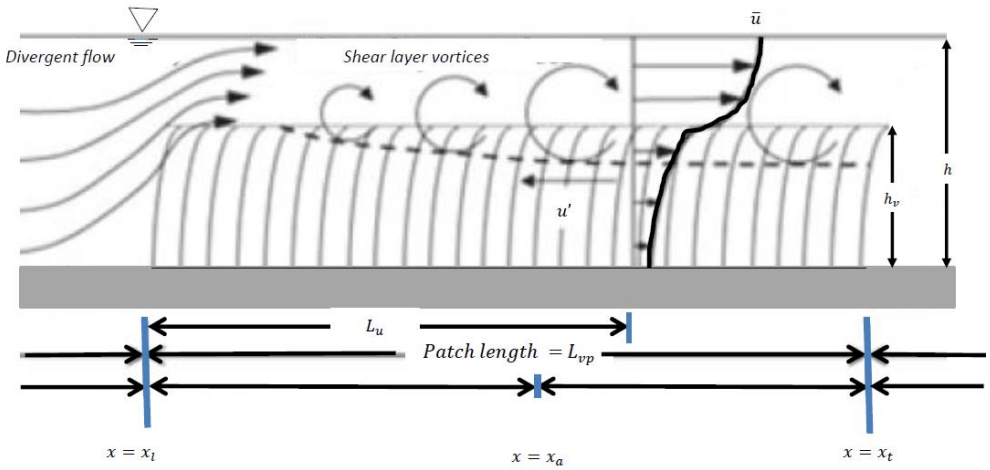

Figure 6.1: Schematic diagram of the longitudinal section of the flume

Table 6.1: Submerged case: Hydraulic parameters of the experiments

(Constant lateral spacing)

Placement patterns of vegetation elements (m)	Q (m^3/s)	h (m)	U (m/s)	Re (-)	λ (m^{-1})
	0.0069	0.2830	0.0901	678	
	0.0083	0.3110	0.0984	740	
$S_Y = 0.0125$	0.0097	0.3300	0.1082	815	72.29
$S_X = 0.0083$	0.0111	0.3400	0.1120	904	
	0.0125	0.3565	0.1287	969	
$S_Y = 0.0125$	0.0083	0.2868	0.1020	768	
$S_X = 0.0125$	0.0097	0.2963	0.1152	867	48.19
	0.0111	0.3043	0.1282	965	
	0.0125	0.3120	0.1406	1059	
	0.0139	0.3190	0.1528	1151	
$S_Y = 0.0125$	0.0083	0.2865	0.0978	736	24.10
$S_X = 0.0250$	0.0097	0.2970	0.1100	829	
	0.0111	0.3040	0.1228	925	
	0.0125	0.3112	0.1350	1016	
	0.0139	0.3178	0.1469	1106	
$S_Y = 0.0125$	0.0083	0.2830	0.0969	730	
$S_X = 0.0500$	0.0097	0.2950	0.1085	817	12.05
	0.0111	0.3020	0.1209	911	
	0.0125	0.3110	0.1321	995	
	0.0139	0.3175	0.1440	1085	
$S_Y = 0.0125$	0.0083	0.2810	0.0960	723	6.02
$S_X = 0.100$	0.0097	0.2935	0.1079	813	
	0.0111	0.3010	0.1203	906	
	0.0125	0.3090	0.1318	992	
	0.0139	0.3145	0.1439	1084	

Table 6.2: Submerged case: Hydraulic parameters of the experiments

(Constant longitudinal spacing)

Placement pattern of vegetation element (m)	Q (m^3/s)	h (m)	U (m/s)	Re (-)	λ (m^{-1})
	0.0083	0.28925	0.0955	719.47	18.83
Sx =0.02	0.0097	0.298	0.1081	814.07	18.83
Sy =0.02	0.0111	0.30625	0.1201	904.64	18.83
	0.0125	0.315	0.1313	988.72	18.83
	0.0139	0.32175	0.1428	1074.95	18.83
	0.0083	0.289	0.0951	716.02	15.06
Sx =0.02	0.0097	0.29725	0.1078	811.67	15.06
Sy =0.025	0.0111	0.30675	0.1193	898.29	15.06
	0.0125	0.314	0.1310	986.77	15.06
	0.0139	0.3215	0.1421	1070.32	15.06
	0.0083	0.285	0.0956	720.19	9.41
Sx =0.02	0.0097	0.297	0.1070	805.82	9.41
Sy =0.04	0.0111	0.301	0.1207	908.54	9.41
	0.0125	0.308	0.1326	998.57	9.41
	0.0139	0.3155	0.1437	1082.27	9.41
	0.0097	0.289	0.1097	826.15	7.53
Sx =0.02	0.0111	0.2965	0.1222	920.04	7.53
Sy =0.05	0.0125	0.304	0.1340	1009.24	7.53
	0.0139	0.3105	0.1457	1097.21	7.53
	0.0097	0.288	0.1096	825.65	4.71
Sx =0.02	0.0111	0.2945	0.1225	922.64	4.71
Sy =0.08	0.0125	0.302	0.1344	1012.02	4.71
	0.0139	0.3085	0.1462	1100.62	4.71
	0.0097	0.288	0.1095	824.51	3.77
Sx =0.02	0.0111	0.297	0.1213	913.59	3.77
Sy =0.10	0.0125	0.304	0.1333	1004.00	3.77
	0.0139	0.3105	0.1450	1092.09	3.77

6.4 Adjustment lengths for fully developed flow velocity measurement

To determine the adjustment length L_u beyond which uniform flow condition is reached, profiles of the longitudinal velocity about the clear water region at different vertical transects along the longitudinal center-line were measured using a 3D side-looking ADV. Figure (6.2) shows the velocity profiles for the case of vegetation with different areal density at x = 4.9, 5.05, 5.2, 5.3 and 5.4m, corresponding to 2.0, 1.75, 1.6, 1.5 and 1.4m downstream of the leading edge of the vegetation edge. Convergence of the profiles is observed and it is expected that the convergence of the velocity profiles within the vegetation zone should also be reached. Consequently, velocity measurements were conducted for the whole vertical transect at 2.2m downstream of the leading edge. Blades were removed to enable the velocity measurements within the vegetation zone.

Further confirmation that the uniform flow condition is reached at 2.2m downstream of the leading edge is done by using the empirical equation proposed by Zeng and Li (2014) for mean velocity.

$$L_u = 1.5 \frac{U_m}{\sqrt{-(u'w')_{\max}}} \tag{6.6}$$

where U_m is the mean velocity, $-(u'w'))_{max}$ is the peak Reynolds stress per unit mass.

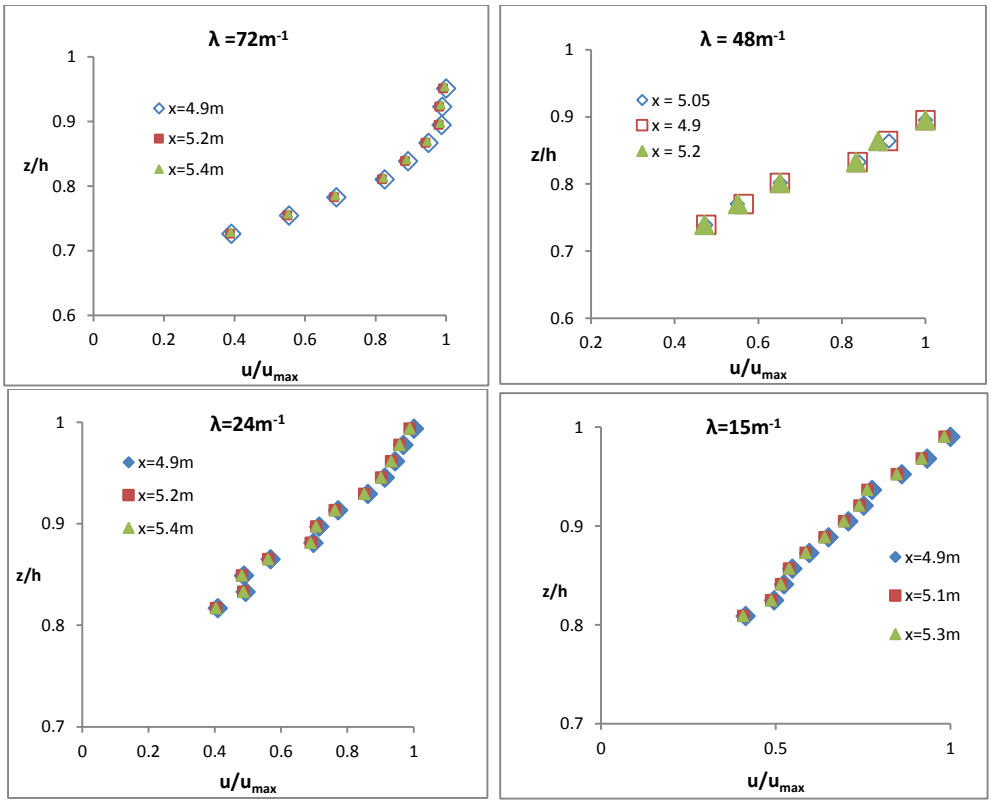

Figure 6.2: Stream-wise mean velocity profiles in clear water zone

Based on the velocity measurements for cases of vegetation with different areal densities and different flow rates, the empirical equation (6.6) yields $0.48m \leq L_u \leq 0.83m$ for $6\ m^{-1} \leq \lambda \leq 72\ m^{-1}$. The adjustment length is found to increase with increasing flow rate and decrease with increasing areal density of vegetation.

Table 6.3: Adjustment length, L_u (m) using empirical equation 6.6

		Q(m^3/hr)					
		25	30	35	40	45	50
λ (m^{-1})	72	0.67	0.48	0.50	0.53	0.56	
	48		0.63	0.62	0.67	0.62	0.74
	24		0.56	0.59	0.57	0.63	0.63
	12		0.69	0.64	0.68	0.73	0.77
	6		0.76	0.75	0.79	0.82	0.83

6.5 Results and discussion

The results are discussed separately for cases with constant lateral spacing and cases with constant longitudinal spacing.

6.5.1 Constant lateral stem spacing

By varying the longitudinal spacing at fixed lateral spacing, the following observations can be drawn on water surface profile, mean stream-wise velocity, vertical distribution of Reynolds stress, and flow regime describing the dependency of C_d on Re and λ.

6.5.1.1 Water surface profiles, velocity profiles and Reynolds stress profiles

The water surface elevations under various hydraulic conditions have been produced and the position of vegetation patch is described with the two red-dot vertical lines (Fig. 6.3). The direction of flow is marked by the arrow line. Figure (6.3) shows all cases except the case with $\lambda = 24 m^{-1}$, which similar trend. For these experiments the resistance force generated by the vegetation is smaller than the gravitational force due to the bottom slope and consequently a backwater appears at the downstream edge with a positive surface slope along the flow. The backwater effect decreases with the areal density of vegetation and the flow rate. The average water surface slope increases with increasing areal density and the surface profiles appear to be rougher. Generally, the larger the longitudinal spacing, the smoother the surface profile irrespective of flow rates.

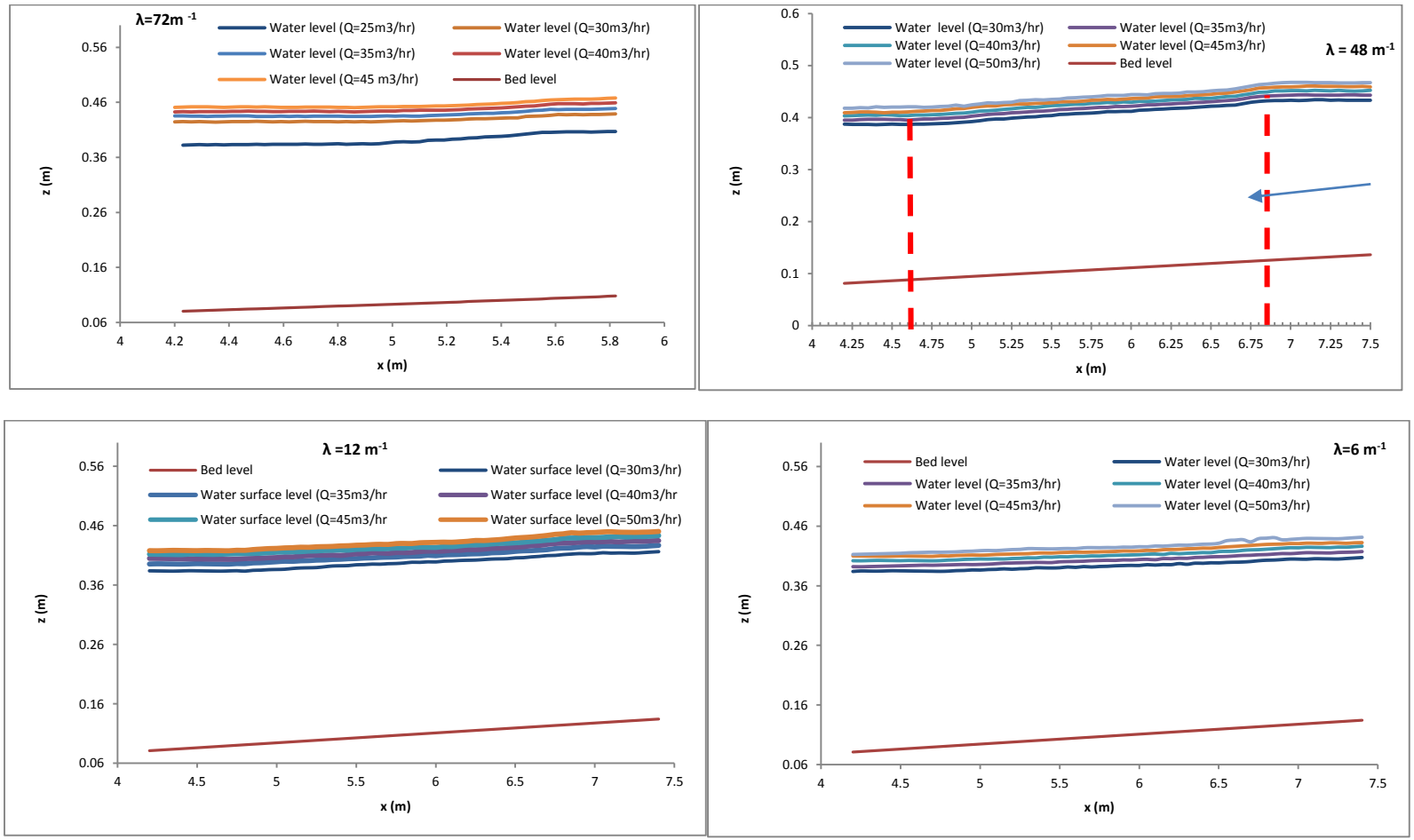

Figure 6.3: Water surface elevation through submerged vegetation (for fixed lateral spacing)

The mean longitudinal, transverse and vertical velocity components (*u*, *v*, *w*) at the centerline of the flume were measured using a 3D side-looking ADV. Figure (6.4), shows the velocity profile for cases with different values of vegetation density λ. For every distribution pattern of blades six sets of experiments of different flow rates (see Table 6.1) were conducted. The velocity profiles for different λ are shown for the ranges of flow rates, the results are of similar trends. Figure (6.4) shows that the velocity profile within the vegetation zone is approximately uniform for all cases. The apparent effect is the increase of water level for increasing flow rate.

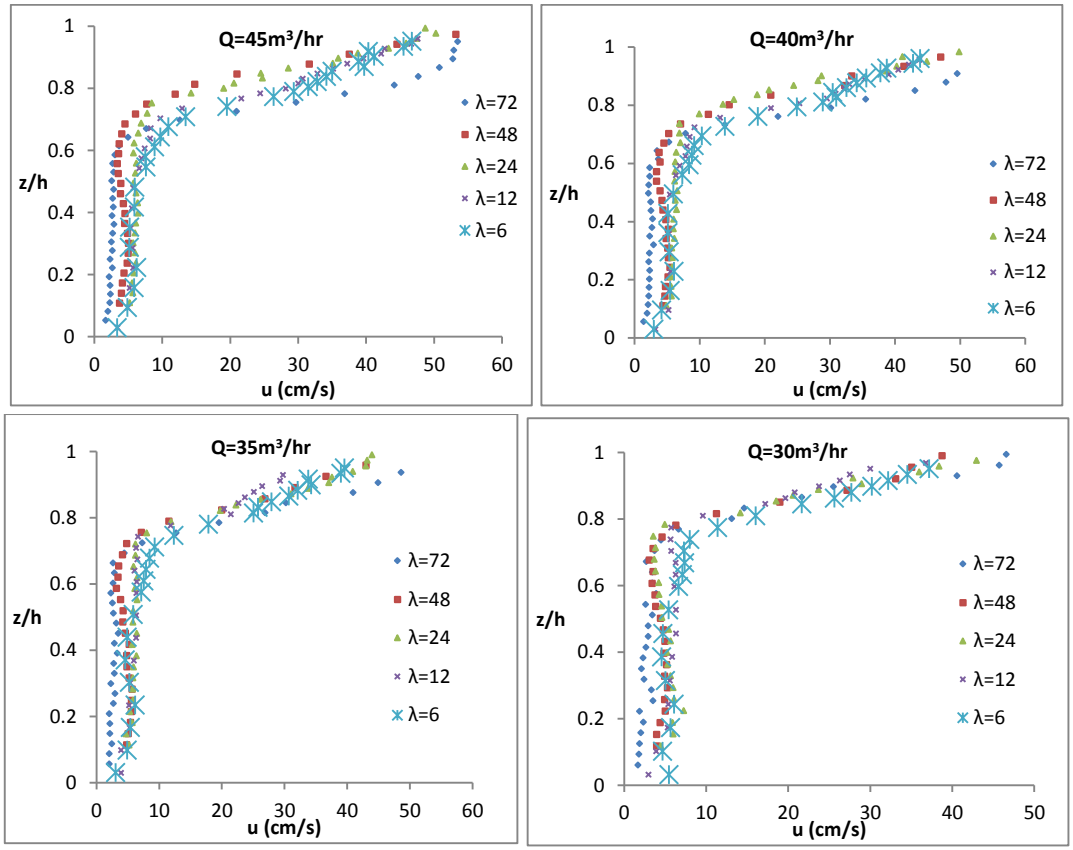

Figure 6.4: Cases with S_y = 0.0125m: Vertical mean velocity profiles

It can be observed that for a given flow rate, the longitudinal velocity in the vegetation zone increases with decreasing λ. The distribution of the velocity in the clear water zone is affected by turbulence penetration. The velocity profile in the clear water zone can be described by an exponential function. A sharp change in the velocity gradient occurs at the interface between vegetation zone and clear water zone for all cases due to the discontinuity of the drag at the top of the vegetation.

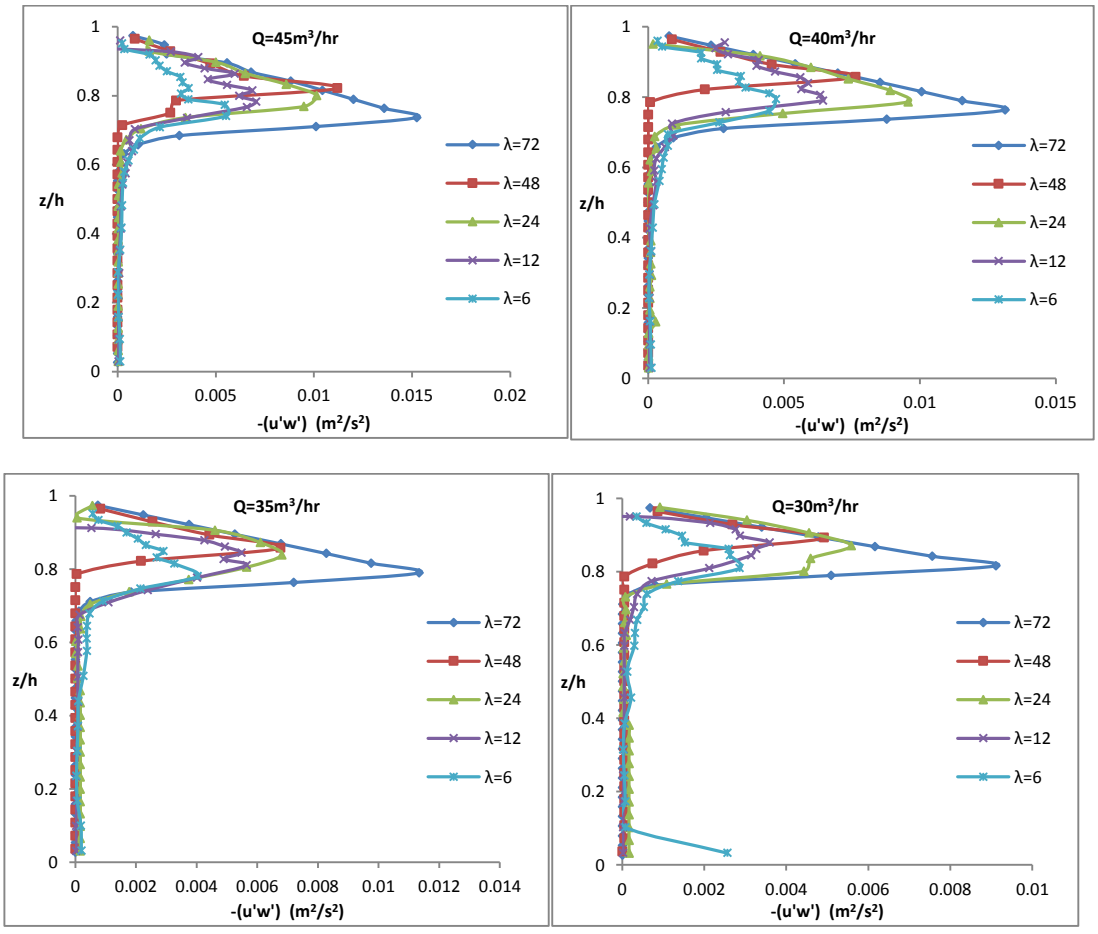

Figure 6.5: Cases with S_y = 0.0125m: Vertical distribution of Reynolds stress

Shear layer vortices are generated which control the exchange of momentum between the vegetation zone and clear water zone. This implies that the shear force on

plant surfaces due to viscous stresses can be significant. Since the vegetation height is close to the water depth, intensive turbulence exchange occurs in the clear water zone. In Figure (6.5), the distribution of turbulence stresses obtained from the measured turbulent velocities (u', v', w') is illustrated. The Reynolds stress increases linearly from the water surface and reaches the maximum at the top of the vegetation. The peak value increases with the vegetation density λ and the turbulence penetration increases with decreasing λ.

6.5.1.2 Flow regime and drag characteristics

The drag coefficient C_d is determined from Eq. (6.3). Figure (6.6a) shows the dependency of drag coefficient on flow regime, the drag coefficient decreases with increasing blade Reynolds number. The relationship yields a resistance equation which is best described as follows:

$$\left.\begin{aligned} C_d &= me^{n\,\mathrm{Re}} \\ m &= f\left(S_x, S_y\right) = 0.906\left(\frac{A_b}{S_x S_y}\right)^{-0.525} \end{aligned}\right\} \qquad (6.7)$$

where m is a parameter that decreases with increasing vegetation density λ, A_b is the blade cross sectional area and n is a constant (= -0.002). The correlation coefficient of the fitting is very high, greater than 0.99. The equation (6.7) is only applicable to describe sheltering effect and cannot be generalized to capture other interference mechanisms. A more holistic equation for computing C_d for submerged vegetation irrespective of the interference mechanisms is proposed in section 6.6. The effect of

increasing flow rate on drag coefficient becomes more significant with increasing longitudinal spacing due to increasing longitudinal velocity in the vegetation zone.

In Figure 6.6b, C_d' is defined based on equation 6.6, where by the vegetative drag term in the longitudinal momentum balance for the patch (in equation 6.3) has been modified to $0.5\rho C_d'\lambda h_v U_v^2$ (Equation 6.4). C_d' is less sensitive to the variation of Re and the values scatter around the best fit line. This result is more realistic than that obtained in Figure 6.6a since the velocity in the vegetation zone is quite low. Therefore, the assumption average pore velocity will affect the results especially for shallow water depth. Hence, C_d' is considered to be the more appropriate bulk drag coefficient for the submerged case. Generally, for the given Re, C_d and C_d' decreases with S_x indicating that the hydraulic resistance is lowered by sheltering.

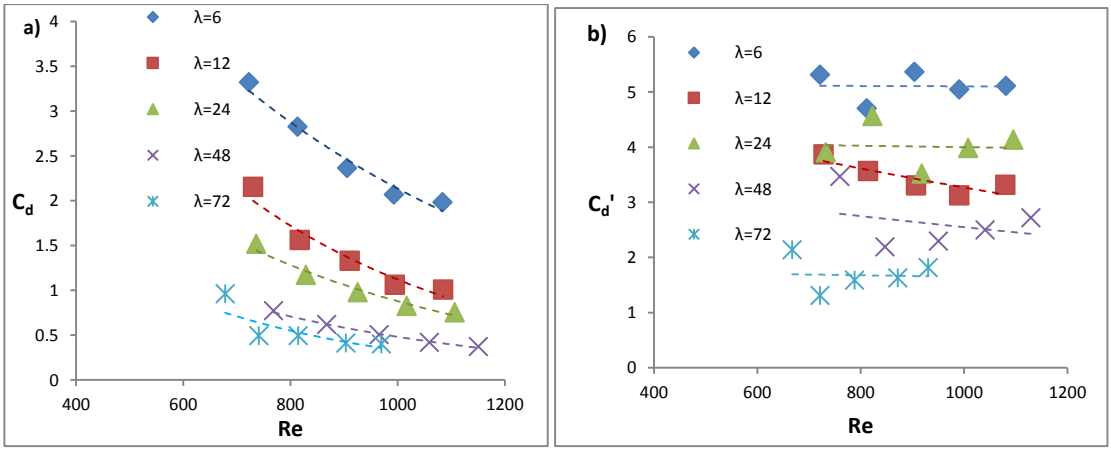

Figure 6.6: Dependence of drag coefficient on Re (S_y = fixed); a) using average pore velocity, b) using mean stem layer velocity.

Figure (6.7) illustrates that for a given discharge, higher areal density of vegetation causes the decrease of drag coefficient due to increasing sheltering effect. The effect of increasing flow rate is less apparent at low density ($\lambda = 6$ m^{-1}) case due to high velocity with increasing penetration depth. Also, the mean value of C_d for different flow rates appears low at high density ($\lambda = 72$ m^{-1}) since the blades behave as a continuum. This result is consistent with the emergent case (Figure 5.5a).

Now that C_d' values have been estimated, the parameter $C_d'\lambda h_v$ proposed by Nepf (2012) can be calculated to evaluate whether the vegetation canopies considered in this study are actually dense. According to Nepf (2012), a canopy with $C_d'\lambda h_v < 0.1$ is considered sparse, otherwise is dense. For the present study, the value of the parameter ranges between 0.99 and 41.82 for the total 62 cases. Therefore, the submerged vegetation in this study are of high areal density and shear layer flows will be formed.

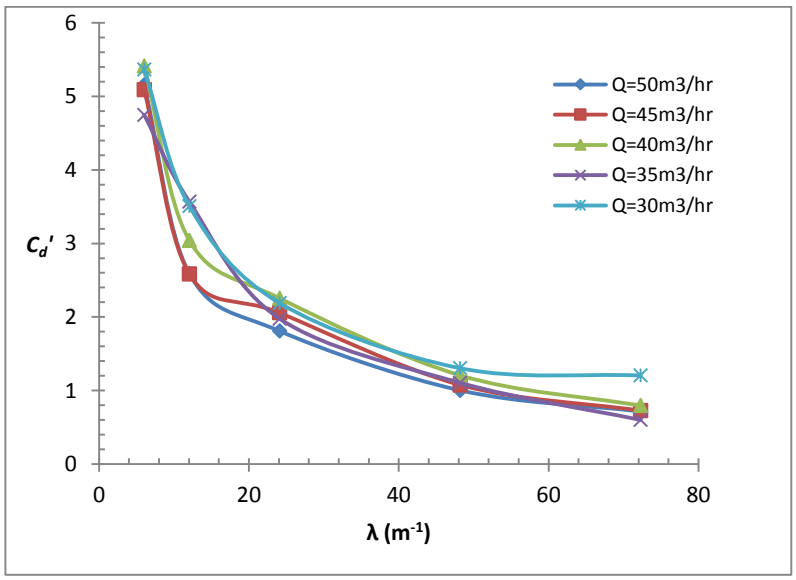

Figure 6.7: Areal density variation (S_y = fixed) and drag coefficient

In Figure (6.8), a normalized drag force ($f_d = F_d/(\mu U)$), where f_d (U_v) and $f_d(U)$ denote the drag force normalized by the mean velocity in the vegetation zone and the drag force normalized by the average pore velocity (Equation 6.1) respectively is presented.

By using the average pore velocity U as the characteristics velocity, the normalized drag force is smaller and the C_d value is underestimated (Busari and Li, 2015c). Using U_v as the characteristic velocity is more proper as it leads to a higher normalized drag force which is more consistent with that in the emergent case.

For small S_x, the flow in the vegetation layer is low and eddies are weak in the gaps and the wake formation is strongly interfered. As S_x increases, the intrusion of flow into gaps becomes stronger and the drag coefficient increases as flow within the blades increases. The effect of flow rate seems insignificant due to the low velocity in the vegetation zone.

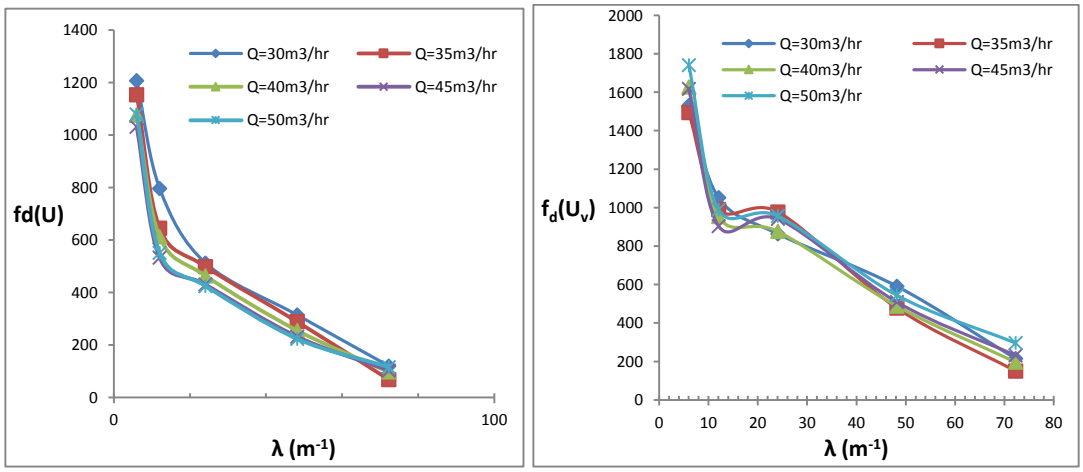

Figure 6.8: Normalized drag force as a function of blade areal density: a) using average pore velocity, b) using mean stem layer velocity.

Figure 6.9 illustrates the normalized drag force f_d as a function of Re for constant S_y, f_d varies approximately linearly with Re for all cases. The slopes of the lines are rather flat, showing that the dependence of f_d on Re is weak. The trend is valid to both velocity scales (Figure 6.9a and Figure 6.9b). However, for large S_x, the f_d – Re relationship deviates slightly from a straight line.

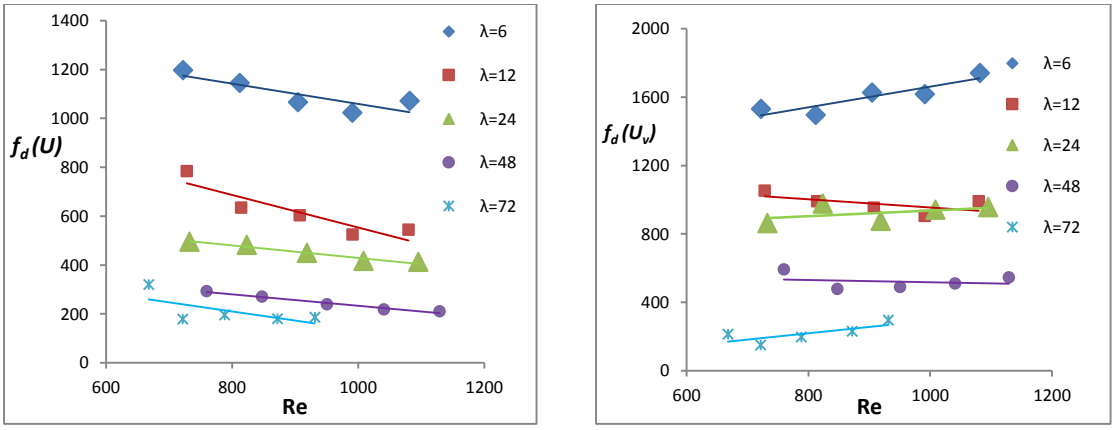

Figure 6.9: Normalized drag force as a function of Re; a) using average pore velocity, b) using mean stem layer velocity.

6.5.2 Constant longitudinal stem spacing

By varying the lateral spacing at fixed longitudinal spacing, the following observations can be drawn on water surface profile, mean stream-wise velocity, vertical distribution of Reynolds stress, and flow regime describing the dependency of C_d on Re and λ.

6.5.2.1 Water surface profiles, velocity profiles and Reynolds stress profiles

The water surface elevations under various hydraulic conditions of varying lateral spacing have been produced and the position of vegetation patch is described with the two red-dot vertical lines (Figure 6.10). The direction of flow is denoted by the arrow line. Figure (6.10) showed selected cases as other sets of results are of similar trends. Compared to the cases with constant lateral spacing, the resistance offered by vegetation is generally less since the λ value ranges from 3 to 18 m^{-1}, while in the cases with constant lateral spacing the λ value ranges from 6 to 72 m^{-1}. The backwater effect is reflected by an approximately horizontal water surface. The water surface profiles generally appear less roughened and flows are quite uniform (as $\Delta h/\Delta x$ is negligibly smaller). The flow regime in the vegetation zone is faster in the gap between blades and less flow is diverted to the clear water zone. However, in case of fixed lateral spacing, the velocity relatively low in the vegetation zone due to hydraulic resistance, hence, resulting larger divergent flow over the surface of the canopy. A backward effect is developed to balance the gravity force leading relatively large surface than experienced under channeling effect. Generally, the larger the lateral spacing (for fixed longitudinal spacing), the smoother the surface profile irrespective of flow rates.

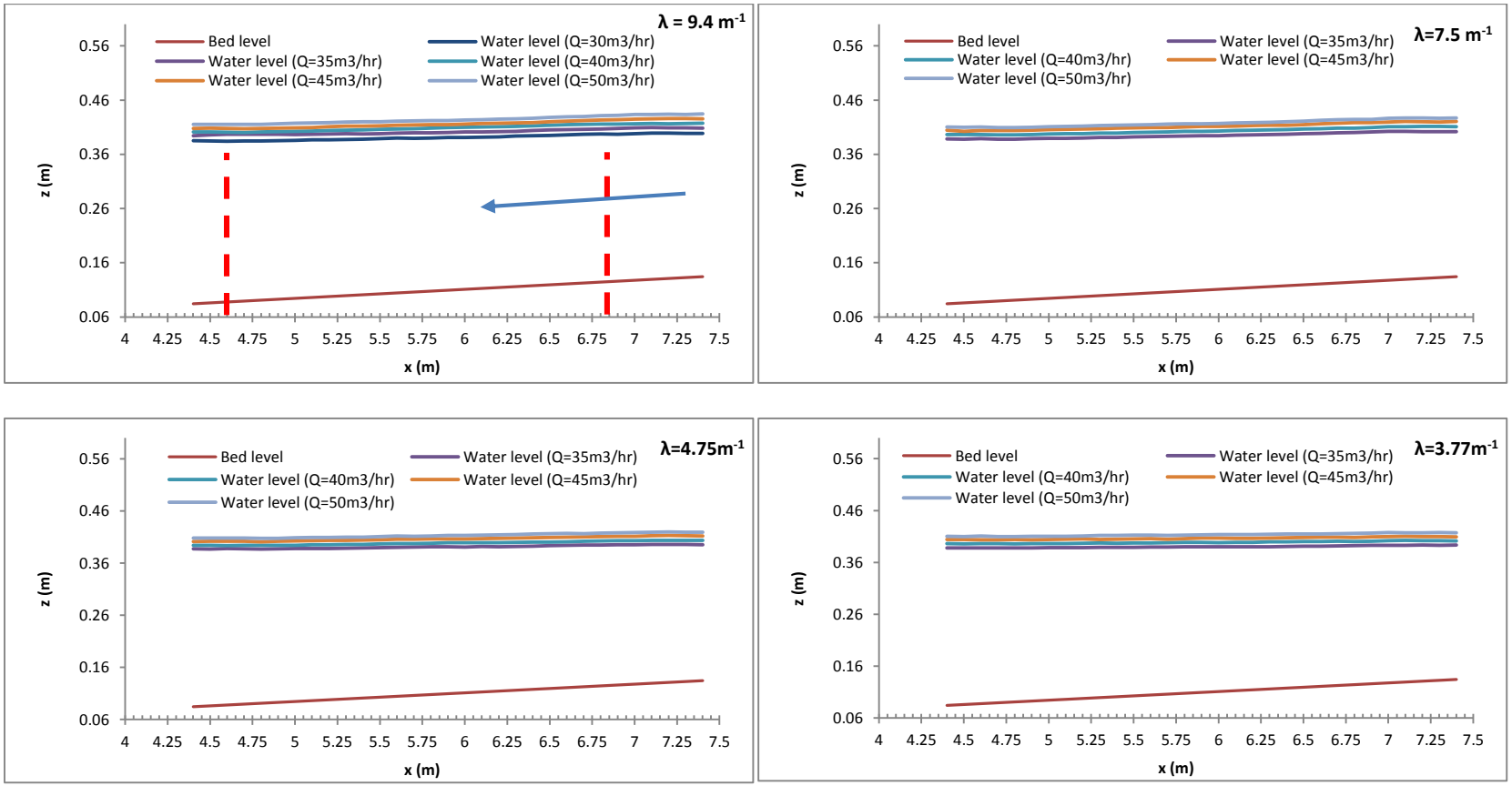

Figure 6.10: Water surface elevation through submerged vegetation (fixed longitudinal spacing)

Figure (6.11), shows the velocity profile for cases with different values of vegetation density λ at constant longitudinal spacing (S_x = 0.02m). The velocity profile within the vegetation zone is approximately uniform for the densities. More so, entire shape of the velocity profiles seem to be similar for both cases). The mean velocity in the vegetation zone is higher and the velocity gradient is less than that for the case with constant lateral spacing, showing that the resistance force is lower.

It can be observed that for a given flow rate, the longitudinal velocity in the vegetation zone increases with decreasing vegetation density λ and this phenomenon is more apparent at lower flow rates. The distribution of the velocity in the clear water zone is much affected by turbulence penetration. The velocity profile in the clear water zone can be described by a logarithmic function. Similar to the cases with constant lateral spacing, a sharp change in the velocity gradient occurs at the interface between vegetation zone and clear water zone for all cases due to the discontinuity of the drag at the top of the vegetation.

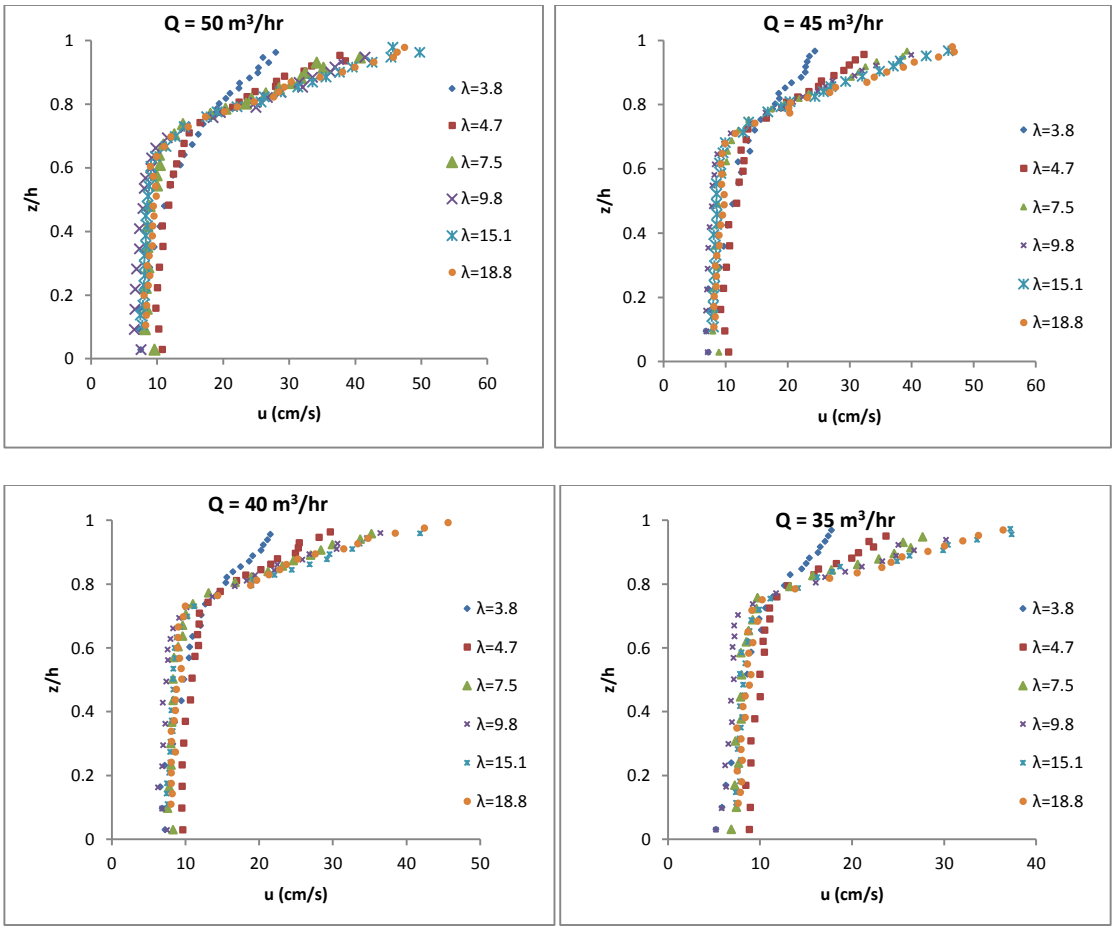

Figure 6.11: Cases with S_x = 0.02m: Vertical mean velocity profiles

Figure (6.12) displays the Reynolds stress profiles obtained from the measure turbulent velocities. The Reynolds stress increases with vegetation density λ. The peak values are less than those in the cases with constant lateral stem spacing because of lower resistance. The Reynolds stresses have near-zero values in the vegetation zone due to a balance between the gravity force and the vegetation resistance force. Also, the turbulence generated by the coherent vortices penetrates slightly deeper into the vegetation zone.

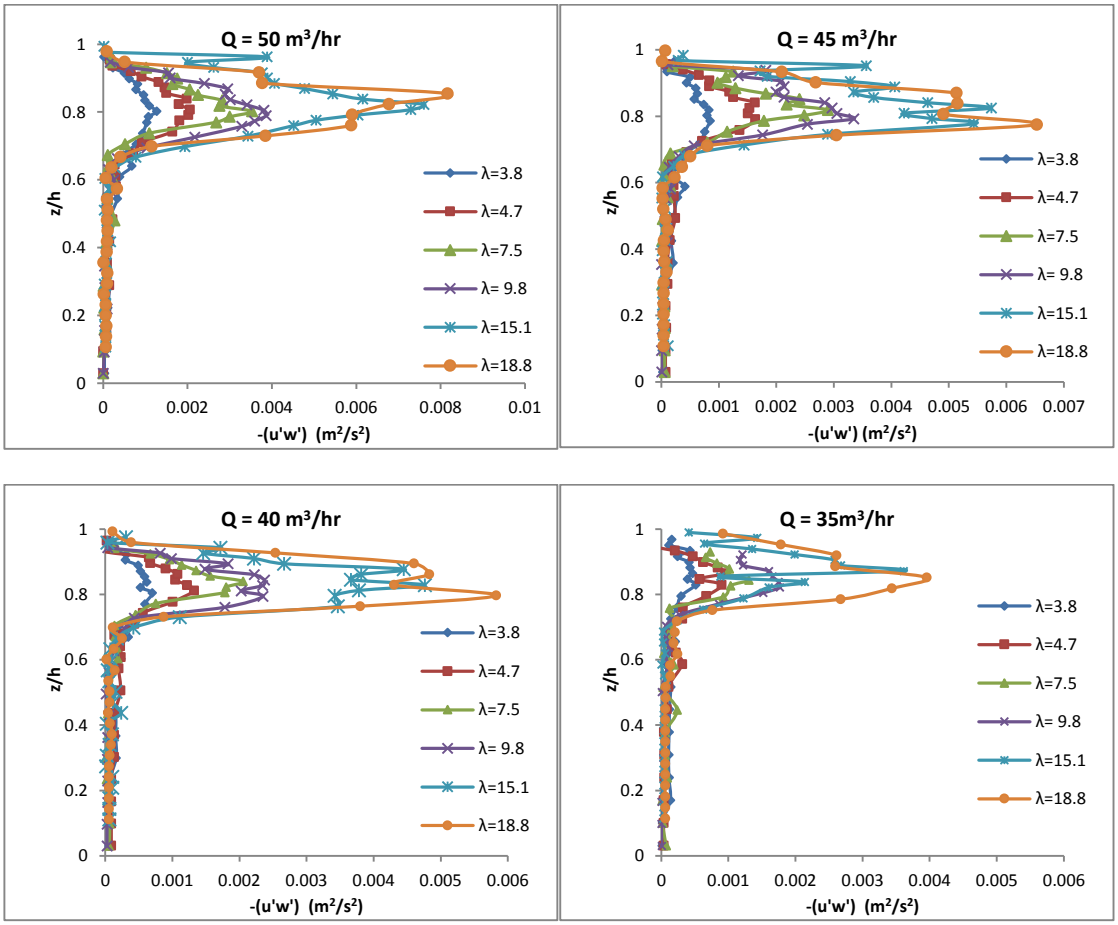

Figure 6.12: Cases with S_x = 0.02m: Vertical distribution of Reynolds stress

6.5.2.2 Flow regime and drag characteristics

The variation of C_d' with Re is shown in Fig. 6.13b. For a given Re, C_d' increases with decreasing lateral stem spacing, S_y. For the case of S_x = 0.0125 and S_y = 0.02m (λ = 30.12m^{-1}), the interpolated value gives $C_d' = 4$. Figure 6.13a shows that the C_d decreases monotonically with increasing Re. Also, from figure 6.13b C_d' decreases monotonically with increasing Re for high density. Similar trend is obtained for the

other interference mechanisms (section 6.5.1) including emergent vegetation case. However, the *bulk drag coefficient* appears insensitive to Re at lower densities irrespective of the velocity scale (Figure 6.13), this indicates that at large S_y channeling effect can be insignificant.

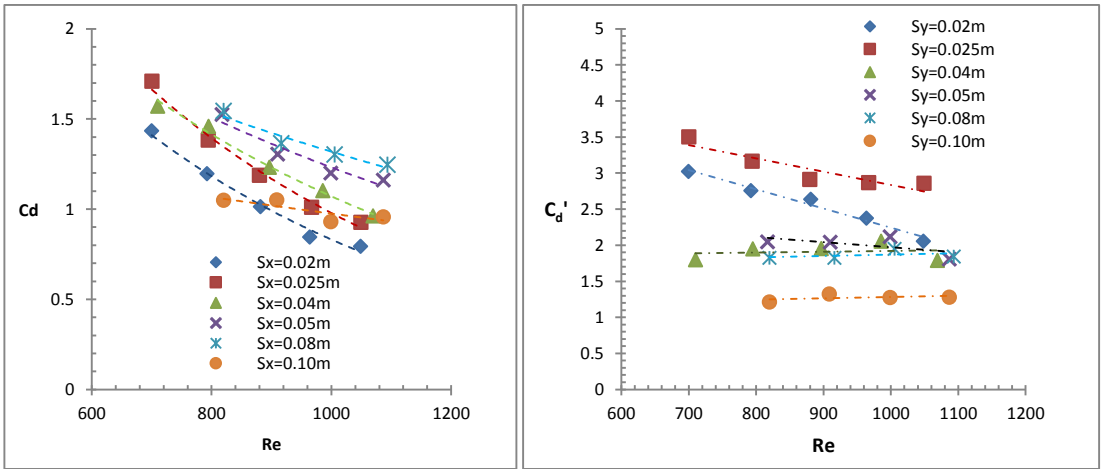

Figure 6.13: Dependence of drag coefficient on Re (S_x = fixed); a) using average pore velocity, b) using mean stem layer velocity.

In Figure (6.14) the effect of increasing lateral stem spacing is investigated. By widening the gap between the blades, more water passes through the vegetation zone and reduces the hydraulic resistance. An increase in drag coefficient with decreasing spacing is resulted. For cases with small S_y (large λ), increasing flow rate produces significant changes in the value of C_d'. This indicates the wake interference is significant and affected by the flow velocity. The effect of increasing flow rate is insignificant for cases with lower vegetation density since the blades are widely separated, and the wake interference is weak.

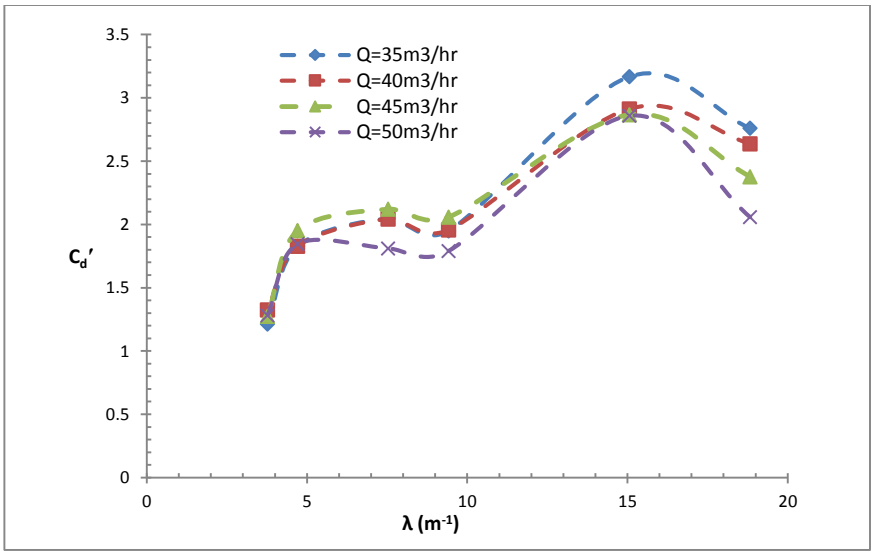

Figure 6.14: Variation of drag coefficient with areal density of vegetation (S_x = constant)

In Figure (6.15), it is observed that irrespective of flow rate, f_d' generally increases with decreasing lateral stem spacing. It can be shown that $f_d' = C_d' h_v \mathrm{Re}$, if U_v is taken as the characteristic velocity.

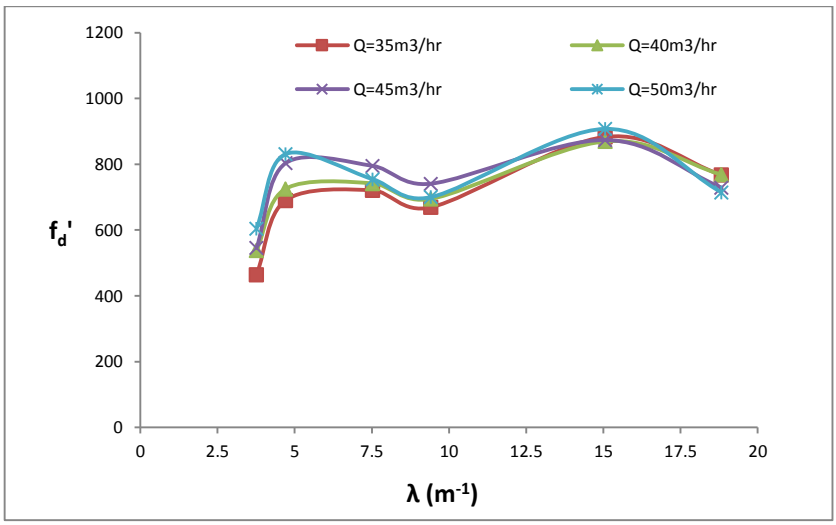

Figure 6.15: Normalized drag force as a function of blade areal density (S_x = constant).

Figure 6.16 illustrates the normalized drag force f_d' as a function of Re for constant S_x, f_d' varies approximately linearly with Re for all cases. However, for large lateral spacing (S_y), the f_d' – Re relationship deviates slightly from a straight line. For a given Re, the f_d' increases with increasing λ, indicating that the channeling effect plays a dominant role. The trend is opposite of Figure 6.9.

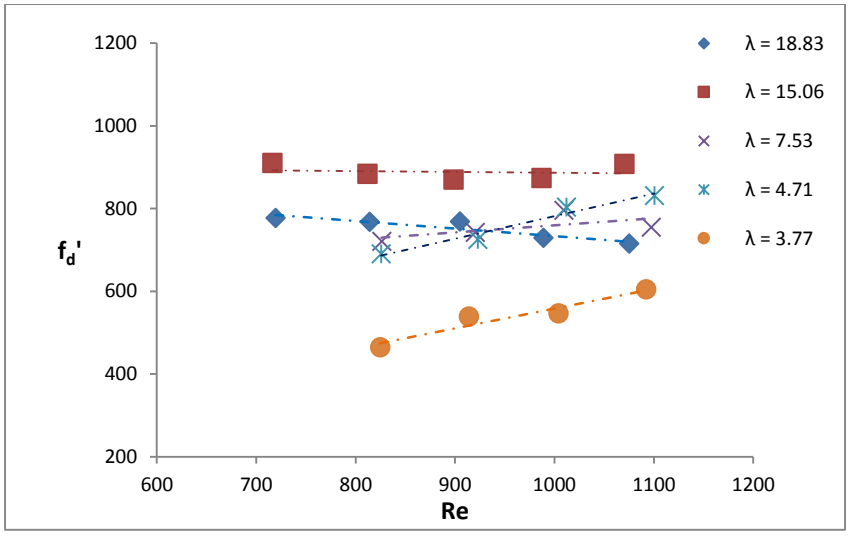

Figure 6.16: Normalized drag force as a function of Re using mean stem layer velocity.

The straight line fitting shows that the intercept on the vertical axis increases with decreasing lateral spacing, S_y, this implies that the shear force on plant surfaces due to viscous stresses is lesser.

6.5.3 The effect of vegetation distribution pattern

The effect of vegetation distribution pattern on the flow characteristics is investigated by using two cases of experiments. The first case is of S_y = 0.0125m, S_x = 0.10m, and the second case is of S_y = 0.05m, S_x = 0.025m. Both cases have the λ value of 6 m^{-1}. Figure (6.17) and Figure (6.18) show the velocity profiles and Reynolds stress profiles for the discharge of 0.0125m^3/s. The difference of the mean velocity in the vegetation zone and that in the clear water zone is lesser for the case with S_y = 0.05m. Thus more water flows over the vegetation for the case with S_y = 0.0125m, indicating that the resistance in the vegetation zone is higher.

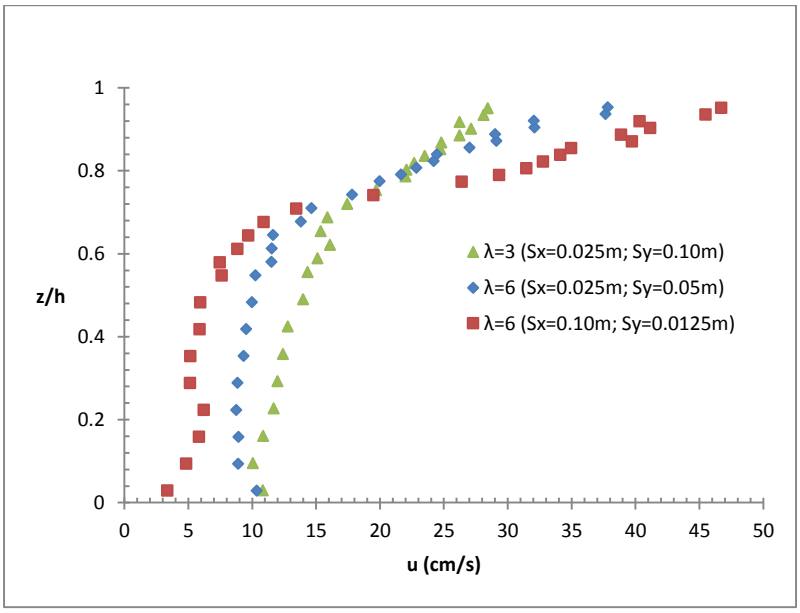

Figure 6.17: Vertical mean velocity profiles for λ = 3m^{-1} and 6m^{-1}.

Figure 6.18 shows that the highest peak Reynolds stress is measured for the case with S_y = 0.0125m, which confirmed that this case has the highest resistance. Physically,

this case has the narrowest lateral stem spacing which allows the least flow to pass through the vegetation zone.

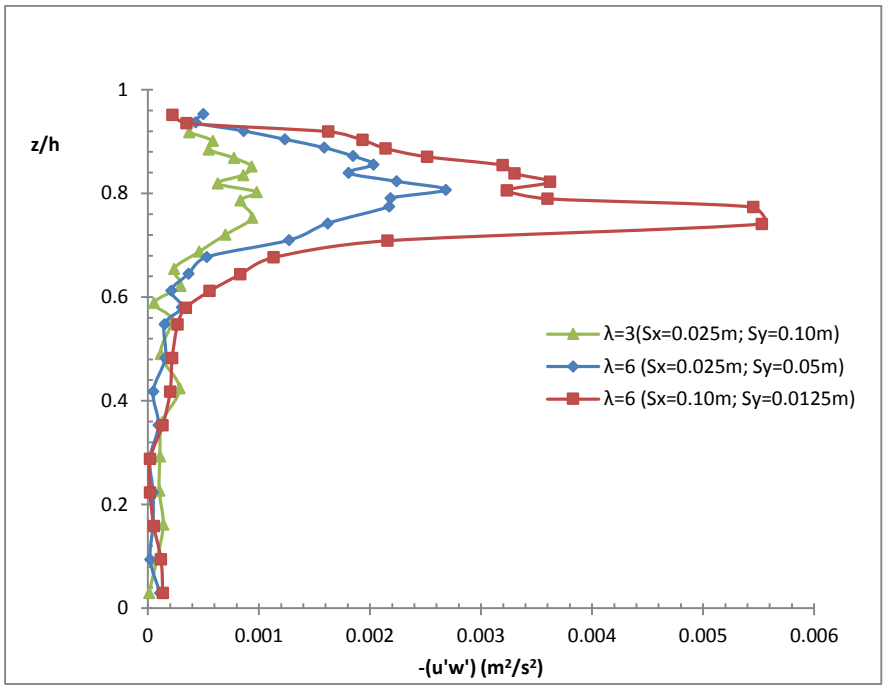

Figure 6.18: Vertical distribution of Reynolds stress for $\lambda = 3m^{-1}$ and $6m^{-1}$.

The effect of increasing the lateral stem spacing is investigated by adding the case with S_y = 0.100m and S_x = 0.025m, with $\lambda = 3m^{-1}$. Comparing to the case with S_y = 0.050m, S_x = 0.025m ($\lambda = 6m^{-1}$), the case with $\lambda = 3m^{-1}$ allows more water pass through the vegetation zone. The flow resistance is smaller and thus the peak Reynolds stress and the drag coefficient is lower (Figure 6.19). This result shows that the drag coefficient increases with the vegetation density λ, which is of the opposite trend with that shown in Figure (6.8) and similar to the observed trend at high lateral stem spacing in Figure (6.14). By keeping the same value of S_x for the two cases, the sheltering effect

remains more or less constant. Increasing S_y allows more water flowing through the vegetation zone and reduces the hydraulic resistance.

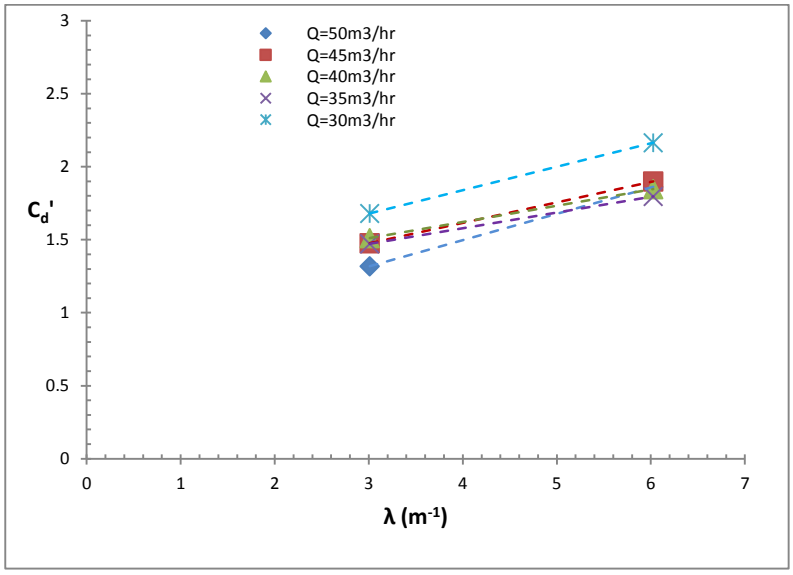

Figure 6.19: Effect of channeling phenomena on drag coefficient (S_x = 0.025m)

6.6 Equation for estimating C_d' for flow through submerged vegetation

Similar to the cases with emergent vegetation, the following equation is proposed to fit data of the bulk drag coefficient for cases with submerged vegetation:

$$C_d' = C_{d0}'\{f(S_x)\}\{g(S_y)\} \tag{6.8}$$

$$\left.\begin{aligned} f(S_x) &= \left\{1 - \beta e^{-K\left(\frac{S_x}{w}\right)}.Re^{-\gamma}\right\} \\ g(S_y) &= \left\{1 + \alpha e^{-L\left(\frac{S_y}{w}\right)}.Re^{-\delta}\right\} \end{aligned}\right\}$$

For $S_x \to \infty$; $S_y \to \infty$ and $R_e \to \infty$, $C_d' \to C_{d0}' = 2$.

Using the multiple regression method, a fairly good match between the fitting equation and the data is obtained (Figure 6.20) with the parameters taking the following values: $\beta = 0.329;\ \alpha = 43.399;\quad K = 0.864;\quad L = 0.3872;\quad \gamma = -0.238;\ \delta = 0.418$. Figure 6.20 shows that the fitting results, the results are scattered around the line of agreement, equation (6.8) slightly overestimate the bulk drag coefficient especially for sheltering effect where the effect of interfacial shear stress is expected to be significant, the coefficient of multiple determination (R^2) of the regression is 0.80.

.

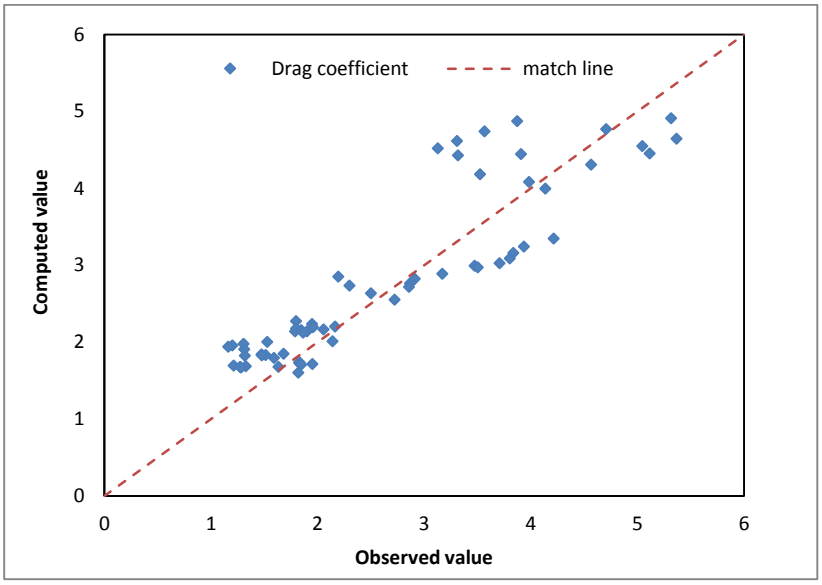

Figure 6.20: Comparison between fitting results of C_d' using equation 6.8 and the observed value.

The mechanisms of coherent motion of flow at the interface between the patch surface and clear water zone are not fully understood. The shear stress at the interface between the top surface of stems and the overflow layer for high areal density vegetation can affect the C_d' values. In this study, the velocity in the clear water zone is much

greater than the velocity within the vegetation zone (i.e. $U_a << U_v$) due to high areal density of vegetation. The influence of interfacial shear stress can be significant.

6.7 Comparison of the bulk drag coefficients of the submerged and emergent cases

The trend of the bulk drag coefficient values produced by the interference effects are very consistent for both emergent and submerged case as shown in Figures 6.21 and 6.22. It can be seen that the bulk drag coefficient for submerged case is smaller than that in emergent case. The physics of flow over vegetation is complex. The possible explanation for the difference in C_d values for the two cases could be:

(i) Due to the additional flow path at the top of the stems, which will reduce the suction (negative pressure) at the wake zone;

(ii) The fact that submerged vegetation is subjected to larger deflection than the emergent case, as a result, the drag will reduce.

These two effects will decrease with increasing vegetation areal density.

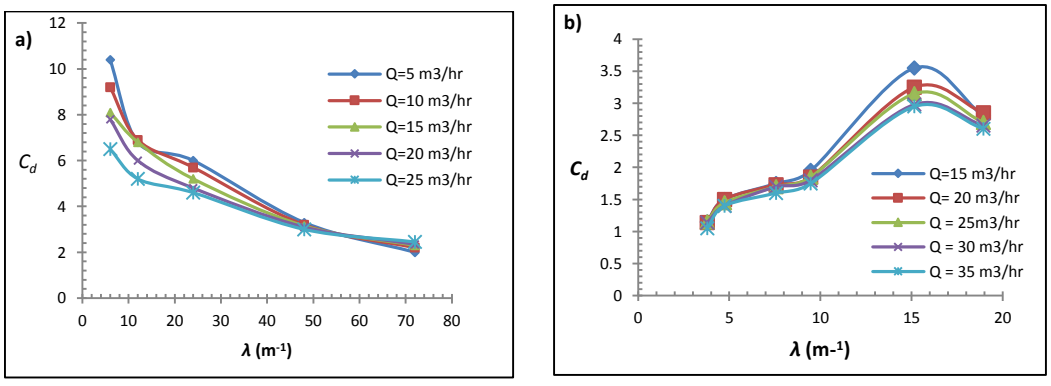

Figure 6.21: Emergent case: (a) Sheltering effect, (b) Channeling effect

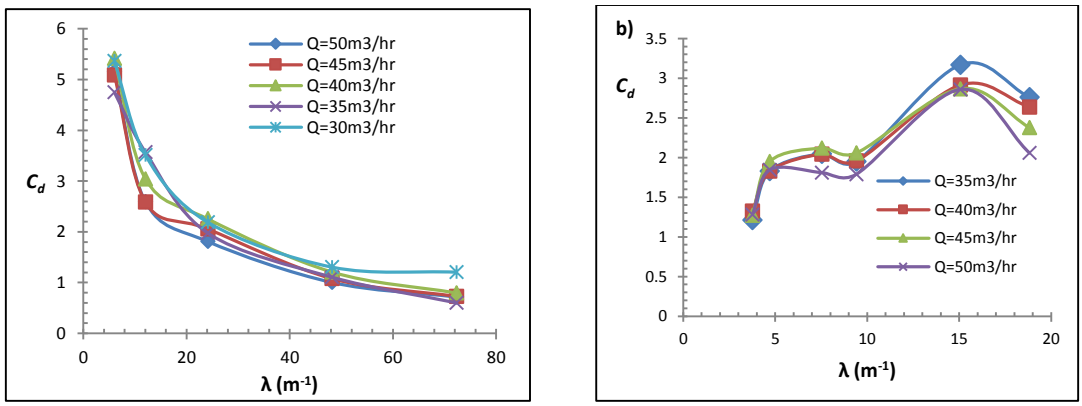

Figure 6.22: Submerged case: (a) Sheltering effect, (b) Channeling effect

6.8 Experimental measurement uncertainty

The bulk drag coefficient for dense vegetation under submerged condition of varying hydraulic conditions and interference effects in sections 6.5.1 and 6.5.2 has been carried out using the centerline mean velocity measured by ADV. Following the methodology in section 4.2.2 using equation (4.3), the measurement uncertainty is displayed in Table 6.4 and Table 6.5 for channeling effect and sheltering effect respectively. Generally, ψ values is between 0.14 and 0.18.

Table 6.4: Error in the measured mean velocity using centerline of the flume

(Constant longitudinal stem spacing)

λ (m^{-1})	18.825	18.825	18.825	18.825	18.825	15.060	15.060	15.060
$\bar{U}$ (m/s)	0.119	0.135	0.147	0.163	0.169	0.123	0.132	0.143
U(m/s)	0.139	0.157	0.171	0.190	0.196	0.143	0.154	0.166
Error (%)	16.244	16.159	16.106	16.193	16.153	16.083	16.219	16.208
λ (m^{-1})	15.060	15.060	9.413	9.413	9.413	9.413	9.413	7.530
$\bar{U}$ (m/s)	0.158	0.167	0.101	0.120	0.136	0.156	0.170	0.117
U(m/s)	0.183	0.195	0.115	0.138	0.155	0.178	0.194	0.134
Error (%)	16.144	16.231	14.286	14.286	14.286	14.286	14.286	14.286
λ (m^{-1})	7.530	7.530	7.530	4.706	4.706	4.706	4.706	4.706
$\bar{U}$ (m/s)	0.138	0.157	0.160	0.104	0.125	0.146	0.163	0.182
U(m/s)	0.158	0.180	0.183	0.119	0.142	0.167	0.186	0.208
Error (%)	14.286	14.286	14.286	14.286	14.286	14.286	14.286	14.286

Table 6.5: Error in the measured mean velocity using centerline of the flume

(Constant lateral stem spacing)

λ (m^{-1})	12.048	12.048	12.048	12.048	12.048	24.096	24.096	24.096	24.096	24.096
$\bar{U}$ (m/s)	0.110	0.111	0.159	0.175	0.187	0.106	0.140	0.131	0.152	0.166
U(m/s)	0.130	0.130	0.188	0.206	0.220	0.121	0.160	0.150	0.173	0.189
Error (%)	18.256	17.878	18.051	17.805	17.938	14.286	14.286	14.286	14.286	14.286
λ (m^{-1})	48.192	48.192	48.192	48.192	48.192	72.288	72.288	72.288	72.288	72.288
$\bar{U}$ (m/s)	0.091	0.087	0.095	0.096	0.144	0.050	0.081	0.084	0.089	0.135
U(m/s)	0.104	0.100	0.108	0.110	0.165	0.057	0.092	0.097	0.102	0.142
Error (%)	14.286	14.286	14.286	14.286	14.286	14.286	14.286	14.286	14.286	5.215

6.9 Summary

A thorough experimental examination of the characteristics of gradually-varied flows through semi-rigid blade-type submerged vegetation have been conducted. The areal density of vegetation is high and ranges from $\lambda = 3m^{-1}$ to $72m^{-1}$. Two interference mechanisms among the vegetation stems have been identified as described under emergent case: sheltering and channeling. It has been found that for regular arrays of blades with constant lateral stem spacing (S_y), the drag coefficient C_d decreases with increasing areal density of vegetation due to sheltering effect. For arrays of blades of constant longitudinal spacing (S_x), C_d increases with increasing areal density of vegetation due to channeling effect. The results showed that C_d should be relating to the lateral spacing and longitudinal spacing instead of solid volume fraction.

The distribution pattern of vegetation elements has been found to have significant effect on the drag coefficient and the associated flow characteristics, including flow adjustment length, peak Reynolds stress and flow division in the clear water zone and vegetation zone. The trend of the bulk drag coefficient values produced by the interference effects are very consistent for both emergent and submerged cases. The slight difference in drag coefficient values for the two cases particularly for longitudinal variation of spacing. This could be attributed to the 3D effect of vortex shedding behind the blades in the mixing layer due to over flow above vegetation for the submerged case.

An empirical equation that relates the (lateral and longitudinal) spacing ratio and Re is proposed for the calculation of the drag coefficient under submerged flow condition. A fairly good match between the fitting equation and experimental data has been observed, the data scattered around the line of agreement.

The flume measurements complement previous laboratory studies and advances our knowledge on the influence of interference effects on flow structure, turbulence distribution, adjustment length and most importantly, the bulk drag coefficient over the canopy length. Further work is required for submerged flexible vegetation. It would be interesting to investigate and quantify the effects of additional flow path at the top of the stems with respect to parameters such as submergence ratio, areal density and surface wave using the interference mechanism in the future work. It has to be emphasized that correct treatment of uncertainty contained in the measurements and proposed equations will implicitly yield better estimate of the C_d' value. Thus the performance of numerical models is enhanced.

7 Uncertainty analysis of vegetated flow modeling

7.1 Introduction

In numerical modelling, there are three principal sources of errors: modeling error, solution error and input error. Modeling error refers to the error induced by the formulation of the model in describing the physical phenomena, mainly is related to the inaccuracy of the modeling of turbulence. Solution error refers to the error induced during the solution processes, such as the grid discretization error, time stepping error and iteration error. Input error refers to the uncertainty in the input parameters, such as the water depth, discharge rate and etc.

For vegetated flows, the major input uncertainty will be the drag coefficient. In the previous two chapters, experimental studies have been carried out to determine more accurately the drag coefficient for flows through vegetation with regular array of stems. This can help to reduce the numerical modelling errors in simulating this kind of problem.

In field conditions, the vegetation parameters (height, stem diameters and etc.) and the flow conditions will be temporarily and spatially varied. For engineering purposes, numerical modelling is generally used to determine the flood water level or the discharge capacity of a vegetated channel. It is thus important to investigate the effect of uncertainty in the input parameters on the model output.

For vegetated flows, the spatiotemporal variation of vegetative resistance parameter (i.e. vegetation density, width, height, flexural rigidity) and flow condition is

very complex and hence, variability of discharge in open channels is inherent. The concept of sensitivity analysis starts with the measure of variance or coefficient of variation (CoV) of the model output by proportionate change in inputs. A larger value of CoV indicates larger degree of uncertainty in the variable (Johnson, 1996; Johnson and Docks, 1998; Tyagi and Haan, 2001). This is a preliminary description of uncertainty in a variable where data are available. Also, information on uncertainty from input random variables can be used to indirectly estimate the uncertainty associated with a response (random) variable using uncertainty approach.

In this chapter, the numerical model is used to reproduce the flume experiments conducted in chapter (6), thereby illustrating the capability of the RANS model to simulate the influence of interference effects on stream-wise mean velocity profile and the vertical distribution of Reynolds stresses using accurate mean drag coefficients obtained from laboratory experiments. In this regard, the accuracy in the formulation of the numerical model can be assessed. In addition, the sensitivity of the model output to changes in the input parameters is examined and the propagation of uncertainty through the numerical model is studied using the Unscented Transform (UT) method

7.2 Simulation set up

The RANS (S-A) model described in chapter three (3) was used to simulate the flume experiments. A total of 39 simulations were shown under different hydraulic conditions using measured bulk drag coefficient. Twenty scenarios are for cases with constant lateral stem spacing (sheltering effect) and the other scenarios are for cases

with constant longitudinal stem spacing (channeling effect). The key parameters are shown in Table 7.1 and Table 7.2. The focus is to assess the accuracy of the S-A model to replicate the mean stream-wise fully developed vertical velocity profiles through and above vegetation patches of different areal densities.

Table 7.1: Experimental hydraulic conditions and measured C_d' (sheltering effect)

λ (m^{-1})	h (m)	U (m/s)	f_{rk} (m^{-1})	f_v (-)	z_o/h_v (-)	gS_w (m/s^2)	C_d' (-)
12.048	0.283	0.097	46.654	11.617	0.900	0.054	3.872
12.048	0.295	0.109	42.979	10.702	0.895	0.069	3.567
12.048	0.303	0.121	39.839	9.920	0.890	0.066	3.307
12.048	0.312	0.132	37.682	9.383	0.886	0.074	3.128
12.048	0.318	0.144	39.964	9.951	0.890	0.064	3.317
24.096	0.287	0.098	94.202	23.456	0.937	0.020	3.909
24.096	0.297	0.110	109.981	27.385	0.943	0.012	4.564
24.096	0.304	0.123	84.918	21.145	0.932	0.010	3.524
24.096	0.311	0.135	96.006	23.905	0.937	0.011	3.984
24.096	0.318	0.147	99.680	23.824	0.937	0.010	4.137
48.192	0.287	0.102	167.295	41.824	0.957	-0.028	3.471
48.192	0.296	0.115	105.765	26.441	0.941	-0.024	2.195
48.192	0.304	0.128	110.870	27.717	0.943	-0.019	2.301
48.192	0.312	0.141	120.536	30.134	0.946	-0.013	2.501
48.192	0.319	0.153	131.171	32.793	0.949	-0.017	2.722
72.288	0.283	0.090	154.779	38.695	0.955	-0.142	2.141
72.288	0.311	0.098	94.833	23.708	0.937	0.002	1.312
72.288	0.330	0.108	115.027	28.757	0.945	-0.017	1.591
72.288	0.340	0.120	117.973	29.493	0.946	-0.014	1.632
72.288	0.357	0.129	131.514	32.879	0.949	-0.022	1.819

Note: *S_w is the average water surface slope*

The input parameters of the model are the flow depth (h), vegetation resistance parameter (f_{rk}), zero-plane displacement parameter (z_o/h_v), time averaged deflected stem height (h_d), gravity (driving) force (gS_w) and bulk drag coefficient. The number of grids

used is 41 and the time step size is in the order of 0.0005s to ensure computational stability. Grid convergence study shows that further reduction of grid size does not affect the results practically. The measured deflected vegetation height is on average 0.249m for cases with constant lateral stem spacing, whereas it ranges from 0.245 to 0.249m for cases of constant longitudinal stem spacing.

Table 7.2: Experimental hydraulic conditions measured C_d' (channeling effect)

λ (m^{-1})	h (m)	U (m/s)	f_{rk} (m^{-1})	f_v (-)	z_o/h_v (-)	gS_w (m/s^2)	C_d' (-)
18.825	0.289	0.096	77.599	19.400	0.928	0.052	4.122
18.825	0.298	0.109	74.090	18.523	0.926	0.048	3.936
18.825	0.306	0.121	72.229	18.057	0.925	0.046	3.837
18.825	0.315	0.132	71.604	17.901	0.924	0.050	3.804
18.825	0.322	0.144	69.789	17.447	0.923	0.04	3.707
15.060	0.289	0.095	52.763	13.191	0.908	0.06	3.504
15.060	0.297	0.108	47.716	11.929	0.902	0.059	3.168
15.060	0.307	0.120	43.868	10.967	0.897	0.057	2.913
15.060	0.314	0.132	43.177	10.794	0.896	0.057	2.867
15.060	0.322	0.143	43.056	10.764	0.896	0.051	2.859
9.413	0.285	0.096	16.930	4.232	0.817	0.105	1.799
9.413	0.297	0.107	18.347	4.587	0.825	0.98	1.949
9.413	0.301	0.121	18.414	4.603	0.825	0.094	1.956
9.413	0.308	0.133	19.365	4.841	0.831	0.090	2.057
9.413	0.316	0.144	16.845	4.211	0.816	0.090	1.790
4.706	0.288	0.110	8.600	2.150	0.735	0.128	1.827
4.706	0.295	0.123	8.603	2.151	0.735	0.125	1.828
4.706	0.302	0.134	9.181	2.295	0.744	0.120	1.951
4.706	0.309	0.146	8.684	2.171	0.737	0.115	1.845

7.3 Uncertainty analysis of input parameters

The reasons for using sensitivity/uncertainty analysis have been clearly spelt out in (Hall et al., 2009). For instance, sensitivity analysis is required to answer questions

like: Which vegetation parameter(s) have the most influence on model prediction? Which vegetation parameters require further investigation in order to improve the confidence in the model prediction? Is the model reproducing the known influences upon the processes it is replicating? The variation of which parameter will give the maximum model output change? In the followings, the influence of the input parameters below on the output of the numerical model will be examined. They are related to the channel discharge *(Q = UBh)* or *U* as response variable by

$$U = f\{h, h_v, Z_o, N, w, t, g, C_d', S_w, E\} \quad (7.1)$$

Based on physics, some variables can be grouped together and equation (7.1) yields

$$U = \{h, h_v, Z_o, EI, gS_w, f_{rk}\} \quad (7.2)$$

Where $f_{rk} = NC_d'w = \lambda C_d'$ and gS_w is the gravity driving force for gradually varied flow, $I = {wt^3}/{12}$ is the second moment of area, for blade type plants.

The model output is the mean horizontal velocity at different flow depth ($0 \leq z \leq h$) which can be aggregated to give the mean stream-wise vertical velocity (*U*) as used in section 7.4.1 to replicate the interference effects. For practical uncertainty analysis, the range of vegetation parameter variation is expected to be correlated with field data.

7.3.1.1 Selection of vegetation data

In nature, aquatic vegetation displays a wide range of geometrical characteristics. Some typical ranges of values of parameters are listed below. For typical vegetation, $0.001 \leq w \leq 0.01m$ (Leonard and Luther, 1995; Lightbody and Nepf,

2006); For seagrasses $0.003 \leq w \leq 0.01m$; $t \approx 10^{-3}m$; $10 \leq \lambda \leq 100\ m^{-1}$(Luhar, et al., 2010, Nepf, 2012); For grasses, $10 \leq h_v \leq 20\ cm$; $5 \times 10^{-6} \leq EI \leq 1 \times 10^{-3}N$ (Nepf and Vivoni, 2000; Ghisalberti and Nepf, 2002).

Assuming a shallow water depth open channel, h = 0.4 ~ 0.8m. The only parameter that requires additional information is f_{rk}, which is a function of bulk drag coefficient C_d'. For the laboratory experiments, the blade geometry satisfy the range of real grass morphology; $w = 0.00753m, t = 0.00168m$ and $3.01 \leq \lambda \leq 72.3\ m^{-1}$. Therefore, the C_d' in this present study, assuming it is accurate including other input vegetation parameters, could be justifiably applied to obtain the vegetation resistance parameter, f_{rk} rather than assuming values. For areal vegetal density; $10 \leq \lambda \leq 100\ m^{-1}$, the bulk drag coefficient is in the range of $1.3 \leq C_d' \leq 4.6$. Therefore, the variation of f_{rk} is between 46 – 130 m^{-1}. Using this information of data range for flow depth and vegetation parameters, the specified values of mean and standard deviation used in this analysis is given in Table 7.3.

Table 7.3: Parameters value for uncertainty analysis

Parameter	μ	σ
h (m)	0.6	0.04
h_v *(m)*	0.15	0.01
f_{rk} *(m^{-1})*	85.00	9.00
EI (Nm^2)	5.03e-04	9.95 e-05
zo/hv (-)	0.78	0.015

Using the data, UT method of uncertainty analysis is employed to propagated input uncertainty in the model.

There are a lot of methods developed for uncertainty analysis, such as the Monte Carlo method, the Automatic Differentiation technique and the Unscented Transform (UT) method. In the Monte Carlo method a large sample of output data is generated for analysis through the known probability distribution of the input parameters. The computational effort can be substantial. This method among other methods and its practical limitation has been discussed in chapter 2, section 2.14. Recently, the UT method has been developed to capture the mean and variance of the output distribution by using the information at multiple points in the input space (e.g., Julier, 2002). The method is derivative-free and requires less function evaluations.

7.3.2 Propagation of uncertainty – Unscented transformation

UT is a deterministic method to obtain the statistical properties (mean and covariance) of an output variable (e.g., Manning roughness coefficient) subjected to a nonlinear transformation through the numerical model. The statistical properties (mean and covariance) of the input parameters are specified, either obtained from measurements or from design requirements. A set of sigma points for the input parameters are then chosen and the corresponding output points are computed. The statistical properties of the output parameter are obtained through a linear combination of the output points with appropriate weightings. The basic idea of the method is that the statistical parameters of an output variable can be more conveniently obtained from the nonlinear transformation of the statistical parameters of the input variables. The method requires less function evaluations and is considered better than the Monte Carlo

simulation method in terms of flexibility, ease of implementation and practicability (Padulo et al., 2007; Menezes et al., 2013; Stephanie et al., 2013).

In UT method, the *m*-dimensional random variable $\boldsymbol{x}$ with mean $\overline{x}$ and covariance Σ is approximated by $2m+1$ weighted samples or sigma points of locations x_i and weights W_i based on the following constraints.

$$\left.\begin{array}{c} \sum_{i=0}^{2m} W_i = 1 \\ \sum_{i=0}^{2m} W_i x_i = \overline{\boldsymbol{x}} \\ \sum_{i=0}^{2m} W_i (x_i - \overline{\boldsymbol{x}})\,(x_i - \overline{\boldsymbol{x}})^T = \sum_x \end{array}\right\} \tag{7.3}$$

The sigma points thus are not unique and one commonly used set is as follows:

$$\left.\begin{array}{rl} x_o = \hat{\boldsymbol{x}} = \mu & \\ x_i = \mu + \left(\sqrt{(m+k_o)\,\Sigma}\right)_i = \mu + \alpha_o\sqrt{(m+\varpi)}\sigma_i & i = 1,\ldots,m \\ x_i = \mu - \left(\sqrt{m+k_o)\,\Sigma}\right)_i = \mu - \alpha_o\sqrt{(m+\varpi)}\sigma_i & i = m+1,\ldots,2m \end{array}\right\} \tag{7.4}$$

The weights for computing the mean, $W_i^{[\mu]}$ and covariance, $W_i^{[c]}$ are

$$\left.\begin{array}{c} W_0^{[\mu]} = \frac{k_o}{m+k_o} \\ W_i^{[\mu]} = W_i^{[c]} = \frac{1}{2(m+k_o)} \text{ for } i = 1,\ldots,2m \\ W_i^{[c]} = W_0^{[\mu]} + (1 - \alpha_o{}^2 + \beta_o) \end{array}\right\} \tag{7.5}$$

where k_o, ϖ, α_o, β_o are scaling parameters (Van der Merwe, 2004; Kim and Park, 2010), m is the dimensionality and $\left(\sqrt{(m+k_o)\,\Sigma}\right)_i$ is the i^{th} column of the matrix square root of $(m+k_o)\,\Sigma$. The optimum choice of scaling parameters is: $0 < \alpha_o < 1$; $\beta_o = 2$; $\varpi > 0$, and $k_o = \alpha_o{}^2(m+\varpi) - m$.

After transformation mapping of the statistical parameters of the input variables, the estimated mean and covariance of the output variable are obtained by:

$$\mu' = \sum_{i=0}^{2m} W_i^{\mu} f\left(x^{[i]}\right) \tag{7.6}$$

$$\Sigma' = \sum_{i=0}^{2m} W_i^{c} \left(f\left(x^{[i]}\right) - \mu'\right)\left(f\left(x^{[i]}\right) - \mu'\right)^T \tag{7.7}$$

In case the number of input parameters is small (say 2) the analytical solution of the mean and covariance of the output variable can be computed easily, knowing that the probability distribution is a normal distribution.

7.3.3 Sensitivity analysis of vegetation parameters

This section investigates the influence changes in vegetation parameters on the hydraulic roughness coefficient for vegetated open channel flows. The spatiotemporal dynamics of vegetative resistance parameter (i.e. vegetation density, height, flexibilty) and flow condition is very complex and hence, variability of hydraulic roughness parameter in open channels is inherent. In engineering practice related problems, information on uncertainty from other random variables can be used to indirectly estimate uncertainty associated with one response (random) variable using sensitivity approach.

The sensitivity analysis of vegetation parameters can be very useful for engineering applications as it can reveals which parameter(s) is/are most critical in contributing to the uncertainty in the hydraulic roughness. The sources of uncertainty are due to the limitations of the model and the variability of the input vegetation and flow parameters. The influence of the following vegetation parameters (h_v, flexibility (I) and f_v) as input data on the output of hydraulic roughness model output are examined using dataset from Boller and Carrington, (2006). The second moment of area, I is defined as a function of blade width assuming uniform blade thickness. It should be noted, that the zero-plane displacement parameter (Z_o) varies with h_v, I and f_v since the

parameters are mutual correlated. Neglecting this effect can lead to overestimation of uncertainty in the model result. This changes is taking into consideration during transformation in the hydraulic roughness model. For each percentage variation in parameter, new sigma points are generated and the algorithms in the flow chart (Figure 2.8) is followed and the average value of the drag coefficient is used. Six numbers of variation are carried out with the mean value inclusive.

7.4 Results and discussion

7.4.1 Assessment of modeling errors

The numerical model is used to replicate all the experimental dataset. Generally, the predictions are quite good. Figures 7.1, 7.2, 7.3 and 7.4 are representative results, showing the comparison between the numerical results and the experimental results of the velocity profiles obtained in this study. Four sets of cases with constant lateral stem spacing and different areal density of vegetation (λ) are displayed. For each set of cases with constant areal density of vegetation, Q increases from $30m^3/hr$ to $50m^3/hr$ at $5m^3/hr$ interval, except for the set of cases with vegetation density $\lambda = 72\ m^{-1}$, for which Q increases from $25m^3/hr$ to $45m^3/hr$. The computed velocity profiles agree well with those measured in the experiments. From the Figures, it can be seen that the numerical model successfully replicate most of the characteristics of the flows.

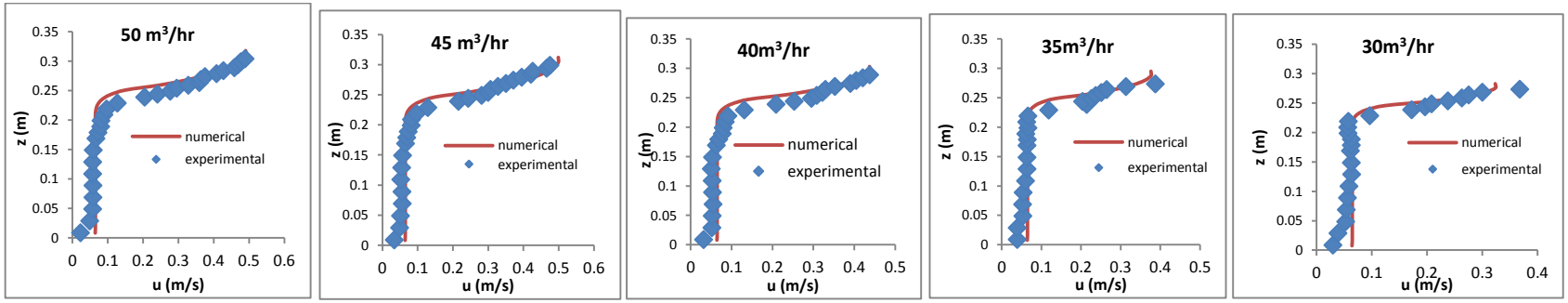

Figure 7.1: Comparison of vertical distribution of mean stream-wise velocity at various flow rates ($\lambda = 12.048\ m^{-1}$)

(Blue square dot – measured, red solid line – computed)

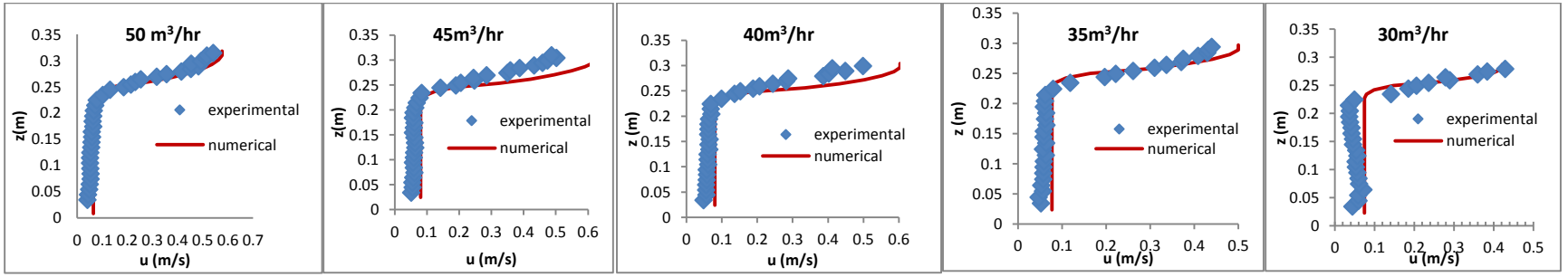

Figure 7.2: Comparison of vertical distribution of mean stream-wise velocity at various flow rates ($\lambda = 24.096\ m^{-1}$)

(Blue square dot – measured, red solid line – computed)

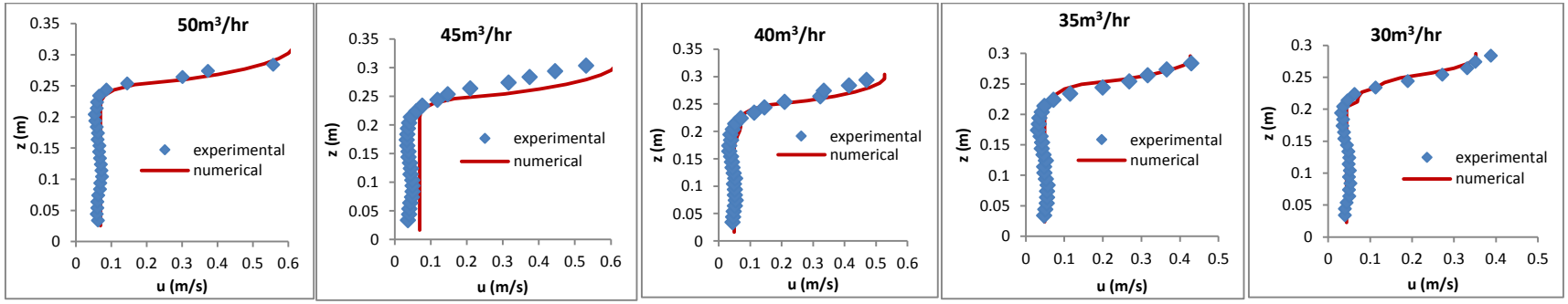

Figure 7.3: Comparison of vertical distribution of mean stream-wise velocity at various flow rates ($\lambda = 48.192\ m^{-1}$)

(Blue square dot – measured, red solid line – computed)

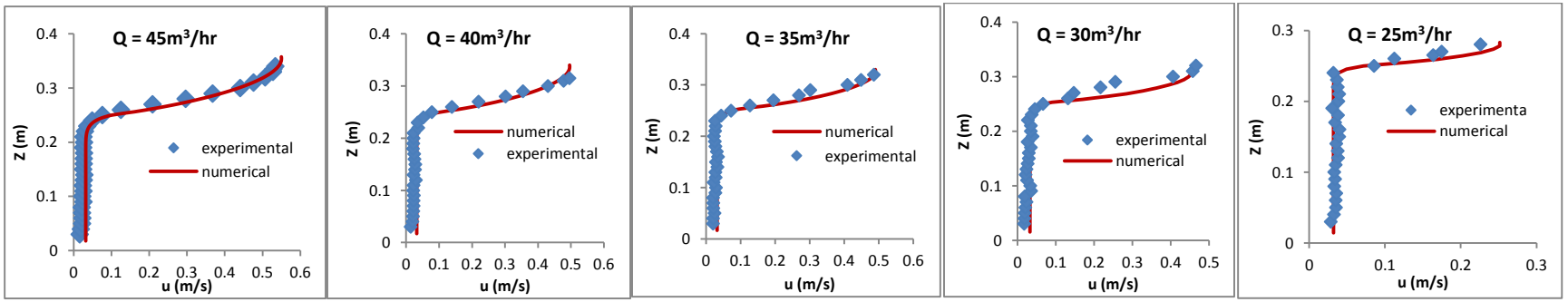

Figure 7.4: Comparison of vertical distribution of mean stream-wise velocity at various flow rates ($\lambda = 72.288\ m^{-1}$)

(Blue square dot – measured, red solid line – computed)

Figures 7.5, 7.6, 7.7 and 7.8 show the computed vertical profiles of stream-wise velocity together with those measured for four sets of cases with different vegetation densities and constant longitudinal stem spacing. From the flume experiments , for each set of cases with constant areal density of vegetation, *Q* increases from 30 to 50m^3/hr at 5m^3/hr interval, except for the set of cases with vegetation density $\lambda = 4.8\ m^{-1}$, for which Q increases from 35m^3/hr to 50m^3/hr, as the case with Q = 30m^3/hr is only partially submerged. Similar to above, the computed results and measured data agree well.

From the second-order velocity fluctuations u' and w', in the longitudinal and vertical directions x and z, respectively, the Reynolds stress has been calculated for the measurement under varying hydraulic conditions. In Figures 7.9, 7.10, 7.11 and 7.12, the predictive capability of the numerical model is further examined by simulating part of the experimentally measured vertical profiles of the Reynolds Shear stress for the two interference effects. The Figures 7.9 and 7.10 illustrate the comparison of the measured vertical profiles of the Reynolds shear stresses and the computed one for the channeling effect under diffirent flow condition and vegetation densities. Similar comparison is shown for sheltering effect in Figures 7.11 and 7.12. The model predicts the maximum Reynolds stress quite well.

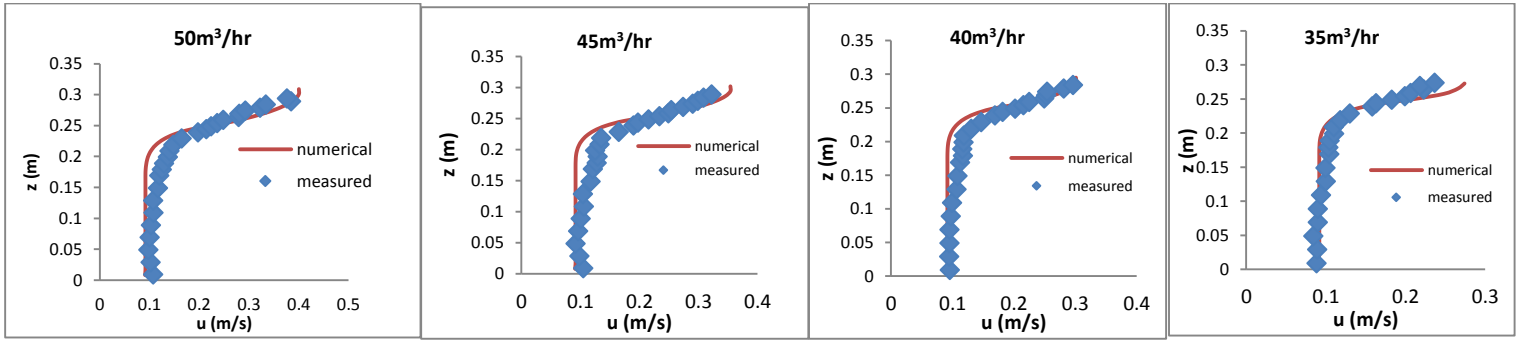

Figure 7.5: Comparison of Vertical distribution of mean stream-wise velocity at various flow rates ($\lambda = 4.80\ m^{-1}$)

(Blue square dot – measured, red solid line – computed)

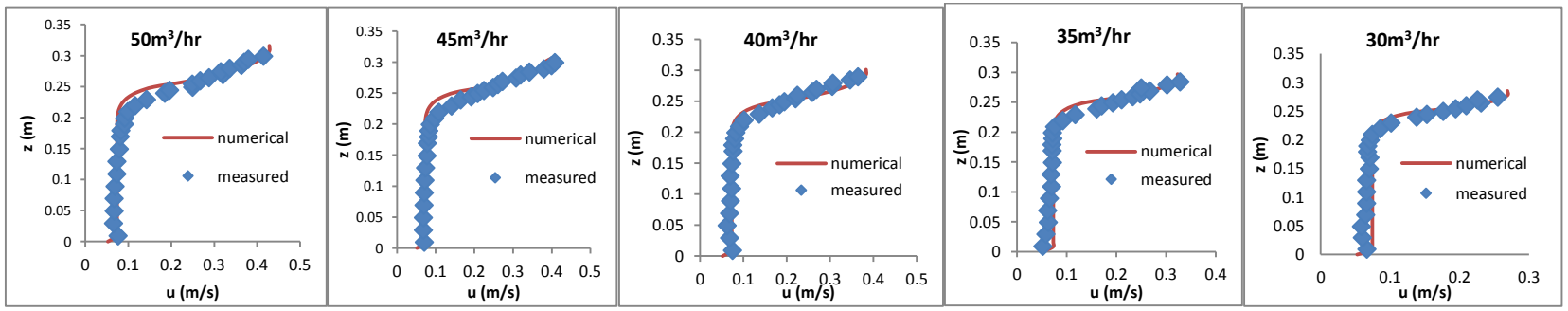

Figure 7.6: Comparison of vertical distribution of mean stream-wise velocity at various flow rates ($\lambda = 9.75\ m^{-1}$)

(Blue square dot – measured, red solid line – computed)

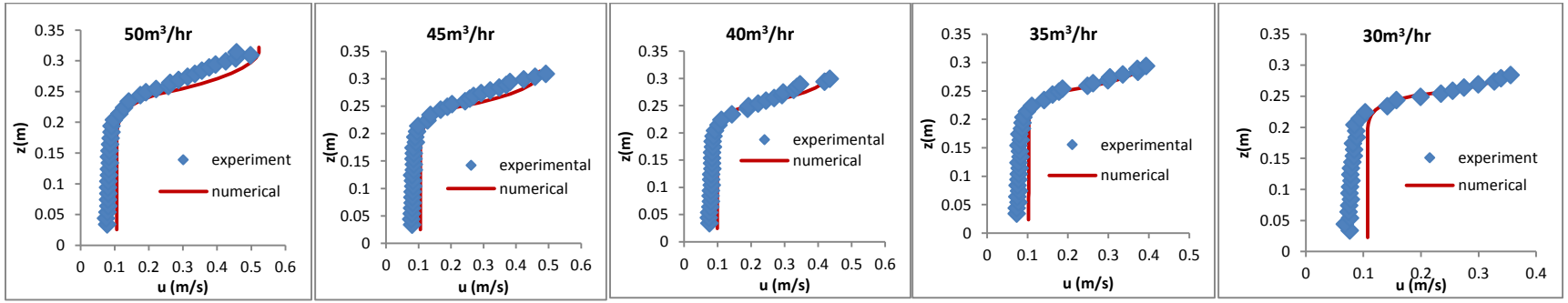

Figure 7.7: Comparison of vertical distribution of mean stream-wise velocity at various flow rates ($\lambda = 15.06\ m^{-1}$)

(Blue square dot – measured, red solid line – computed)

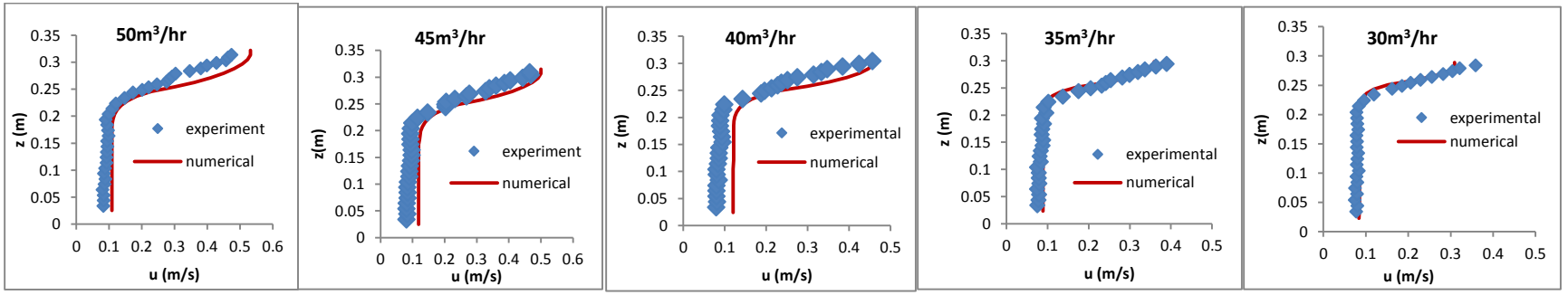

Figure 7.8: Comparison of vertical distribution of mean stream-wise velocity at various flow rates ($\lambda = 18.825\ m^{-1}$)

(Blue square dot – measured, red solid line – computed)

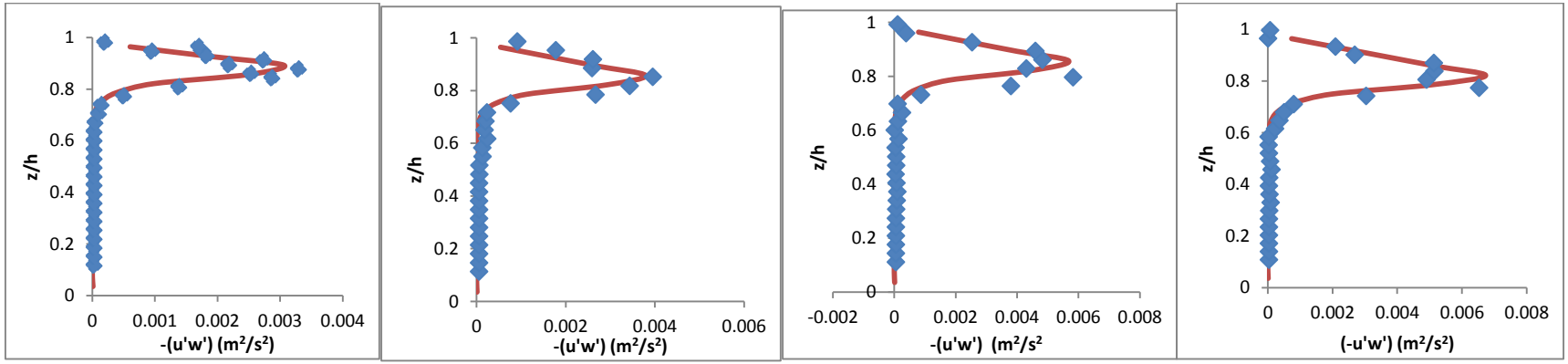

Figure 7.9: Comparison of vertical distribution of the Reynolds shear stress at 30, 35, 40 and 45m^3/hr (λ = 18.825 m^{-1})

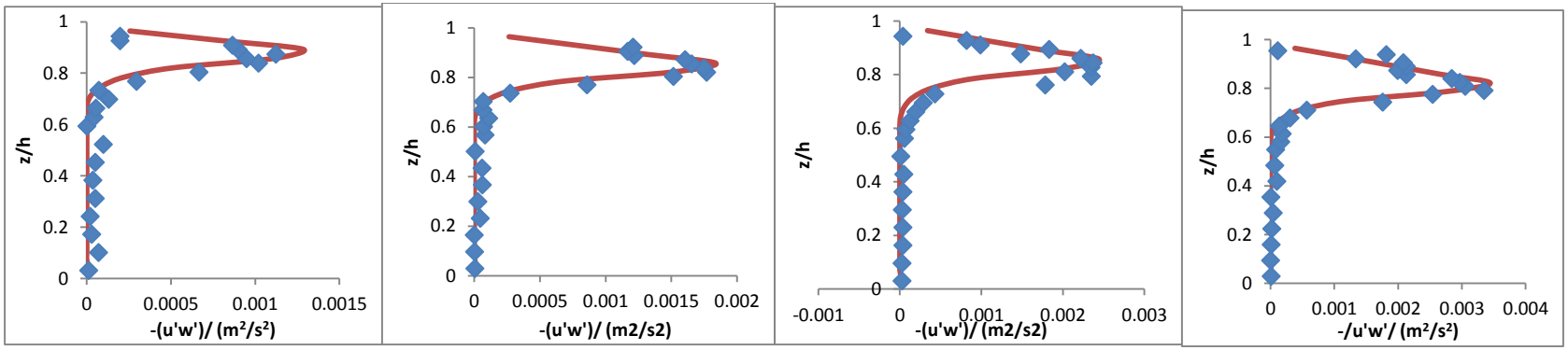

Figure 7.10: Comparison of vertical distribution of the Reynolds shear stress at 30, 35, 40 and 45m^3/hr (λ = 9.75 m^{-1})

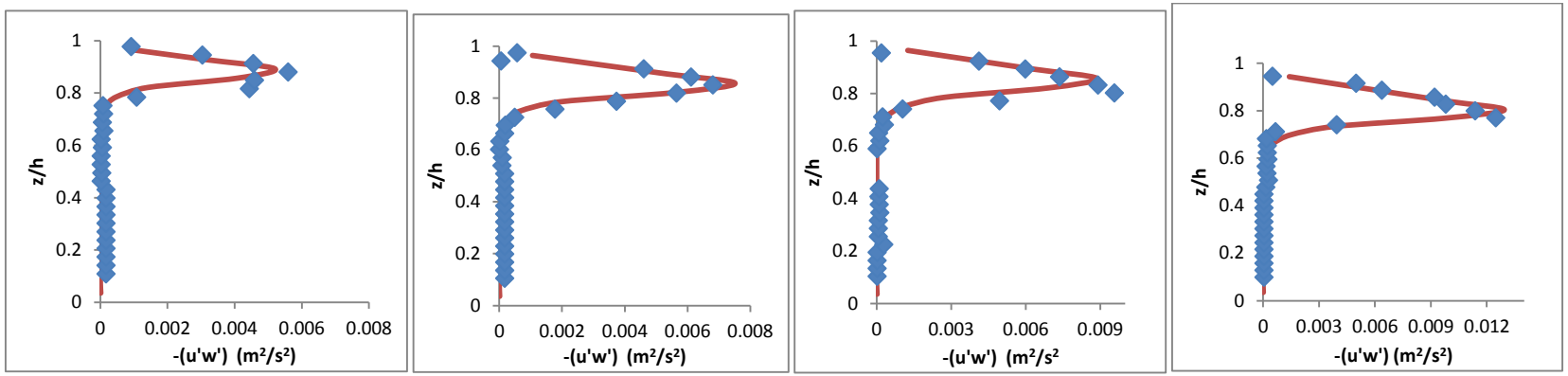

Figure 7.11: Comparison of vertical distribution of the Reynolds shear stress at 30, 35, 40 and 50m^3/hr ($\lambda = 24.10\ m^{-1}$)

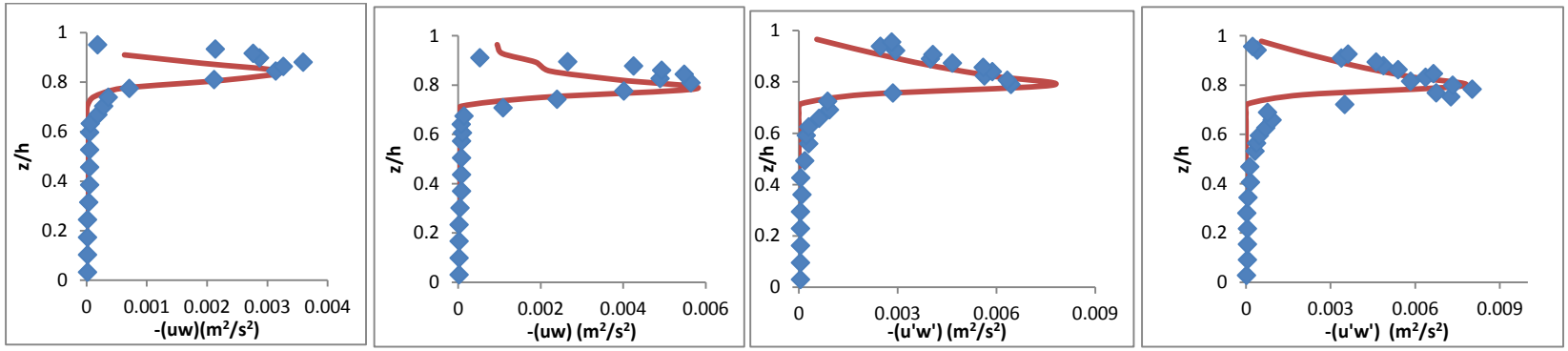

Figure 7.12: Comparison of vertical distribution of the Reynolds shear stress at 30, 35, 40 and 50m^3/hr ($\lambda = 12.05\ m^{-1}$)

The modeling error is assessed through the comparison of the computed and measured mean velocities. The errors of input parameters are taken from experiments and thus are minimized. For the cases with constant longitudinal stem spacing (channeling effect), the percentage errors between the computed velocities and the corresponding measured values U are shown in Table 7.4, and are within $\pm 9.5\%$. For the cases with constant lateral stem spacing (sheltering effect), the percentage errors between the computed velocities and the corresponding measured values (U) are shown in Table 7.5, and are within $\pm 10\%$. The errors are expected to include model formulation errors and measurement errors.

Table 7.4: Uncertainty in the computed mean velocity obtained from mean stream-wise vertical velocity profile (for constant longitudinal stem spacing)

λ (m^{-1})	18.825	18.825	18.825	18.825	18.825	15.060	15.060	15.060
U *(m/s)*	0.096	0.109	0.121	0.132	0.144	0.095	0.108	0.120
$U_{computed}$ *(m/s)*	0.098	0.111	0.131	0.144	0.153	0.093	0.110	0.124
Error *(%)*	-2.266	-2.029	-7.939	-9.177	-6.270	2.211	-1.944	-3.083
λ (m^{-1})	15.060	15.060	9.413	9.413	9.413	9.413	9.413	7.530
U *(m/s)*	0.132	0.143	0.096	0.107	0.121	0.133	0.144	0.110
$U_{computed}$ *(m/s)*	0.141	0.152	0.099	0.110	0.124	0.125	0.139	0.104
Error *(%)*	-7.045	-6.364	-3.526	-2.764	-2.781	6.241	3.240	5.173
λ (m^{-1})	7.530	7.530	7.530	4.706	4.706	4.706	4.706	
U *(m/s)*	0.122	0.134	0.146	0.11	0.123	0.134	0.146	
$U_{computed}$ *(m/s)*	0.117	0.129	0.142	0.114	0.125	0.138	0.152	
Error *(%)*	4.242	3.752	2.547	-3.744	-1.301	-2.732	-3.802	

Table 7.5: Uncertainty in the computed mean velocity obtained from computed mean stream-wise vertical velocity profile (for constant lateral stem spacing)

λ (m^{-1})	12.048	12.048	12.048	12.048	12.048	24.096	24.096	24.096	24.096	24.096
U *(m/s)*	0.097	0.109	0.121	0.132	0.144	0.098	0.11	0.123	0.135	0.147
$U_{computed}$ *(m/s)*	0.096	0.109	0.125	0.143	0.141	0.093	0.120	0.124	0.141	0.152
Error *(%)*	0.628	0.055	-3.012	-8.234	1.748	5.204	-9.182	-0.569	-4.667	-3.469
λ (m^{-1})	48.192	48.192	48.192	48.192	48.192	72.288	72.288	72.288	72.288	72.288
U *(m/s)*	0.102	0.115	0.128	0.141	0.153	0.09	0.098	0.108	0.12	0.129
$U_{computed}$ *(m/s)*	0.109	0.104	0.122	0.146	0.147	0.091	0.098	0.110	0.123	0.132
Error *(%)*	-6.730	9.721	4.484	-3.422	4.230	-1.222	0.204	-1.944	-2.583	-2.403

7.4.2 Uncertainty in input parameters and fitting equations

The uncertainty in the input parameters and fitting equations illustrated in chapter (3) is estimated. Table (7.6) summarizes the estimated errors induced by equations (3.25), (3.28), (3.31), (3.32) and (3.33) which represent the proposed equation for this study, its simplified form, Baptist et al.'s model, Yang and Choi's model, and Cheng's model respectively. The errors are computed by using Normalized Root Mean Square Deviation (NRMSD) method which is defined as follows:

$$\left.\begin{aligned} NRMSD &= RMSD/\left(n_{measured,max} - n_{measured,min}\right) \\ RMSD &= \sqrt{\frac{1}{m}\sum_{j=1}^{m}\left(n_{measured,j} - n_{computed,j}\right)^2} \end{aligned}\right\}$$

The normalization using the range of measured value is considered more reasonable than that using the mean value due to the high degree of variability in the data, especially for the field data. On average, the equations proposed by Baptist et al., (2007), Cheng (2011) and Yang and Choi (2010) and the present study appear to be more accurate for rigid vegetation. Equation (3.30) and (3.32) appear to be less accurate

for flexible vegetation. The proposed equations (3.24) and (3.27) in this study perform almost the best. Generally, the equations perform worse for cases requiring estimation of the drag coefficient. The estimated NRMSD uncertainty using the present fitting equations are less than 18% for the entire verification stage.

Table 7.6: NRMSD (%) generated by different empirical equations

(*nc* = number of cases)

Verification stage	Investigators	Equation	Manning Coefficient (%)	Reference Busari and Li, (2015b)
1.	Baptist et al., (2007)	3.30	13.2	Figure 8 (*nc = 23*)
	Proposed model	3.27	12.6	
	Proposed model	3.24	11.1	
	Baptist et al., (2007)	3.30	16.9	Figure 9 (*nc = 21*)
	Proposed model	3.27	18.8	
	Proposed model	3.24	15.9	
	Baptist et al., (2007)	3.30	56.2	Figure 10 (*nc = 105*)
	Proposed model	3.27	25.5	
	Proposed model	3.24	49.8	
2.	Baptist et al., (2007)	3.30	8.8	Figure 11 (*nc = 60*)
	Yang and Choi, (2010)	3.31	7.2	
	Cheng, (2011)	3.32	8.7	
	Proposed model	3.27	8.0	
	Proposed model	3.24	8.1	
	Baptist et al., (2007)	3.30	94.5	Figure 12 (*nc = 172*)
	Yang and Choi, (2010)	3.31	26.7	
	Cheng, (2011)	3.32	136	
	Proposed model	3.27	14.8	
	Proposed model	3.24	16.1	
3	Proposed model	3.27	7.4	Figure 13 (*nc = 18*)
	Proposed model	3.24	9.6	

7.4.3 Propagation of input uncertainty in 1-D model using UT method.

The application of UT method is demonstrated using data from Table 7.3 and considering two vegetative parameter (i.e., f_{rk} and h_v). The flow depth and other

parameters are fixed at their respective mean values. These two parameters are correlated with the roughness parameter (z_o). They are both assigned their respective mean and standard deviation values in Table 7.3. The cross covariance is set to zero for simplicity. The problem becomes 2 - dimensional and $2m$+1 simulation is required. The average stem width of 7mm was selected, with C_d = *1.6* and considering an open channel width of 0.5m.

Using equations 7.3 through 7.5, the sigma points and associated weights are computed as follows, noting that $m = 2, k_o = 1$.

Mean = $\begin{bmatrix} \mu_{fv} \\ \mu_{hv} \end{bmatrix}$ and the covariance matrix = $\begin{bmatrix} 9 & 0 \\ 0 & 0.01 \end{bmatrix}$

For two dimensional random variables, there are 2 coordinates for each sigma points and $2m + 1$ or 5 sigma points are required, and are as follows:

$x_0 = (\mu_{f_{rk}}, \mu_{h_v}) \quad = (85, \quad 0.15)$

$x_1 = \left(\mu_{f_v} + 9\sqrt{3}, \mu_{h_v}\right) = (100.5885, \quad 0.15)$

$x_2 = \left(\mu_{f_v} - 9\sqrt{3}, \mu_{h_v}\right) = (69.4115, \quad 0.15)$

$x_3 = \left(\mu_{f_v}, \mu_{h_v} + 0.01\sqrt{3}\right) = (85, \quad 0.1673)$

$x_4 = \left(\mu_{f_v}, \mu_{h_v} - 0.01\sqrt{3}\right) = (85, \quad 0.1327)$

The associated weights are $W_0 = {}^1/_3$ and $W_i = {}^1/_6$, where $i = 1,2,3,4$

Using the sigma points, the associated zero-plane displacement parameter is computed. The data are fed into the 1-D model and the corresponding output points are computed. The statistical properties of the output parameter are obtained through a linear combination of the output points with above weightings. The computed results for the mean and covariance of the discharge are obtained using equation 7.6 and equation 7.7. The results are shown in Table 7.7. The estimated mean values of the output variable (discharge) for the model using the mean values ($\boldsymbol{x}_o$) of the input parameters are also included in Table (7.7).

Table 7.7: Computed discharge (m^3/s) by 1-D model based on UT method.

Mean	Variance	CoV	x_o
0.0777	0.00003	0.215	0.0755

The computed coefficient of variation (CoV) is around 0.22, showing that the discharge can have a significant variation arising from the variability in the vegetation parameters. The computed discharge for the case using the mean values ($\boldsymbol{x}_o$) of the input parameters is about 3% lower than that computed by UT. This indicates that the dispersion of the input parameters exerts an effect on the mean output values. Therefore, the estimation of the mean discharge using the mean vegetation and flow parameters will have errors.

7.4.4 Propagation of input uncertainty of the hydraulic roughness model

In Chapter 3, the numerical model is used to generate synthetic data for the development of a hydraulic roughness model. For the model the uncertainty in the output hydraulic roughness coefficient can be related to the uncertainties of the input parameters using the UT method. Following Padula et al., (2007), the accuracy of the UT method is demonstrated against the exact solution obtained by using Monte Carlo simulation. Using equations (3.24) and (3.27), the input variables chosen are f_v (= C_dNwh_v) and plant height h_v. They are both assigned the same mean value of 1, same standard deviation σ (= 0.05, 0.1, 0.15, 0.2) and zero cross covariance for simplicity. The water depth was assumed uniform. The average stem width of 4mm was selected, assuming a very flexible vegetation with $C_d = 0.5$. The vegetation is totally submerged.

The computed results are shown in Table 7.8 and Table 7.9. The difference between the computed and exact mean and covariance values is around 1% and 3% respectively. The estimated mean values of the output variable (Manning roughness coefficient) for the two equations using the mean values ($\boldsymbol{x}_o$) of the input parameters are also included in Table 7.8 and denoted by *E(n).* These mean values are commonly taken as the expected value of the output parameter if no information about the covariance is given. It can be seen that this method is slightly less accurate than the UT method as the information of covariance is not used.

Table 7.8: Uncertainty propagation analysis: Mean

Test case	σ	Exact solution	UT method	Relative uncertainty (%)	Mean *E(n)*
		Mean ($\bar{n}$)	Mean (n_{UT})		
Equation 3.24	0.20	0.1219	0.1219	0.00	0.122
	0.15	0.1208	0.1221	1.07	
	0.10	0.1221	0.1223	0.16	
	0.05	0.1224	0.1224	0.00	
Equation 3.27	0.20	0.1149	0.1149	0.00	0.115
	0.15	0.1141	0.1152	0.96	
	0.10	0.1152	0.1154	0.17	
	0.05	0.1155	0.1155	0.00	

Table 7.9: Uncertainty propagation analysis: Covariance

Test case	σ	Exact solution	UT method	Relative uncertainty (%)
		Covariance	Covariance	
Equation 3.24	0.20	6.777e-4	6.799e-4	0.3246
	0.15	3.763e-4	3.876e-4	3.0029
	0.10	1.721e-4	1.737e-4	0.9297
	0.05	4.359e-5	4.361e-5	0.0459
Equation 3.27	0.20	3.997e-4	4.029e-4	0.8006
	0.15	2.112e-4	2.172e-4	2.8409
	0.10	9.281e-5	9.371e-5	0.9697
	0.05	2.299e-5	2.302e-5	0.1305

7.4.5 Application of UT to experimental dataset

The UT method is then used to study the uncertainty of the Manning roughness coefficient induced by the propagation of the variability of shape and flexibility of vegetation during reconfiguration. Boller and Carrington (2006) conducted hydrodynamic experiments of 19 samples of macro-alga to determine their drag characteristics. The measured parameters are shown in Table 7.10, where $C_{d(hv)}$ = drag coefficient in high velocity condition ($u = 1.9m/s$); $C_{d(lv)}$ = drag coefficient in low velocity condition ($u = 0.5m/s$).

Table 7.10: Measured parameters (Boller and Carrington, 2006)

	h_v	w	$C_{d(\mathrm{hv})}$	$C_{d(\mathrm{lv})}$
Mean	0.0735	0.0424	0.265	0.594
Covariance	0.0003	0.0001	0.0071	0.0359
CoV	0.222	0.225	0.318	0.319

The data are sparse and the distribution does not strictly follow the normal distribution. In the test case, the water depth is assumed to be approximately uniform ($h = 0.15m$), the vegetation density is set to 1000. The dimensionality of the problem is $m = 3$ and 7 sigma points are required. The sigma points are computed using equations 7.3 to 7.5.

The analysis is carried out for the two flow regimes. The computed results by UT using equation (3.28) and the 7 sigma points are shown in Table 7.11.

Table 7.11: Sigma points for $m = 3$ dimensions

i	h_v (m)	w (m)	$C_{d(hv)}$	$C_{d(lv)}$
x_o	0.0735	0.0424	0.2647	0.5942
x_1	0.0931	0.0424	0.2647	0.5942
x_2	0.0535	0.0424	0.2647	0.5942
x_3	0.0735	0.4371	0.2647	0.5942
x_4	0.0735	0.4116	0.2647	0.5942
x_5	0.0735	0.0424	0.4181	0.8753
x_6	0.0735	0.0424	0.1672	0.3820

h_v and l_v denote high velocity and low velocity respectively

In Table 7.12, the computed coefficient of variation (CoV) for both cases is around 0.2, showing that the Manning roughness can have a significant variation arising from the variability in the vegetation parameters. The computed Manning roughness coefficient for the case using the mean values ($\boldsymbol{x}_o$) of the input parameters is 2 - 5% lower than that computed by UT.

Table 7.12: Computed Manning's roughness coefficient by Eqn. (3.27) based on UT method.

	Mean	Variance	CoV	x_o
Low velocity (0.5m/s)	0.0721	0.00026	0.226	0.0760
High velocity (1.9m/s)	0.0705	0.00020	0.197	0.0721

7.4.6 Sensitivity studies of vegetation parameters

In this section, the effect of changes in the vegetation parameters on vegetative Manning's roughness coefficient is investigated using the dataset by (Boller and Carrington, 2006) as discussed in section 7.4.5. The methodology for the analysis has been presented in section 7.3.3. The range of variation of ($\pm$30%) of each parameter around the mean value are within the experimental values from Boller and Carrington, (2006). The parameters are varied at (10%) interval around the mean values (see Table 7.10) and the influence of these changes on the output (that is the Manning's roughness coefficient) is presented in Table 7.13.

In Table 7.13, for low velocity of flow, the changing the plant diameter does not have significant effect on the mean value of the Manning's coefficient. The plant's flexibility is low with moment of inertia in the range of 2.5 x 10^{-8} - 6.4 x10^{-7} m^{-4}. At higher velocity, the effect of change in plant diameter appear slightly significant especially for smaller diameter. The change in plant height produces are significant change in the roughness coefficient, around $\pm$23% changes of the mean value irrespective of the flow condition. Similarly, the vegetation density imposed significant effect on the Manning roughness value in the order of 18% changes.

Table 7.13: Sensitivity of vegetative Manning's roughness coefficient by Eqn. (3.27) to change in vegetation parameter based on UT method.

Low velocity (u = 0.5m/s)									
S/N		Mean	Covariance		Mean	Covariance		Mean	Covariance
1		0.0938	0.0066		0.0759	0.0045		0.0552	0.0023
2		0.0858	0.0055		0.0760	0.0046		0.0598	0.0028
3	h_v	0.0652	0.0032	w	0.0759	0.0045	N	0.0635	0.0031
4		0.0586	0.0026		0.0756	0.0045		0.0690	0.0037
5		0.0519	0.0021		0.0750	0.0044		0.0716	0.0040
High velocity (u = 1.9m/s)									
S/N		Mean	Covariance		Mean	Covariance		Mean	Covariance
1		0.0919	0.0064		0.0743	0.0043		0.0625	0.0030
2		0.0844	0.0054		0.0737	0.0043		0.0668	0.0035
3	h_v	0.0645	0.0032	w	0.0711	0.0040	N	0.0696	0.0038
4		0.0581	0.0026		0.0698	0.0038		0.0722	0.0040
5		0.0515	0.0020		0.0681	0.0036		0.0662	0.0035

7.5 Summary

The model formulation uncertainty of the S-A model used in the present study is assessed. The model input parameters are determined accurately from experiments. The computed velocity profiles (in the vegetation zone and clear water zone) and the vertical distribution of the Reynolds stresses agreed well with those measured in the experiments. Using the mean velocity as reference, the relative percentage difference between the computed and measured values is 10%, including the modeling error and measurement error.

The propagation of the uncertainty due to the variability of the highly sensitive vegetation parameters is investigated by using the method of UT. The method is found

efficient and gives accurate estimation of the mean output (velocity or roughness coefficient) and more information on covariance of the output. By measuring the vegetation and flow parameters with uncertainty ranges, the numerical model together with the UT method can be used to compute the mean and covariance of the channel discharge or hydraulic roughness coefficient.

For engineering applications, the response of the hydraulic roughness model to change in vegetation parameters is further assessed using sensitivity analysis. The sources of uncertainty are due to the limitations of the model and the variability of the input vegetation and flow parameters. The relative sensitivity of the model results to the change in input parameters shows that vegetation height and vegetation density are critical in contributing to the hydraulic roughness uncertainty.

8 Conclusion and Future Works

8.1 Conclusion

The present study deepens the understanding of flow resistance model by taking into consideration the influence of zero-plane displacement parameter. The study also deepens the understanding of the effect of dense vegetation on hydraulic resistance through thorough laboratory flume experiments and numerical simulation of open channel flow with blade-type vegetation roughness. The effect of different vegetation distribution pattern on hydraulic roughness parameter reveals the need for this study. The results from both the laboratory observation and numerical runs are quite consistent. In addition, the field conditions are always with uncertainty. There is a practical need to assess fitting equations and modeling error as well as the propagation of uncertainty input uncertainties in the hydraulic roughness parameter or discharge.

8.1.1 Development of a hydraulic roughness model for flow over submerged vegetation

At the beginning of this study, the reviews have indicated the need for vegetative resistance model for submerged flexible vegetation. For submerged vegetation, the flow characteristics between the clear water zone and vegetation can be distinctively different. Part of the flow in the surface layer can penetrate into the vegetation layer and the depth of penetration is a function of vegetation characteristic and flow condition. Therefore, turbulence length scale between the two layers can be different. To this end, a zero-plane displacement parameter (equation 3.19) is introduced into the new inducing

equation (equation 3.24) and its simplified form (equation 3.27) to differentiate the difference in the turbulence characteristic between the two zones and account for the resulting hydraulic resistance effects. This induced equations are calibrated from the synthetic velocity profile data (see Figure 3.12) using extensively verified numerical model. The fitting is the best at lower values of h/h_v, and has larger discrepancy when f_v is low and h/h_v is high (that is, in the low hydraulic resistance range).The predicted Manning's roughness coefficients by derived equations are highly correlated with that from well-documented experimental data and field data. The equation performed better than the existing equations without zero-plane displacement parameter especially for submerged flexible vegetation (Figure 3.15).

8.1.2 Laboratory experimental study

For the laboratory work, the laboratory study was divided into two parts: submerged and emergent vegetated flow modeling. For each study, a systematic laboratory study has been carried out to investigate the effect of the distribution pattern of vegetation stems on the hydrodynamics of gradually varied flow (GVF) using two interference mechanisms. The drag induced by flow through vegetation is affected by the velocity, shape of vegetation stems and wake interference among stems. Based on this, an extensive laboratory studies was embarked upon using blade-type vegetation under emergent and submerged flow condition.

8.1.2.1 Emergent flow conditions

For emergent case, the solid volume fractions ranging from 0.005 to 0.121 have been used and the stem Reynolds number tested ranges from 500 – 2600. The longitudinal water surface profiles have been measured and the effect of increasing areal

density of vegetation with respect to varying longitudinal and lateral spacing under the flow conditions is examined. The momentum equation (equation 5.7) that relates the vegetation resistant force and water surface profile has been used to obtain the value of C_d. A good agreement is observed between the measured and semi-theoretical results which shows the high reliability of the estimated C_d value. Generally, the water level increases with increase in λ under the same flow rate. The results shows that C_d decreases with increasing stem Reynolds number for the range of Reynolds number examined, the dependence is more or less linear. The results indicates that for cases with fixed lateral spacing, at a smaller value of S_x, the change in velocity will not alter the flow pattern since the wake region is limited by the longitudinal spacing of adjacent blades, S_x. Hence, the resulting C_d becomes more not less a constant. For a larger value of S_x, the flow pattern is affected by the magnitude of the velocity and a decreasing trend of C_d with Re is resulted. For cases with fixed longitudinal spacing, at a larger value of S_y, the lateral spacing between adjacent blades is sufficiently wide and the flow pattern is not affected by the variation in velocity. When S_y is small, the interference effect between two laterally adjacent blades becomes strong and is affected by the magnitude of the velocity.

Generally, the C_d decreases with increasing ϕ at fixed lateral spacing due to sheltering effect (Figure 5.6a), and increases with ϕ at fixed longitudinal spacing due to channeling effect (Figure 5.6b). The flow through vegetated channel is turbulent and subcritical (Fr < 1) as can be observed from (Figure 5.10), as a result, the increasing flow rate does not lead to sudden change in drag coefficient (Figure 5.6). The findings show that normalized drag force, f_d varies approximately linearly with Re and the

linearity depends on the longitudinal spacing between blades for fixed lateral spacing. In addition, at larger longitudinal spacing the effect of vortex shedding and jet spreading are significant. The inertial contribution due to pressure loss in the stem wake decreases with increase in transverse and longitudinal spacing, while the effects of viscous shear stress, vortex shedding and jet spreading increases with the increase in longitudinal spacing over the experimental range.

The analysis of distribution of dimensionless drag force and Re revealed that flow and wake interference are more influenced by the (longitudinal and lateral) spacing than by vegetation density. In the case of Froude number (F_r), it can be concluded that the normalized drag is insensitive to F_r in the range of experimental condition tested. For channeling effect, f_d increases with increasing ϕ due increasing wake interference and decreases with increasing ϕ for sheltering effect. This is because interaction in dense vegetation reduces the flow speed in the canopy relative to distribution of less dense vegetation. The results, also show that different distribution pattern for regular array of the same solid volume fraction will produce different drag force.

Finally, based on the fitting equation (5.14), it has been demonstrated that the relationship between C_d and ϕ for a fixed Reynolds number is not unique(see Figure 5.15), therefore, an empirical equation relating C_d to the lateral and longitudinal spacing instead of ϕ has been obtained and validated (in Figure 5.13).

8.1.2.2 Submerged flow conditions

For similar patches arrangement as for emergent case set up, the hydrodynamic behaviour of GVF through submerged blade-type vegetation is investigated. The blade

Reynolds number (Re) ranges from 670 to 1150 and six flow rates are used in each set of the experiments. The vertical profile of the stream-wise velocity have been measured using Acoustic Doppler Velocimeter (ADV). The theoretical longitudinal momentum equation relating the vegetation resistant force, water surface slope and mean velocity in the vegetation layer is used to determine the C_d value. Also, a comparison is drawn by replacing the mean velocity in vegetation layer with the average pore velocity in the channel. Using a regular-array pattern of vegetation elements, the interference effects have been studied independently by varying the longitudinal element spacing (S_x) and lateral element spacing (S_y) respectively.

For cases of stems with constant lateral spacing, at high areal density, the resistance force generated by the vegetation is smaller than the gravitational force due to the bottom slope and consequently a backwater appears at the downstream edge with a positive surface slope along the flow. The backwater effect decreases with the areal density of vegetation and the flow rate. The average water surface slope increases with increasing areal density and the surface profiles appear to be rougher. For a given discharge, the longitudinal velocity in the vegetation zone increases with decreasing vegetation density λ. The distribution of the velocity in the clear water zone is affected by turbulence penetration. The Reynolds stress increases with vegetation density λ and turbulence penetration increases with decreasing λ. Generally, for the given Re, C_d and C_d' increase with S_y indicating that the hydraulic resistance is lowered. The normalized drag, f_d varies approximately linearly with Re for all cases. For a given Re, the f_d decreases with increasing λ, indicating that the sheltering effect. This trend is the same for both the velocity scales.

For cases of stems with constant longitudinal spacing, the resistance offered by vegetation is generally less since the λ value ranges from 3 to 18 m^{-1}, while in the cases with constant lateral spacing the λ value ranges from 6 to 72 m^{-1}. The backwater effect is reflected by an approximately horizontal water surface. The water surface profiles generally appear less roughened and flows are quite uniform. Generally, the larger the lateral spacing, the smoother the surface profile irrespective of flow rates. The C_d' decreases monotonically with increasing Re for high density, but appears insensitive to Re at lower densities, indicating the significance of channeling effect. For different flow rates, the f_d' increases with decreasing lateral stem spacing. Broadly, f_d' varies approximately linearly with Re for all cases.

By using emergent cases as reference for the interference effects, the results shows that average pore velocity under-predict the C_d values due to zero drag above the vegetation. The C_d' values obtained using the mean velocity in the vegetation zone is similar but slightly less than that of emergent case (Figures 6.21 and 6.22). This can be attributed to larger deflection experienced by submerged vegetation and also, influence of additional flow at the top of vegetation can reduce the negative pressure at the wake zone. It is also shown that both effects increase with decreasing vegetation areal density.

Generally, the results shows that the distribution pattern of vegetation elements can exert significant effect on the C_d values, and the associated flow characteristics, including flow adjustment length, peak Reynolds stress and flow division in the clear water zone and vegetation zone. For the same vegetation density, but different distribution pattern of the vegetation, the drag coefficient, velocity profiles and Reynolds stresses distribution vary significantly (Figures 6.17 and 6.18). An empirical

equation relating C_d to the lateral and longitudinal spacing is proposed for submerged flexible vegetation (equation 6.8). For the same vegetation distribution pattern, the C_d values obtained for submerged and emergent conditions are similar for cases with high areal density of vegetation. A good estimate of the interfacial shear stress with the vegetation layer and clear water layer can increase the correlation in the C_d for emergent and submerged cases.

8.1.3 Numerical simulation and Uncertainty estimation

To assess uncertainties in the vegetative parameters as well as modeling error, numerical simulation of flows over dense vegetation has been carried out using the experimentally determined C_d as input. The flow evolution within the vegetation patches and the clear water zone due to sheltering and channeling effects among vegetation stems have been successfully replicated (Figure 7.1 through 7.12).

For practical applications, the accuracy of the prediction by the proposed equations and numerical model is further assessed. The sources of uncertainty are due to the limitations of the equations and the variability of the input vegetation and flow parameters. From Table 7.6, the uncertainty of the inducing equations in the estimation of the roughness coefficients expressed by the Normalized Root Mean Square Deviation (NRMSD) is generally less than 10% where C_d values are specified and overall average of 18% (including where C_d values are assumed). The percentage deviation from observed mean velocity in the open channel compared with that computed using 1-D model is within $\pm 10\%$ for the interference effects (Tables 7.4 and 7.5).

The propagation of the uncertainty due to the variability of the vegetation and flow parameters existing in nature is thoroughly investigated by introducing the method of Unscented Transformation (UT). By measuring the vegetation and flow parameters with uncertainty ranges, the inducing equations together with the UT method is used to compute the mean and covariance of the Manning roughness coefficient using laboratory dataset. In the same manner, the uncertainty of the numerical model in the estimation of the open channel discharge due to the variability of the vegetation and flow parameters existing in nature from selected vegetation data is propagated using numerical model with the method of UT. The results indicates that the dispersion of the input parameters exerts an effect on the mean output values. The method is found efficient and gives a more accurate estimation of the Manning roughness coefficient (or mean channel discharge) with less computational effort.

The investigation of how the hydraulic roughness coefficient is affected by the changes in the vegetation parameter using sensitivity analysis (Table 7.13) reveals that vegetation height and vegetation density are critical in contributing to the hydraulic roughness uncertainty.

8.2 Future work

This study contributes to the knowledge and understanding of vegetated flows. It advances the previous studies in that the dependence of the hydraulic roughness parameter (drag coefficient) on the distribution pattern of vegetation has been investigated both numerical and experimentally. The propagation of the uncertainty in

the parameter estimation is also quantified. The proposed equations and numerical model have shown promising results. Nevertheless, there are still areas for improvement. To enhance the use of the equations and the model for river/wetland restoration and vegetation management projects, the following future works are recommended:

- A further refinement of the hydraulic roughness equations is needed especially in the low hydraulic resistance range.
- Further laboratory, and more importantly, field research and data collection for submerged blade-type vegetation is required to possibly reduce some model prediction uncertainties.
- More sophisticated measuring instrument can be adopted (e.g., PIV) to replicate the present study to deepen the understanding of the physics through capturing the flow velocity field and the coherent vortices at interfacial shear layer between the edge of vegetation and the clear water zone.
- A real life case study is expected to give better understanding of the vegetation parameters and associated flow conditions. To this end, a seasonal field study is required to obtain the cross covariance among vegetative parameters so that the values can be included in uncertainty estimation to avoid overestimation of model responses.
- It would be interesting to investigate and quantify the effects of additional flow path at the top of the stems with respect to parameters such as submergence ratio, areal density as well as the influence of surface wave using the interference effects.

- In case of data availability, a comparative study of the uncertainty propagation methods (including UT methods) for vegetated flows is worthwhile

References

Abdel-Khalik, H. S., Bang, Y and Wang, C., (2013). Overview of hybrid subspace methods for uncertainty quantification, sensitivity analysis. Annals of Nuclear Energy, volume 52, pp 28 – 46.

Aberle, J and Jarvela, J., (2013). Flow resistance of unsubmerged rigid and flexible floodplain vegetation. Journal of Hydraulic research, Volume 51, number 1, pp 33 – 45.

Abrishamchi, A., Tajrishi, M and Shafieian, P, (2005). Uncertainty analysis in QUALSE model of Zayandeh - Rood River. Journal of Water Environmental Research, Volume 77, No 2, pp 1 – 8.

Afzalimehr, H., Moghbel, R., Gallichand, J and Sui, J., (2011). Investigation of turbulence characteristics in channel with dense vegetation. International Journal of Sediment Research 26, pp 269 – 282.

Ahmadi, M., Khayatian, A and Karimaghaee, P., (2012). Attitude estimation by divided difference filter in quaternion space. Journal of Acta Astronautica, vol. 75, pp 95 –107.

Alam, M.M., Zhous, Y and Wang, X.W., (2011). The wake of two side - by -side square cylinders. Journal of Fluid Mechanics, volume 669, pp 432 – 471.

Ascough, C. J., Maier, H. R., Ravalico, J. K., and Strudley, M. W. (2009). Future research challenges for incorporation of uncertainty in environmental and ecological decision making. Ecological Modelling. Volume 219, pp 383 – 399.

Anagnostopoulos, P and Seitanis, S.A., (2014). Numerical study of aperiodic phenomena past two staggered rows of cylinders in cross flow. Journal of Ocean Engineering, volume 92, pp 212-233.

Ang, A.H.-S and Tang, W.H. (1975). Probability Concepts in Engineering Planning and Design, Vol. 1, Basic Principles, John Wiley and Sons Ltd, New York.

Armanini, A., Righetti, M., Grisenti, P., (2005). *Direct measurement of vegetation resistance in prototype scale*. Journal of Hydraulic Research. Volume 43, issue 5, pp 481– 487.

Arulampalam, M.S., Maskell, S., Gordon, N., Clapp, T., (2002). A tutorial on particle filters for online nonlinear/non-Gaussian Bayesian tracking. IEEE Transactions on Signal Processing. Volume 50, number 2, pp 174 - 188.

Ata, M. Y., (2007). A convergence criterion for the Monte Carlo estimates. Journal of Simulation Modelling Practice and Theory. Volume 15, pp 237–246.

Aven, T. (2010). On the need for restricting the probabilistic analysis in risk assessments to variability. Risk Analysis, volume 30, number 3, pp 354 – 360.

Azamathulla, H.M., Ahmad, Z and Ab.Ghani, A., (2012). An expert system for predicting Manning's roughness coefficient in open channels by using gene expression programming. Neural Comput & Application. Springer publishing.

Bakry, M.F., Gates, T.K and Khattab, A.F., (1992). Field - measured hydraulic resistance characteristics in vegetation-infested canals. Journal of Irrigation and Drainage Engineering, volume 118, number 2, pp 256 – 274.

Baptist, M. J., Babovic, V., Keijzer, M, Uttenbogaard, R. E., Mynett, A and Verwey, A., (2007). On inducing equations for vegetation resistance. Journal of Hydraulic Research, Volume. 45, number 4, pp 435 -450.

Beven, K.J, (2009). Environmental modelling: an uncertain future? : An introduction to techniques for uncertainty estimation in environmental prediction. Routledge, London,

Boller, M.L and Carrington, E., (2006). The hydrodynamic effects of shape and size during

reconfiguration of a flexible macroalga. Journal of Experimental Biology, volume 209, pp 1894 – 1903.

Bowmer, K.H., Jacobs, S.W.L and Sainty, G.R., (1995). Identification, Biology and Management of Elodea Canadensis, Hydrocharitaceae. Journal of aquatic management. Volume 33, 13-19.

Bruno, O.S.T., Leonardo, A.B.T., Paulo, I and Luis A. A., (2011). Flight path reconstruction – A comparison of nonlinear Kalman filter and smoother algorithms. Journal of Aerospace Science and Technology. Volume 15, pp 60 – 71.

Burgman, A. M., Wintle, B. A., Thompson, C. A., Moilanen, A., Runge, M. C., and Ben-Haim, Y. (2010). Reconciling uncertain costs and benefits in Bayes nets for invasive species management. Risk Analysis, volume 30, pp 277 – 284.

Busari, A.O and Li, C.W., (2013). A hydraulic roughness model for submerged flexible vegetation. Proceedings of 35th IAHR World Congress, September 8-13, 2013 at Chengdu, China.

Busari, A.O and Li, C.W., (2015). A laboratory study of gradually varied flow through semi-rigid emergent blade-type vegetation. Proceedings of Engineering Mechanics Institute (ASCE) 2015 International conference. Held in January 7-9, 2015 at The Hong Kong Polytechnic University, Hong Kong SAR, China.

Busari, A.O and Li, C.W., (2015b). A hydraulic roughness model for submerged flexible vegetation with uncertainty estimation. Journal of Hydro-environment Research, volume 9, issue 2, pp 268 – 280.

Busari, A.O and Li, C.W., (2015c). Modeling of gradually-varied flow through submerged semi-rigid blade-type vegetation**.** Presented at the 36th IAHR World Congress 28 June – 3 July, 2015 Delft-The Hague, the Netherlands.

Camacho, R.A. and Martin, J.L., (2013). Bayesian Monte Carlo for evaluation of uncertainty in hydrodynamic models of coastal systems. Journal of Coastal Research, Special issue number 65, pp 886 – 891.

Carollo, F.G., Ferro, V and Termini, D., (2002). Flow measurement in vegetated channels. Journal of Hydraulic Engineering. Volume 128, number 7, pp 664-673.

Carollo, F.G., Ferro, V and Termini, D., (2005). Flow resistance law in channels with flexible submerged vegetation. Journal of Hydraulic Engineering, Volume.131, No.7. pp 554-564.

Carrasco, I.J and Chang, S (2005). Random Monte Carlo simulation analysis and risk assessment for ammonia concentrations in wastewater effluent disposal. Journal of Stochastic Environ Risk Assessment. Volume 19, pp 134- 145.

Cengel, Y.A and Cindala, J.M., (2010). Fluid mechanics- Fundamentals and applications. Second edition. McGraw-Hill Company, New York.

Chen, X. and Chen, X., (2003). Sensitivity analysis and determination of streambed leakance and aquifer hydraulic properties. Journal. Hydrology volume 284, pp 270 – 284.

Cheng, N.S., (2011). Representative roughness height of submerged vegetation. Journal of Water resources research, volume 47, pp 1 – 18.

Cheng, N.S and Nguyen, H.T., (2011). Hydraulic radius for evaluating resistance induced by simulated emergent vegetation in open channel flows. Journal of Hydraulic Engineering, Volume.137, No.9. pp 995 - 1004.

Colburn C. H., Cessna, J. B. and Bewley, T. R., (2011). State estimation in wall-bounded flow systems, Part 3. The ensemble Kalman filter. Journal of Fluid Mechanics. Volume 682, pp. 289–303.

Coleman, H.W and Steele, W.G., 2009. Experimentation, validation, and uncertainty analysis for engineers. Third Edition, published by John Wiley and Sons, Inc., Hoboken, New Jersey.

Collins, G. W., (2003). Fundamental Numerical Methods and Data Analysis.

Confalonieri, R., Bellocchi, G., Bregaglio, S., Donatelli, M and Acutis, M., (2010). Comparison of sensitivity analysis techniques: A case study with the rice model WARM. Ecological Modelling. Volume 221, pp 1897–1906.

Daum, F., (2005). Nonlinear Filters: Beyond the Kalman filter. IEEE A and E Systems magazine, volume 20, number 8, pp 57 – 69.

David, V., (2008). Risk analysis: A quantitative guide. Third Edition, published by John Wiley and Sons Limited, The Atrium, Southern gate, West Sussex, England.

Defina, A and Bixio, A.C., (2005). Mean flow and turbulence in vegetated open channel flow. Journal of Water Resources research, volume 41, pp 1 – 12.

DeGroot, M.H and Schervish, M.J., (2002). Probability and Statistics. Fourth edition. Addision – Wesley, Pearson Education, Inc. Boston.

Dharmasiri, N., Yang, S. Q and Han, Y., (2012). Effects of roughness density on the determination of flow resistance in spatially averaged vegetated open channel flow. World Environmental and Water Resources Congress 2012: Crossing Boundaries, ASCE 2012, pp 1349 – 1365

Drainage Services Department/ Mott Macdonald report (2009). Mangrove growth: Management and hydraulic impacts, Hong Kong.

Dunn, C., Lopez, F and Garcia, M., (1996). Mean flow and turbulence in a laboratory channel with simulated vegetation. Civil Engineering studies. Hydraulic engineering Series No.51.

Dupont, S and Brunet, Y., (2009). Coherent structures in canopy edge flow: a large-eddy simulation study. Journal of Fluid Mechanics., volume 630, pp. 93–128.

Edoardo, P., Pradlwarter,H, J and Schueller, G.I., (2010). Global sensitivity of structural variability by random sampling. Computer Physics Communications. Volume 181, pp 2072 - 2081.

Erduran, K.S and Kutija, V., (2003). Quasi-three-dimensional numerical model for flow through flexible, rigid, submerged and non-submerged vegetation. Journal of Hydroinformatic. Volume 5, number 3, pp 189-202. IWA publishing.

Eric, S., (2002). Uncertainty Analysis. Encyclopedia of Environmetrics. Volume 4, pp 2283–2297. John Wiley & Sons, Limited, Chichester.

Evangelos, A. E., (2009). Bayesian and Frequentist Methods for Approximate Inference in Generalized Linear Mixed Models. Doctoral Thesis, University of North Carolina.

Fathi-Maghadam, M and Kouwen, N., (1997). Non rigid, non-submerged, vegetative roughness on floodplains. Journal of Hydraulic Engineering, volume 123, number 1, pp 51 – 57.

Ferreira, R. M. L., Ricardo, A. M., and Franca, M. J., (2009). Discussion of Laboratory investigation of mean drag in a random array of rigid, emergent cylinders by Yukie Tanino and Heidi M. Nepf. Journal of Hydraulic Engineering, Volume 135, number 8, pp 690–693.

Ferson, S and Ginzburg, L.R., (1996). Different methods are needed to propagate ignorance and variability. Journal of Reliability Engineering and System Safety. Volume 54, pp 133 - 144.

Gates, T. K and AI-Zahrani, M. A, (1996). Spatiotemporal Stochastic Open-Channel Flow II: Simulation Experiments. Journal of Hydraulic Engineering, Volume 122, Number. 11, pp 652 - 661.

Geza, S., (2007). Introduction to probability with statistical applications. Published by Birkhauser Boston, New York, USA.

Ghisalberti, M and Nepf, h.M., (2002). Mixing layers and coherent structures in vegetated aquatic flows. Journal of Geophysical Research, volume 107, (C2) 3011.

Girish, C and Ravindra, J., (2010). Aerodynamic parameter estimation from flight data applying extended and unscented Kalman filter. Journal of Aerospace Science and Technology. Volume 14, pp 106 – 117.

Gove, J. H and Hollinger, D. Y., (2006). Application of a dual unscented Kalman filter for simultaneous state and parameter estimation in problems of surface-atmosphere exchange. Journal of Geophysical Research, volume 111, pp 1 – 21.

Gu Feng-feng., (2007). Roughness coefficients for un-submerged and submerged reed. Journal of Hydrodynamics. Volume 19, number 4, pp 421-428.

Haldar, A and Sankaran, M., (2000). Probability, reliability, and statistical methods in engineering design. John Wiley Publication.

Hall, J.W (2006). Uncertainty-based sensitivity indices for imprecise probability distributions. Journal of Reliability Engineering and System Safety. Volume 91, pp 1443-1451.

Hall, J.W., Boyce, S.A., Wang, Y., Dawson, R.J., Tarantola, S and Saltelli, A., (2009). Sensitivity Analysis for Hydraulic Models. Journal of Hydraulic Engineering, Volume 135, Number 11, pp 959 – 969.

Hamed, M.M and El-Beshr, M.Z (2004). Uncertainty analysis in Dissolved Oxygen modeling in streams. Journal of Environmental Management, volume 34, no 2, pp 233 – 244.

Hayes, K.R., (2011). Uncertainty and uncertainty analysis methods. Issues in quantitative and qualitative risk modeling with application to import risk assessment ACERA project (0705). Report Number: EP102467.

He, T and Herose, S., (2013). Observation-driven Bayesian filtering for global location estimation in the field area. Journal of Field Robotics. Volume 30, number 4, pp 489–518.

Helen M. Regan, H, M., Colyvan, M and Burgman, M.A., (2002). A taxonomy and treatment of uncertainty for ecology and conservation biology. Ecological Applications, volume 12, number 2, pp. 618–628.

Helton, J.C., (1999). Uncertainty and sensitivity analysis in performance assessment for Waste Isolation Pilot Plant. Computer Physics Communication, volume 117, pp 156 – 180.

Helton, J. C and Davis, F. J, (2002). Illustration of Sampling-Based Methods for Uncertainty and Sensitivity Analysis. Risk Analysis, volume 22, number 3, pp 591 – 622.

Helton, J.C., Johnson, J.D., Sallabery, C.J and Storlie, C.B., (2006). Survey of sampling – based methods for uncertainty and sensitivity analysis. Reliability Engineering and System safety, volume 91, pp 1175 – 1209. Elsevier publishing.

Hoerner, S.F., (1965). Fluid dynamic drag, published by the author.

Hofstra, D.E., Gemmill, C.E.C and Winton, M.D., (2006). Preliminary genetic assessment of New Zealand Isoetes and Nitella, using DNA sequencing and RAPDs. Science for Conservation 266.

Horritt, M. S., (2006). A linearized approach to flow resistance uncertainty in a 2-D finite volume model of flood flow. Journal of Hydrology, volume 316, pp 13 – 27.

Huai, W., Chen, Z and Han, J., (2009). Mathematical model for the flow with submerged and emerged rigid vegetation. Journal of Hydrodynamics. Volume 21, number 5, pp722-729.

Huthoff, F., (2012). Theory of flow resistance caused by submerged roughness elements. Journal of Hydraulic Research, volume 50, number 1, pp 10 – 17.

Huthoff, F and Augustijn, D.C.M., (2006). Hydraulic resistance of vegetation: predictions of average flow velocities based on a rigid-cylinders analogy. Project report no: U2/430. 9/4268. University of twenty, Water Engineering and Management, Enschede, The Netherlands

Ikeda, S and Kanazawa, M., (1996). Three dimensional organized vortices above flexible water plants. Journal of Hydraulic Engineering, volume 122, number 11, pp 634-640.

Ingham, B.D., Tang, T and Morton, B.R., (1990). Journal of Fluid Mechanics, volume 210, pp 281 – 302.

Ishikawa, Y., Mizuhara, K., and Ashida, S. (2000). Effect of density of trees on drag exerted on trees in river channels. Eurasian Journal of Forest Research, Volume 5, number 4, pp 271–279.

James, C. S., Birkhead, A. L., Jordanova, A. A., and O'Sullivan, J. J., (2004). Flow resistance of emergent vegetation. Journal of Hydraulic Research, Volume 42, number 4, pp 390 – 398.

Jarvela, J., (2002). Flow resistance of flexible and stiff vegetation: a flume study with natural plants. Journal of Hydrology, Volume 269, pp 44–54. Elsevier publishing.

Jarvela J., (2004). Determination of flow resistance caused by non-submerged woody vegetation. International of Journal of River Basin Management. Volume 2, number 1, pp 61–70.

Jarvela, J., (2005). Effect of submerged flexible vegetation on flow structure and resistance. Journal of Hydrology, Volume307, pp 233–241.

Jazwinsky, A., (1970). Stochastic processes and filtering theory. Academic Press, New York.

Jial, Y., Alonso, C., Simon, A., Wells, R and Wang, S.Y., (2008). World Environmental and Water Resources Congress 2008, Ahupua'a.

Johnson, P.A., (1996). Uncertainty of hydraulic parameters. Journal of Hydraulic Engineering, volume 122, number 2, pp 112 – 114.

Johnson, P.A and Docks, D.A., (1998). Probabilistic bridge scour estimates. Journal of Hydraulic Engineering, volume 124, number 7, pp 750 – 754.

Julier, S.J., (2002). The scaled unscented transformation. Proceedings of the American Control Conference, Anchorage. Volume 6, pp 4555 -4559.

Julier, S and Uhlmann, J.K., (2004). Unscented filtering and nonlinear estimation. Proceeding of IEEE. Volume 92, number 3, pp 401 – 422.

Julier, S., Uhlmann, J. K and Durrant-Whyte, H. F., (2000). A new method for the nonlinear transformation of means and covariances in filters and estimators. IEEE Transaction on automatic control. Volume 45, number 3, pp 477 – 482.

Kabala, Z. J., (2001). Sensitivity analysis of a pumping test on a well with wellbore storage and skin. Advances in Water Resources, volume 24, pp 483 – 504.

Kalman, R.E., (1960). A new approach to linear filtering and prediction problems. Transactions of the ASME–Journal of Basic Engineering, volume 82, Series D, pp 35 – 45.

Kapelan, Z., Savic, D.A., Walters, G.A and Babayan, A.V (2006). Risk- and robustness – based solutions to a multi-objective water distribution system rehabilitation problem under uncertainty. Water science and Technology. Volume 53, number 1, pp 61 – 75. IWA publishing.

Karanki, D.R., Jadhav, P.A., Chandrakar, A., Srividya, A., and Verma, A.K., (2010). Uncertainty analysis in PSA with correlated imput parameters. International Journal of System Assurance Engineeing Management. Volume 1, pp 66 – 71.

Kays,W., and A. London, (1955). Compact Heat Exchangers. National. Press, Palo Alto, Calif.

Kessler, M., Alexander, L and Michael, S., (2012). Statistical methods for stochastic differential equations. Published by CRC Press, Taylor and Francis Group, London.

Kevin, C., Johlene, K., and Paul, C., (2007). Regional guidelines for ecological assessments of freshwater environments: Aquatic plant covers in wadeable streams. Environment Waikato Technical report 2006/47.

Kim, K and Park, C.G., (2010). Non-symmetric unscented transformation with application to in-flight alignment. International Journal of Control, Automation, and Systems, volume 8, number 4, pp 776 – 781.

Kim, S., Paul, A. S., Wan, E. A and McNames, J., (2010). Multi-harmonic frequency tracking method using the Sigma-point Kalman smoother. EURASIP Journal on Advances in Signal Processing, Hindawi Publishing Corporation. Article ID 467150, pp 1 – 13.

King, D. M and Perera, B. J. C., (2013). Morris method of sensitivity analysis applied to assess the importance of input variables on urban water supply yield – A case study. Journal of hydrology, volume 477, pp 17 – 32.

Klopstra, D., Barneveld, H.J, Noortwijk, J.M and Velzen, E.H., (1997). Analytical model for hydraulic roughness of submerged vegetation. The 27th Congress of IAHR, San Francisco, pp 775-780.

Kothyari, U. C., Hayashi, K., and Hashimoto, H., (2009). Drag coefficient of unsubmerged rigid vegetation stems in open channel flows. Journal of Hydraulic Research, Volume 47, number 6, pp 691–699.

Koutsoyiannis, D., Yao, H. and Georgakakos, A., (2008). Medium-range flow prediction for the Nile: a comparison of stochastic and deterministic methods. Journal of Hydrological Sciences. Volume 53, number 1, pp 142 - 164.

Kouwen, N and Fathi-Moghadam, M., (2000). Friction factors for coniferous trees along rivers. Journal of Hydraulic Engineering, Volume 126, number 10, pp 732 – 740.

Kouwen, N. and Unny, T.E., (1973). Flexible roughness in open channels. Journal of Hydraulic Division, ASCE. Volume 99, number 5, pp 713 - 728.

Kouwen, N and Li, R., (1980). Biomechanics of vegetative channel linings. . Journal of Hydraulic Division. ASCE, volume 106, number HY6, pp 1085 – 1103.

Kubrak, E., Kubrak, J & Rowiński, P.M., (2008). Vertical velocity distributions through and above submerged, flexible vegetation. Journal of hydrological sciences. Volume 53, number 4, pp 905 – 920.

Kutija, V and Hong, H.T.M., (1996). A numerical model for assessing the additional resistance to flow introduced by flexible vegetation. Journal of Hydraulic Research, volume 34, number 1, pp 99 – 114.

Kumar, K and Sung, C-J, (2011). Autoignition of Methanol:Experiments and Computations. International Journal of chemical Kinetics, volume 43, issue 4, pp 161 – 218.

Lam, K and Zou, L., (2010). Three dimensional numerical simulations of cross flow around four cylinders in an in-line square configuration. Journal of Fluids and Structures, volume 26, pp 482 – 502.

Larocque, G.R., Bhatti, J.S., Boutin, R and Chertov, O., (2008). Uncertainty analysis in carbon cycle models of forest ecosystems: Research needs and development of a theoretical framework to estimate error propagation. Ecological modeling, volume 219, pp 400 – 412. Elsevier publishing.

Leonard, L and Luther, M., (1995). Flow hydrodynamics in tidal marsh canopies. Limnology oceanogr., volume 40, pp 1474-1484.

Li, C.W and Tam, Y.F., (2002). Gradually varied flow through semi-rigid vegetation. The proceedings of the 14th Congress of International Association of Hydraulic Engineering and Research (IAHR), Hong Kong, 15-18 December, 2004, pp 859-864.

Li, C.W and Xie, J.F., (2011). Numerical modeling of free surface flow over submerged and highly flexible vegetation. Advances in Water Resources, Volume 34, pp 468–477. Elsevier publishing.

Li, C. W and Yan, K., (2007). Numerical Investigation of Wave–Current–Vegetation Interaction. Journal of Hydraulic Engineering, Volume 133, number 7, pp 794–803.

Li, C.W and Yu, L. H., (2010). Hybrid LES/RANS modelling of free surface flow through vegetation. Computers & Fluids, volume 39, pp 1722–1732.

Li, C.W and Zhang, M. L., (2010). 3D modelling of hydrodynamics and mixing in vegetation field under waves. Journal of Computers and Fluids, volume 39, pp 604–614. Elsevier publishing.

Li, C.W and Zeng, C., (2009). 3D numerical modeling of flow divisions at open channel junctions with or without vegetation. Journal of Advances in Water Resources, Volume 32, pp 46-60.

Li, L., Lu, H., Campbell, D.E and Ren, H., (2011). Methods for estimating the uncertainty in emergy table – form models. Ecological Modelling, volume 222, pp 2615 – 2622. Elsevier publishing.

Lightbody, A and Nepf, H.M., (2006). Prediction of velocity profiles and longitudinal dispersion in emergent salt marsh vegetation. Limnology Oceonogr, volume 51, (C1) 2005.

Liu, D., Diplas, P., Fairbanks, J. D., and Hodges, C. C., (2008). An experimental study of flow through rigid vegetation. Journal of Geophysical Research, Volume 113, F04015, pp 1 – 16.

Lohrmann, A., Cabrera, R., and Kraus, N.C., (1994). Acoustic – Doppler Velocimeter (ADV) for laboratory use. In fundamentals and Advancements in Hydraulic Measurements and Experimentation, C.A. Pugh (editions), pp 351 – 365.

Londhe, S and Charhate, S., (2010) Comparison of data-driven modelling techniques for river flow forecasting. Journal of Hydrological Sciences. Volume 55, number 7, pp 1163 – 1174.

Lopez, F and Garcia, M.H., (2001). Mean flow turbulence structure of open-channel flow through non-emergent vegetation. Journal of Hydraulic Engineering, Volume.127, number, 5, pp 392-402.

Liu, D., P. Diplas, J. D. Fairbanks, and C. C. Hodges (2008), An experimental study of flow through rigid vegetation. Journal of Geophysical Research, volume 113, pp 1 – 16.

Ludovic, C., Gilles, B., Jea, P.B., Cyril, D and Fredric, M., (2015). Velocity profiles in a real vegetated channel. Journal of Environmental Fluid Mechanics, Volume 15, pp 1263 - 1279.

Luhar, M., Contu, S., Infante, E., Fox, S and Nepf, H.M., (2010). Wave induced velocities inside a model seagrass bed. Journal of Geophysical Research, volume 115, pp 218 – 228.

Luhar, M and Nepf, H.M., (2013). From the blade scale to the reach scale: A characterization of aquatic vegetative drag. Journal of advances in Water Resources, volume 51, pp 305 – 316.

Luo, X. and Moroz, I.M., (2009). Ensemble Kalman filter with the unscented transform. Journal of Physica D, Volume 238, pp 549 – 562.

Luo, X., Moroz, I. M and Hoteit, I., (2010). Scaled unscented transform Gaussian sum filter: Theory and application. Journal of Physica D, volume 239, pp 684 – 701.

Mailhot, A and Villeneuve, J., (2003). Mean – value second – order uncertainty analysis method: application to water quality modeling. Journal of Advances in Water Resources, volume 26, pp 491- 499. Elsevier publishing.

Mansouri M., Dumont, B and Destain, M. F., (2013). Modeling and prediction of nonlinear environmental system using Bayesian methods. Journal of Computer and Electronics in Agriculture. Volume 92, pp 16 – 31.

Mattis, S.A., Dawson, C.N, Kees, C.E and Farthing, M.W., (2015). An immersed structure approach for fluid – vegetation interaction. Advances in Water Resources, volume 80, pp 1-16.

McIntyre, N.R., (2004). Analysis of uncertainty in River water quality modelling. PhD thesis, Civil and Environmental Engineering Department, Imperial College London.

Mckay, M. D., Beckman, R. J. and Conover, W. J., (2000): A comparison of three methods for selecting values of input variables in the analysis of output from a computer code, Technometrics, 42:1, 55-61.

Meijer, D.G., (1998). Modelproeven overstroomd riet. Technical report PR177, HKV Consultants, Lelystad, The Netherlands.

Melching, S.C, (1995). Reliability estimation. In Singh, V.P., editor, Computer models of watershed hydrology, Water Resources Publications, pp 69 – 118.

Menezes, L.R., Soares, A.J.M., Silva, L.M and Ishihara, J.Y., (2013). Using unscented transform as alternative to Monte Carlo in bit error rate calculations. Electronics Letters, 2013, Volume 49, number 10, pp 675 – 677.

Miler, O., Albayrak, I, and Nikora, V., (2012). Biomechanical properties of aquatic plants and their effects on plant-flow interactions in streams and rivers. Journal of Aquatic Sciences, Volume 74, pp 31 – 44.

Mochnac, J., Marchevsky, S and Kocan, P., (2009). Bayesian filtering techniques: Kalman and extended Kalman filter basics. 19th International Conference, Radioelectrica'09, Slovak Republic. Pg 119 -122.

Morgan, M.G. and Henrion, M. (1990). Uncertainty: A guide to dealing with uncertainty in quantitative risk and policy analysis, Cambridge University Press, Cambridge, U.K.

Morris, M. D, (1991). Factorial Sampling Plans for Preliminary Computational Experiments. Technometrics, Volume 33, number 2, pp. 161-174.

Muluye, G. Y., (2011). Improving long-range hydrological forecasts with extended Kalman filters, Journal of Hydrological Sciences. Volume 56, number 7, pp 1118-1128.

Murphy, E., Ghisalberti, M. and Nepf, H., (2007). Model and laboratory study of dispersion in flows with submerged vegetation. Journal of Water Resources Research, Volume 43, W05438, doi: 10.1029/2006WR005229, 2007.

Zhang, M., Li, C.W and Shen, Y., (2012). Depth-averaged modeling of free surface flows in open channels with emerged and submerged vegetation. Journal of Applied Mathematical Modelling, volume 37, pp 540 – 553. Elsevier publishing.

Nehal, L., Yan, Z.M., Xia, J.H and Khaldi, A., (2012). Flow through non-submerged vegetation: A flume experiment with artificial vegetation. The 16th International Water Technology Conference, IWTC, Istanbul, Turkey

Nept, H.M., (1999). Drag, turbulence, and diffusion in flow through emergent vegetation. Journal of Water Resources Research, volume 35, number 2, pp 479 – 489.

Nepf, H.M, (2012). Flow and Transport in Regions with Aquatic Vegetation. Annual Review in Advance on Fluid Mechanics. Volume 44, pp123–142.

Nepf, H.M. (2012b). Hydrodynamics of vegetated channels. Journal of Hydraulic Research, volume 50, number 3, pp 262 – 279.

Nepf, H.M and Vivoni, E.R., (2000). Flow structure in depth-limited, vegetated flow. Journal of Geophysical Research, volume 105, number C12, pp 547 – 557.

Nezu, I and Sajou, M., (2008). Turbulence structure and coherent motion in vegetated canopy open-channel flows. Journal of Hydro-environment Research, volume 2, pp 62 – 90. Elsevier publishing.

Nikora, V., Scott, L., Nina, N., Koustuv, D., Glenn, C. and Michael, R., (2008). Hydraulic resistance due to aquatic vegetation in small streams: Field study. Journal of Hydraulic Engineering, Volume 134, number 9, pp 1326-1332.

Noarayanan, L., Murali, K and Sundar, V., (2012). Manning's 'n' co-efficient for flexible emergent vegetation in tandem configuration. Journal of Hydro-environment Research, volume 6, pp 51 – 62.

Noorgaard, M., Poulsen, N. K., and Ravn. O., (2000). New developments in state estimation for nonlinear systems. Journal of Automatica, volume 36, pp 1627 – 1638.

Okamoto, T and Nezu, I., (2010). Large eddy simulation of 3-D flow structure and mass transport in open-channel flows with submerged vegetation. Journal of Hydro-environment Research, volume 4, pp 185 – 197. Elsevier publishing.

Okamoto, T., Nezu, I and Ikeda, H., (2012). Vertical mass and momentum transport in open-channel flows with submerged vegetation. Journal of Hydro-environment Research, volume 6, pp 287 - 297. Elsevier publishing.

Osidele, O.O., Zeng, W and Beck, M.B (2006). A random search methodology for examining parametric uncertainty in water quality models. Journal of Water science and Technology. Volume 53, number 1, pp 33 – 40. IWA publishing.

Padulo, M., Campobasso, M.S and Guenov, M. D., (2007). Comparative analysis of uncertainty propagation methods for robust engineering design. International Conference on Engineering Design, ICED'07. 28 - 31 August 2007, Cité Des Sciences et De L'industrie, Paris, France. Page 1 -12.

Paul, M., Thomas, R.E., Dijkstra, J.T., Penning, W.E and Vousdoukas, M.I., (2014). Plants, hydraulics and sediment dynamics, Book chapter 6; Users Guide to Ecohydraulic Modelling and Experimentation. Published by CRC Press/Balkema, Leiden,The Netherlands.

Pirim,T., Bennett, S and Barkdoll, B., (2000). Effect of Riparian Vegetation Density on Stream Flow Velocity. Water Resources 2000.

Podsechin, V., Tejakusuma, I., Schernewski, G., and Pejrup, M., (2006). On parameters estimation in dynamic model of suspended sediments. Journal of Hydrology, volume 318, pp 17 – 23.

Poggi, D., Porporato, A., Ridolfi, L., Albertson, J. D and Katul, G. G., (2004). The effect of vegetation density on canopy sub-layer turbulence. Journal of Boundary-Layer Meteorology, volume 111, pp 565–587.

Raadgever, G. T., Dieperink, C., Driessen, P.P.J., Smit, A.A.H and Rijswick, H.F.M.W, (2011). Uncertainty management strategies Lessons from the regional implementation of the Water Framework directive in the Netherlands. Journal of Environmental Science and Policy, volume 14, pp 64 – 75.

Ramroth, W.T., Krysl, P and Asaro, R.J., (2006). Sensitivity and uncertainty analysis for FE thermal model of FRP panel exposed to fire. Composites: Part A, volume 37, pp 1082 – 1091. Elsevier publishing.

Raupach, M.R., (1994). Simplified expression for vegetation roughness length and zero-plane displacement as functions of canopy height and area index. Boundary Layer Meteorology, Volume 7, pp 211- 216.

Regan, H. M., Colyvan, M., and Burgman, M. A. (2002). A taxonomy and treatment of uncertainty for ecology and conservation biology. Journal of Ecological Applications, volume 12, pp 618 – 628.

Regan, H. M., Ferson, S., and Berleant, D. (2004). Equivalence of methods for uncertainty propagation of real-valued random variables. International Journal of Approximate Reasoning, volume 36, pp1 – 30.

Righetti, M., Armanini, A., (2002). Flow resistance in open channel flows with sparsely distributed bushes. Journal of Hydrology. Volume 269, pp 55 – 64.

Ross, S.M., (2004). Introduction to probability and Statistics for engineers and scientists. Third Edition, Elsevier Academic Press, Burlington, USA.

Rubinstein, R. Y, (1981). Simulation and Monte Carlo Method. John Wiley & Sons, lnc., New York. Pp 26 – 36.

Saowapon, C. and Kouwen, N., (1989). A physically based model for determining flow resistance and velocity profiles in vegetated channels. Symposium on Manning's equation. B.C. Yen, Ed., Virginia, pp. 559-568.

Schneider, R and Georgakis, C., (2013). How to not make the extended Kalman filter fail. Journal of Industrial and Engineering Chemistry Research. Volume 52, pp 3354 – 3362. American Chemical Society publication.

Schoneboom, T., Aberle, J and Dittrich, A., (2011). Spatial Variability, Mean Drag Forces, and Drag coefficients in an array of rigid cylinders. Experimental Methods in Hydraulic Research. P. Rowinski (ed.), Geoplanet: Earth and Planetary Sciences, DOI 10.1007/978-3-642-17475-9_18, © Springer-Verlag, Berlin, Heidelberg.

Sébastien, D., Philippe, D., Paulo, E and Guillen, P., (2002). Development and application of Spalart–Allmaras one equation turbulence model to three-dimensional supersonic complex configurations. Aerospace Science and Technology, volume 6, pp 171–183.

Shimizu, Y. and Tsujimoto, T., (1994). Numerical analysis of turbulent open channel flow over a vegetation layer using a k-ε turbulence model. Journal of Hydroscience and Hydraulic Engineering, volume 2, pp 55 - 67.

Sigel, K., Klauer, B and Paul-Wostl, P., (2011). Conceptualizing uncertainty in environmental decision - making: The example of EU water framework directive. Journal of Ecological Economics. Volume 69, pp 502 – 510. Elsevier publishing.

Simon, D., (2010). Kalman filtering with state constraints: a survey of linear and nonlinear algorithms. IET Control Theory and Applications. Volume 4, issue 8, pp 1303 – 1318.

Simo, S and Jouni, H., (2010). Sigma point methods in optimal smoothing of non-linear stochastic state space models. 2010 IEEE International Workshop on Machine Learning for Signal Processing, August 29 – September 1, 2010, Kittila, Finland.

Soong, T.T, (2004). Fundamentals of probability and statistics for engineers. John Wiley and Sons Limited, the Atrium, Chichester, England.

Sowonski, M (2006). An uncertainty analysis of the flood – stage upstream from a bridge. Water Science and Technology. Volume 53, number 1, pp 77 – 84. IWA publishing.

Spalart, P. R., and Allmaras, S. R., (1994). A one-equation turbulence model for aerodynamic flows. La Recherche Aerospatiale, volume 1, number 1, pp 5-21.

Speyer, L.J and Chung, W.H., (2008). Stochastic processes, estimation, and control. 1st Edition, Published by Society for Industrial and Applied mathematics, Philadelphia, USA.

Stephan, U and Gutknecht, D., (2002). Hydraulic resistance of submerged flexible vegetation. Journal of Hydrology, volume 269, pp 27-43.

Stéphanie, M., Hervé, D., Maxime, S and Nicholas, A., (2013). Fast parameter calibration of a cardiac electromechanical model from medical images based on the unscented transform. Biomechanic Model Mechanobiology, volume 12, pp 815 – 831.

Stoesser, T., Kim, S. J., and Diplas, P., (2010). Turbulent flow through idealized emergent vegetation. Journal of Hydraulic Engineering, Volume 136, number12, pp 1003 – 1017.

Stone, B. A. M. and Shen, H. T., (2002). Hydraulic Resistance of Flow in Channels with Cylindrical Roughness. Journal of Hydraulic Engineering, Volume. 128, number 5, pp 500 -506.

Su, X., Li, C. W and Chen, B., (2003). Three - dimensional large eddy simulation of free surface turbulent flow in open channel within submerged vegetation domain. Journal of Hydrodynamics, volume 3, pp 35 – 43. China Ocean Press, Beijing, China.

Taka-aki, O and Nezu, I., (2010). Flow resistance law in open-channel flows with rigid and flexible vegetation. River Flow 2010.

Tanino, Y and Nepf, H.M., (2008).Laboratory investigation of mean drag in a random array of rigid, emergent cylinders. Journal of Hydraulic Engineering, volume 134, number 1, pp 34 – 41.

Taylor, H.M and Karlin, S., (1998). An introduction to stochastic modeling. Third Edition. Academic Press Limited, London.

Temple, D. M., (1986). Velocity distribution coefficients for grass-line channels. Journal of Hydraulic Engineering, volume 112, number 3, pp 193-205.

Tine, L., Herman, B and Joris, D. S., (2002). Comment on a new method for the nonlinear transformation of means and covariances in filters and estimators. IEEE Transactions on Automatic Control. Volume 47, number 8, pp 1 -3.

Tomlin, A.S, (2012). The role of sensitivity and uncertainty analysis in combustion modelling. Proceeding of the combustion Institute, pp 1 -18. Published by Elsevier Inc.

Turanyi, T., (2008). Sensitivity Analysis in Chemical Kinetics. International Journal of Chemical Kinetics. Volume 40, issue 11, pp 754 -768.

Tyagi, A and Haan, C.T., (2001). Reliability, risk and uncertainty analysis using generic expectation functions. Journal of hydraulic Engineering, volume 127, number 10, pp 938 – 945.

Van Asselt, M. B. A.: 2000, Perspectives on Uncertainty and Risk: The PRIMA Approach to Decision Support, Kluwer Academic Publishers, Dordrecht.

Van Asselt, M.B.A and Rotmans, J., (2002). Uncertainty in integrated assessment modelling: From Positivism to Pluralism. Journal of Climatic Change, volume 54, pp75–105. Kluwer Academic Publishers. Printed in the Netherlands.

Van de Klis, H., (2003). Uncertainty analysis applied to numerical models of river bed morphology. PhD thesis, Department of Civil Engineering, Technical University, Deflt, The Netherlands.

Van der Merwe, R., (2004). Sigma-Point Kalman Filters for Probabilistic Inference in Dynamic State-Space Models. Doctoral Thesis, Oregon Health & Science University, United State.

Van der Merwe, R and Wan, E.A., (2004). Sigma-point Kalman filters for integrated navigation. Paper presented at the 60th annual meeting of Institute of Navigation, Dayton, Ohio.

Van Gelder, P.H.A.J.M., (2000). Statistical methods for the risk-based design of civil structures. PhD thesis, Department of Civil Engineering and Geosciences, Technical University, Deflt, The Netherlands.

Van vuren, B.G., (2005). Stochastic modelling of river morphodynamics. Doctoral thesis, Department of Civil Engineering and Geosciences, Technical University Delft, The Netherlands. Published and distributed by DUP Science.

Vassilios, A. T and Edgar E. M., (2000). Hydraulic Resistance Determination in Marsh Wetlands. Journal of Water Resources Management, volume 14, pp 285–309. Kluwer Academic Publishers.

Velasco, D, Bateman, A., Redondo, J.M and Medina, V., (2003). An open channel flow experimental and theoretical study of resistance and turbulent characterization over flexible vegetated linings. Flow, Turbulence and Combustion. Volume 70, pp 69–88.

Velasco, D, Bateman, A. and Medina, V., (2008). A new integrated, hydro-mechanical model applied to flexible vegetation riverbeds. Journal of Hydraulic Reseach, Volume 46, number 5, pp 579-597.

Wahl, T.L., (2000). Analyzing ADV data using WinADV. Proceedings of Joint Conference on Water Resources Engineering and Water Resources Planning and Management. July 30-august 4, 2000, Minneapolis, Minnesota.

Walker, W.E., Harremoes, P., Rotmans, J., Van der Sluijs, J.P and Van Asselt, M.B.A., (2003). Defining uncertainty: A conceptual basis for uncertainty management in model-based decision support. Journal of Integrated Assessment, volume 4, number 1, pp 5 – 17.

Wang, C., Zhang, J and Mu, J., (2012). Maximum likelihood-based iterated divided difference filter for nonlinear Systems from discrete noisy measurements. Journal of *Sensors* volume *12*, pp 8912 – 8929.

Wang, Q., Rizos, C., Li Y and Li, S., (2008). Application of a Sigma-point Kalman Filter for alignment of MEMS-IMU. 2008 IEEE/ION Position, Location and Navigation Symposium, May 2008, pp 44 - 52.

Welch, G and Bishop, G., (2006). An introduction to the Kalman Filter. UNC – Chapel Hill, TR 95 – 045, July 24, 2006.

White, F.M, (1991). Viscous fluid flow. Second Edition, McGraw-Hill Company, USA.

White, B and Nepf, H., (2007). Shear instability and coherent structures in a flow adjacent to a porous layer. Journal of Fluid Mechanics, volume 593, pp 1 - 32.

William, H.W., Douglas, C.M., Davis, M.G, and Connie, M. B., (2003). Probability and statistics in engineering. Published by John Wiley and Sons Limited, USA.

Wilson, C.A.M.E, (2007). Flow resistance models for flexible submerged vegetation. Journal of Hydrology, volume 342, pp 213 – 222.

Wilson, C.A.M.E., Hoyt, J and Schnauder, I., (2008). Impact of foliage on the drag force of vegetation in aquatic flows. Journal of Hydraulic Engineering, volume 134, number 7, pp 885 – 891.

Wu, F.C., Shen, H.W., and Chou, Y.J., (1999). Variation of roughness coefficients for unsubmerged and submerged vegetation. Journal of Hydraulic Engineering, Volume 125, number 9, pp 934 – 942.

Wu, L and Yang, X., (2011). Factors influencing bending rigidity of submerged vegetation. Journal of Hydrodynamics. Volume 23, number 6, pp 723 – 729.

Wu, W and He, Z., (2009). Effects of vegetation on flow conveyance and sediment transport capacity. International Journal of Sediment Research, volume 24, pp 247- 259.

Wu, Y. T and Mohanty, S., (2006). Variable screening and ranking using sampling -based sensitivity measures. Reliability Engineering and System Safety, vol. 91, pp 634 – 647.

Xiaojun, T., Jie, Y., and Dudu, Z., (2010). Square-root sigma-point Kalman filtering for spacecraft relative navigation. Journal of Acta Astronautica. Volume 66, pp 704 – 713.

Yang, W. (2008), Experimental study of turbulent open-channel flows with submerged vegetation, Ph.D. thesis, Yonsei University, Korea.

Yang, W and Choi, S., (2009). Impact of stem flexibility on mean flow and turbulence structure in depth limited open channel flows with submerged vegetation. Journal of Hydraulic Research, volume 47, number 4, pp 445- 454.

Yang, W and Choi, S.U, (2010). A two-layer approach for depth-limited open-channel flows with submerged vegetation. Journal of Hydraulic Research. Volume 48, number 4, pp. 466 – 475.

Yu, P-S., yang, T-C and Chen, S.J., (2001). Comparison of uncertainty analysis methods for a distributed rainfall – runoff model. Journal of hydrology, volume 244, pp 43 – 49.

Zdravkovich, M., (1993). Interstitial flow field and fluid forces, in Technology for the '90's, edited by M. K. Au-Yang, p. 634, American Society of Mechanical Engineers, New York.

Zeng, C., (2012). Numerical and experimental studies of flows in open channels with gravel and vegetation roughnesses. PhD thesis, Department of Civil and Structural Engineering, The Hong Kong Polytechnic University.

Zeng, C and Li, C.W., (2014). Measurements and modeling of open-channel flows with finite semi-rigid vegetation patches. Journal of Environmental Fluid Mechanics. Volume 14, pp 113 – 134.

Zong, L and Nepf, H., (2010). Flow and deposition in and around a finite patch of vegetation. Journal of Geomorphology, volume 116, pp 363 – 372.

Zhong, C., Zhang, W and Zhu, S., (2010). Experimental research on shear stress of submerged vegetation in ecological river bank. Earth and Space 2010: Engineering, Science, Construction and Operations in Challenging Environments, 2010 ASCE.

Ziehn, T., Hughes, K. J., Griffiths J. F., Porter, R and Tomlin, A. S., (2009). A global sensitivity study of cyclohexane oxidation under low temperature fuel-rich conditions using HDMR methods. Combustion Theory and Modelling, volume 13, issue 4, pp 589 - 605.

Ziehn, T and Tomlin, A. S., (2008). A global sensitivity study of sulfur chemistry in a premixed methane flame model using HDMR. International Journal of chemical Kinetics, volume 40, issue 11, pp 742 – 753.